2013

OPTIMIZATION OF THE OPTICAL AND ELECTROCHEMICAL PROPERTIES OF DONOR-ACCEPTOR COPOLYMERS THROUGH FUNCTIONAL GROUP AND SIDE CHAIN MODIFICATION

Mark J. Seger
University of Kentucky, mjsege2@gmail.com

STUDENT AGREEMENT:

I represent that my thesis or dissertation and abstract are my original work. Proper attribution has been given to all outside sources. I understand that I am solely responsible for obtaining any needed copyright permissions. I have obtained and attached hereto needed written permission statements(s) from the owner(s) of each third-party copyrighted matter to be included in my work, allowing electronic distribution (if such use is not permitted by the fair use doctrine).

I hereby grant to The University of Kentucky and its agents the non-exclusive license to archive and make accessible my work in whole or in part in all forms of media, now or hereafter known. I agree that the document mentioned above may be made available immediately for worldwide access unless a preapproved embargo applies.

I retain all other ownership rights to the copyright of my work. I also retain the right to use in future works (such as articles or books) all or part of my work. I understand that I am free to register the copyright to my work.

REVIEW, APPROVAL AND ACCEPTANCE

The document mentioned above has been reviewed and accepted by the student's advisor, on behalf of the advisory committee, and by the Director of Graduate Studies (DGS), on behalf of the program; we verify that this is the final, approved version of the student's dissertation including all changes required by the advisory committee. The undersigned agree to abide by the statements above.

Mark J. Seger, Student

Dr. Mark D. Watson, Major Professor

Dr. John Anthony, Director of Graduate Studies

OPTIMIZATION OF THE OPTICAL AND ELECTROCHEMICAL PROPERTIES OF DONOR-ACCEPTOR COPOLYMERS THROUGH FUNCTIONAL GROUP AND SIDE CHAIN MODIFICATION

DISSERTATION

A dissertation submitted in partial fulfillment of the
requirement for the degree of Doctor of Philosophy
in the College of Arts and Sciences
at the University of Kentucky

By

Mark J. Seger

Lexington, Kentucky

Director: Dr. Mark D. Watson, Professor of Chemistry

Lexington, Kentucky

2013

ABSRTACT OF DISSERTATION

OPTIMIZATION OF THE OPTICAL AND ELECTROCHEMICAL PROPERTIES OF DONOR-ACCEPTOR COPOLYMERS THROUGH FUNCTIONAL GROUP AND SIDE CHAIN MODIFICATION

Donor-acceptor copolymers have received a great deal of attention for application as organic semiconductors, in particular as the active layers in low-cost consumer electronics. The functional groups grafted to the polymer backbones generally dictate the molecular orbital energies of the final materials as well as aid in self-assembly. Additionally, the side chains attached to these functional groups not only dictate the solubility of the final materials, but also their morphological characteristics.

The bulk of the research presented in this dissertation focuses on the synthesis and structure-property relationships of polymers containing novel acceptor motifs. Chapter 2 focuses on the synthesis of 1,2-disubstituted cyanoarene monomers as the acceptor motif for copolymerization with known donors. It was found that cyanation of both benzene and thiophene aromatic cores resulted in a decrease of the molecular orbital energy levels. Additionally, the small size of this functional group allowed favorable self-assembly and close π-stacking to occur relative to related acceptor cores carrying alkyl side chains as evidenced by UV-Vis and WAXD data.

Chapter 3 describes the systematic variation of side chain branching length and position within a series of phthalimide-based polymers. Branching of the side chains on bithiophene donor units resulted in the expected increase in solubility for these materials. Furthermore, a correlation was found between the branching position, size, and the HOMO energy levels for the polymers. Additionally, it was demonstrated that branching the alkyl side chains in close proximity to polymer backbones does not disrupt conjugation in these systems.

A novel acceptor motif based on the 1,3-indanedione unit is presented in Chapter 4. Despite the stronger electron withdrawing capability of this functional group relative to phthalimide, it was found that polymers based on this unit have the same HOMO molecular orbital energy levels as those presented in Chapter 3. It was found, however,

the presence of orthogonal side chains greatly enhanced the solubility of the final polymers. Additionally, UV-Vis and WAXD measurements revealed that thermal annealing had a profound effect on the ordering of these polymers. Despite the presence of orthogonal side chains, long range order and close π-stacking distances were still achieved with these materials.

Finally, alkynyl "spacers" were used in Chapter 5 to separate the solubilizing alkyl side chains from the polymer backbones on bithiophene donor monomers. The alkynyl groups allowed for conjugated polymer backbones to be achieved as well as low HOMO energy levels. A correlation between the side chain size, π-stacking distances and HOMO-LUMO energy levels was measured in this polymer series.

KEY WORDS: Conjugated polymers, organic thin-film transistors (OTFTs), organic photovoltaic devices (OPVs), polymer electrochemistry, polymer spectroscopy

Mark Seger

5/2/2013

OPTIMIZATION OF THE OPTICAL AND ELECTROCHEMICAL PROPERTIES OF DONOR-ACCEPTOR COPOLYMERS THROUGH FUNCTIONAL GROUP AND SIDE CHAIN MODIFICATION

By

Mark J. Seger

Dr. Mark D. Watson
Director of Dissertation

Dr. John E. Anthony
Director of Graduate Studies

5/2/2013
Date

DEDICATED TO

My family and friends

ACKNOWLEGMENTS

First and foremost I thank my research advisor, Professor Mark Watson. He allowed me to join his lab and work on the interesting research projects – culminating in the creation of this dissertation. His approach toward advising me during my graduate education was a delicate combination of guided and independent research. The expectations of thoroughly knowing and critically thinking about all of the aspects associated with the projects have undoubtedly catalyzed my continuing transformation from a college-educated chemist into a scientist. His patience with teaching students and passion for chemistry have had a significant impact my own teaching and research philosophies, things I will carrying into the future with me.

I thank our collaborators, the Jenekhe group at the University of Washington and the Polyera Corporation. Their device fabrication and measurements provided valuable information about the materials I synthesized during my time at UK.

My committee members, Professor John Anthony, Professor John Selegue and Professor Zach Hilt also deserve my thanks. Both my Oral Examination and Final Defense felt more like a round-table discussion with genuinely interested scientists, rather than a stressful pass-fail examination. They gave me valuable suggestions on my projects and also helped to craft my research skills and critical-thinking ability. Additionally, my outside examiner, Professor Tianyan Gao deserves acknowledgment. She provided some useful insight to me during my Final Defense.

I thank Mr. John Layton and Dr. Sean Parkin for their help with NMR and X-ray experiments, respectively. Both of these instruments played key roles in my research, and their expertise was invaluable.

Finally, and most importantly, I express my deepest thanks to my family and friends. They have fully supported me without prejudice through my entire journey through graduate school.

TABLE OF CONTENTS

LIST OF TABLES

LIST OF FIGURES

LIST OF ABBREVIATIONS

BCBG	Bottom gate bottom contact
BCTG	Bottom contact top gate
BHJ	Bulk heterojunction
BOBT	3,3'-dibutyloctyl-2,2'-bithiophene
BuLi	n-butyllithium
Bu_3SnCl	Tributyltin chloride
CT	Charge transfer
CV	Cyclic voltammetry
D-A	Donor-acceptor
DBT	3,3'-didodecyl-2,2'-bithiophene
DCM	Dichloromethane
DPV	Differential pulsed voltammetry
DSC	Differential scanning calorimetry
EA	Electron affinity
E_g	HOMO-LUMO energy gap
E_{HOMO}	HOMO energy level
E_{LUMO}	LUMO energy level
EtOAc	Ethyl acetate
EtOH	Ethanol
eV	Electron volts
Fc/Fc^+	ferrocene/ferrocenium
FF	Fill factor
FMO	Frontier molecular orbital
GPC	Gel permeation chromatography
HH	Head-to-head
HT	Head-to-tail
HOMO	Highest occupied molecular orbital
I_{on}/I_{off}	On/off current ratio
IP	Ionization potential
IPN	Interpenetrating network
J_{SC}	Short-circuit current density
LUMO	Lowest unoccupied molecular orbital
μ	Mobility
NBI	Naphthalene bisimide
n-type	Electron transporting (negative-type)
OE	Organic electronics
OFET	Organic field effect transistor
P3HT	Poly(3-hexylthiophene)
PAT	Poly(alkylthiophene)
PBI	Perylene bisimide
PCBM	[6,6]-phenyl-C_{61}-butyric acid methyl ester
PCE	Power conversion efficiency
PDI	Polydispersity index
p-type	Hole transporting (positive-type)

RvB	Rosenmund-von Braun
TMSCl	Chlorotrimethylsilane
TCBG	Top contact bottom gate
UPS	Ultraviolet photoelectron spectroscopy
V_{OC}	Open-circuit voltage
V_{th}	Threshold voltage
WAXD	2-D wide angle x-ray diffraction
3,3’-ROT2	3,3’-dialkoxy-2,2’-bithiophene

Chapter One: Introduction to Organic Semiconductor Materials

1.1 Organic Electronics Introduction

Conjugated polymers, for electronic applications, first appeared in the literature with the reports of conductive, doped polyacetylene in 1977.[1] Since then, a large research effort has taken place to further this technology, resulting in large scientific advances through the past 36 years. Specifically, a major goal of the organic electronics (OE) field is to replace/supplement conventional Si-based technologies in applications such as thin-film transistors,[2] photovoltaic devices,[3] sensors[4], and radio-frequency identification (RF-ID) tags.[5] One main attraction of "going organic" rather than using traditional silicon and metalloid semiconductor materials lies in the reduced cost of fabricating devices from soluble organic compounds, rather than the costly and energy intensive methods required for traditional devices fabricated from insoluble silicon. A number of cheap, simple, high-throughput deposition techniques such as spin coating and inkjet printing have been developed that can be applied to process soluble semiconductor materials.[6] Recent developments in the field have also produced organic-based devices that can compete with, and even outperform amorphous-Si (a-Si) in certain figures of merit for thin-film transistor applications.[8,9,10] Solution processability also allows these materials to be compatible with temperature sensitive device substrates such as plastics and fabrics. Novel products can be created using these materials that otherwise would not be possible using metalloid semiconductors requiring high temperature processing steps.[7] Despite impressive technological advances over the past five years, OE have not found wide-spread use in real-world devices on the market today. Indeed the majority of low-end contemporary electronic technologies are still dependant on semiconductors

based on the metalloid compounds. This is due to the fact that organic materials still have a host of unsolved issues. The main drawback to OE technology is that these carbon-based materials are simply not stable during device operation.[68] These materials undergo redox processes with ambient species such as O_2 and H_2O when operated in devices, thus greatly limiting device efficiency and lifetime.[11,12, 13] One solution to this issue is to encapsulate the active organic layer, shielding it from contact with the atmosphere.[13] This approach, however, requires extra materials and steps in processing, driving up the final cost of devices and taking away the most attractive feature of cost savings associated with going organic. Other approaches, which are a major topic of this dissertation, rely on the design of compounds to thermodynamically and/or kinetically prevent the active materials from undergoing redox chemistry with atmospheric species.[69]

1. 2 Organic Thin-Film Transistors

In particular, research in the past 5 years has produced large increases in device performances in the field. Such advances necessitate a multidisciplinary approach to achieve efficient final devices. This and the following section describe the basic device structures and operating principals of organic thin-film transistor (OTFT) and organic photovoltaic (OPV) devices. These sections are intended to give just enough background to understand the motivation for the synthesis of polymers presented in later sections and are by no means comprehensive. Both p-type and n-type organic semiconductors are known, but the focus of this dissertation is p-type semiconductors so only those materials will be discussed in this section. Sections 1.4 and 1.5 summarize the bulk of the topics for this dissertation; molecular design principals and materials synthesis.

OTFTs, as mentioned above, have numerous practical uses as the active components in many modern devices. In addition to functional devices they also provide valuable fundamental information and may be considered a characterization tool for OE materials. The four basic device structures for OTFTs are shown in figure 1.1.

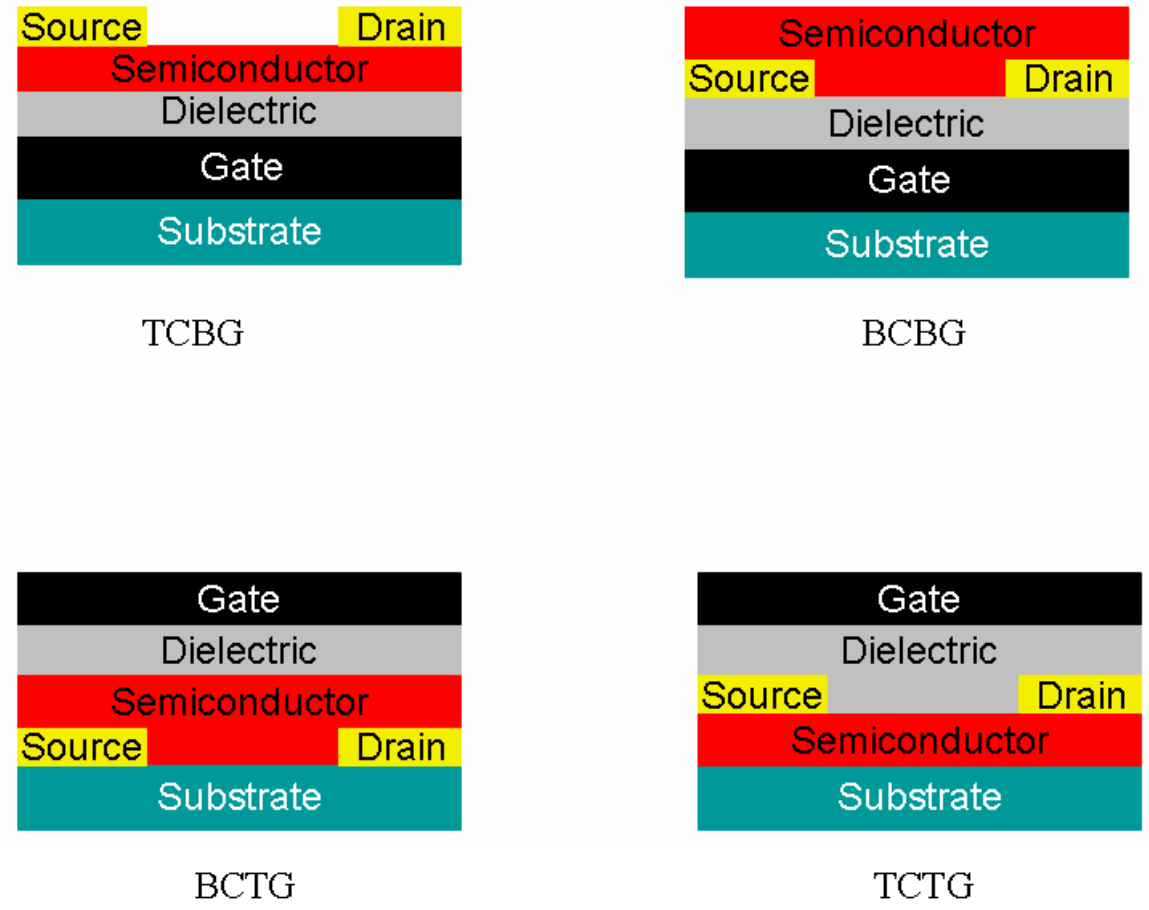

Figure 1.1: Basic device architecture for OTFTs: Top contact bottom gate (TCBG), bottom contact bottom gate (BCBG), bottom contact top gate (BCTG) and top contact top gate (TCTG).

While the overall configurations for these devices are different, the basic components are all the same. A three electrode set-up consisting of source, drain and gate electrodes are present in all configurations. The source and drain electrodes are typically made from

gold, but other materials may be used. The gate electrode is generally heavy doped silicon although other materials may be used as well. An insulating dielectric layer separates the gate electrode from the semiconductor in all cases; the gate electrode is capacitively coupled to the semiconductor through the dielectric layer. Inorganic or polymeric dielectrics are commonly used for this purpose. The semiconducting layer is not purposely doped, so ideally the concentration of charge carriers (holes or electrons) is extremely low when no gate voltage is applied and the device is in the "off" state. Application of a gate voltage induces an increase in charge-carrier concentration in the semiconducting layer (accumulation layer) and the device is said to be "on". Finally, after charge accumulation, a potential difference between the source and drain electrodes is applied and holes are injected into the highest occupied molecular orbital (HOMO) energy level of polymer. Current then flows between the two electrodes as illustrated

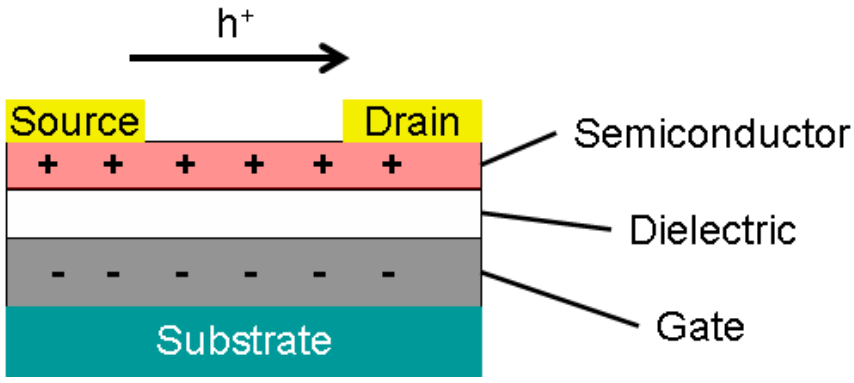

Figure 1.2: Schematic of OTFT device function.

in figure 1.2. Although this diagram and the operating principles described above are an oversimplification of how OFETs work, the focus of this dissertation is not on the device

engineering and solid-state physics aspect of OFETs. Rather, this basic idea of OFET operation will be sufficient to understand the molecular design principals presented later. Three important figures of merit are used when evaluating the performance of OFETs.[76]

Charge carrier mobility (μ): The charge carrier mobility, by definition, is the drift velocity of a charge (electron or hole) per unit of the applied electric field. Mobility greater than 0.5 cm^2/Vs is desirable for real world applications.[76]

On/off current ratio (I_{on}/I_{off}): The on/off current ratio is simply a ratio of the current flowing through the device in the "on" state and the "off" state. When no gate voltage is applied, there should be minimal mobile charges in the active layer and hence, no current flowing through the device. However, if impurities are present they may act as dopants, creating mobile charges while the device is in the "off" state. I_{on}/I_{off} then, can be an indicator of the purity and stability of the semiconductor, with desirable values of $> 10^5$.[76]

Threshold voltage (V_{th}): The threshold voltage is the gate voltage at which the accumulation layer is formed. Generally, hole or electron traps are present in the films of semiconductors that must be filled before the device can conduct. Numbers close to zero are desirable for V_{th}.

1.3 Organic Photovoltaic Devices

Photovoltaic cells, otherwise known as solar cells, utilize light to create electrical current employing a photoactive semiconducting material. Traditionally, solar cells have been based on inorganic materials; specifically on silicon, making up 85% of the market as of 2010.[14] While the prospect of using a clean, non-CO_2 releasing, renewable energy source such as the sun has been attractive to many scientists and politicians for years, the practical aspects of solar energy capture have hampered widespread adoption. The main issue associated with solar energy, based on classic inorganic cells, is the prohibitively high cost of manufacturing crystalline silicon. Silicon must be highly purified and processed at high temperatures under vacuum, a very costly and energy-expensive process. Additionally, large-scale grid operations of silicon solar cells cannot compete with traditional grid-type electricity.[15] The active materials for OPVs on the other hand, may be easily synthesized and purified by routine laboratory procedures and solution processed at or near room temperature into devices, greatly decreasing manufacturing cost. The attractive features of large-area, low-cost solar cells have generated extensive research interest in the field of OPVs. However, organic-based cells have serious limitations of their own, generally associated with their low power conversion efficiencies (PCEs) and poor long term stability. Considering that silicon solar cells have certified efficiencies >25%[10] while their organic counterparts have just begun to achieve efficiencies exceeding 10%, OPVs appear to be purely an academic exercise as of now. It has been estimated, however, that OPVs operating with 10% PCE with device stability of ~ 10 years could reduce the overall cost of ownership to less than that of silicon solar cells making real world OPV cells a reality.[15] The lower manufacturing costs of OPVs

relative to their higher performing inorganic counterparts will compensate for their lower device performance and stability.[16] Recent progress further suggests this may become reality as the PCEs of some OPV devices are topping the 12% mark.[80]

Operating Mechanism

While various architectures for OPVs have been proposed and tested throughout the years the current state of the art is known as the bulk heterojunction (BHJ) design. The key feature of the bulk heterojunction design is the blending of a p-type conjugated polymer or small molecule with an n-type electron acceptor, almost exclusively a soluble fullerene derivate such as PCBM or $P_{71}BCM$ (figure 1.3).

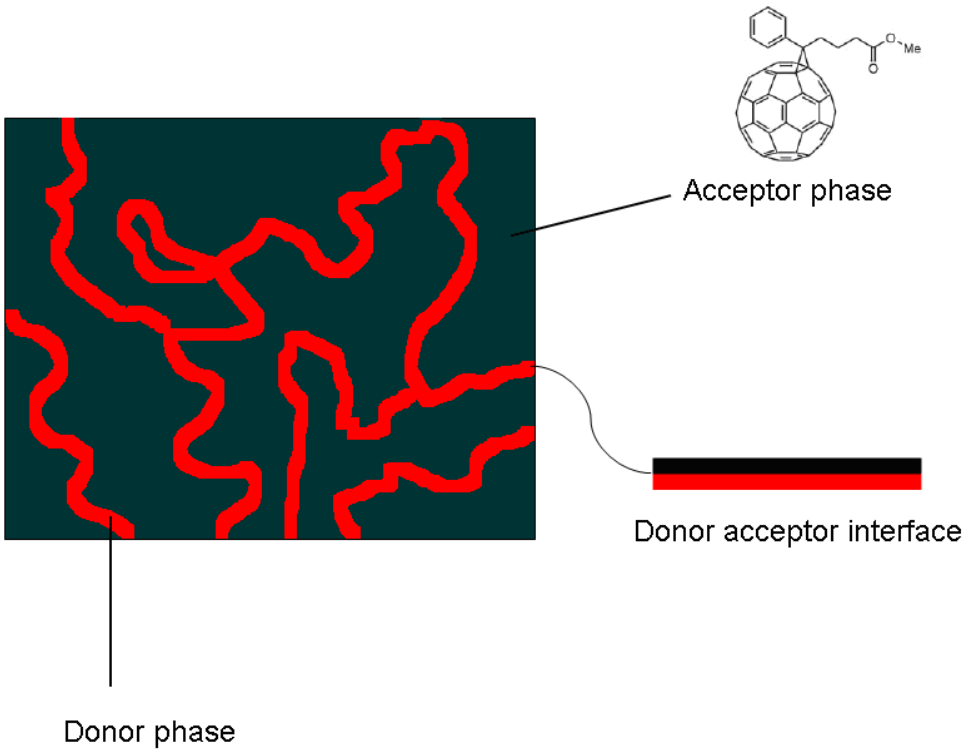

Figure 1.3: Schematic representation of the active layer of an OPV (not to scale) with the structure of commonly used acceptor PCBM .

The overall performance of an OPV is expressed as the power conversion efficiency (PCE) represented by equation 1.

$$PCE = \frac{Voc \times Jsc \times FF}{Pin} \qquad \textbf{eq. 1}$$

It can be seen from equation 1 that the overall PCE is represented by three terms that may be extracted from the J-V output curve of an OPV device. These terms are briefly defined here:

Open-circuit voltage (V_{OC}): The open-circuit voltage is the voltage across an OPV when there is no current flowing.

Short-circuit current density (J_{sc}): The short-circuit current density is the current flowing through the OPV when the potential across the cell is zero. It is proportional to the area of the cell illuminated by light; therefore it is expressed as a ratio of current to area (mA/cm^2).

Fill Factor (FF): Fill factor is the ratio of the maximum power produced by the cell to the product of V_{oc} and J_{sc}.

The general operating mechanism for BHJ OPVs is illustrated in figure 1.4 and described as follows:[18]

1) Absorption of photons by the conjugated polymer creating a exciton (a bound electron-hole pair).
2) Diffusion of the exciton to the donor-acceptor interface.
3) Dissociation of the exciton, charge generation and diffusion to the proper electrodes.

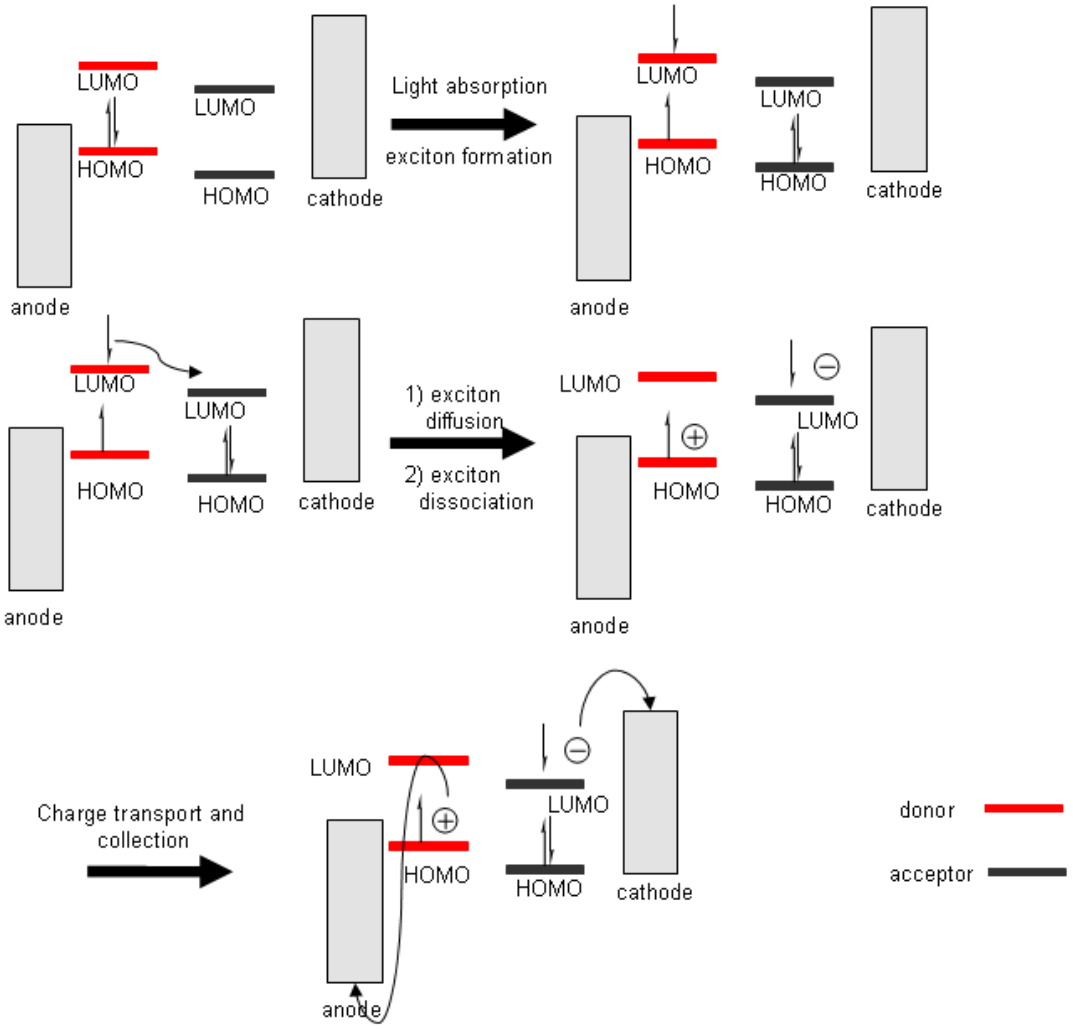

Figure 1.4: Diagram of optical excitation, charge transfer and charge collection in BHJ OPV.

It becomes apparent from figure 1.3 that intimate mixing of the donor and acceptor phases as well as the overall morphology of the blend are crucial for high-performance cells to be realized. The blends must form an interpenetrating network (IPN) with domains of the donor and acceptor on the scale of the exciton diffusion length, about 10 nm.[70] Fullerene derivatives are, as of now, the prime materials used as electron acceptors

in BHJ cells. Fullerenes possess a number of unique characteristics. Their triply degenerate LUMO allows them to be reduced with up to six electrons in solution[77] and they possess high electron mobility, up to 1 cm^2/Vs in OTFTs[78]. Electron transfer from excited donors to fullerenes is ultra fast, on the order of 45 fs, while competing relaxation processes are much slower, on the order of 1 ns.[20] Their energetically deep lying LUMO of -4.2 eV[19] (high electron affinity) provides the thermodynamic driving force for step 3, charge dissociation at the donor/acceptor interface. Their spherical structure also allows 3-dimensional electron transport. In order to obtain the necessary energetic driving force for forward electron transfer to fullerene, a minimum energetic offset of ~ 0.3 eV between the LUMOs of the donor and acceptor materials is generally reported to be sufficient to overcome the exciton binding energy.[21] The V_{OC} is also partially dependent on the difference in HOMO energy level of the donor and LUMO energy level of the acceptor. Brabec et al. found a direct relationship between the electron acceptor strength of 4 different fullerene derivatives with the donor poly(phenylene vinylene), MDMO-PPV.[22] Further studies by Brabec et al. showed that a similar trend was observed using PCBM as the acceptor while varying the donors.[23] Assuming PCBM will be used as the electron acceptor phase we are searching for materials with HOMO energies of -5.4 eV and a HOMO-LUMO energy gap (E_g) ~ 1.5 eV to achieve maximum cell efficiency. The second key factor for materials to be used in OPVs is the light harvesting capability of the polymers. Approximately 70% of the sun's light flux is distributed in the wavelength region between 900 and 380 nm.[24] Ideal donor polymers will have a broad absorption profile across this range and low E_g to obtain high overall efficiency. From the molecular design and synthetic chemistry point of view we are mostly concerned with

synthesizing polymers with the appropriate E_g and FMO energies as to maximize both V_{OC} and J_{SC}. We also wish to maintain high levels of solubility for our materials to facilitate processing, ideally with good self-organization properties.

1. 4 Molecular Properties

The major focus of this dissertation is optimizing the molecular properties of conjugated polymers for applications in OTFTs and OPVs and will be introduced here. A qualitative model for the prediction of the E_g of conjugated polymers was first presented by Roncali in 1997.[25] As shown in figure 1.5 the E_g may be thought of as a function of five interrelated contributions described below.

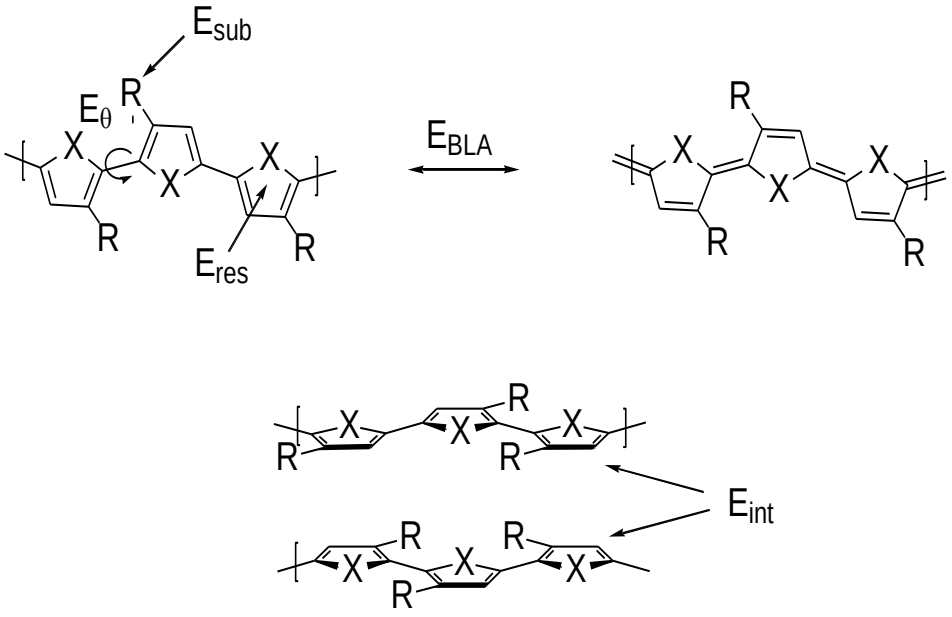

$$E_g \approx E_{BLA} + E_\theta + E_{res} + E_{sub} + E_{\text{int}}$$

Figure 1.5: Qualitative model and "equation" for E_g contributions. [25]

E_{BLA}: (BLA = bond-length alternation) The two "resonance" structures shown in figure 1.5 are not energetically equivalent.[26] The quinoidal structure of the polymer has been calculated to have a smaller E_g, hence, its contributions to the ground state structure will result in systems with smaller E_g.[27]

E_θ: Twisting of the repeating units relative to one another decreases π-orbital overlap and overall conjugation in the system. The result is an increase in the E_g.

E_{res}: This term refers to the intrinsic resonance stabilization energy of the units in the polymer backbone. For example, benzene has a higher resonance stabilization energy than thiophene, 1.56 and 1.26 eV respectively.[25] Therefore, based on this alone, one may predict thiophene-based polymers would have smaller E_g than the analogous benzene-based polymers.

E_{sub}: The substitution of hydrogen by various functional groups on the aromatic moieties in CPs has a large influence on the E_{HOMO} and E_{LUMO}, and hence, the E_g of the polymer. This will be discussed in greater detail later.

E_{int}: Intermolecular interactions, specifically interchain coupling, in solution and especially the solid state can impact the E_g. Generally, decreases in E_g are observed for CPs as interchain coupling increases.

Returning to the definition of E_g as difference in energy between HOMO and LUMO energies in conjugated systems, any of the above contributions that affect the E_g of the CP does so by affecting the FMO energies of the polymer. As will be shown in the next sections, the magnitude of the changes of the FMO energies is not always equal.

1. 4. 1 Structural Considerations

Conjugated π-electron system

Charge transport in OE materials typically occurs through conjugated p-orbitals in aromatic systems. First, ionization potentials (IP) for electrons in the HOMO of conjugated molecules, very commonly part of the π-framework, are much lower than those associated with the σ-framework, or isolated π-orbitals of non-conjugated alkenes.[2] This, from a practical point of view, means that charges may be injected into the HOMO of π-conjugated molecules from common metal electrodes. Second, following injection, the charge must be delocalized throughout the molecule in order to travel to the necessary electrodes. Figure 1.6 shows a resonance structure for a commonly used OE material, P3HT. The ideal situation, illustrated in figure 1.6 suggests that if P3HT were sandwiched between two electrodes it would function essentially as a wire; fast charge delocalization would occur through the whole polymer leading to high charge carrier mobility. However, it is well known that this is not the case. Defects in the polymer chain from chemical synthesis and (photo)chemical decomposition may block complete charge delocalization. Physical defects, such as tilting of the monomer units relative to one another (E_θ) also limits the conjugation within a polymer chain. Limiting these chemical and physical defects through molecular design and choice of synthetic route can increase carrier mobility. These implications will be discussed in detail later.

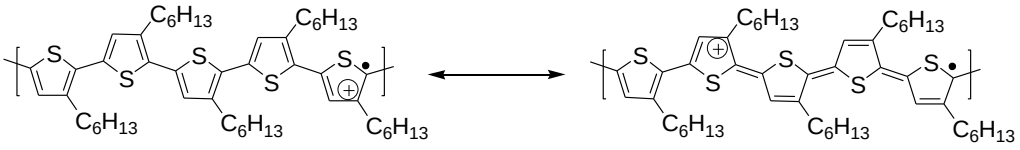

Figure 1.6: Resonance structure for a segment P3HT showing charge delocalization.

Solid State Ordering

Another mode of charge transport is believed to be dominant in organic semiconductors. Charges "hop" from one polymer chain to adjacent polymer chains as illustrated in figure 1.7, i.e. in an intermolecular fashion.[71] Therefore, it is important to design materials that preferentially adopt face-to-face π-stacking at close intermolecular distances in order to maximize charge transport rates and overall mobility.

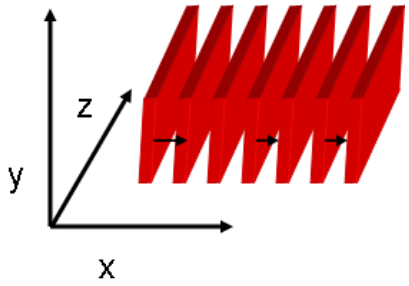

Figure 1.7: Schematic diagram of charge delocalization in a polymer OE device. The solid red blocks represent CP backbones (side chains omitted). The arrows between the backbones show the movement of charge from one chain to another. Intrachain delocalization occurs in the Z direction, interchain hopping occurs in the X direction.

The relationship between intra- and interchain electron delocalization and hopping leads to two dimensional charge transport. The insulating alkyl chains would generally populate the Y direction in figure 1.7 and do not contribute to charge transport.[71] It is however, a difficult task to predict whether polymers will order in this fashion or not *a priori.*

Appropriate FMO energies

Not only must the π-electron system of conjugated polymers have accessible HOMO energy levels for hole injection from common metal electrodes such as gold, they

must also have suitable energies to impart ambient stability. One of the biggest issues facing commercialization for OE devices, as noted before, is their lack of ambient stability when operated in devices. The general design of polymeric OE semiconductors incorporates electron-rich aromatics in the backbone of the polymer. These highly electron-rich species are prone to undergo oxidation processes with ambient species such as O_2, H_2O and ozone. de Leeuw and co-workers applied the standard redox potentials of common ambient species to derive a relationship between a polymer's E_{HOMO} and operational device stability.[28] It is worth noting here that the Nernst equation was used for their calculations, which is valid for aqueous solutions. The polymers in question, of course, are generally not deposited from aqueous solution. More importantly, these materials are in the solid state when operated in devices and sandwiched between electrodes with different work functions. Additionally, the free energy of activation (overpotential) for electrochemical reactions to occur was also neglected in their calculations, which may amount up to a volt.[69] Nonetheless, they found that semiconductors in OTFTs must have an E_{HOMO} deeper than - 4.9 eV relative to vacuum in order to be stable against redox chemistry with O_2 and H_2O. In order to achieve this, electrons in the HOMO must be somehow stabilized relative to vacuum level.

Small HOMO-LUMO energy gap

The E_g is an important consideration for materials specifically in OPVs. As shown in figure 1.8, and stated in section 1.3, approximately 70% of the sun's energy is distributed in wavelength region between 900 and 380 nm. In order to capture as many photons as possible it is necessary for the polymer to have a narrow E_g of ~ 1.4 eV, and, ideally a large spectral distribution in this wavelength region.[24] For example, the

absorption spectrum of polymer "B", shown as the black line in figure 1.8, has an E_g of 1.4 eV and a broad absorption profile in the 900 to 380 nm range. A material with such absorption characteristics would be expected to efficiently capture photons in this wavelength region. Polymer "A" on the other hand, has an E_g of 2.6 eV and a narrow absorption profile in this region, and would not be capable of harvesting a large fraction

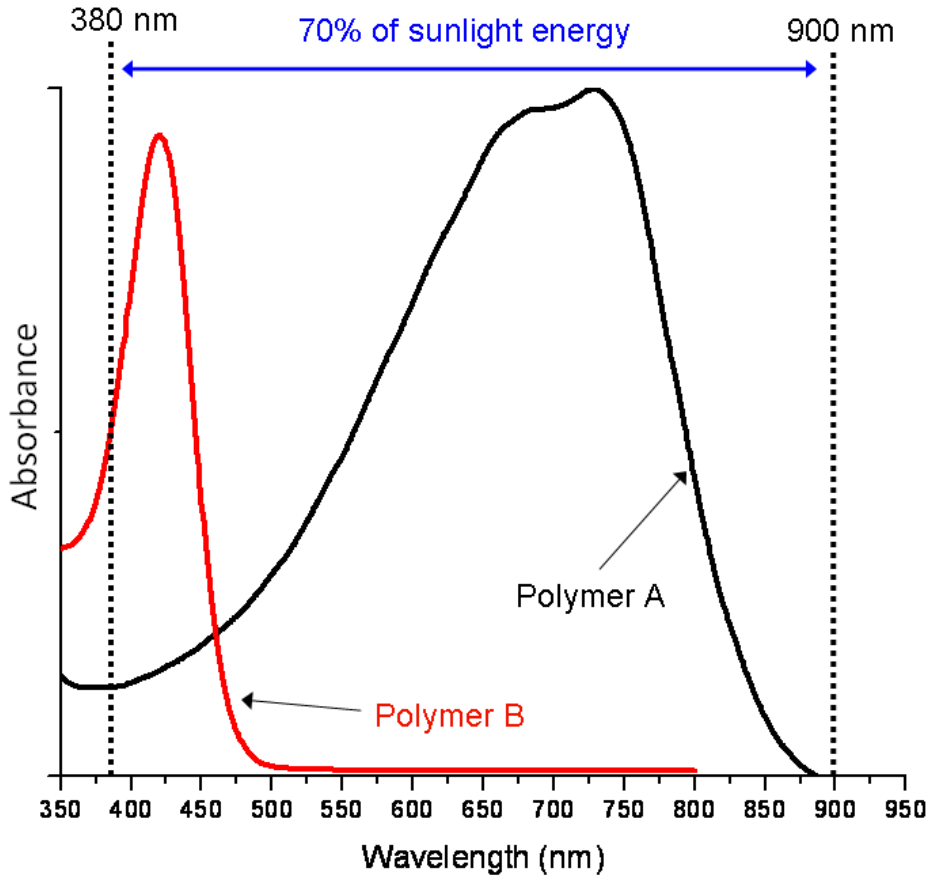

Figure 1.8: Absorption of spectrum of a low-energy gap polymer "A" (black line) with a broad spectral distribution and a large energy gap polymer "B" (red line) with a narrow spectral distribution.

of solar photons in this wavelength region.

1. 4. 2 The Donor-Acceptor Approach to Conjugated Polymers

In order to satisfy the above requirements for conjugated polymers the contemporary strategy is to synthesize polymers comprised of alternating electron-

donating and accepting monomers; otherwise known as the donor acceptor (D-A) approach. All of the highest performing polymers to date (as will be shown in the following section) are D-A materials. The main benefits of the D-A approach are thought to be in the areas of polymer self organization and FMO energy level control. Alternating electron-rich and electron-poor monomers within a polymer backbone can provide a driving force for favorable self-assembly (π-stacking); the electron-rich and electron-poor units may assemble in a close, face-to-face fashion (figure 1.9), as observed, for example, in benzene and hexafluorobenzene mixtures,[72] necessary for good performance in OTFTs.

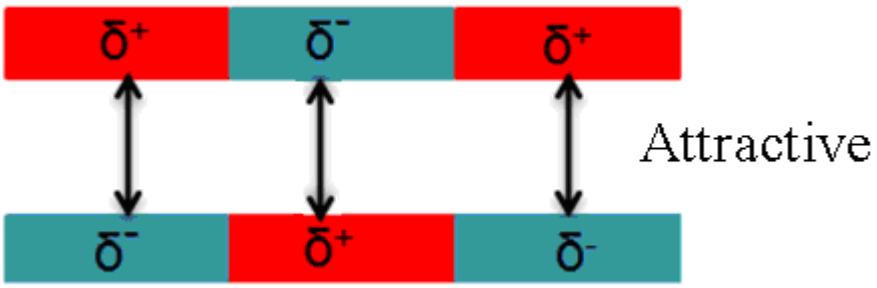

Figure 1.9: Illustration of attractive interactions between electron-rich (donor) and electron-poor (acceptor) units of a D-A polymer.

Second, this approach allows for the E_g, as well as the FMO energy levels of polymers to be rationally varied as illustrated in figure 1.10. Copolymerization of donor and acceptor monomers generally raises the HOMO energy of and stabilizes the LUMO energy of the resulting D-A polymer relative to the isolated monomers, thus narrowing the E_g.[73] Additionally, the HOMO in many D-A systems is concentrated more on, or the E_{HOMO} is

more strongly governed by the E_{HOMO} of, the donor unit while the LUMO is concentrated more on, or the E_{LUMO} is more strongly governed by, the acceptor unit.[73,74] Therefore, by

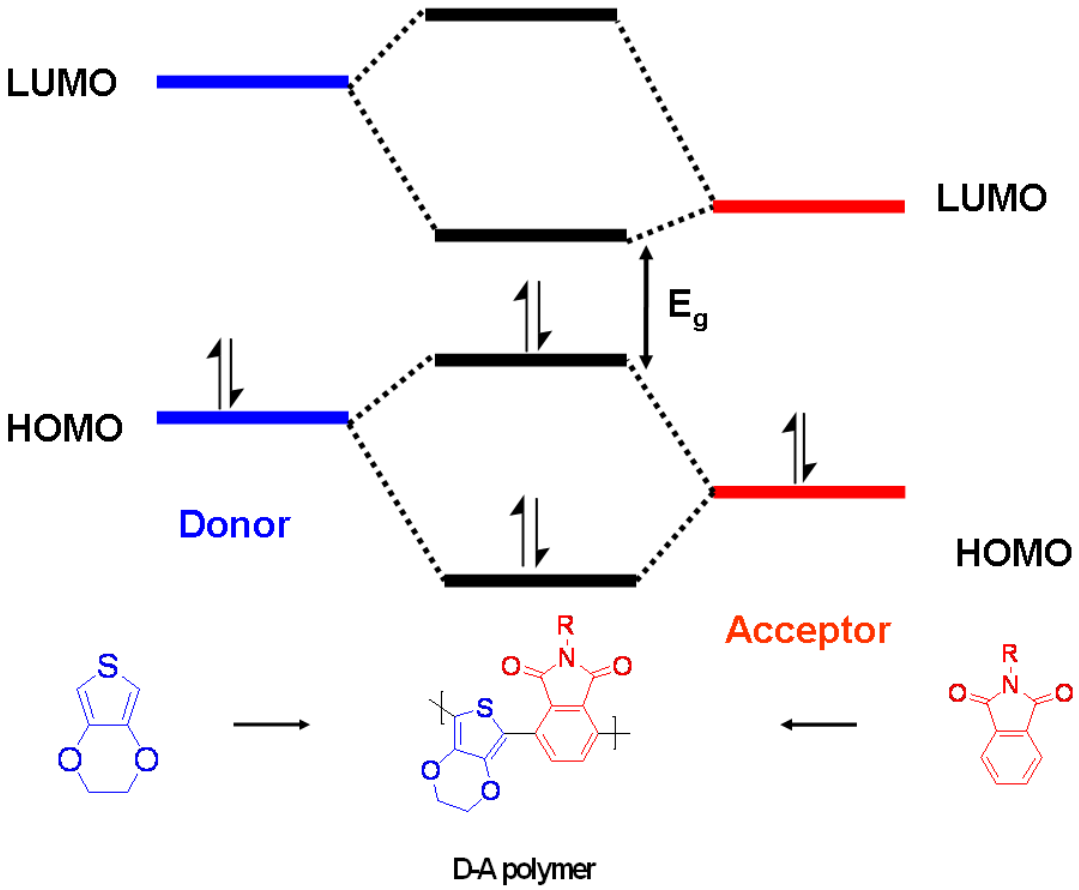

Figure 1.10: Qualitative molecular orbital diagram for donor and acceptor monomers and the resulting D-A polymer after polymerization.

appropriately choosing the relative FMO energy levels of the monomers, the FMO energies of the resulting D-A polymers may also be varied in a rational fashion.

1. 4. 3 Design Strategies Used in This Dissertation

Simple structural modifications can tune the FMO energies of CPs to provide suitable FMO energy levels for ambient stability and small E_g for OPV applications. The following section describes the molecular design strategies used in this dissertation to achieve the appropriate FMO energies and E_g, in addition to solubility and self-assembly, for the conjugated polymers.

1) **Use the D-A approach** to obtain polymers with the appropriate FMO energies and high propensity for favorable self organization.

2) **Use head-to-head bithiophene linkages.** Head-to-head (HH) linkages refers to the relative alkyl chain positions on adjacent thiophene rings as illustrated in figure 1.11.

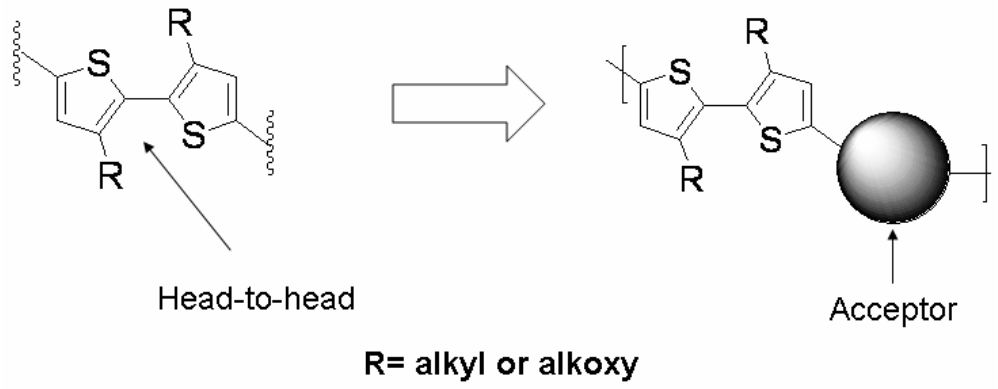

Figure 1.11: HH-linkages in a D-A copolymer.

This motif allows for the regular placement of alkyl chains along the polymer backbone while minimizing steric interaction with adjacent acceptor units, thus allowing the

concomitant highest possible loading of acceptor and solubilizing side chains whilst still allowing backbone coplanarity. It has been shown that HH bithiophene linkages in poly(alkylthiophenes) (PATs) results in twisting of the polymer backbones.[29] However, it has also been shown that the presence of these linkages in D-A polymers does not hinder backbone planarization, likely due to additional driving forces for self organization such as donor acceptor interactions.[30] Furthermore, 3,3'-dialkoxy-2,2'-bithiophene units (3,3'-ROT2) are also used in this dissertation on the donor motif as illustrated in figure 1.11(R= OC_nH_{2n+2}). The presence of alkoxy linkages between the π-system and the alkyl chains will have large effects on both E_g and the FMO energies of the polymers. Additionally, it has been proposed that there are attractive, rather than repulsive intramolecular interactions between the pendant oxygen atoms and adjacent thiophene units.

For example, Reynolds and co-workers collected crystal structures of monomers **A** and **B**, shown in figure 1.12, and found the dihedral angle between the thienyl and phenyl groups became drastically reduced upon alkoxylation of the 2- and 5-positions of the benzene ring.[31, 32] Furthermore it was found the distance between the phenylene oxygen atom and the sulfur atom in the thiophene ring was 2.63 Å, less than the sum of the van der Waals radii of 3.2 Å for the two atoms. After electrochemical polymerization they found the resulting polymer from monomer **A** had both a lower E_g and than polymers from monomer **B** by 0.6 eV. The difference in space filling demands of the large alkoxy side chains in monomer **A** relative to hydrogen in monomer **B** was likely another factor that affected the properties of the polymers in these studies.

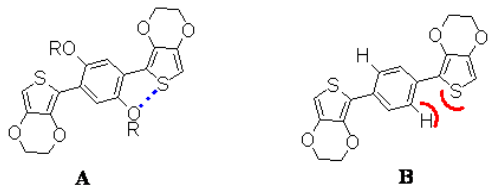

Figure 1.12: Close contacts and restricted dihedral angles between thienyl sulfur and phenylene pendant oxygen atoms.[31,32]

Many other groups have observed the close contacts and restricted dihedral angles in crystal structures of similar small molecules containing adjacent oxygen and thienyl sulfur atoms.[85,34,35] The same general observations of red-shifted absorption maxima and lower ionization potential in alkoxylated thiophene-containing polymers has also been reported.[36,37] Theoretical works on the source of these attractions[38] have not clearly provided an explanation for these interactions in polymers-whether they are purely electrostatic in nature or p-σ^* type bonding. Nonetheless the experimental evidence clearly shows that this motif is effective in lowering the band gap of conjugated polymers. This approach will allow low E_g materials to be synthesized for OPV applications. Unfortunately, as will be discussed in later chapters, a significant decrease in the solubility of polymers containing 3,3'-ROT2 units is generally observed, limiting the choices of acceptor monomers that may be used for polymerization.

3) **Use novel acceptors to acquire the appropriate energy levels for FMOs** as illustrated in figure 1.10. Known D-A polymers in the literature and knowledge of basic organic chemistry allows rational functional group choices to be made to obtain appropriate FMO energies.

4) **Use branched side chains**, when necessary, to increase solubility and decrease polymer HOMO energies by sterically modifying π-conjugation in the backbone and/or solid state organization and interchain coupling.

1. 5 The State of the Art in Materials Performance

Impressive advances in the mobilities of OTFTs and efficiencies of OPVs have been made in the past 5 years. This section focuses solely on p-type semiconductors which are the focus of this dissertation.

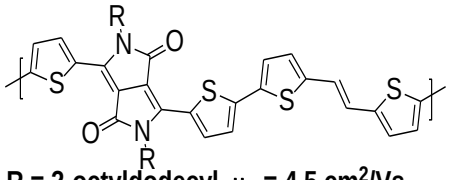

PDVT-8: R = 2-octyldodecyl, μ_h = 4.5 cm^2/Vs
PDVT-10: R = 2-decyltetradecyl, μ_h = 8.2 cm^2/Vs

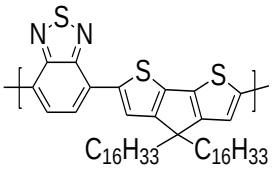

CDT-BTZ-C_{16}, μ_h = 3.3 cm^2/Vs

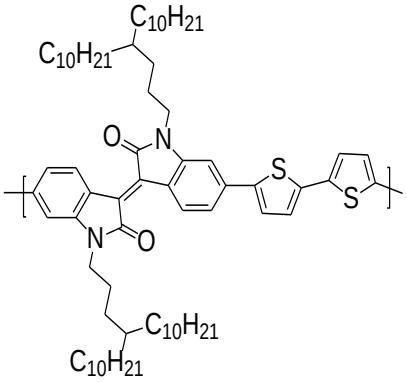

IIDDT-C_3, μ_h = 3.6 cm^2/Vs

Figure 1.13: Polymers with highest OFET hole mobilites reported in the literature, **PDVT**[10] **CDTBTZ-C_{16}**[9] and **IIDDT-C_3**[39]

Figure 1.13 shows the structures of the highest performing semiconducting polymers in OTFTs to date reported in the literature. It is worth noting here that all of the polymers contain a strongly electron-accepting group copolymerized with a weakly electron-

donating group in the backbone. Furthermore, it is worth noting that all of these materials contain branched side chains, and in the case of **CDT-BTZ-C_{16}**, orthogonal side chains with respect to the polymer backbone. The highest mobility polymer reported in the literature to date is **PDVT-10**[10], shown in figure 1.13 with a maximum measured mobility of 8.2 cm^2/Vs. Devices based on small molecules such as 6,13-dichloropentacene[173] and dioctylbenzothienobenzothiophene[174] were reported to have mobilites of 9.0 and 9.1 cm^2/Vs, respectively.

Figure 1.14 shows the highest performing polymers in OPVs to date. The same general motifs found in high performance OTFT materials are also present in OPV materials such as the D-A motif, branched side chains, as well as orthogonal side chains. The highest performing (proprietary) OPV material to date was recently reported by Heliatek. They used vacuum-deposited small molecules rather than solution processed polymers to fabricate OPVs with PCEs of 12%.[80]

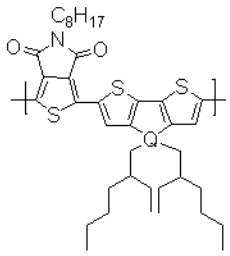

PDTSiTPD: Q = Si, PCE = 7.3%

PDTGeTPD: Q = Ge, PCE = 8.5 %

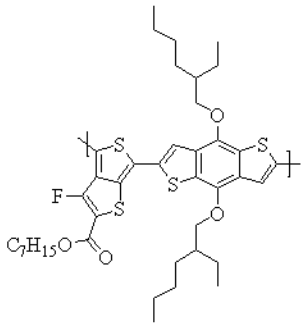

BnDT-TT: PCE = 7.4%

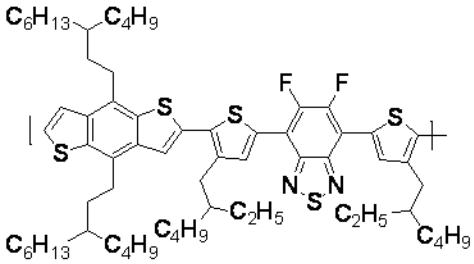

PBnDT-DTffBT: PCE = 7.2%

Figure 1.14: Polymers with highest PCEs reported in the literature, **PDTSiTPD**[40] **PDTGeTPD**[41] **BnDT-TT**[42] **PBnDT-DTffBT.**[43]

1.6 Methods

This section summarizes the methods used for the measurements of the optical properties, FMO energies, and solid state ordering of the final polymers. The polymerization reaction conditions used throughout this dissertation are also presented.

1. 6. 1 Electrochemistry

Molecular orbital energy, as stated in the previous sections, is a very important factor to consider when designing polymers for synthesis. Therefore, it is of interest to easily and accurately estimate the energy required for both the oxidation and reduction of

our polymers. Specifically, we are interested in measuring the ionization potential (IP) for p-type doping and electron affinity (EA) for n-type doping. These may then be related to the HOMO and LUMO energy levels of the polymers, respectively, via Koopmans' theorem.[45] IP, by definition, is the energy required to remove an electron from a gaseous atom or molecule to vacuum. The method best suited to measure IP then, is ultraviolet photoelectron spectroscopy (UPS). This method involves exposing a sample of analyte to ultraviolet light under high vacuum. Electrons are ejected and their kinetic energy varies according to which molecular orbital from which it was ejected.[46] However, this method is costly and time consuming compared to the more commonly employed electrochemical measurements. In a classical cyclic voltammetry experiment, a forward then a reverse linear potential scan are applied to a working electrode that is immersed in a solution containing dissolved analyte and a supporting electrolyte. If oxidation of the analyte (and reduction of the oxidized species) is accessible within the experimental window the average of the oxidation (E_{pc}) and reduction peak (E_{pa}) potentials may be used to approximate the formal potential of the redox couple according to equation 2.[47]

$$E_{1/2} = 1/2(E_{pc} + E_{pa}) = E_o + (RT/nF)\ln(D_R/D_O)^{1/2} \qquad \textbf{eq. 2}$$

The electrochemical oxidation potentials may then be related to vacuum level using an internal standard such as the ferrocene/ferrocenium (Fc/Fc^+) redox couple.[48] However, electrochemical analysis of conjugated polymers involves deposition of a polymer thin film on the working electrode and immersion into a solvent in which the polymer is insoluble. Therefore, the analyte is not dissolved and diffusion of (un)charged analyte to the working electrode does not occur as in the established CV methods. Furthermore,

redox processes for conjugated polymers result in large conformational and energy level reorganization relative to small molecules.[47, 49] Therefore redox processes being studied with conjugated polymers are often non- or quasi-reversible and standard equation 2 is not valid.[49] Indeed large hysteresis and broad peaks are generally observed in CVs of conjugated polymers. Charging of the polymer backbone during the experiment adds further error to the measurement.[49] As a result, the onset of oxidation, rather than peak oxidation is generally used to probe the energies of charge injection in the ground state of conjugated polymers. Although CV is generally used to determine polymer FMO energies in the literature, it came to our attention that this electrochemical technique was not the best suited for measuring the onset of oxidation. Differential Pulse Voltammetry (DPV) may be a superior method for measuring the onset of oxidation potentials for conjugated polymers. The DPV technique provides greater sensitivity than CV due to the fact that the current sampling points allows for the decay of the capacitive current during the experiment, thus producing a more sensitive measurement of the Faradic current.[50, 51] Indeed, it has been reported that DPV produces sharper oxidations allowing for more accurate determinations for the onset of oxidation for conjugated polymers.[52, 53, 54] To test the relative merit of DPV versus CV, a sample of P3HT was used for measurement. The CV E_{HOMO} values for P3HT reported in the literature range from -4.8 eV[55] to -5.2 eV[56] with UPS measurements producing the former value.[75] Figure 1.15 shows the DPV and CV voltammograms of thin-films of P3HT drop cast from toluene. This came after days of repeated measurements, changing variables such as preconditioning the polymer film with incomplete scans, until reliable technique could be established in-house.

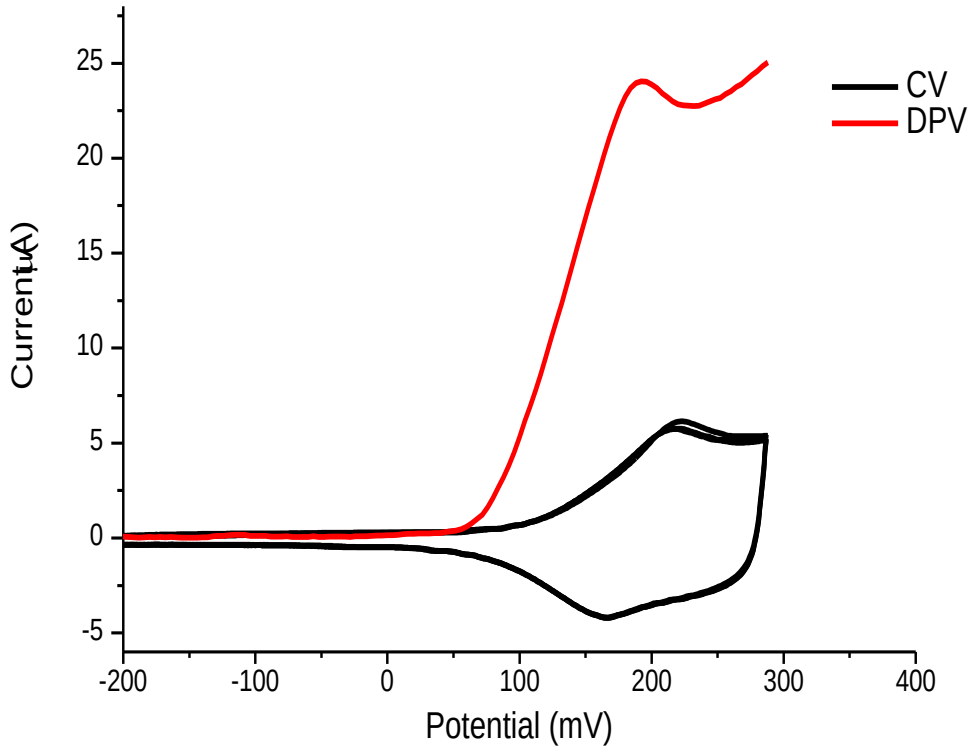

Figure 1.15: DPV versus CV of P3HT calibrated versus Fc/Fc^{+}.

A clear difference between the onsets of oxidation is seen between the two methods. In fact, the difference between the onsets of the two peaks is 40 mV, corresponding to the difference in the upper and lower limits for the P3HT ionization potential reported in the literature. The DPV method gave an E_{HOMO} of -4.8 eV relative to vacuum, in agreement with UPS measurements.[75] Accordingly, DPV was adopted for all electrochemical measurements reported in this dissertation.

1 . 6. 2 Optical Spectroscopy

Optical spectroscopy, in particular UV-Vis spectroscopy, is a useful tool for gaining a preliminary understanding of the molecular order present in polymer solutions and thin-films. The onset of absorption (λ_{onset}) is generally used to estimate the E_g of a

given material as illustrated in figure 1.16. This method must be used with caution as onset of absorption does not necessarily correspond to the formation of free charge

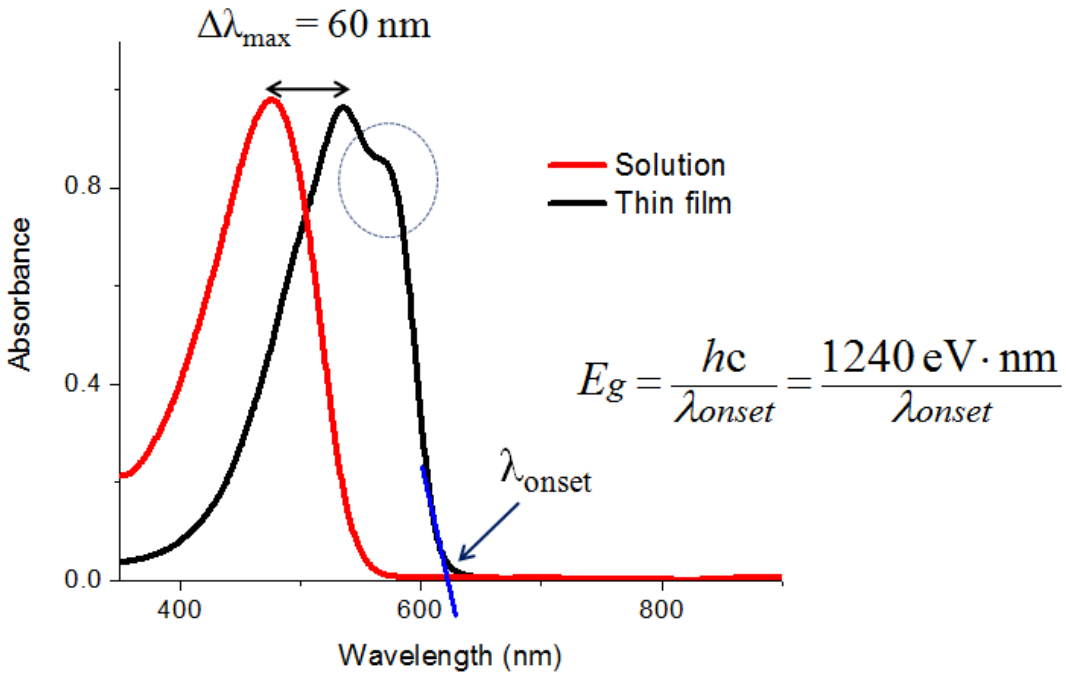

Figure 1.16: Example of a UV-Vis spectrum of a D-A polymer illustrating the estimation of E_g from a polymer thin-film, the $\Delta\lambda_{max}$ between the solution and thin-film spectra and the presence of fine structure (circled region).

carriers, rather a bound electron-hole pair is formed.[49] In many cases the energy gap measured by electrochemical methods such as DPV yields higher values of E_g when compared to the optical energy gaps.[49,81-83] Nonetheless, in many cases reduction peaks are not observed in electrochemical voltammograms of p-type semiconductors (or oxidization peaks for n-type) and this method is commonly used in the literature. The term E_g, used for the remainder of this dissertation refers to the optical energy gap measured by the method described above.

Comparison of the solution and solid state absorption spectra provides information about differences or similarities in two states. For example, similar solution and thin-film absorption profiles implies similarities in the two states, whether the peaks are broad and featureless (dissolved polymers in solution/amorphous polymers in the solid state) or structured (ordered polymers). A large red-shift in the absorption profile (as illustrated as $\Delta\lambda_{max}$ in figure 1.16) upon going from solution to the solid state implies a large difference between the two states. The red-shifts in going from solution to the solid state are thought to be a product to increased backbone planarity, increased conjugation and increased intermolecular orbital overlap relative to polymers dissolved in solution.[84] Finally, fine structure (circled region in figure 1.16) is sometimes observed in thin-films of conjugated polymers.[79] The fine structure is generally attributed to "inter-chain" interactions of π-stacked polymer backbones in the solid state, implying polymers displaying fine structure in their absorption spectra are relatively ordered.

1. 6. 3 2-D Wide Angle x-ray Diffraction (WAXD)

A schematic representation of a WAXD experiment is shown in figure 1.17. In a typical WAXD experiment, a sample of polymer is mechanically forced through a home-built extruder to align the polymer backbones vertically. The polymer fiber is then

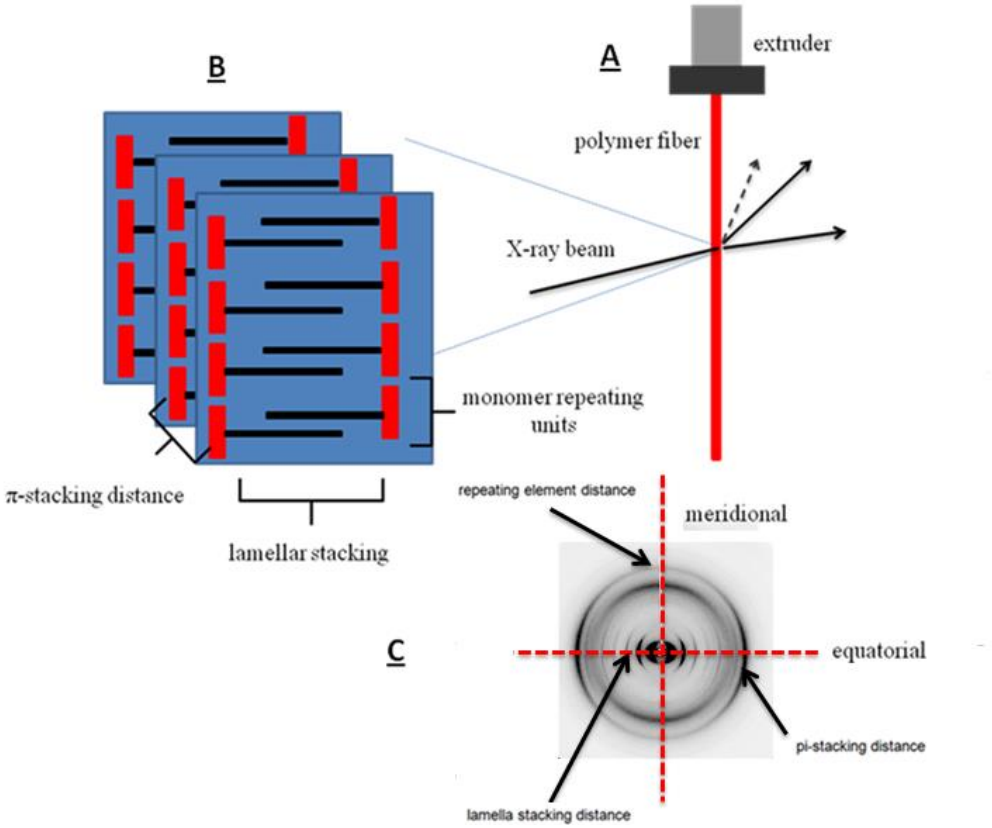

Figure 1.17: Schematic diagram illustrating a WAXD experiment. A) Alignment of polymer fibers through extruder. B) Illustration of lamellar packing of side chains and π-stacking of polymer backbones. The red blocks represent monomer repeating units and the black blocks represent alkyl side chains. C) 2D-WAXD pattern of a mechanically aligned polymer fiber.

mounted perpendicular to the incoming X-ray beam and diffracted X-rays are collected by an area detector. Diffraction maxima along the meridian provide information about the repeating element distance along the polymer backbones. Maxima along the equatorial provide information about the lamellar stacking and π-stacking distances between polymer backbones.

1. 6. 4 General Remarks About Stille Polymerization

The general route used to produce all of the final polymers in this dissertation was Stille coupling.[57] In general, materials for electronics applications must be extremely

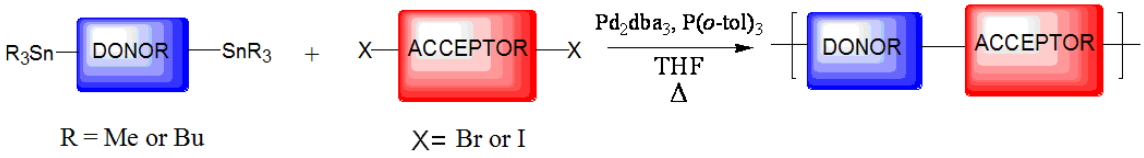

Scheme 1.1: General Stille polymerization for D-A polymers.

pure because impurities can, among other things, act as defects in packing and charge carrier traps.[58] For polymers in particular, a synthetic method is necessary that will give little or no side reaction products that are permanently (covalently) contained within the polymers. Additionally, high molecular weights with reproducible PDIs are desirable. The monomers used for polymerization should also be stable enough to withstand routine purification procedures and have a reasonable shelf life. The mild reaction conditions, high selectivity, functional group compatibility and overall reliability of the Stille coupling makes it the reaction of choice for most research groups synthesizing polymers for OE applications. In addition to the attractive reaction features, the final monomers are generally able to be purified by recrystallization or basic alumina column chromatography and have relatively long shelf lives in air. The published reaction conditions reported vary little between research groups and are briefly discussed below.

Mechanism

The general (simplified) catalytic cycle for the Stille reaction is show in scheme 1.2. Like all other Pd-catalyzed coupling reactions the mechanism is thought to involve at least 3 steps:

Oxidative Addition: In this step of the catalytic cycle, Pd^0, acting as a nucleophile, inserts into the long, weak carbon halogen bond. Pd is oxidized from Pd^0 to Pd^{II}.

Transmetalation: The oxidative addition adduct undergoes a ligand "swap", replacing the halogen atom on palladium with a carbon containing residue. This is generally believed to be the rate determining step of the Stille coupling.[59]

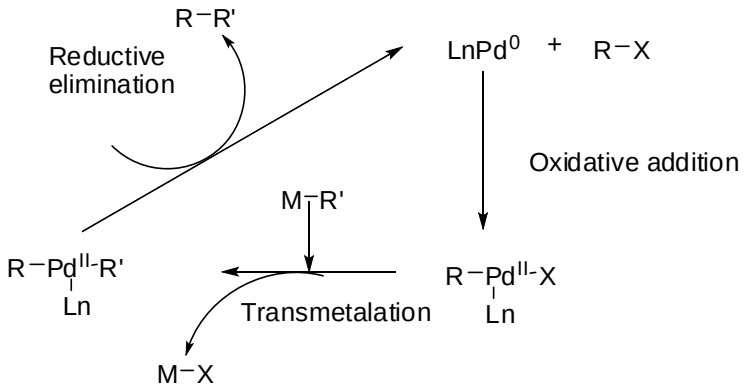

Scheme 1.2: General catalytic cycle for transition metal coupling reactions.

Reductive Elimination: With the two carbon residues placed in a favorable position relative to one another, carbon-carbon bond formation takes place regenerating the Pd^0 catalyst and completing the catalytic cycle.

Palladium Source

The catalyst system employed, Pd_2dba_3, and P(*o*-Tol)$_3$ was specifically chosen based on the following parameters: First and foremost, a relatively air-stable source of palladium(0), Pd_2dba_3 was chosen. The dba ligand is weakly coordinating ligand[60] that may easily be displaced by other more strongly coordinating ligands such as phosphines after simply mixing. Here, the assumption is made that the dba ligand will be inert throughout the reaction and can be removed from polymer products during subsequent Soxhlet extractions. A Pd^0 precatalyst is essential for obtaining high molecular weights

for the polymerization reactions. If a Pd^{II} precatalyst were used, it must be reduced to Pd^{0} by the stannyl reagent before it may enter the catalytic cycle. This has two consequences. First, as predicted by the Carothers equation, the stoichiometric imbalance between the two monomers will result in lower molecular weights.[60,61] Of course this may be partially circumvented by adding excess stannyl monomer to compensate for this side reaction. Secondly, and perhaps more importantly, this side reaction will result in structural defects being incorporated into the conjugated backbones as illustrated in scheme 1.3.

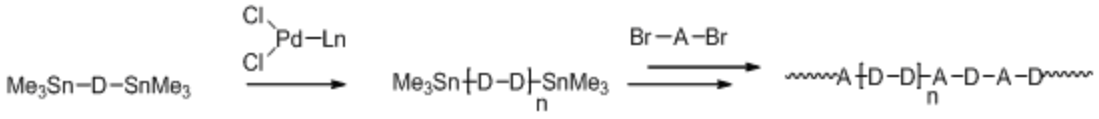

Scheme 1.3: Incorporation of defects in polymer backbones by reduction of a Pd^{II} catalyst.

It is well known that highly regio-regular structures are required for good electrical performance of these materials. The commonly used "McCullough Method"[62] of synthesizing rr-P3HT uses a Ni^{II} precatalyst and is known to generate terminal as well as internal tail to tail (TT) defects in the polymer backbone (scheme 1.4). Indeed, rr-P3HT synthesized using a Ni^{0} catalyst has been found to possess slightly increased crystallinity, lower PDIs and longer conjugation lengths[63] relative to rr-P3HT synthesized using a Ni^{II} catalyst.

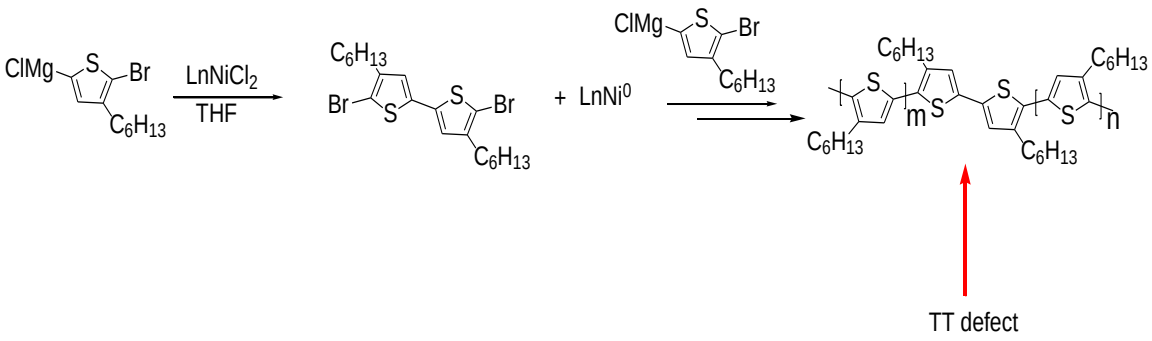

Scheme 1.4: Effects of reductive elimination of Ni(dppp)Cl_2 by the Gringard reagents used for the preparation of rr-P3HT.

Phosphine Ligands

The choice of the ligand to be used on the palladium center when performing small molecule synthesis is generally triphenylphosphine (PPh_3). However, for polycondensations the ligand most commonly reported in the literature, as well as in this dissertation is tri(*o*-tolyl)phosphine, P(*o*-Tol)$_3$. The scrambling of the R groups on the phosphine ligand with oxidative addition products to palladium has been well documented.[64] During their work on poly(*p*-phenylenes) employing the related Suzuki polymerizations, Novak and co-workers found that instead of producing the expected anisotropic rods they isolated branched isotropic materials.[65] They proposed that the unexpected results were due to an exchange reaction between the oxidative addition adduct of the aryl bromides and the phenyl groups in triphenylphosphine (scheme 1.5).

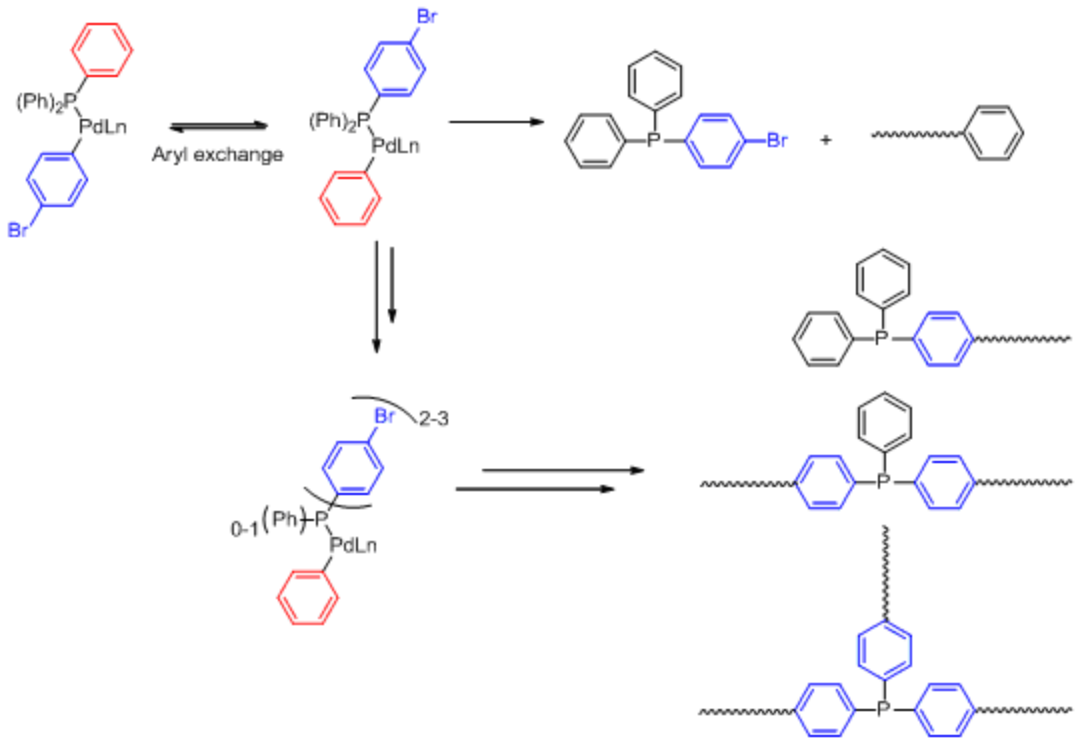

Scheme 1.5: Ligand scrambling in a Pd-catalyzed coupling reaction.[65]

This reaction would terminate growing polymer chains with phenyl end groups as well as incorporate phopshine-containing impurities into the polymer backbone. If all three phenyl groups are exchanged onto the phosphine then a cross linking unit would be incorporated into the backbone. All of these side reactions could seriously affect the electronic performance of materials without being directly detectable by conventional methods.

Further mechanistic studies revealed that an intermediate phosphonium salt could be formed via reductive elimination, followed by oxidation addition into a different phosphorus carbon bond (scheme 1.6).[66]

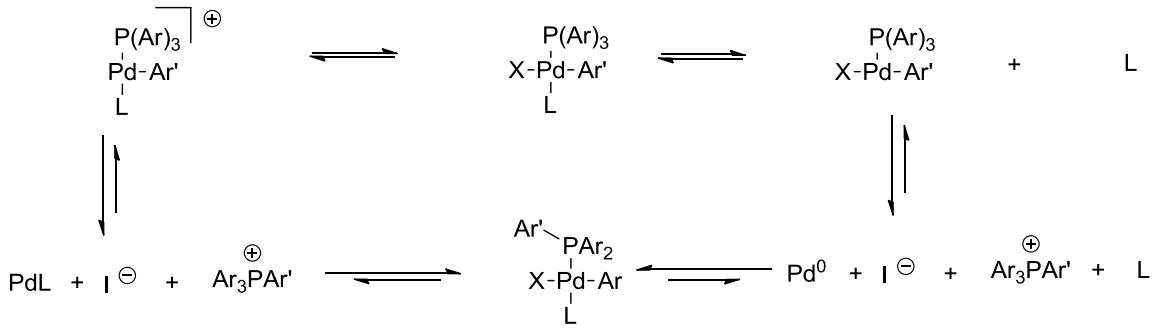

Scheme 1.6: Proposed mechanism for aryl exchange with phosphine ligands.[66]

Optimization of the reaction conditions showed that using a hydrophobic solvent such as dichloromethane (DCM) nearly suppressed all of the ligand exchange reaction.[66] Unfortunately, typical D-A polymers used in our work are rarely soluble in DCM. An alternative solution exploits bulkier ligands on the phosphine. Heck earlier realized that using P(*o*-Tol)$_3$ in vinylic substitution reactions significantly reduced the amount of exchanged products, presumably due to the steric bulk around the phosphine center, slowing the rate of reductive elimination.[67] Of the ligands tested in their polymerization reactions, P(*o*-Tol)$_3$ in THF as solvent gave considerably smaller amounts of the exchanged product.

Coupling partners

The first step of the catalytic process, oxidative addition, is essentially nucleophilic insertion of the palladium center to the carbon halogen bond. In this context, the aryl halide may be considered an electrophile and the rate of oxidative addition will follow the bond disassociation energies of the carbon halogen bond resulting in the trend Cl << Br < I. The second step of the catalytic process, transmetalation (generally regarded as the rate limiting step),[59] involves nucleophilic attack of the organometallic coupling partner on the palladium center, displacing the

halogen. Thus, the organometallic reagent may be considered a nucleophile in these reactions. Following this, it is desirable to make the aryl halide as electron deficient as possible and the organometallic as electron rich as possible to maximize the rates for each of these steps. Since we are focused on D-A polymers, the acceptor fragment always contains the halide and the donor fragment is always organometallic as illustrated in scheme 1.1.

1. 7 Summary of the Remaining Chapters

The goal of the work presented in the remainder of this dissertation is to rationally design, synthesize and characterize novel D-A polymers for use in OTFT and OPV devices. Chapter 2 describes the synthesis and characterization of novel cyanothiophene- and (tere)phthalonitrile-based acceptor units and D-A polymers with the goal of enhancing the self organization properties and optimization of the FMO energies for the resulting polymers. Branched alkyl side chains on 3,3'-ROT2 units are explored in Chapter 3 as a tool to tune the solubility and FMO energies of phthalimide-based D-A polymers. Chapter 4 describes an example of a functional group interconversion (FGI) strategy, from imide-based phthalimide acceptor units to diketone-based indanedione motifs to tune FMO energies and the solubilities for D-A polymers. Finally, some of the problems associated with the currently used donor motifs is addressed in Chapter 5 and an effort to overcome those problems is presented with the introduction of 3,3'-dialkynylbithiophene donor motifs for D-A polymers.

Chapter Two: Cyanoarene-Based Donor-Acceptor Copolymers

2.1 Introduction

The organic chemist has a large number of functional groups to choose from when considering electron withdrawing groups for D-A polymers. An ideal candidate would be a powerful electron withdrawing group that does not impede close intermolecular packing of the polymer backbones. Additionally the group should not induce intramolecular twisting between adjacent monomer units, which could disrupt conjugation, and possess reasonable chemical stability. One of the obvious functional groups that falls into this category is the nitrile group. The strong electron-withdrawing capability (Hammett parameter $\sigma_{para} \sim 0.6$)[110] as well as its small size make it ideally suited for incorporation into D-A polymers to be used in OE applications.

Indeed, much work with respect to OE has already been performed on materials containing this functional group. According to DFT calculations, cyanation lowers both HOMO and LUMO energy levels,[85] decreases internal reorganization energy and encourages π-stacking,[86] as well as enhances self organization by CN···H and RCN···NCR interactions[87] in acenes and oligothiophenes. Calculations performed on a series of cyanated pentacene derivates suggested that this functional group provides a 3-in-1 advantage relative to other popular electron withdrawing groups such as fluorine.[86] The calculated EA and IP for cyano-substituted pentacenes both became larger relative to unsubstituted pentacene. The reorganization energies for both hole and electron transfer also became smaller, the difference in the reorganization energy (relative to unsubstituted pentacene) being larger for electron transfer. It was also found that larger intermolecular

electronic couplings were present in dimers of cyanated pentacenes relative to unsubstituted pentacene.[86] The findings from this theoretical study suggested that cyanation could lead to higher charge carrier mobilites and increased air stability for pentacene chromophores.

Experimentally, cyanation of small molecules has proven to be an efficient strategy for tuning orbital energies and switching inherently p-type materials into n-type materials. Di-cyanation of naphthalene bisimide (NBI) and perylene bisimide (PBI) cores was found to be an effective method to tune orbital energetics (figure 2.1).

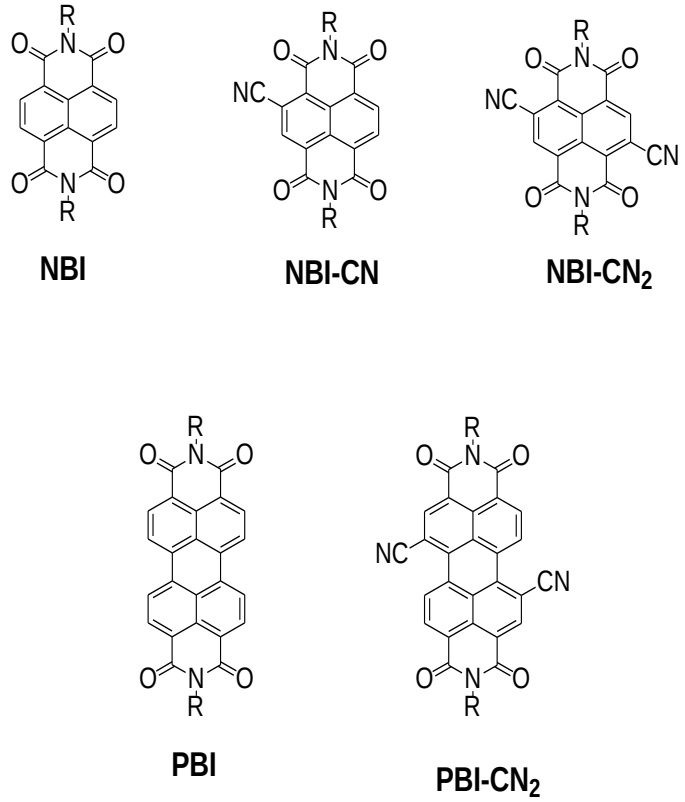

Figure 2.1: Unsubstituted and core cyanated NBI (top) and PBI (bottom), R = n-octyl.

Both the E_{HOMO} and E_{LUMO} were decreased by approximately 0.7 eV and 0.4 eV for NBI and PBI respectively, while the energy gaps remained essentially constant.[69] This, in

addition to fluoroalkylation of the N-imide positions produced active materials for air stable n-type devices with electron mobilites of 0.24 and 0.11 cm^2/V s in air for PDI and NDI respectively.[69]

Similar decreases in FMO energies were observed experimentally with cyanated trialkylsilylethynyl pentacene derivates (figure 2.2); the number of nitrile groups added to the aromatic core lowered both E_{HOMO} and E_{LUMO} without having a significant impact on the E_g.[88,90]

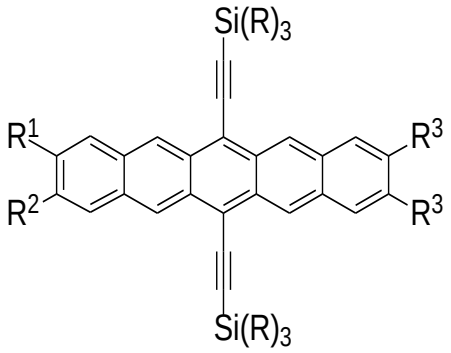

R*	R1	R2	R3	E_{HOMO} (eV)	E_{LLUMO} (eV)
Isopropyl	H	H	H	-5.16	-3.35
Cyclopentyl	CN	H	H	-5.31	-3.50
Cyclopentyl	CN	CN	H	-5.47	-3.64
Isopropyl	CN	CN	CN	-5.75	-3.90

Figure 2.2: Cyanated trialkylsilylethynyl pentacene derivatives and FMO energies. *The authors note that varying the "R" groups on silicon does not affect the FMO energies.[89]

A series of mono-, di- and tetracyano derivatives were synthesized and the FMO energy levels were found to decrease by ~ 0.15 eV per pendant cyano group while the energy

gap remained constant.[88,89] Electron transport in these materials was observed and they were used as electron acceptors with P3HT donors in bulk heterojunction OPV's.[89]

Fewer examples of nitrile-functionalized conjugated polymers have been reported in the literature. The well studied system MEH-CN-PPV, containing cyanovinylene linkages has a lower E_{HOMO} relative to its unsubstituted parent MEH-PPV by ~ 0.5 eV, without a significant difference in E_g (figure 2.3).[91] This material was recently used in place of PCBM in a solution processed all polymer OPV yielding a 2.0% PCE, which is among the highest reported for an all-polymer solar cell.[92] However, cyanovinylene moieties are known to be relatively unstable and easily photooxidized, [107] decreasing their usefulness for OPV applications. A related material to MEH-CN-PPV, DOCN-PPV,

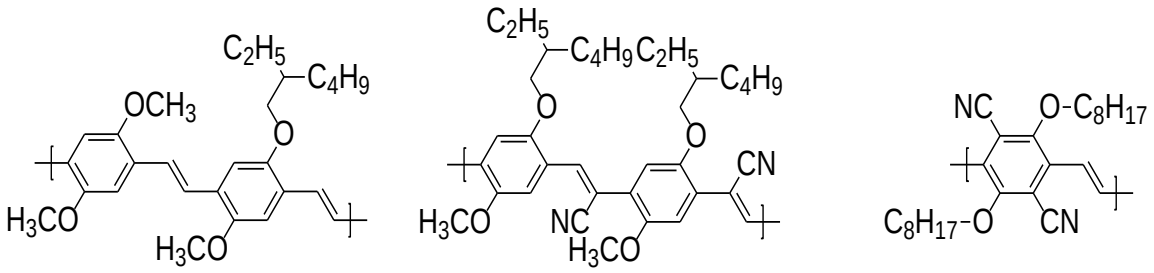

MEH-PPV **MEH-CN-PPV** **DOCN-PPV**

Figure 2.3: Cyanovinylene and cyanobenzene MEH-PPV derivatives.

where the cyano groups are transferred from the vinylene linkage of parent MEH-CN-PPV to the phenylene core is known and has been used as an acceptor in all-polymer OPV cells with an efficiency of 1%.[93]

Heeger et al. synthesized insoluble films of poly(3,4-dicyanothiophene) from vacuum pyrrolysis of 2,5-iodo-3,4-dicyanothiophene.[94] They estimated a very deep E_{HOMO} of -6.3 eV and E_{LUMO} of -3.6 eV for this material. The absorption maximum for

the given polymer was only 366 nm (blue-shifted relative to polythiophene) suggesting that the backbone of this system is highly twisted, which in turn would affect film morphology and electron transport. Additionally, this material was highly insoluble, taking away all of the attractive advantages of OE. Nonetheless this material was used

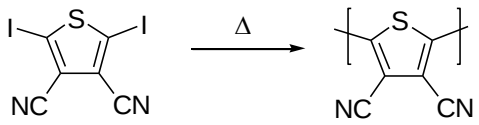

Figure 2.4: Poly(3,4-dicyanothiophene) synthesized by Heeger and coworkers.[94]

to fabricate rectifying heterojunction bilayer devices with MEH-PPV as the donor. The *in device* FMO energies for poly(3,4-dicyanothiophene) were estimated to be -6.7 and -3.6 eV for the HOMO and LUMO respectively. Further characterization was lacking due to insolubility.

Janssen and coworkers carried out a systematic study on the substitution patterns of regio-regular head-to-tail poly(3-dodecylthiophene) (**PDDT**) derivates.[95] All of the materials (shown in figure 2.5) were prepared using the McCullough method[111] producing a low molecular weight nitrile containing polymer with $M_n \sim 2{,}875$ g/mol. Four polymers were synthesized to compare to the parent **PDDT**; a dodecyl side chain in the repeat unit was replaced with a hydrogen (**PTDDT**), phenyl (**PPhDDT**), and a cyano group (**PCNDDT**). Optical measurements revealed that the absorption profiles were nearly identical for **PDDT**, **PTDDT** and **PCNDDT** with almost no variation in the E_g for all of the polymers. Furthermore, they found a large decrease in the HOMO energy for **PCNDDT** relative to **PDDT** of about 0.5 eV after cyano substitution (LUMO energy not estimated). Comparing the hydrogen (**PTDDT**) and cyano (**PCNDDT**) substituted

polymers, a decrease of 0.4 eV was estimated in the LUMO energy, again with essentially no effect on the energy gap. This study showed that incorporation of the

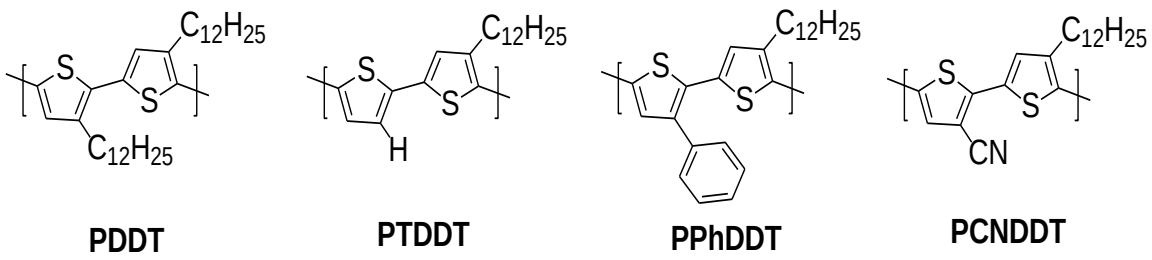

Figure 2.5: Janssen and coworkers P3DDT derivatives.[95]

nitrile functional group into the poly(alkylthiophene) backbone lowered the E_{HOMO} of the parent polythiophene, thus increasing its ambient stability and theoretically increasing V_{oc} for solar cell applications. Furthermore, the optical characteristics of the materials were not greatly affected by cyano substitution.

The purpose of the work reported in this chapter was to synthesize and carry out preliminary measurements to elucidate structure-property relationships of a series of cyanoarene based D-A polymers. Emphasis was placed on two different donors in this project, a weakly electron donating 3,3'-didodecyl-2,2-bithiophene (DBT) unit, and a strongly electron donating 3,3'-dibutyloctyloxy-2,2'-bithiophene (BOBT) unit. Additionally, a cyclopentadithiophene (CPDT) unit was included in one example for comparison of the effects of a covalently fused CPDT bithiophene donor, versus non-fused DBT and BOBT donors. A series of different cyanated-thiophene and (tere)phthalonitrile based acceptors were used for copolymerization. The number and placement of nitrile groups on the aromatic rings, as well as the identity of the rings they

are attached to were varied to study the effects on the optical and electrochemical properties of the resulting D-A copolymers.

2. 2 Synthesis

Cyanothiophene monomers were prepared from the commercial bromothiophenes using CuCN under standard Rosenmund-von Braun (RvB) conditions, shown in scheme 2.1.[96] Bromination of 3,4-dicyanothiophene was achieved with NBS in a mixture of trifluoroacetic acid and sulfuric acid at room temperature. The harsh halogenation

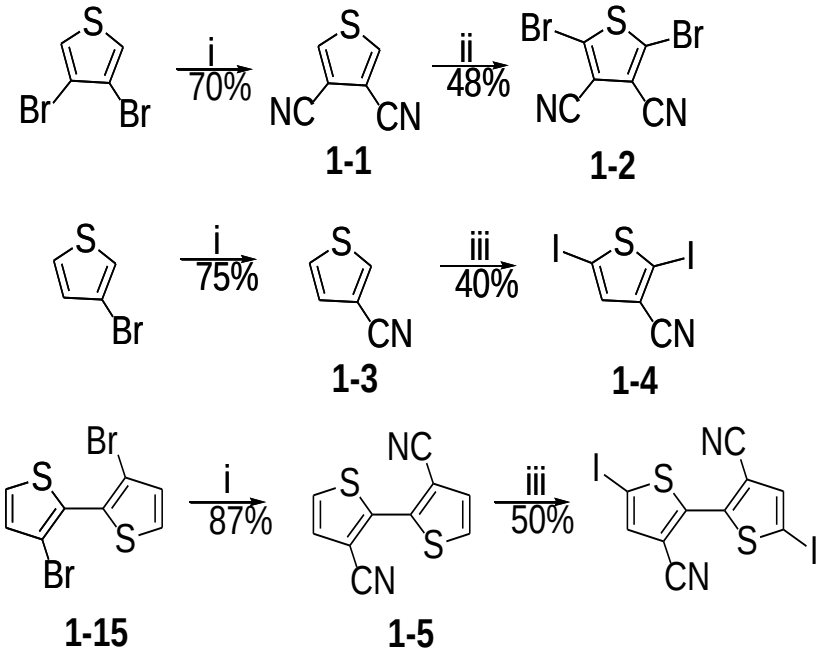

Scheme 2.1: Synthesis of cyanothiophene acceptor monomers. Reagents and conditions: i: a). CuCN, DMF, reflux; b). $FeCl_3$ aq. HCl; ii: TFA, H_2SO_4, NBS, r.t. 5 h; iii: a). LiTMP, THF, -78 °C 1 h; b). I_2, THF, - 78 °C → rt 3 h;

conditions produced inseparable mixtures of di- and tri-brominated products when applied to **1-3** and **1-5**. All other electrophilic substitution reaction conditions failed to produce the desired products. Ortho-lithiation using lithium tetramethylpiperidine

(LiTMP) as base followed by quenching with I_2 produced the final halogenated thiophene-based acceptor monomers **1-4** and **1-6** in acceptable yield.

(Tere)phthalonitrile based acceptors were obtained by "dehydration" of the corresponding diamides **1-8** and **1-10** using either P_2O_5 or $SOCl_2$ as shown in scheme 2.2.[97] In the case of 2,5-dibromoterephthalonitrile, **1-9**, the starting material was 2,5-dibromo-*p*-xylene; no halogenation steps were required to secure the final monomer. 3,6-diiodophthalonitrile[98] was obtained by ammonolysis of phthalimide, followed by dehydration of the diamide. Ortho-lithiation and iodination of phthalonitrile was then carried out as described for the thiophene-based monomers.

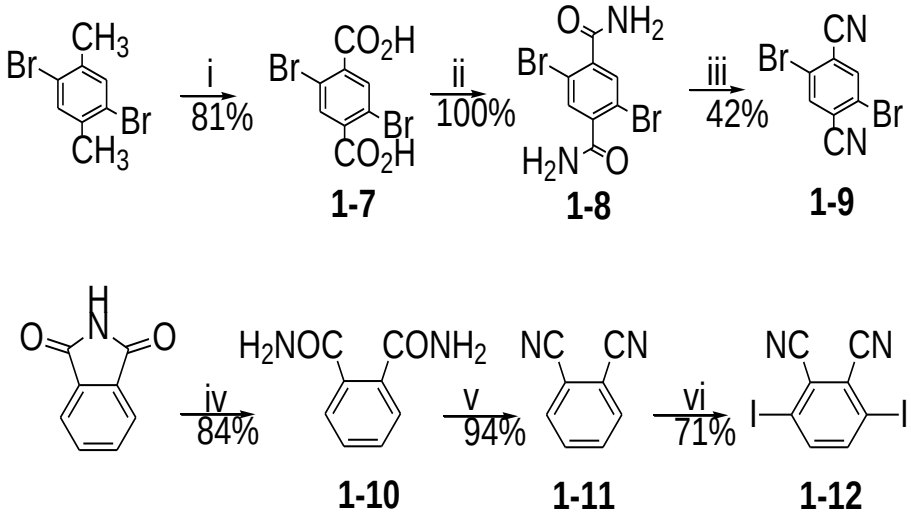

Scheme 2.2: Synthesis of (tere)phthalonitrile acceptor monomers i: a). $KMnO_4$, pyridine, H_2O reflux; b). $KMnO_4$, KOH, H_2O, reflux; c). aq HCl; ii: a). ClCOCOCl, DMF (cat.), PhH; b). NH_3 (aq.); iii: P_2O_5, 170 °C, neat; iv: NH_3 (aq), EtOH, reflux, overnight; v: $SOCl_2$, DMF, 70 °C; vi: a) LiTMP, THF, -78 °C, b) I_2, THF, -78 °C to rt.

Donor bithiophene monomers were prepared according to published procedures (scheme 2.3).[99]

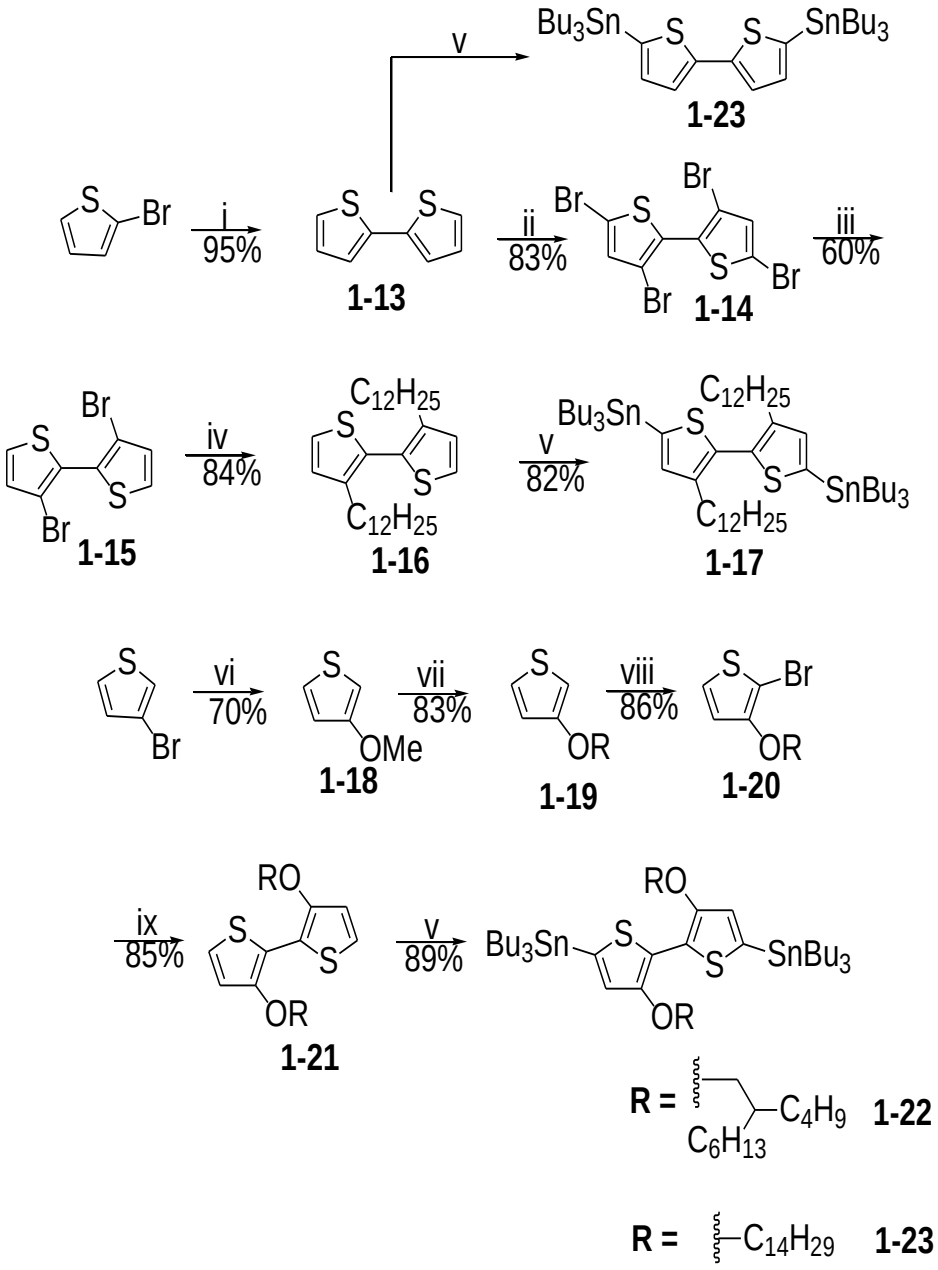

Scheme 2.3: Synthesis of bithiophene donor monomers. Reagents and conditions; i: a). Mg, Et_2O reflux, 1 h; b). Ni(dppp)Cl_2, reflux, overnight; ii: a). Br_2, $CHCl_3$, AcOH, 0 °C → r.t, reflux 24 h; b). KOH, reflux, 5 h; iii: Zn, AcOH, HCl (aq), reflux, 5 h; iv: $C_{12}H_{25}MgBr$, Ni(dppp)Cl_2, Et_2O, 0 °C → reflux, 3 h; v: a). BuLi, THF, -78 °C 2 h, b). Bu_3SnCl, - 78 °C → r.t.; vi: MeONa, MeOH, CuI, reflux ;vii: ROH, PTSA (cat.), PhMe, 110 °C; viii: NBS, DMF, 0 °C; ix: Ni(COD)$_2$, COD, 2,2'-dipyridyl, DMF, PhMe, 80 °C.

Polymerization

Stille polymerizations were carried out under standard conditions as described in Chapter One with THF as solvent giving acceptable molecular weights for the polymers. All of the polymers have relative number-average molecular weights (GPC vs polystyrene) of ~ 15-20 kDa with the exception of **P6b** (table 2.1).

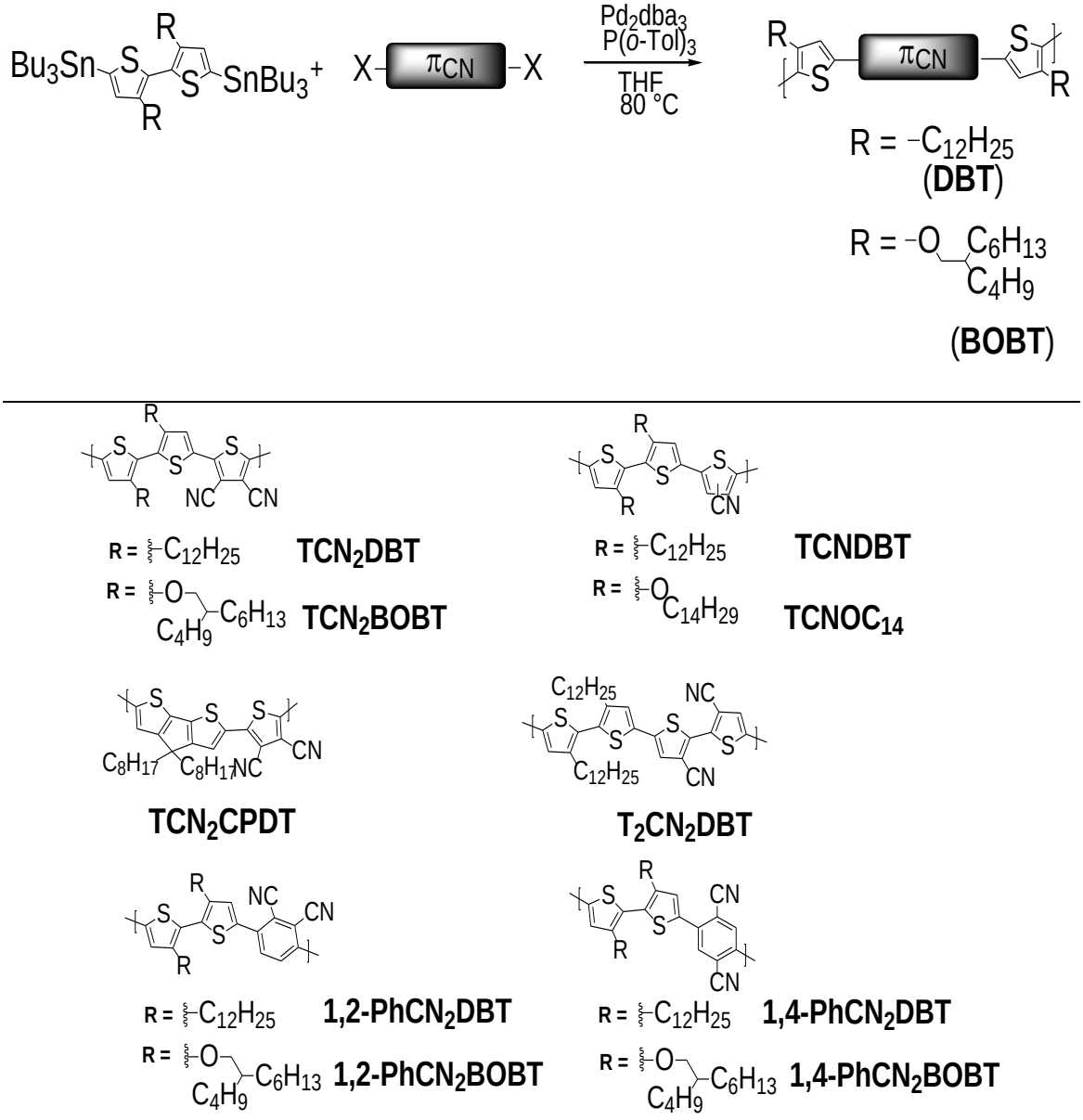

Scheme 2.4. Synthesis and structures of the final polymers

Table 2.1. Yields, molecular weights and (opto)electronic properties of the polymers.

	Yield (%)	Mn (kDa) [PDI]	λ_{max} soln[a]/film[b] (nm)	E_{HOMO} (eV)[c]	E_{LUMO}[d] (eV)	E_g (eV)[e]
TCN_2DBT	89	17.4 [1.47]	465/566	5.70 ± 0.04	4.00	1.70
TCN_2BOBT	15[g]	N/A[f]	730/745	5.14± 0.04	3.82	1.32
TCNDBT	89	22.8 [1.72]	433/452	5.70 ± 0.05	3.64	2.06
$TCNOC_{14}$	89	N/A[f]	709/650, 712	4.95 ± 0.006	3.45	1.50
TCN_2CPDT	90	N/A[f]	621/645	5.33 ± 0.04	3.78	1.55
T_2CN_2DBT	49[h]	N/A[f]	463/500	5.75 ± 0.05	3.79	1.96
1,2-$PhCN_2DBT$	92	22.5 [1.45]	397/419	6.02 ± 0.02	3.88	2.14
1,2-$PhCN_2BOBT$	91	14.8 [2.30]	567/609	5.32 ± 0.02	3.67	1.65
1,4-$PhCN_2DBT$	92	21.2 [1.89]	423/463	6.04 ± 0.02	3.83	2.21
1,4-$PhCN_2BOBT$	61	176 [3.16]	660/664	5.33 ± 0.02	3.66	1.67

[a] 10^{-5} M in chloroform, chlorobenzene used for **P4**. [b] Spin cast from 1 mg/mL toluene solutions and thermally annealed. [c] Measured by DPV and relative to Fc/Fc^+. [d]Estimated using $E_{LUMO} = E_{HOMO} - E_g$. [e]Estimated from the low-energy absorption edge of annealed thin-films using $E = 1240\ eV \cdot nm/\lambda$. [f]Insoluble in THF. [g]$CHCl_3$ fraction, insoluble material remained in Soxhlet thimble. [h]Collected using chlorobenzene as final Soxhlet solvent.

2.3 Optical Properties

Thin-film and solution absorption spectra for all of the polymers are shown in figure 2.6 and relevant values are listed in table 2.1. Large relative red-shifts are observed for the 3,3'-ROT2-based polymers (BOBT) versus the alkylated polymers (DBT) and are in agreement with observations reported in the literature[99,100] and as described in Chapter One. As expected, the polymers containing the smaller thiophene-based acceptor units (**TCN_2** and **TCN)** have a red-shifted λ_{max} relative to the analogous polymers containing (tere)phthalonitrile acceptor units (**1,2-** and **1,4-$PhCN_2$**) .

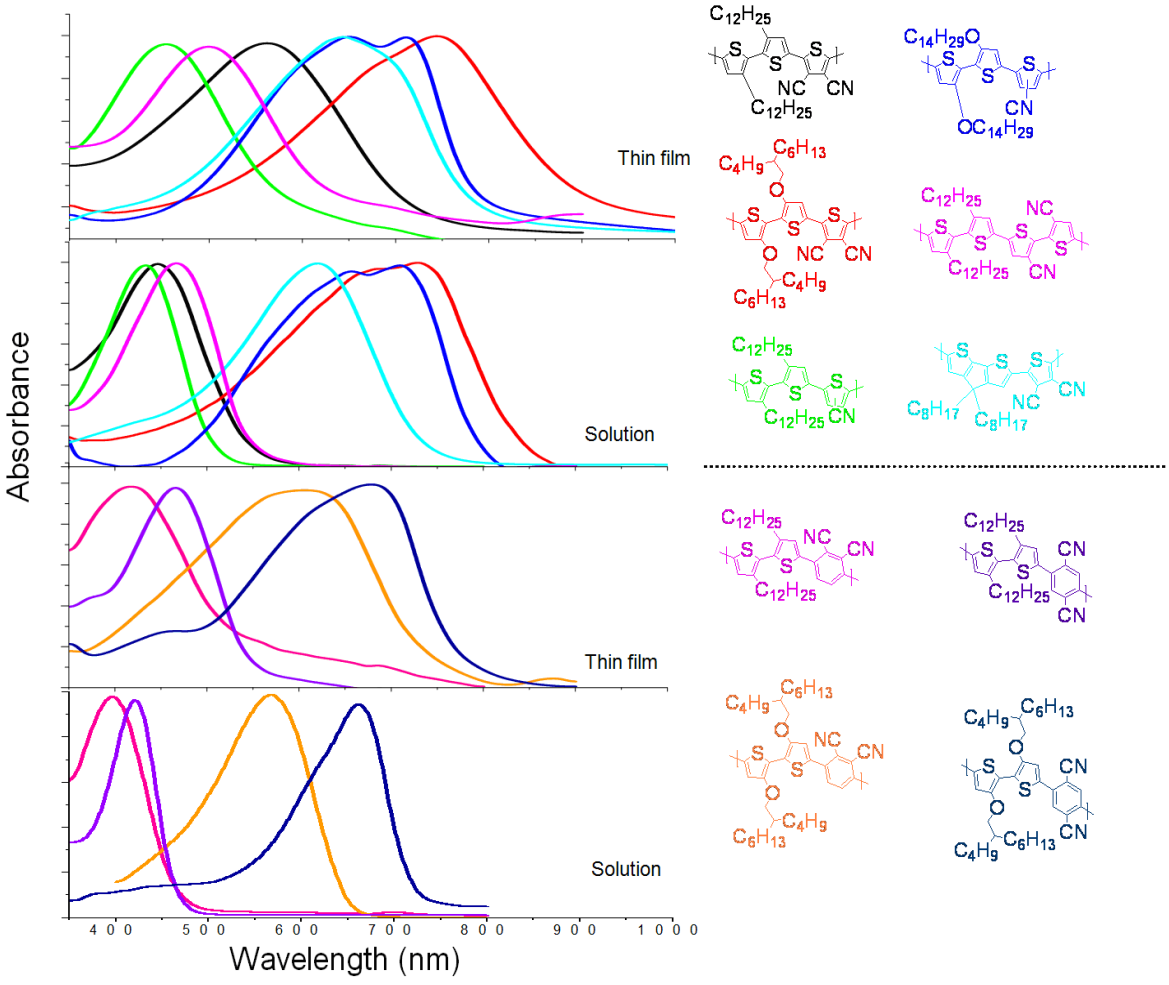

Figure 2.6. Normalized thin-film and solution absorption spectra of thiophene-based (top two) and benzene-based (bottom two) polymers.

Both the smaller size and the lower resonance energy of the thiophene ring relative to the benzene ring probably contribute to better orbital overlap and decreased bond length alternation (BLA) for the **TCN_2** series relative to the **1,2- and 1,4-$PhCN_2$** series. Removing one cyano group from the thiophene ring (**TCN_2** vs. **TCN** series**)** does not greatly affect the solution absorption profiles, blue-shifts of ~ 30 nm are observed for the **TCN**-based polymer relative to **TCN_2.** However the change in λ_{max} ($\Delta\lambda_{max}$) upon going from solution to the solid state is much smaller for the **TCN**-based polymers. This is possibly a result of its regio-irregular structure, leading to a more amorphous-like structure in the solid state. Similar observations in absorption spectra have been made on amorphous regio-irregular P3HT and semi-crystalline regio-regular P3HT.[101] Another possibility is weaker D-A interactions in the solid state for **TCNDBT** relative to **TCN_2DBT**. A much smaller difference in λ_{max} is observed for the **TCN_2** and **TCN** polymers carrying alkoxy-side chains, **TCN_2BOBT** and **$TCNOC_{14}$.** This is likely due to both the planarization effects of the 3,3'-ROT2 units as well as the branched chains on the BOPT units versus the straight chains on **$TCNOC_{14}$.** Branched side chains, as will be discussed in detail in Chapter Three, result in both a larger intramolecular dihedral angle between adjacent monomer units as well as larger intermolecular π-stacking distances (interchain coupling). This results in blue-shifts in the absorption profiles for polymers carrying branched alkyl side chains relative to straight alkyl side chains leading to a smaller $\Delta\lambda_{max}$ for **TCN_2BOBT** versus **$TCNOC_{14}$**. "Spreading" the two cyano-groups out over two thiophene rings in a HH fashion (**T_2CN_2DBT**) produces an intermediate shift between **TCN_2DBT** and **TCNDBT.** The low solubility of this material containing DBT donor units prohibited the synthesis of BOBT containing polymers with this acceptor as

described in Chapter One. The cyclopentadithiophene containing polymer, **TCN$_2$CPDT**, containing a fused donor unit, has λ_{max} intermediate between the **TCN$_2$DBT**and **TCN$_2$BOBT** polymers containing non-fused donors. This is likely due to the covalently bridged backbone, reinforcing co-planarity (red-shift) relative to DBT and the weaker electron donating effect of the alkyl chains on the CPDT unit (blue-shift) relative to BOBT.

The differences of *ortho* versus *meta* dicyano-substitution patterns of the **1,2-PhCN$_2$** and **1,4-PhCN$_2$** polymers yields non-negligible effects on the absorption profiles. However, the large difference in molecular weights (> 150 kDa) and solubility may explain the shifts observed based on solution aggregation which further transfers into the solid state.[102] The effect on the E_g of the polymers follows the same trend as discussed above for λ_{max}; the cyanothiophene-acceptor based polymers have a smaller E_g than the (tere)phthalonitrile based acceptor polymers for both DBT and BOBT donors.

Interestingly, **TCN$_2$DBT** showed a casting solvent dependence on the thin-film absorption profile (figure 2.7). Spin-coating films from chloroform or toluene solutions produced films with only small shifts in λ_{max} relative to solution as observed for many amorphous polymers containing HH bithiophene linkages.[105] Indeed, the other DBT polymers in these experiments only showed small shifts on going from solution to the solid state regardless of casting solvent. However, using THF as casting solvent led to a large relative red-shift of ~ 100 nm in the absorption profiles of the thin-films. Thermally annealing the thin-films cast from $CHCl_3$ and toluene produced absorption profiles nearly identical to that of the pristine film from THF. Furthermore, solvent vapor annealing (which will be discussed in greater detail in Chapter Three) of the $CHCl_3$ and toluene thin

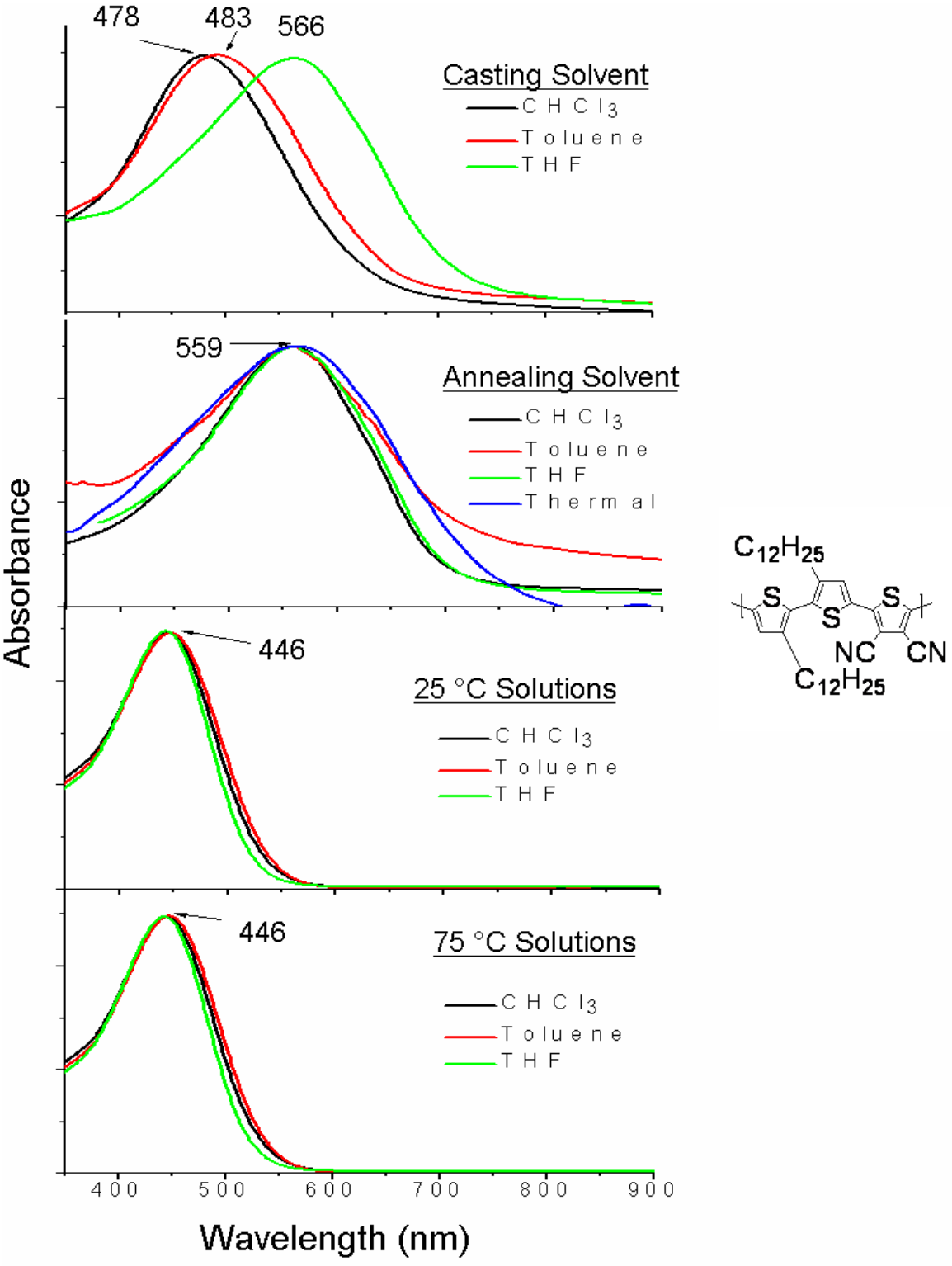

Figure 2.7. Normalized thin-film absorption spectra of **TCN$_2$DBT** before and after (top two spectra) solvent annealing. Solution absorption spectra in the casting solvents (10^{-5} M) at room temperature and 70 °C (bottom two spectra).

films with the respective casting solvents also caused a shift in λ_{max} similar to that of thermal annealing (figure 2.7). The absorption spectra of the films after solvent annealing all converged to yield very similar absorption profiles. Solution absorption measurements were made in all three solvents at 25 °C and at 70 °C (figure 2.7) to investigate the difference in solvent "quality". Polymer aggregates formed in "marginal" solvents (solvents in which the polymers are marginally soluble but form aggregates) tend to display structured and red-shifted absorption profiles relative to a molecularly dissolved solution. Elevated temperatures generally are required to better solvate the polymer in marginal solvents which may be measured by UV-Vis as relative blue-shifts and loss of fine structure.[112] No difference was observed in the two sets of spectra. Indeed, the spectra collected as THF solutions were slightly blue-shifted relative to the other solvents both at room temperature and at elevated temperature, suggesting that the polymer is better solvated in THF than the other solvents.

The origin of the differences are not yet clear but similar observations in thin films of 3[2(*S*2-methylbutoxy)ethyl]-polythiophene (PMBET) spin-coated from THF/methanol solutions have been made.[106] Addition of increasing concentrations of methanol (bad solvent) to the casting solution (THF) caused the absorption maximum of the thin-films to red-shift from 546 nm to 628 nm. The authors attributed this red-shift to solution aggregation as poor solvent is added, introducing rigid rod character to the polymers in which is then transferred to the films during spin-coating. However, in the case of **TCN$_2$DBT** different degrees of aggregation for the different solvents were not detected by the variable-temperature solution UV-vis spectra (at the concentrations measured) and no color difference was discernable by eye of the casting solutions. It is

also known that P3HT forms more highly ordered films when cast from high boiling solvents such as 1,2,4-trichlorobenzene, due to the slower evaporation rate of the solvent.[108] However, THF has a significantly lower boiling point (66 °C) than toluene (110 °C). Bao et al. observed that P3HT films *drop cast* from lower boiling point solvents THF and chloroform had greater crystallinity than films from toluene as well as different morphologies.[109] The absorption profile dependence of **TCN_2DBT** is likely due to a subtle interplay between solvent properties (evaporation rate and polymer solubility) and differing polymer morphologies produced from the various solvents. Absorption of solvents by the polymer films (partially dissolving the polymer) during the solvent vapor annealing process, followed by slow evaporation would allow the materials to reorganize to (average) lower energy states from kinetically trapped states formed during spin-coating and possibly explain the convergence of the absorption profiles.

2. 4 Electrochemistry

The FMO energy levels of the polymers were estimated from thin, drop-cast films using DPV and are listed in table 2.1. The E_{HOMO} of the DBT-based copolymers with cyanothiophene- and cyano-bithiophene acceptors are constant at ~ 5.7 eV, regardless of the number of nitrile groups and thiophene rings per repeat unit (**TCN_2DBT, TCNDBT** and **T_2CN_2DBT**). The same constancy is observed for the phthalonitrile isomers **1,2-$PhCN_2DBT$** and **1,4-$PhCN_2DBT$** with E_{HOMO} at ~ 6.0 eV for each polymer. The E_{LUMO} of these polymers were, however, dependant on the number of nitrile groups. The E_{LUMO} was raised from -4.00 eV in **TCN_2DBT** with two nitrile groups to -3.64 eV in **TCNDBT** containing only a single nitrile group. The same difference in E_{LUMO} of ~ 0.4 eV was observed for the dicyano- and mono-cyanothiophene polymers **TCN_2BOBT**and

$TCNOC_{14}$ with 3,3'-ROT2 donors. An intermediate effect on the E_{LUMO} was observed with **T_2CN_2DBT**. "Spreading" the two nitrile groups out over a bithiophene unit, relative to thiophene in **TCN_2DBT,** resulted in a shallower E_{LUMO} by 0.21 eV.

Replacement of the DBT donor portion with BOBT results in a large E_{HOMO} destabilization for all the polymers as well as a large decrease in E_g. The E_{HOMO} for all of the polymers increased by nearly 0.7 eV and a constant change in E_{LUMO} of 0.2 eV was also observed for all of the BOBT-based polymers relative to DBT. The large increase in E_{HOMO} relative to the small increase in E_{LUMO} led to a decreased E_g of in between 0.4 to 0.6 eV for BOPT donors relative to DBT donors. This is accordance with the E_{sub} parameter shown in figure 1.5 in Chapter One. The strong electron donating effects of the alkoxy side chains in BOBT relative to the alkyl side chains in DBT raises E_{HOMO} for the polymers and decreases the E_g. Replacement of the strongly electron donating 3,3'-ROT2 side chains in **TCN_2BOBT** with a relatively weak fused donor in **TCN_2CPDT** produced a polymer with the same E_{LUMO}, consistent with observations that LUMO energies of D-A polymers are strongly dependant on the electron accepting unit, not the electron donor.[103,104] The weaker electron donating effects of the CPDT unit in **TCN_2CPDT** resulted in a deeper E_{HOMO} by 0.2 eV relative to **TCN_2BOBT,** which would be expected to have favorable impact on OTFT stability and open-circuit voltage in OPVs.

According to solution DPV measurements of the non-halogenated acceptor *monomers*, (tere)phthalonitrile acceptors reduce at potentials 300 mV more positive than 3,4-dicyanothiophene, with $E_{red}^{1/2}$ of 2.34 V and 2.64 V, respectively. The larger E_g as well as the blue-shifted absorbance maxima for the (tere)phthalonitrile copolymers

suggests that poorer orbital overlap (reduced conjugation) is responsible for the deeper HOMO levels and shallower LUMO levels for the phthalonitrile-based polymers. Additionally, the differences in the FMO energies of the polymers is likely also effected by different contributions of MO mixing/symmetry and energetics between the two different acceptors. This possibility, however, cannot be addressed without calculations.

2. 5 WAXD

WAXD was employed to further study the solid state ordering for these materials. Based on the absorption spectra and previous experience it is assumed that **1,2-PhCN$_2$DBT** and **1,4-PhCN$_2$DBT** are both amorphous polymers and they are omitted from this discussion. Polymers **TCN$_2$DBT, TCN$_2$BOBT** and **TCN$_2$CPDT**, containing the dicyanothiophene acceptor motif all show some degree of order. **TCN$_2$DBT**, containing HH-dialkyl units, only shows faint diffractions for π-stacking, at a distance of 3.90 Å. **TCNOC$_{14}$** , shows sharper diffractions and possibly long-range order and gives a stacking distance of 3.77 Å. Interestingly, the π -stacking distance for **TCN$_2$BOBT** is larger than that of **TCN$_2$CPDT (**3.65 Å), containing orthogonal side chains. Polymer **TCNOC$_{14}$**, containing the mono-cyanothiophene motif shows high order and close π-stacking (3.60 Å) most likely attributable to linear side chains rather than the bulky branched chains present in the other polymers. Interestingly **T$_2$CN$_2$DBT**, containing HH donor and acceptor units appears to have a relatively ordered structure as well despite both repeating units have HH linkages.

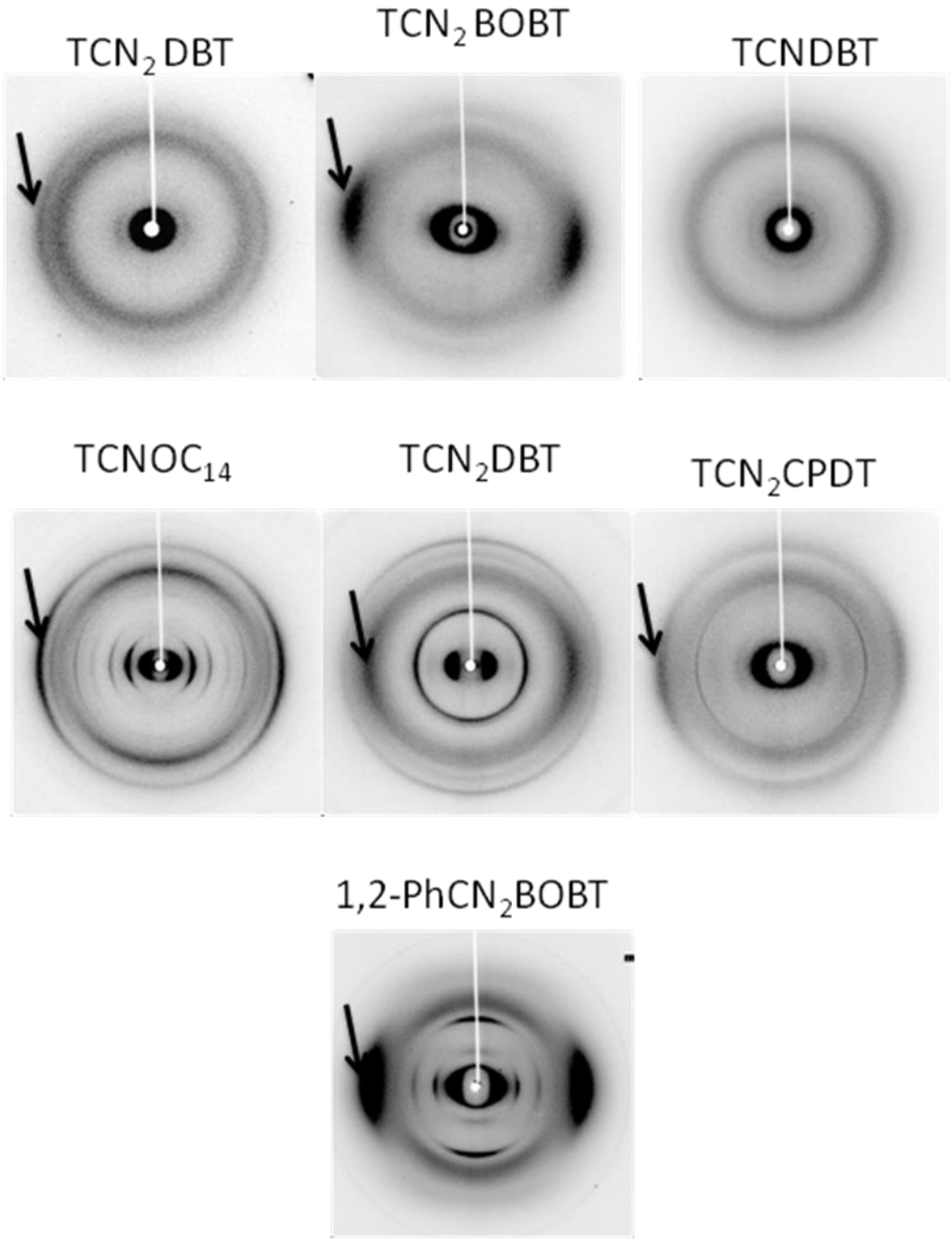

Figure 2.8: WAXD of the polymers. Arrows indicate the diffractions attributed to π-stacking.

2. 6 Conclusions

Novel cyanothiophene and phthalonitrile acceptor monomers were successfully synthesized and copolymerized with different bithiophene donors. Two different

acceptors were employed to study the effects of changing the aromatic acceptor core from thiophene to benzene. Electrochemical measurements revealed that the (tere)phthalonitrile polymers have HOMO energies ~ 0.25 eV deeper than 3,4-dicyanothiophene polymers for both DBT and BOBT donors. The difference in the relative HOMO energies for polymers with DBT and BOBT donors is 0.7 eV (within experimental error). LUMO energies for all of the polymers containing the BOBT donors was ~ 0.2 eV higher than those with DBT donors. The LUMO for the 3,4-dicyanothiophene based acceptor is ~ 0.2 eV deeper than its (tere)phthalonitrile counterparts.

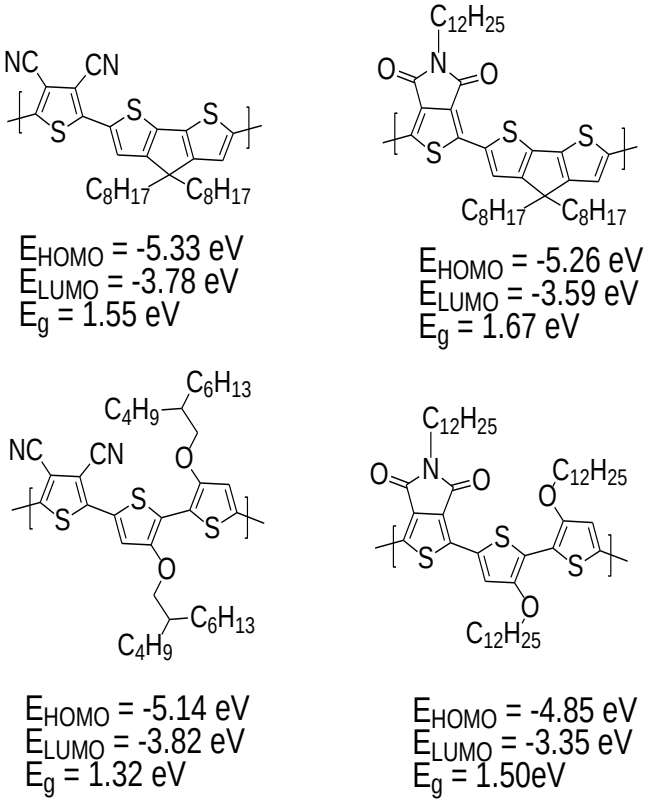

Figure 2.9: Structures and FMO energies of dicyanothiophene (left) and thiophenediimide[115] (right) polymers.

Related 1,2-difunctionalized polymers based on phthalimide[113,114] and 3,4-thiophenediimide,[115] have been reported to both have good charge transport characteristics in OTFTs and high performance in bulk heterojunction OPVs. The measured energies of the dicyanothiophene-based polymers shows they have deeper HOMO and LUMO energies, as well as smaller E_g than their diimide counterparts shown in figure 2.8. It is worth noting that the literature on the diimide copolymers does not contain donor units with 3,3'-ROT2 donor units and this certainly would affect HOMO energies to some extent as will be discussed in Chapter Three. This implies that the cyano-substituted D-A copolymers may be higher performing materials in OPVs with increased V_{OC} and increased ambient stability in OTFTs all other things being equal. These new materials may be promising for future applications in OE.

Chapter Three: Branched Side Chains on 3,3'-dialkoxy-2,2'-bithiophene Donor Units in Phthalimide-Based Copolymers. Increasing Solubility and Tuning FMO Energies

3. 1 Introduction

One of the drawbacks associated with the cyanoarene based polymers presented in Chapter Two was the absence of solubilizing alkyl chains on the acceptor units. On one hand, this is likely beneficial for solid state polymer self organization on the basis of steric interactions and space filling demands. One the other hand, this greatly reduces the solubility of the resulting polymers, demanding compensation with a higher relative volume fraction of solubilizing side chains on donor monomers. Realizing this drawback of using unsubstituted acceptor monomers, many research groups have incorporated electron deficient nitrogen containing functional groups into polymer backbones. An attractive and commonly used functional group for small molecules to be used in OE materials is the imide functional group. In addition to its strong electron withdrawing capability, the "free" N-position allows for incorporation of a wide variety of alkyl chains to be attached to this acceptor unit to tailor solubility and to optimize self organization. Additionally, the presence of alkyl chains on the acceptor monomer allows a wider range of donor monomers to be used for copolymerization, relative to non-alkylated acceptors like those presented in Chapter Two.

Di-imide based OE materials were first introduced in Chapters One and Two and

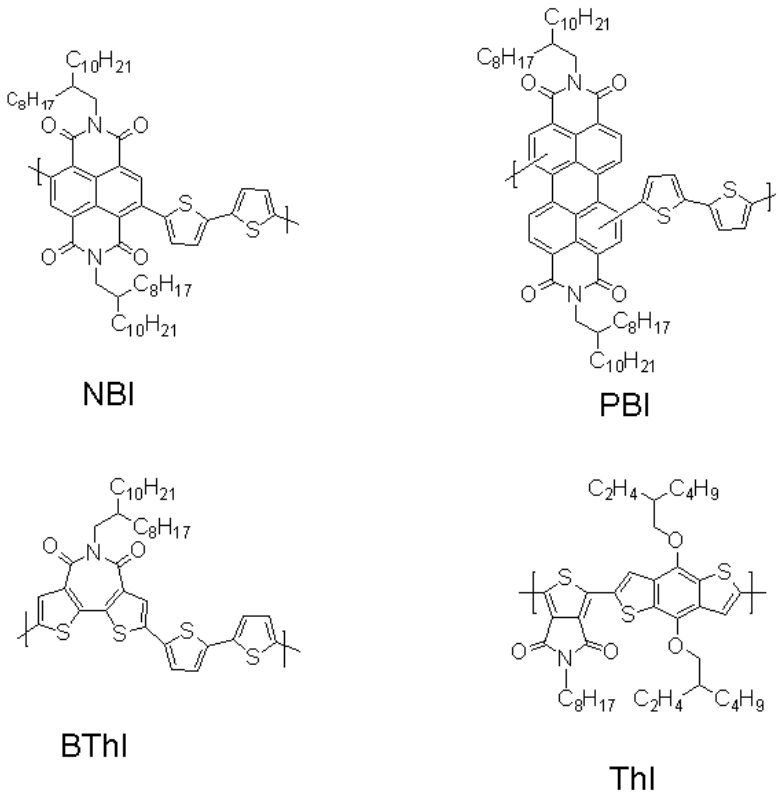

Figure 3.1: Examples of imide functionalized polymers based on naphthalene bisimide (NBI)[116] perylene bisimide (PBI)[117], bithiophene imide (BThI)[118,148] and thiophene imide (ThI)[119].

have been extensively reported in the literature, examples of which are shown in figure 3.1. The majority of the di-imide based materials, in particular rylene di-imides such as NDI and PBI (figure 3.1) are efficient n-type semiconductors.[33,116,117] Mono-imide based materials such as ThI are generally p-type[119] while bithiophene-imide polymers such as BThI may be p- or n-type[3] based on the donor used for copolymerization.[37] Our group was the first to report NBI-based D-A copolymers,[61] as well as phthalimide based D-A polymers (e.g. **PhBT-12** figure 3.2, patented[144]) with structures optimized to provide then state of the art OFET performance. [61,113] Phthalimide based D-A polymers, containing only one electron withdrawing imide motif per repeat unit were found to be efficient p-type semiconductors. The average hole mobility for **PhBT-12** was measured to be 0.17

cm^2/Vs, one of the highest reported in the literature at that time,[113] with much higher values obtained by an industrial partner exploiting proprietary device fabrication. Furthermore the oxidation potential was measured (via CV) to be ~ 0.1 V more positive the P3HT, suggesting OTFTs fabricated from this material should display enhanced

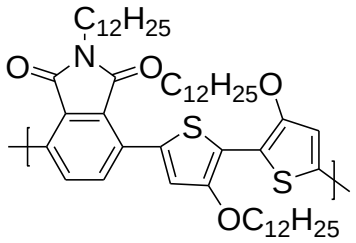

PhBT-12

Figure 3.2: Structure of PhBT-12.

relative ambient stability. Unfortunately, even though devices fabricated from **PhBT-12** initially performed well in air, performance rapidly degraded. [113] In addition to performance degradation issues this material could not meet industrial demands for room-temperature solubility in non-halogenated solvents. Nonetheless, the high hole mobility and narrow E_g (1.64 eV) of this polymer warranted OPV fabrication with **PhBT-12** as the donor polymer. Relatively low PCE values (maximum 1.92%) were obtained from the devices.[120] This may, in part, be due to the high lying HOMO energy level of **PhBT-12**, -5.12 eV (measured independently in this work via DPV) relative to vacuum, leading to low V_{oc} values of ~ 0.55 V when blended in devices. Furthermore, severe macroscopic phase separation occurred in thermally annealed blends of **PhBT-12** and fullerenes[6] limiting the opportunity for further optimization of OPVs based on this material via this approach. In line with the observations described in Chapter One, that higher OPV performance seems to be somehow associated with branched side chains, an

analogue with N-2-ethylhexyl side chains gave modestly better performance with PCE topping 4%.[145]

Working with the industrial licensee of our PhBT technology, we sought to increase the solubility of phthalimide based D-A polymers for ease of device fabrication. Additionally, we sought to address the issues of device instability and low open-circuit voltages encountered with **PhBT-12** by synthesizing similar materials with increased ionization potential relative to the parent polymer. Ideally, the new materials would also retain the attractive features of **PhBT-12** such as the small E_g and high hole mobility. We chose to attach bulky, branched side chains to the 3,3'-ROT2 donor units to increase the solubility of the polymers relative to **PhBT-12**. Additionally, large branched side chains could possibly induce sterically driven twisting of the polymer backbones and/or effect polymer packing and interchain coupling, thus lowering HOMO energy levels resulting in increased ambient stability for OTFT applications and increased V_{OC} for OPV applications.

Indeed it has been demonstrated that increasing the percentage of branched 2-ethylhexyl chains in the backbone of P3HT in a regioregular, random fashion does lower the HOMO energy of the resulting polymers relative to vacuum as illustrated in figure 3.3.[121] The authors stated that the origin of the observed trend in the HOMO energies was not clear, i.e. whether it was due to intramolecular backbone twisting or reduced intermolecular orbital coupling. It was noted that the onset of absorption of thin-films for all of the polymers was identical (with the exception of the 100% branched chain 2-ethylhexyl polymer), and relatively small blue-shifts in λ_{max} were observed with increasing percentages of 2-ethylhexyl side chains relative to 100% P3HT.

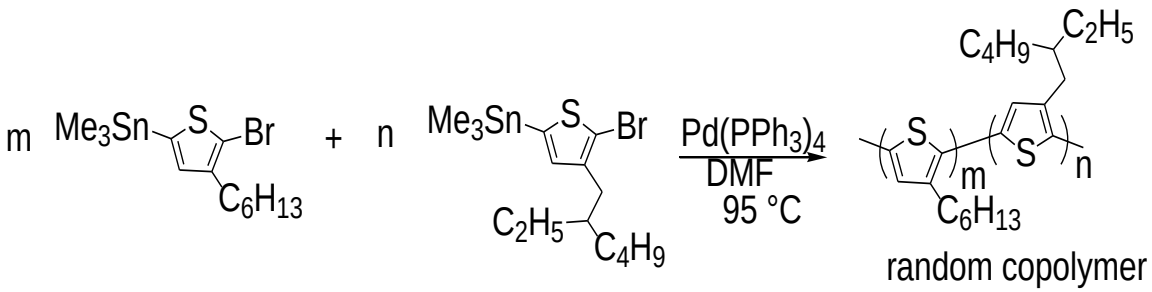

m (%)	n (%)	E_{HOMO} (eV)	E_g (eV)
100	0	-5.17	1.9
75	25	-5.43	1.9
50	50	-5.48	1.9
0	100	-5.57	2.0

Figure 3.3: Structures, HOMO energies and energy gaps for rr-P3HT with an increasing percentage of branched side chains randomly incorporated into the polymer. "m" and "n" refer to the feed ratio of the monomers used for the polymerization reaction.[121]

This study suggested that incorporation of branched side chains in the backbones of poly(3-alkylthiophenes) could efficiently lower the HOMO energy levels relative to P3HT without having a large detrimental impact on light harvesting capabilities of the polymers. Ideally, similar results would be obtained for our materials. Additionally, the S···O interactions and/or strong electron donating effects of the ether oxygen atoms in the 3,3'-ROT2-units used for this project should enhance the degree of backbone planarity relative to the PATs from the published study discussed above.

With these observations in mind a series of materials was developed in order to simultaneously increase the solubility and ionization potential of phthalimide based polymers. The final results of these efforts were expected to be deeper HOMO energy levels, leading to increased ambient stability, higher V_{OC} in OPV applications and small

increase in the E_g. Ideally, a large increase in V_{OC} would be achieved to counteract the possible drop in J_{sc} due to the increased E_g and lead to higher overall PCEs. We proposed the following structures shown in figure 3.4 to fill these criteria.

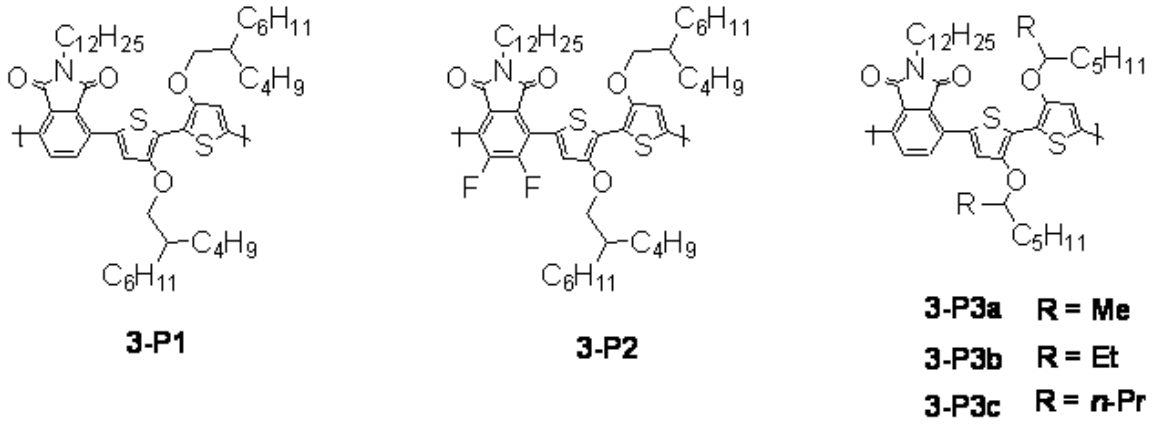

Figure 3.4: Proposed materials.

Initially, we envisioned using a large β-branched side chain (β- relative to the oxygen atom) under the assumption that the butyl and octyl groups would impart sufficient solubility to the resulting polymer, **3-P1**. The **3-P3** series was then chosen as an extreme; I assumed that creating an α-branched alkyl chain in close proximity to the polymer backbone would likely result in twisting between adjacent thiophene units and destroy conjugation along the polymer backbone. However, such a study has not been published on materials containing the 3,3'-ROT2. The presence of S···O interactions could preserve backbone planarity in this extreme situation.

The motivation for the synthesis of **3-P2** is based on the demonstrated favorable impact that fluorination has on aromatic systems for supramolecular organization and FMO energy control. Our group, in addition to other groups, has shown that alternating

copolymers of 3,3'-dialkyl-2,2'-bithiophene donors and hexafluorobenzene leads to increased order, π-stacking, and backbone planarization relative to the non-fluorinated analogues.[122] These properties arise from the unique characteristics of the fluorine atom. It is the most electronegative element (Pauling scale = 4.0) with a small van der Walls radius of 1.35 Å (hydrogen = 1.22 Å). Fluorinated aromatics generally show an inverted charge distribution[123] possibly leading to the enhanced π-stacking observed in these D-A polymers and solid state order is greatly enhanced by C-F··H, F··S and C-F··π_F interactions.[124] Both HOMO and LUMO energies are generally lowered relative to vacuum upon fluorination, resulting in increased ambient stability and possibly larger V_{OC} when these materials are used in devices. Furthermore, fluorinated organic compounds generally show greater hydrophobicity and lipophobicity compared to their non-fluorinated counterparts.[125] This can favorably impact film forming properties of the polymer and lead to higher J_{sc} and FF in OPV devices.

You et al. recently applied these concepts to synthesize PBnDT-DTffBT and compared OPV performance relative to the non-fluorinated analogue PBnDT-DTBT (figure 3.5).[126] Both polymers had similar molecular weight distributions and identical side chains, differing only in the replacement of two hydrogen atoms with two fluorine atoms in the polymer backbone. The two polymers had similar energy gaps as estimated

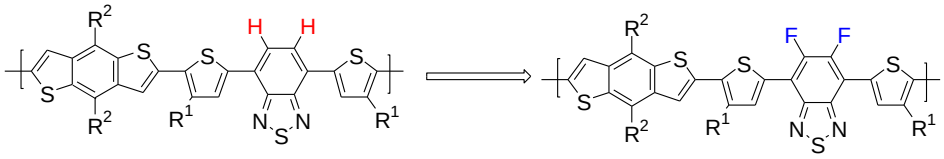

Figure 3.5: Fluorinated and non-fluorinated DTBT-containing polymers for OPV applications. [126]

from the onset of absorption. The FMO energies of the fluorinated polymer, PBnDT-DTffBT, were lower than PBnDT-DTBT by 0.14 and 0.2 eV for HOMO and LUMO respectively. Slightly larger V_{OC} and J_{SC} values of 0.04 V and 2.90 mA were measured for PBnDT-DTffBT relative to PBnDT-DTBT leading a high overall PCE of 7.2%.

3. 2 Synthesis

Synthesis of phthalimide acceptor monomers was carried out following published procedures in two simple steps.[113] Bromination of phthalic anhydride in oleum afforded key intermediate **3-1**. A mixture of all possible isomers is produced under these reaction conditions. Fortunately the target isomer selectively crystallizes from glacial acetic acid, albeit in low yield.[127] Imidization in glacial acetic acid gives the desired phthalimide monomers in acceptable overall yield.

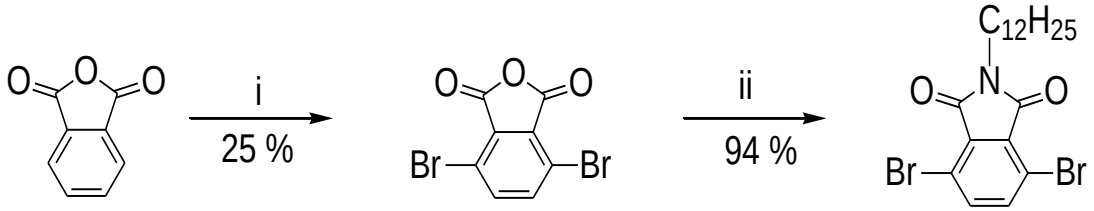

3-1 **3-2**

Scheme 3.1: Reagents and conditions: i) Br_2, I_2 (cat), 30% oleum: ii) H_2N-R, AcOH, 80 °C

During the course of this project an alternate synthetic procedure to produce **3-1** became desirable. Replacing oleum with concentrated sulfuric acid produced no detectable bromination products. Elevated temperatures in H_2SO_4 produced a tar-like mixture that presumably contained self condensation products. The same results were observed when switching to NBS as the bromine source in concentrated sulfuric acid.[128]

Changing brominating agents from NBS to 1,3-dibromo-5,5-dimethylhydantoin (DBMH),[129] in concentrated sulfuric acid at 80 °C however, produced **3-1** in yields comparable to the oleum/Br_2 system. This method has the added benefit of not producing large amounts of HBr gas during large scale synthesis. Workup of the reaction mixture when oleum was used as solvent involved the addition of water to precipitate the solid product and filtration. Oddly, employing this workup with the DBMH/H_2SO_4 system resulted in 0% recovery of any products. Presumably, hydrolysis of the anhydride occurred to produce water soluble products. It was important to extract the crude reaction products from the H_2SO_4/ DBMH reaction with DCM, without the addition of water, followed by neutralization of the organic layer with solid base before adding aqueous solvent. Recrystallization of the solids in same manner afforded **3-1** in comparable yield.

Synthesis of the novel fluorinated phthalimide derivative, **3-7**, employing similar methodologies as those applied to the cyanoarene monomers in Chapter One failed. Rosenmund von Braun nitrile synthesis from 1,2-dibromo-4,5-difluorobenzene produced the target in <5% yield. The reaction mixture produced a deep blue solid that was insoluble in all solvents, presumably the corresponding copper phthalocyanine which is known to be a by-product of the RvB nitrile synthesis when applied to *ortho*-substituted systems.[130] A mild alternative to the RvB synthesis utilizes zinc cyanide and palladium as catalyst to effect the cyanation of aromatic halides.[130,131] This method allowed

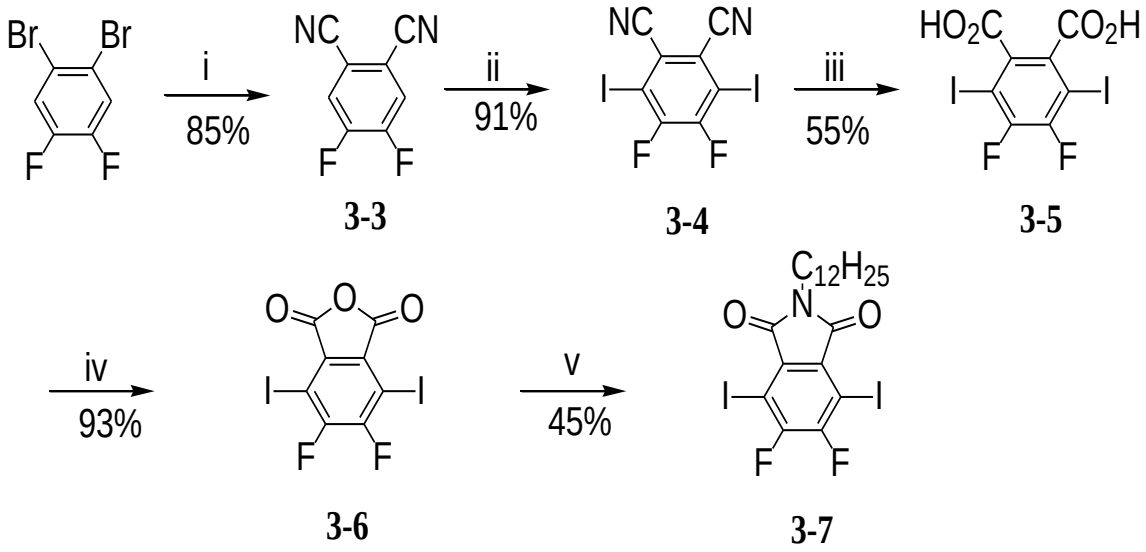

Scheme 3.2: Reagents and conditions: i) $Zn(CN)_2$, Pd_2dba_3, DPPF, DMAc, 100 °C: ii) LiO*t*Bu, I_2, DMF, 100 °C: iii) 50% H_2SO_4, 150 °C, sealed tube: iv) Ac_2O, reflux: v) H_2N-R, AcOH, 80 °C

isolation of **3-3** in > 80% yield. Traditional electrophilic bromination of **3-3** either resulted in zero conversion or decomposition of the starting material. No **3-4** was detected under a variety of conditions. Switching to the basic conditions employed in Chapter One for iodination of cyanoarene monomers produced mixtures of products from which the target could not be isolated. Starting material was consumed, but significant amounts of benzyne derived products were produced using various lithium amide bases. Fortunately, Daugulis and co-workers have shown that for sufficiently acidic aromatics, deprotonation and halogenation can be achieved simultaneously using the much milder lithium *tert*-butoxide as base.[132] This method presumably produces a small equilibrium concentration of the lithiated arene, which is then be quickly halogenated under the reaction conditions. [132] Yields of **3-4** greater than 90% were obtained on 1 mmol scale, however this method did not scale up well, giving < 30% yield on 10 mmol scale.

Once again, brominated products could not be obtained using this method with various electrophilic bromine sources. The final steps were nitrile hydrolysis to produce **3-5**, followed by anhydride formation and imidization like the sequence shown for **3-2** to give the final monomer, **3-7**, in acceptable overall yield.

Polymerization reactions were carried out under the standard conditions reported in Chapter One yielding high molecular weight polymers. Additionally, all of the polymers, with the exception of **3-P2**, had similar molecular weight distributions between 110 and 145 kDa (table 3.1).

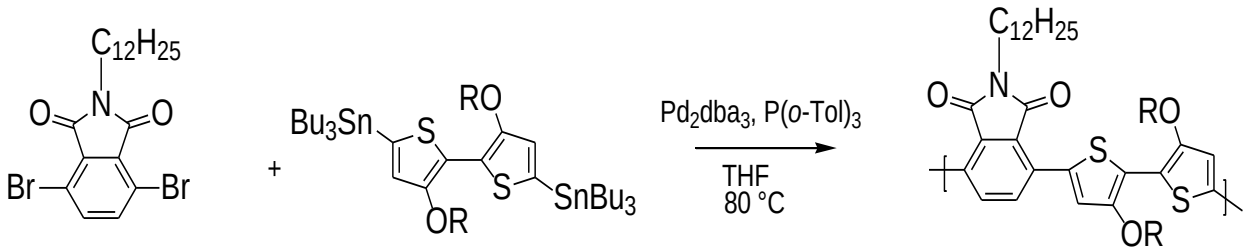

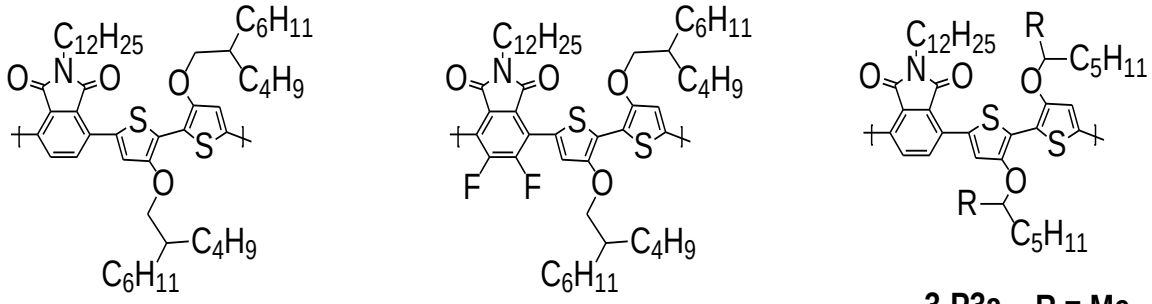

Scheme 3.3: Synthesis and structures of the phthalimide polymers.

The solubility of the branched chain polymers relative to **PhBT-12** was greatly increased. Polymers **3-P1**, **3-P3b** and **3-P3c** were all soluble in a wide range of non-halogenated solvents such as toluene, anisole and warm hexanes. Polymer **3-P3a** displayed better solubility than **PhBT-12** in aromatic solvents such as toluene and anisole, however it dissolved to a lesser extent than the other polymers with larger branched chains. The solubility of polymer **3-P2** was decreased relative to **PhBT-12**, despite the presence of the branched side chains, likely due to fluorination of the acceptor core. [126]

Table 3.1: Yields, molecular weights and melting points of the polymers.

	Yield (%)	**M_n (kDa) [PDI][a]**	**T_m (°C)[b]**
3-P1	92	130 [2.8]	247, 295
3-P2	80	60.2 [1.73]	N/A
3-P3a	81	115 [2.5]	348
3-P3b	83	110 [2.7]	340
3-P3c	89	145 [3.1]	330

[a]GPC versus polystyrene standards. [b]Measured byDSC at a scan rate of 10 °C per minute.

3. 3 Optical Properties

3. 3. 1 Solution and Thin-Film Measurements

Solution and thin-film absorption spectra of the polymers are shown in figure 3.6. All of the polymers have featureless absorption profiles in $CHCl_3$ solution with λ_{max}

centered at ~ 560 nm, suggesting all of the polymers, regardless of branching position and size have similar solution state conjugation lengths and main chain conformation. The fluorinated polymer, **3-P2**, has the most blue-shifted λ_{max} of the series suggesting that the presence of fluorine atoms on the phthalimide unit is causing twisting of the polymer backbones in solution, or differential shifts in FMO energies. The magnitude of the blue-shift of **3-P2** relative to **3-P1** is similar to observations made in the literature when comparing other fluorinated and non-fluorinated polymers. [133] Slight blue-shifts also occur in the onset of absorption as the steric bulk of the side chains increases.

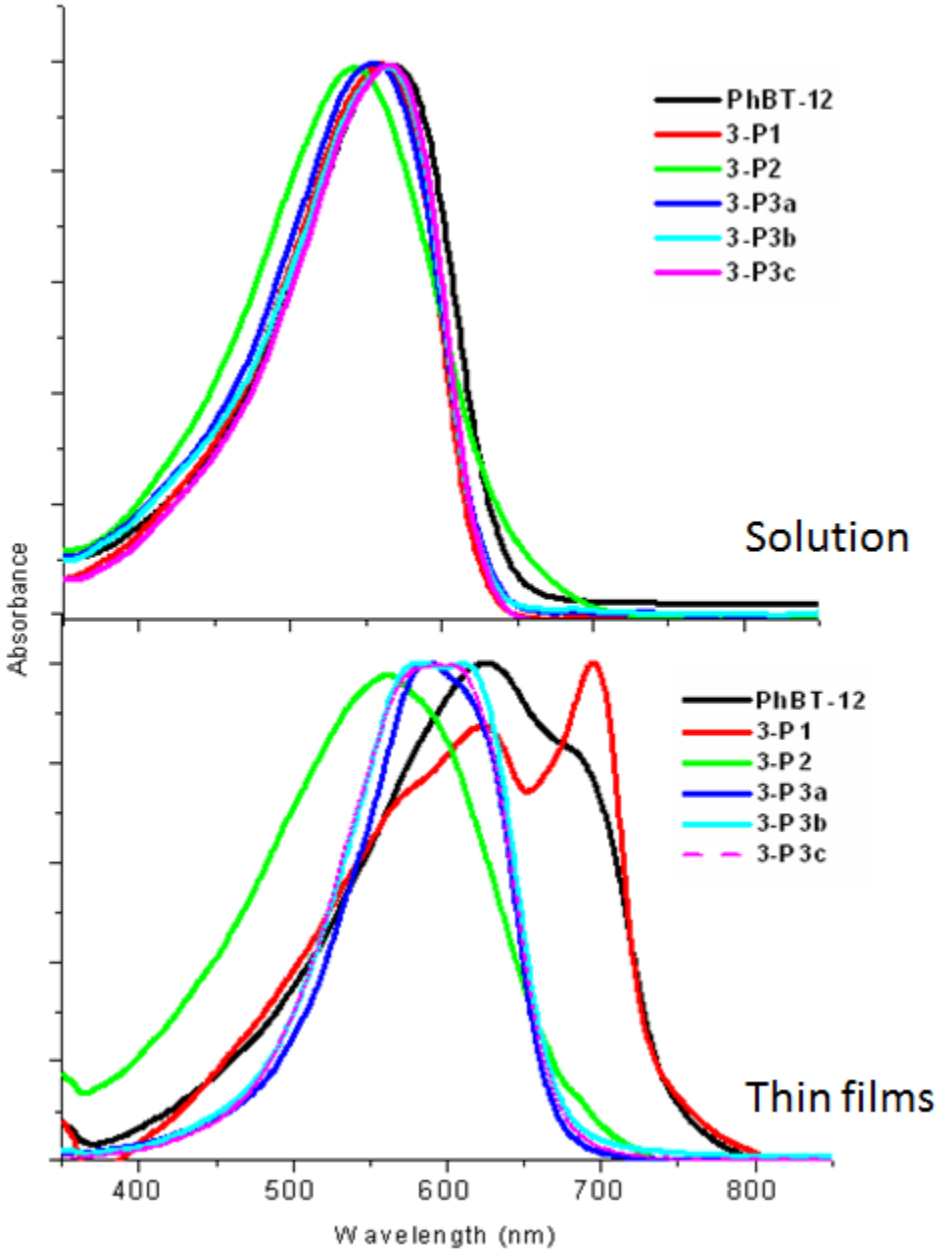

Figure 3.6: Absorption spectra of 10^{-5} M chloroform solutions (top) and thin-films spin-coated from 1 mg/ mL toluene solutions (bottom).

The thin-film absorption profiles for all of the polymers are shown in the bottom spectrum in figure 3.6. The α-branched **3-P3** series all have λ_{max} centered at ~ 590 nm. Weak shoulders are present in the spectra at approximately 608 nm, increasing in

intensity as the size of the α-branch increases (**3-P3a → 3-P3c**). These λ_{max} values are blue-shifted from that of the **PhBT-12** film by ~ 36 nm. The small blue-shifts relative to **PhBT-12** suggest that while a small degree of backbone twisting is likely occurring, the polymer backbones of the α-branched **3-P3** series are still relatively conjugated in thin films. If the steric bulk of the branched side chain were the only variable, however, it would be reasonable to predict that the β-branched polymer, **3-P1** should have λ_{max} - intermediate between the α-branched polymers (**3-P3**) and **PhBT-12**. This trend is reasonably followed for the solution state measurements, but, as can be seen from figure 3.6, this is clearly not the case for the polymers in the solid state. Two distinct peaks are present for **3-P1** with a small shoulder on the high energy side of the spectrum. Interestingly, the spectra for both **3-P1** and **PhBT-12** appear to be quite similar in peak position, differing only in the relative intensities of the peaks at 696 and 626 nm. The position of the low-energy shoulder in **PhBT-12** nearly matches λ_{max} for **3-P1** at 696 nm, while λ_{max} for **PhBT-12** corresponds to the second higher energy peak for **3-P1** at 626 nm. This suggests that similar low-energy-absorbing species are being formed for both polymers, a larger fraction of which being formed for **3-P1**. The low-energy absorption bands can either be attributed to planarization[122] and extended conjugation of the polymer backbones, or interchain (π-stacking) interactions of the of the polymer backbones[38]. Filtering solutions of both polymers through a 0.2 μm PTFE filter before spin-coating resulted in no change in the absorption spectrum excluding

Table 3.2: Optical and electrochemical properties of the polymers.

	$\lambda_{max\ soln}$ (nm)[a]	$\lambda_{max\ film}$ (nm)[b]	$\Delta_{film\text{-}soln}$	$E_{abs\ onset}$ (nm)	E_g^{opt} (eV)[c]	E_{HOMO} (eV)[d]	E_{LUMO} (eV)[e]
PhBT-12	565	629	64	741	1.64	-5.12 ± 0.03	-3.48
3-P1	559	620	60	775	1.60	-5.27 ± 0.04	-3.67
3-P2	543	564	21	711	1.74	-5.27 ± 0.02	-3.53
3-P3a	557	588	21	692	1.79	-5.12 ± 0.04	-3.33
3-P3b	565	558	-7	692	1.79	-5.23 ± 0.06	-3.44
3-P3c	567	568, 619	52	706	1.76	-5.27 ± 0.03	-3.51

[a] Solutions 10^{-5} M in $CHCl_3$. [b] Thin-films spin-coated from 1 mg/mL toluene solutions and thermally annealed. [c] Optical energy gap estimated from the absorption edge of thin- films annealed at 200 °C. [d]DPV measurements of films drop cast thin from 1 mg/mL PhMe solutions versus Fc/Fc^+. [e]Estimated from $E_{LUMO} = E_{HOMO} + E_g$.

aggregates greater than that length scale as the source of the low-energy shoulder.

3. 3. 2 Thermal Annealing Experiments

To examine the effect of thermal history on the absorption profiles, spectra of the same thin-films were collected after thermal annealing (guided by phase transitions observed in DSC). Thermal annealing has been shown to promote self organization of rr-P3HT resulting in longer range chain stacking, increased film crystallinity and overall morphological order[134,135], i.e. this is a macroscopic effect. This is generally observed by UV-Vis spectroscopy as a red-shift in the absorption profile and the appearance of low-energy shoulders.[135] Figure 3.7 shows the thermally annealed thin-film absorption spectra for all of the polymers in comparison to the non-annealed pristine films.

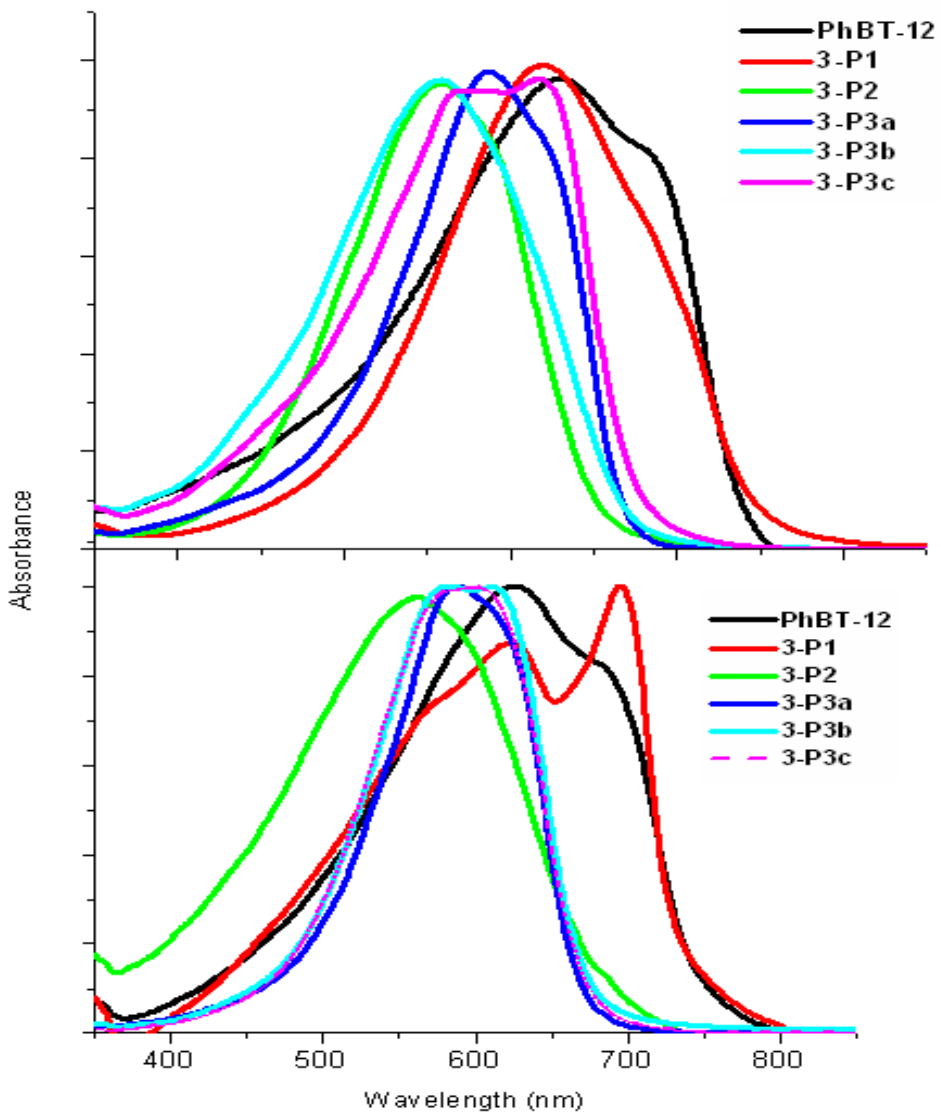

Figure 3.7: Thermally annealed thin-film absorption profiles for the polymers (top) compared to as-cast films (bottom). Annealing was performed at 200 °C for 10 minutes under N_2 with a heating and cooling rate of 10 °C/min.

The annealing effects for the **3-P3** α-branched polymers are for now puzzling. Little change in the absorption profile of **3-P3a** is observed. A blue-shift and loss of fine structure is observed for **3-P3b** while the absorption for **3-P3c** is broadened with more fine structure. A large difference is observed for **3-P1**. The low-energy peak at 696 nm

is reduced to a small shoulder while the high energy shoulder completely disappears. λ_{max} remains essentially constant at 620 nm. Under these conditions, λ_{max} for **3-P1** is intermediate between the α-branched polymers and **PhBT-12** as one would predict based solely on steric bulk around the polymer backbone as noted earlier. The shoulder at 696 nm at 80% intensity of λ_{max} is still present in **PhBT-12** after thermal annealing as well. This finding suggests that a low-energy polymer domain (intra- or intermolecular) of **3-P1** is likely being kinetically trapped during the spin coating process.

Furthermore, it was found that the low-energy peaks for **3-P1** completely disappeared in the spectra of thin-films annealed at temperatures much lower than the polymer's melting point observed by DSC (table 3.1).

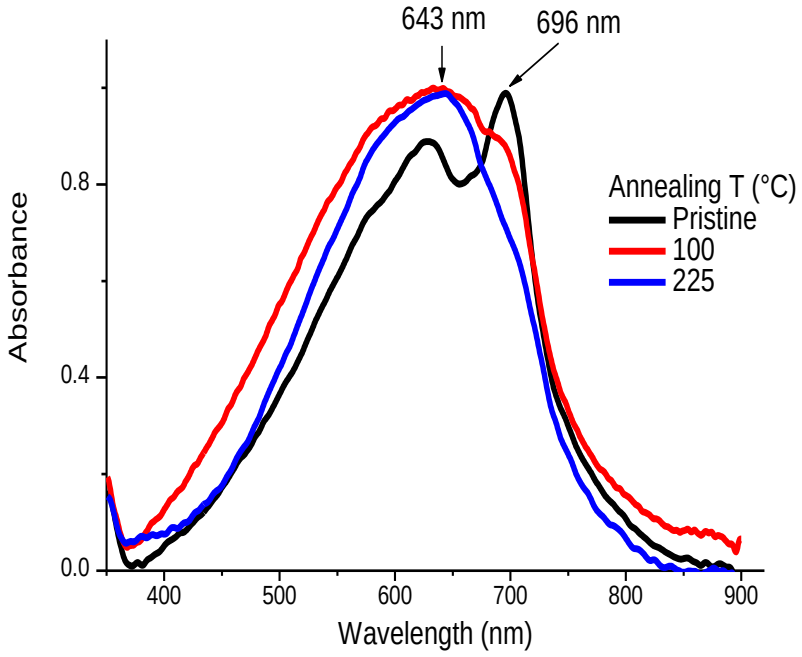

Figure 3.8: Absorption spectra of thin-films of **3-P1** annealed at various temperatures.

Figure 3.8 shows the absorption spectra for films of **3-P1** at various annealing temperatures. The peak at 696 nm became less intense after annealing at temperatures as low as 80 °C (not shown) and is reduced to a shoulder after annealing at 100 °C although no phase changes were observed by DSC below 240 °C. This observation further suggests the nature of this change is due to kinetic trapping of the polymer chains in a low-energy state due to rapid solvent evaporation during the spin-coating process. In a typical DSC experiment performed for this work, solid polymer (generally precipitated from $CHCl_3$ solution with methanol) is placed directly into an aluminum crucible and placed in the instrument. Phase changes of the polymer are then measured as a function of temperature. An extrinsic variable is introduced when the materials are spin-coated onto quartz plates. It is known that the solvent used for spin coating has a significant impact on the final film morphology.[27] Low-energy domains formed by the spin coating process may be detected optically, but not by the DSC measurement in this fashion. Unfortunately, our instrument is not sufficiently sensitive to make measurements on such thin-films. These findings suggest that the artifact at 696 nm in the absorption spectrum of **3-P1** is a product of solvent driven self organization of the polymer backbones in solution with is then transferred to the thin-films.

3. 3. 3 Casting Solvent Experiments

To further examine the hypothesis of solvent driven self assembly, thin-films were cast from other solvents varying in polarity and boiling point. Experiments in the literature have linked the crystallinity of P3HT with OTFT and OPV performance as a function of the boiling point of the solvent used for deposition. For example, it was

found that OTFTs fabricated using 1,2,4-trichlorobenzene (bp = 214 °C) as solvent had mobility one order of magnitude higher than those fabricated from chloroform (bp = 61 °C).[136] The difference in mobility was explained in terms of the solvents' boiling points. Higher boiling point solvents evaporate more slowly, giving the polymer chains more time to interact with one another and form more crystalline structures.[136] The differences in absorption profiles for P3HT as a function of the boiling point of the solvent has also been studied. The general trend is as the solvent boiling point increases, the absorption profiles red-shift and fine structure becomes more intense as a result of longer range order and higher crystallinity present within the polymer films.[137]

If solvent boiling point were the only factor affecting the morphology for the polymer thin-films in this project, however, it would be reasonable to expect a similar, or slightly blue-shifted absorption profile for **3-P1** relative to **PhBT-12** based solely on the identical polymer backbones and differences in the steric bulk of the side chains. The spectra in figure 3.6 were measured from films cast from the same solvent, toluene. It has also been shown with P3HT the solvent "quality" has a major influence on the resulting film morphology and crystallinity.[138-140] In this context, solvent quality is defined as good, marginal or bad. The term good solvent refers to any solvent that will molecularly dissolve the polymer sample. Marginal solvents either only partially dissolve the polymers, or result in solutions of strongly aggregated polymer chains. Poor solvents are those that the polymers are completely insoluble in. Solvents of marginal quality enhance crystallization and interchain interactions which then may be transferred to films during the spin-coating process. To disentangle these variables thin-films were cast from a wide variety of solvents, varying in both polarity and boiling points. **PhBT-**

12 is poorly soluble at room temperature in the majority of organic solvents, limiting the solvents used for this study. This discussion will be limited to 4 solvents and two good/bad solvent mixtures. It is worth noting here that these experiments were performed on the **3-P3** series as well, however significant changes were not observed and they are omitted from this discussion for clarity. Table 3.3 shows the Hildebrand solubility parameters and boiling points for the solvents used in this study and are listed in order of increasing polarity. Spin-coating films from chloroform solutions produced absorption profiles markedly different than those from toluene solutions as shown in figure 3.9.

Table 3.3: Casting solvents, Hildebrand solubility parameters[146] and solvent boiling points[147].

Solvent	**δ ($cal^{1/2}/cm^{3/2}$)**	**Boiling point (°C)**
Toluene	8.91	110.6
Chloroform	9.21	61.2
1% acetone/chloroform	9.22	N/A
5% acetone/chloroform	9.24	N/A
Chlorobenzene	9.50	131
Tetrahydrofuran	9.52	66.0
Acetone	9.77	56.5

No fine structure is present in the spectra for either polymer. Indeed, both of the profiles are nearly identical. The featureless spectra for both polymer films obtained from chloroform, relative to toluene is consistent with the difference in their boiling points

(61.2 and 110.6 °C, respectively) and the observations from the literature noted above. Spin-coating films from a solvent with a similar boiling point to chloroform, THF (66.0 °C), results in a large difference in the absorption profile. **3-P1** films produce a similar absorption spectrum as films from toluene with an increased relative intensity of the lower energy peak. **PhBT-12** even produces a spectrum with increased intensity in the absorption shoulder at 696 nm. The similar boiling points of chloroform and THF suggest that slow evaporation of solvent alone is not the only factor affecting the fine structure in the spectra. Spin-coating films from chlorobenzene also produced structured

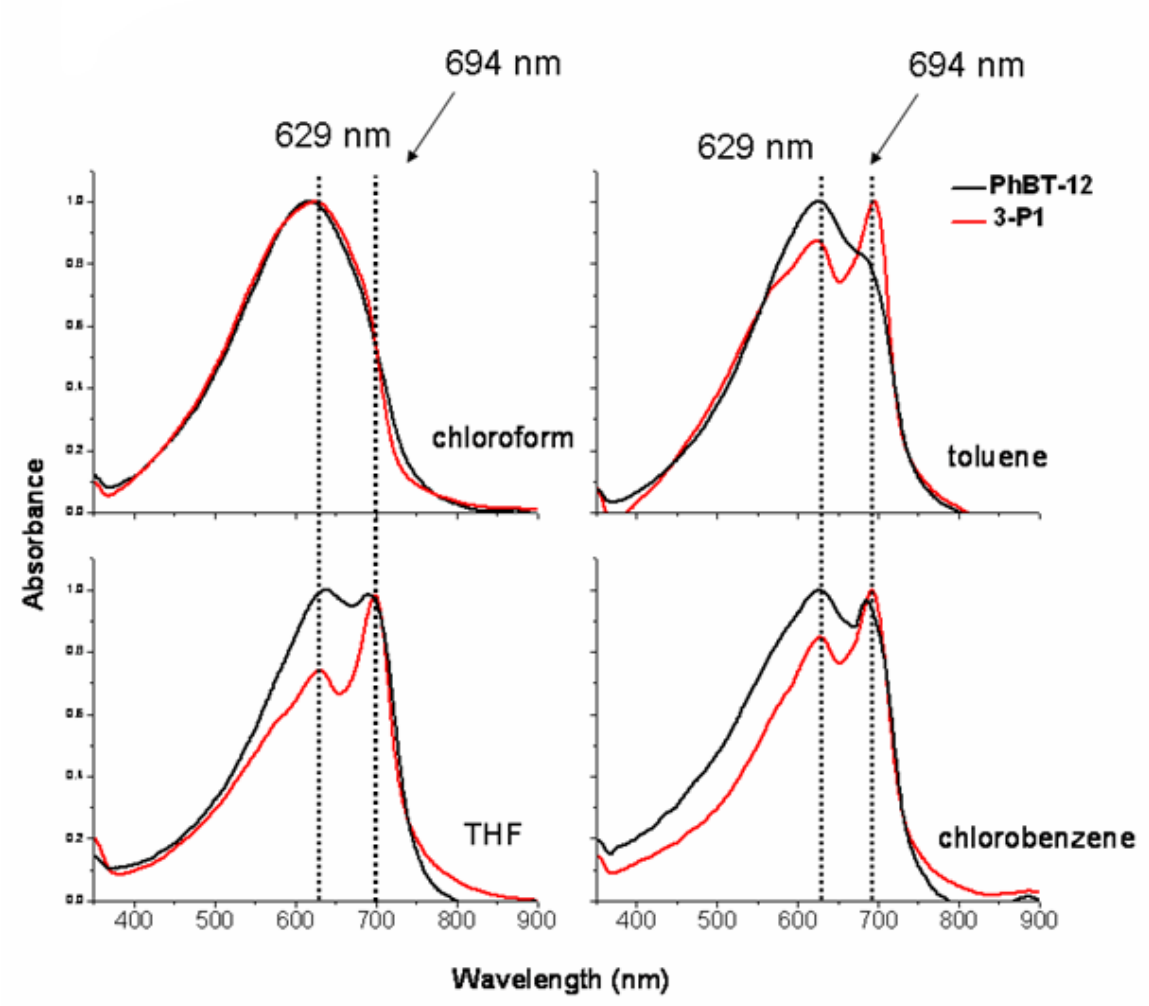

Figure 3.9: Films of **PhBT-12** and **3-P1** cast from various solvents, chloroform (top left), THF (bottom left), toluene (top right) and chlorobenzene (bottom right).

spectra with two distinct peaks for each polymer. The trend of solvent boiling point and the fine structure present in the spectra is consistent following from chloroform, toluene and chlorobenzene. The fine structure present in films cast from THF however, cannot be explained using the solvents' boiling points alone. The δ values of the solvents and the presence of fine structure in the films shows no clear trend either. THF and chlorobenzene have similar δ values of 9.50 and 9.52 $cal^{1/2}/cm^{3/2}$. The least polar solvent used, toluene, has δ = 8.91 $cal^{1/2}/cm^{3/2}$, and these three solvents produce structured spectra despite their large differences in polarity. Chloroform, having an intermediate polarity (δ = 9.21 $cal^{1/2}/cm^{3/2}$) and a similar boiling point to THF is the only solvent that produces unstructured spectra. These observations suggest that both solvent quality and boiling point are factors affecting the absorption spectra for these polymers.

To further elucidate the nature of solvent quality on the absorption profiles of the polymers, a poor co-solvent (acetone) was added to the chloroform casting solution before spin casting. Figure 3.10 shows the absorption spectra of the polymers cast from binary acetone/$CHCl_3$ solvent mixtures with differing compositions. The δ values for the mixtures change little relative to pure $CHCl_3$ as shown in table 3.3, however, it can be seen clearly from figure 3.10 that even 1% of acetone, when mixed in the casting solution has a large influence on the absorption profile of the thin-films. Indeed, when the acetone concentration reaches 5% the absorption profiles for both polymers are nearly identical to the profiles for films cast from toluene. Since the boiling point of the acetone/$CHCl_3$ solvent mixture should not significantly change relative to pure $CHCl_3$,

this should be a reflection of the quality of the casting solvent mixture, not the boiling points.

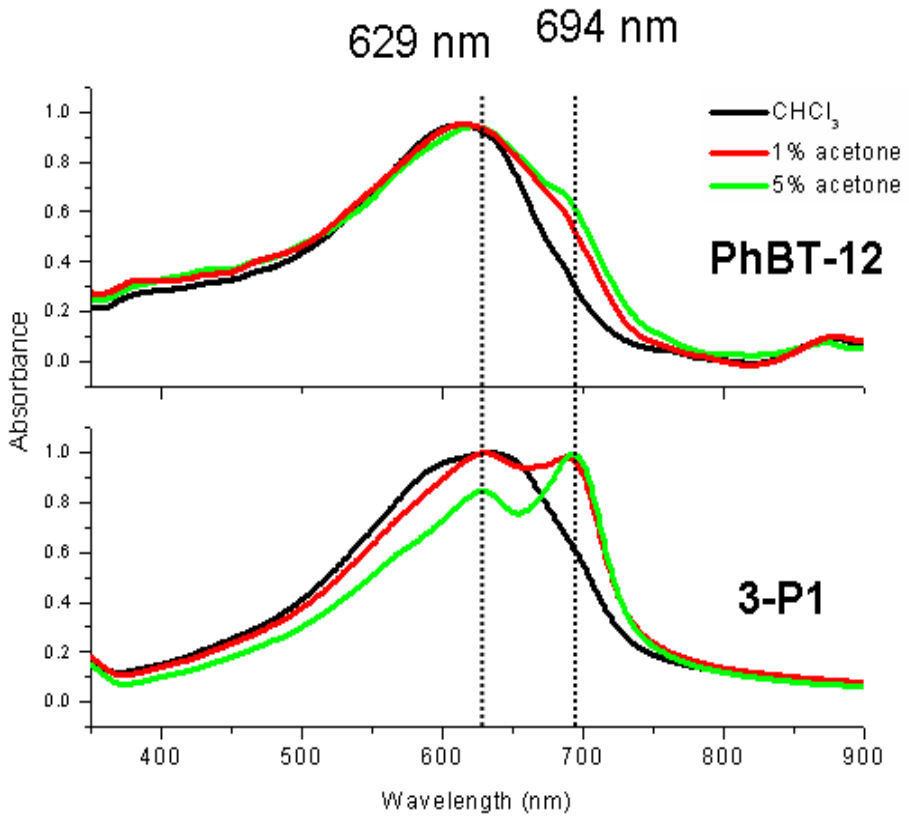

Figure 3.10: Thin-films cast from good solvent ($CHCl_3$) and good/bad solvent (acetone) mixtures.

3. 3. 4 Solvent Vapor Annealing Experiments

Finally, under the assumption that marginal to poor solvent quality was the driving factor for self organization of the polymers, solvent vapor annealing (SVA) was performed. SVA, first introduced in Chapter Two, is a widely used process to promote crystallization and rearrangement within thin-films of both small molecules[143] and

polymers[141]. Additionally, if self organization of the polymers is occurring in solution and fast solvent removal during spin coating is trapping that particular polymer conformation, annealing the thin-films for a prolonged period of time may allow structural rearrangement to occur to the thermodynamically preferred solid state arrangement. Figure 3.11 shows the absorption spectra for SVA thin-films of **PhBT-12**.

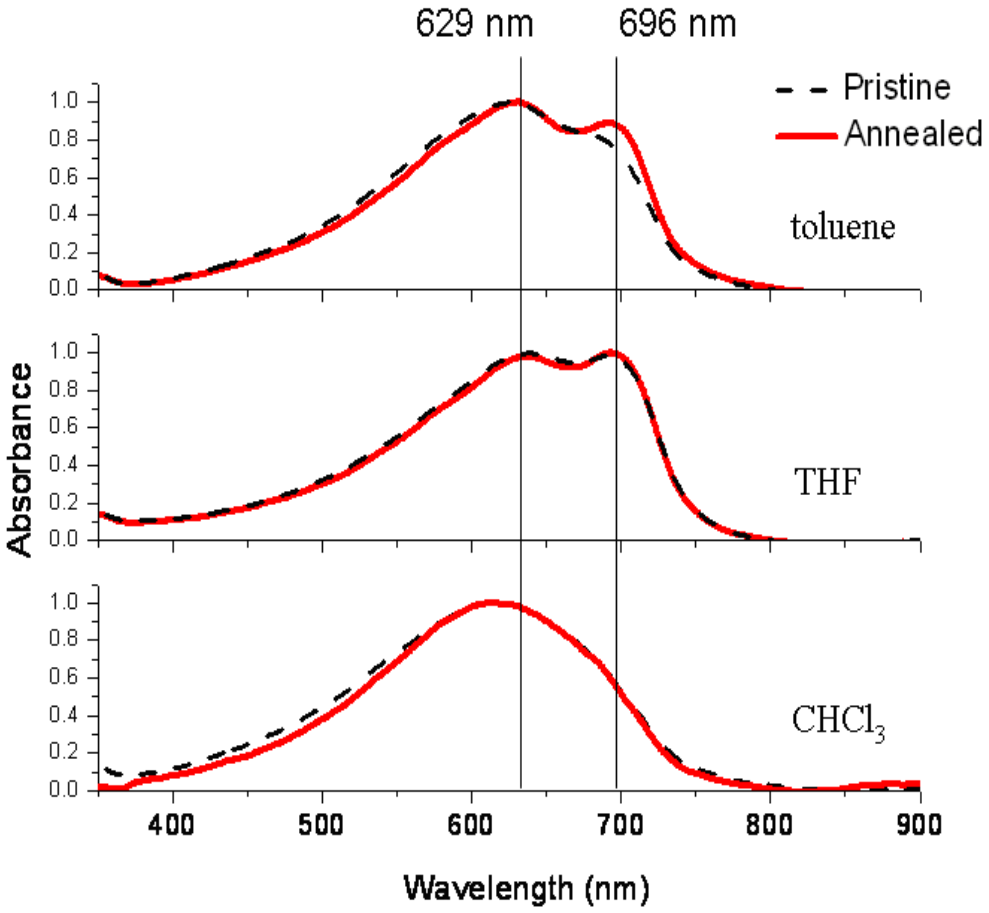

Figure 3.11: Solvent annealing of **PhBT-12.** The thin-films were placed in a 25 mL beaker and sealed in a Mason jar (height = 15 cm, inside diameter = 6 cm) containing 10 mL of annealing solvent. The sealed jars were left in the dark, undisturbed for 4 h. The beaker containing the film was removed from the solvent pool and air dried for 5 minutes followed by drying under a high flow of N_2 for 5 minutes immediately before measurement. Spectra were also collected (not shown) after vacuum drying the films for 1.5 h and no changes were observed.

An increase in the intensity of the shoulders is observed in the films annealed with toluene. Little change is seen with both THF and $CHCl_3$ vapor.

Interestingly, large changes are observed for the films of **3-P1** annealed with THF and toluene vapor as shown in figure 3.12. The fine structure is destroyed for both of the

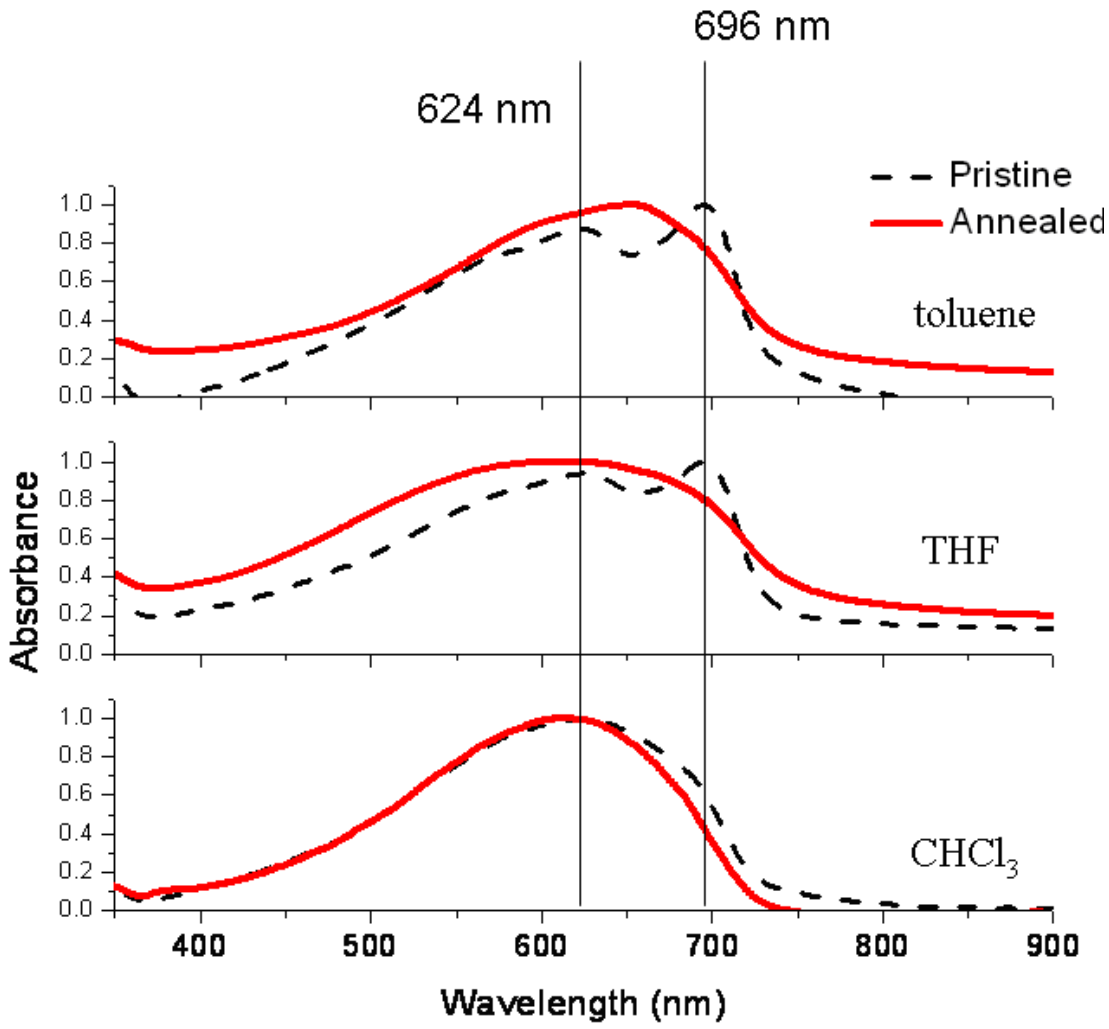

Figure 3.12: Solvent annealing of **3-P1**. The conditions were identical to those described for **PhBT-12.**

films and a single peak is observed, similar to the effects of thermal annealing. Again, only a minor difference is observed from the thin-films annealed with $CHCl_3$.

Based on these data alone an unambiguous conclusion cannot be reached. It does appear the same low-energy domain of the polymer (evidenced by the shoulder at 696 nm) for both **PhBT-12** and **3-P1** can be obtained through appropriate solvent choice and film processing. **3-P1** is qualitatively more soluble than **PhBT-12** in all of the solvents used. Solvent molecules likely penetrate the films **3-P1** during SVA to a much greater extent than **PhBT-12** causing structural reorganization of polymers within the films and loss of fine structure. The fast evaporation of solvent during spin coating precludes such relaxation. The low-energy shoulder at 696 nm is not observed in films of either of the polymers cast from $CHCl_3$, likely because both polymers are more fully solvated, limiting pre-assembly. Addition of a poor solvent (acetone) to the $CHCl_3$ casting solutions causes aggregation of the polymer backbones, which is then transferred to the films. In a similar fashion, after casting from marginally good solvents such as toluene and THF, the absorption peak at 696 nm is observed. These findings cannot be ascribed to boiling point alone due to the similar boiling points of THF and $CHCl_3$. Using a good solvent with a high boiling point, such as chlorobenzene, produces a similar effect in the absorption profile, likely due slower solvent evaporation and increased polymer crystallinity as reported in the literature. The difference between the solubilities for **PhBT-12** and **3-P1** is likely the source for the differences in their thin-film absorption profiles. **PhBT-12** has poor solubility in both toluene and THF. These solvents likely do little to actually solvate the polymer backbone before spin coating i.e. they are marginal solvents for this polymer; it is still trapped in the conformation produced by workup (precipitation into methanol). **3-P1** on the other hand has increased solubility in these solvents relative to **PhBT-12**, these solvents likely fall closer to the "good" category

described above. This polymer is solvated enough to undergo solvent driven re-organization/aggregation to a different conformation which is then transferred to the film during the spin-coating process. Prolonged exposure to solvent vapor then destroys these re-organized/aggregated phases in the thin-films and the absorption profile becomes to similar to that observed for films cast from a good solvent such as $CHCl_3$.

3. 4 Electrochemistry

DPV was preformed to estimate the relative FMO energy levels for all of the polymers. It is emphasized here that only the alkyl-side chains on the donor portion of the polymers were varied in this study. **PhBT-12**, the only material containing linear side chains on the 3,3'-ROT2 unit has a E_{HOMO} of -5.12 eV (relative to the reported CV measurement of -5.2 eV).[5] Branching the side chain on the 3,3'-ROT2 unit in the α-position with smallest methyl group, **3-P3a**, had no effect on the estimated HOMO energy. Increasing the branch size in the α-position to ethyl in **3-P3b**, however, did result in a decrease in the HOMO energy to -5.22 eV. The trend of deepening HOMO energy with larger branches is followed for the α-propyl branched polymer and β-butyl branched polymer **3-P3c** and **3-P1.** Both of these materials have an E_{HOMO} of -5.27 eV.

Fluorination of the phthalimide core in **3-P2** also produced a material with a HOMO energy equivalent to those of **3-P3c** and **3-P1**, despite the presence the presumably stronger electron accepting nature of the fluorinated phthalimide unit. This is likely due to backbone twisting due to steric effects of the fluorine atoms as evidenced by UV-Vis, or the E_{HOMO} of the polymer is not affected by substitution of the fluorine atoms on the phthalimide acceptor unit. Figure 3.13 shows the DPV traces for all of the

polymers, calibrated to the oxidation onset of Fc/Fc^+ at 0 V. A clear decrease in the onset of oxidation as a function of branch size can been seen. LUMO energies follow a similar trend. As the branches become larger, the LUMO energies become more negative relative to vacuum.

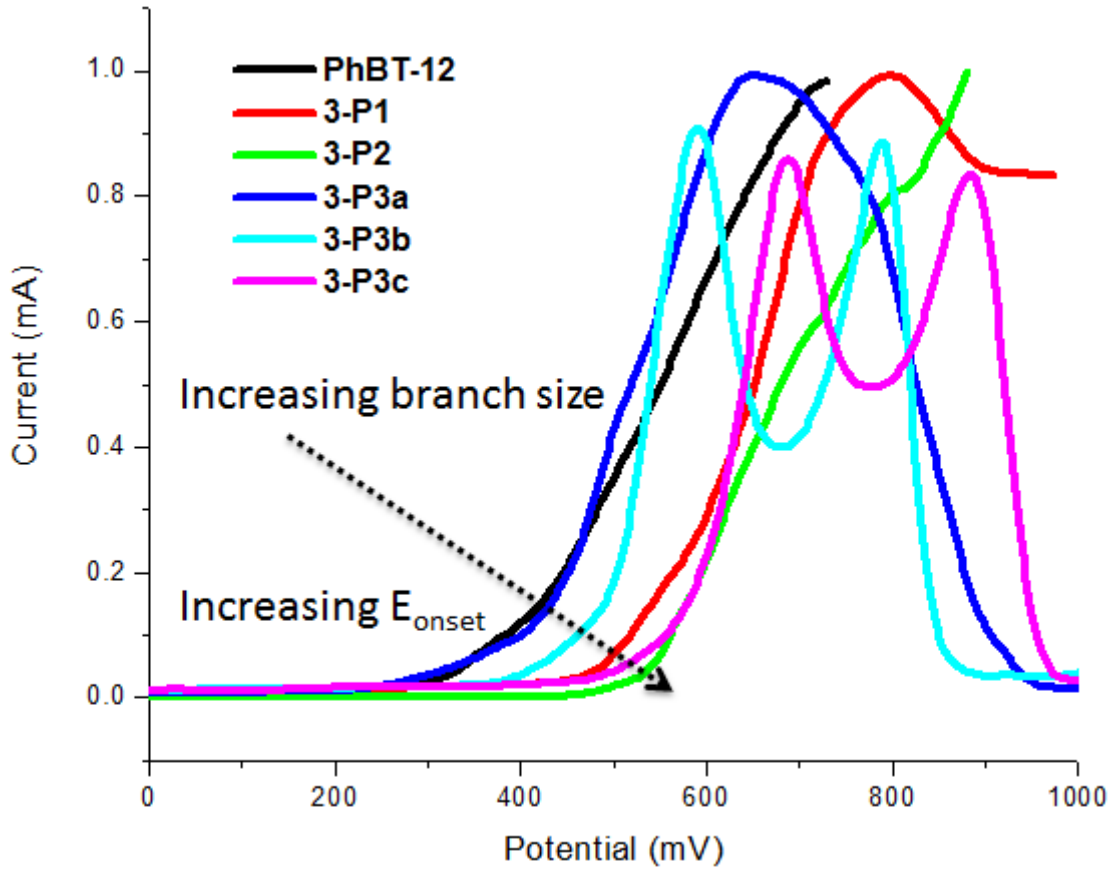

Figure 3.13: DPV of the phthalimide polymers referenced to Fc/Fc^+.

These effects, again, may be taken as intramolecular or intermolecular. As the branching of the side chains becomes larger, it would be expected for some degree of twisting of the polymer backbones to take place. This would be observable as blue-shifts in both λ_{max} and the onset of absorption in UV-Vis experiments. A clear trend in the film UV-Vis spectra for these polymers, however, was not observed. Additionally, **3-P1** has

the second most red-shifted λ_{max} and onset of absorption, but has the lowest HOMO energy of the materials. This suggests these effects are likely not due to intramolecular backbone twisting.

A second possibility would be a restircted dihedral angle between the oxygen lone electron pairs on the 3,3'-ROT2 units and the polymer π-electron system. If the bulky side chains narrows the population of solid-state rotational states about this bond, the oxygen atom could act as an electron accepting group, inductively removing electron density from the π-system which could result in a lower E_{HOMO} for the polymers. If this were the operating mechanism then it would be expected that this could be detected by UV-Vis as well; weaker D-A interactions would be present within the polymers and this would be observable as blue-shifts in the absorption spectra. Again there is no clear trend in the UV-Vis spectra for these polymers, and in particular the α-branched **3-P3** series. Finally, this could be an intermolecular phonemenon, as the branching of the polymer alkyl chains becomes larger, less efficient interchain coupling is present resulting in lower HOMO energies for the polymers .

3. 5 WAXD

In order to try to disentangle these effects, WAXD patterns were collected from extruded fibers of the polymers. The diffraction patterns are shown in figure 3.15, listed with the measured π-stacking distances. All of the polymers, with the exception of **3-P2,** show clear diffractions attributable to π-stacking between the polymer backbones. As expected, polymers containing larger branched alkyl side chains gave larger measured π-

stacking distances. **PhBT-12**, carrying straight chains on the 3,3'-ROT2 donor units, has a π-stacking distance of 3.7 Å. Polymer **3-P3a**, carrying the smallest branched side

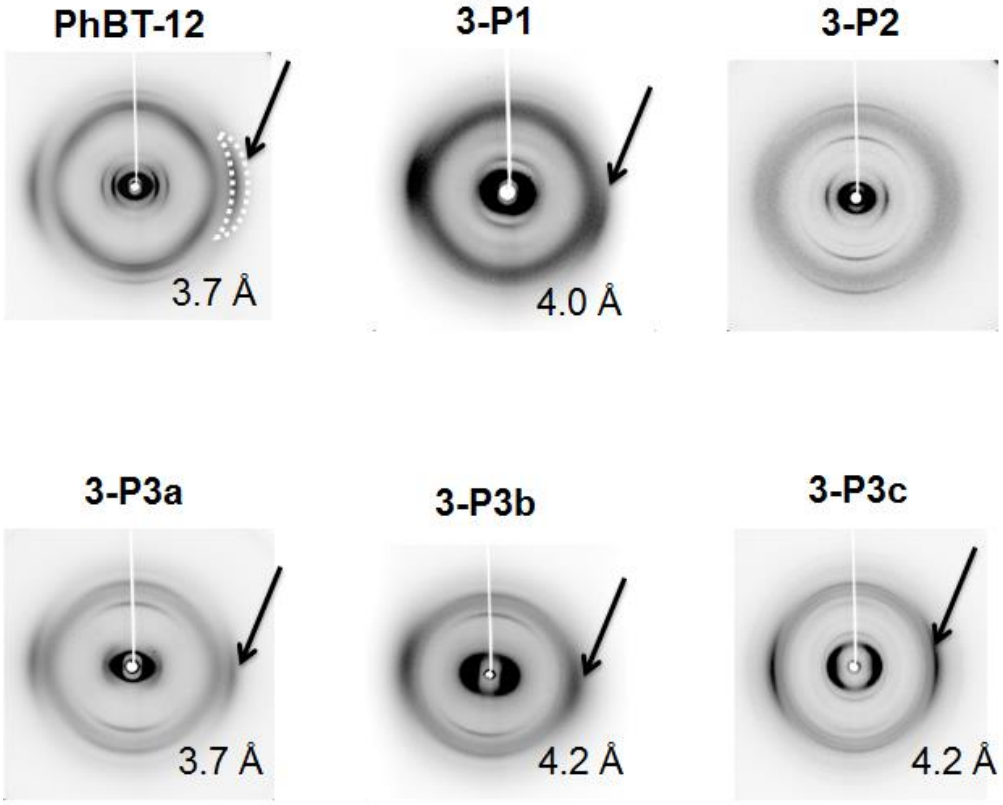

Figure 3.14: WAXD for the phthalimide polymers. **PhBT-12** from reference 7. Arrows indicate diffractions attributed to π-stacking.

chain (α-methyl) has the same π-stacking distance as **PhBT-12** and the diffraction patterns as whole look similar. Increasing the branch size in the **3-P3** series to ethyl (**3-P3b**) and propyl (**3-P3c**) resulted in an increased π-stacking distances of 4.2 Å, a difference of 0.5 Å relative to **PhBT-12**. **3-P1**, with the largest branched side chain in the β-position has a π-stacking distance intermediate between **PhBT-12** and the larger α-

branched polymers **3-P3b** and **3-P3c** at 4.0 Å. From this data it appears that both the branch size and position play important roles in how close the polymer backbones may stack with adjacent chains. Assuming S··O interactions of some nature are operative in these systems then this becomes an issue of side chain position. The attractive S··O interactions, provide a kinetic "block" against free rotation around the 2,2'-bithiophene linkage. As the branches become larger so do the π-stacking distances commensurate with the size of the side chains. Moving the branching position to the β-position would alleviate some the intermolecular steric congestion and allow the backbones to come in closer proximity to one another.

The fluorinated polymer **3-P2** shows no clear diffraction attributable to π-stacking. The blue-shifted absorption profile relative to the other polymers suggests that this material is less coplanar than the others and/or the fluorine atoms do not affect the FMO energies of these materials. A twisted polymer backbone would certainly not allow close π-stacking.

This data could explain the change in the onset of oxidation observed by DPV. Less interchain coupling could certainly lead to the lower E_{HOMO} values measured for the polymers.[142] This trend is supported by the WAXD measurements and the π-stacking distances.

3. 6 Conclusions

Branching the side chains on the 3,3'-ROT2 units for the phthalimide-based polymers in this chapter greatly increased their solubility relative to the straight chain polymer **PhBT-12**. UV-Vis studies suggested that conjugation within the polymer backbone is preserved, despite the presence of bulky side chains in close proximity to the

polymer backbones. This is likely a product of the attractive S···O interactions operating in these systems. Only slight blue-shifts were observed for the branched polymers relative to **PhBT-12**. The solid state absorption behavior of **3-P1** was complicated and likely a product of self organization in solution. DPV measurements revealed that branching the side chains affected the FMO energy levels of the polymers, driving them more negative relative to vacuum as a function of steric bulk. Assuming S···O interactions of some nature are operative in these systems the relative coplanarity for all of the polymers should be equal. Thus, the measured differences in the optical and electrochemical properties are likely due to differences in intermolecular coupling.

Chapter Four: Improving Phthalimide-Based Copolymers by Functional Group Interconversion. Indanedione-Based Copolymers.

4. 1 Introduction

The limited success seen with the new, branched-chain donors employed with phthalimide acceptors presented in Chapter Three motivated the synthesis of a related, novel acceptor for polymerization. The HOMO energies of the phthalimide polymers carrying branched 3,3'-ROT2 units did decrease relative to **PhBT-12**, however we desired to produce materials with FMO energies slightly lower than those presented in Chapter Three. The initial solution to further reduce FMO energies of branched chain phthalimide-based polymers, fluorination of the phthalimide core, resulted in unaffected HOMO energies and decreased solubility of the polymer.

We suspected that changing the imide moiety in phthalimide-based copolymers to a di-ketone moiety should allow for further lowering of the HOMO energy level and increased solubility due to the presence of the orthogonal side chains on the acceptor unit.

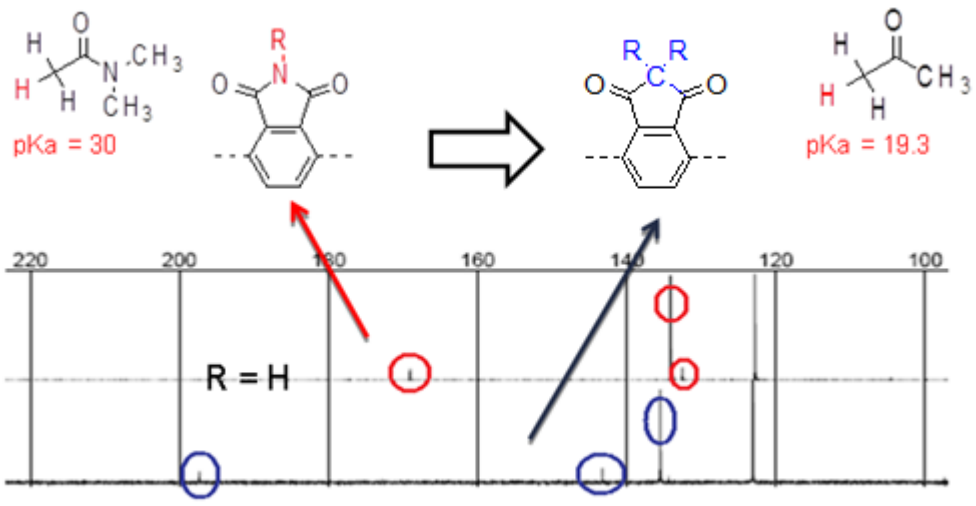

Figure 4.1: ^{13}C NMR comparison of 1,3-indanedione and phthalimide adapted from Sigma Aldrich.[186]

Figure 4.1 shows the ^{13}C NMR spectra for N-methylphthalimide and 1,3-indanedione (indanedione). It can be seen that the carbon resonances for indanedione are slightly farther downfield than the resonances for phthalimide. This implies that the benzene ring in indanedione is more electron deficient than the benzene ring in phthalimide, suggesting that it might act as a stronger electron acceptor unit in D-A polymers. Furthermore, comparison of the pK_a values for acetone versus N,N'-dimethylacetaminde (DMAc) shows that acetone is ~ 1.5 times more acidic than DMAc, reflecting the stronger electron accepting nature of the carbonyl group in ketones relative to amides.

At first glance, the orthogonal side chains relative to the polymer backbones present in the indanedione acceptors would be expected to have a negative impact on solid state ordering by preventing close interactions of the polymer backbones and efficient π-stacking. However, the presence of such tetrahedral atoms in the backbones of conjugated polymers has been well established in the literature, with, for example, the donor monomers fluorene[149,150] and (hetero)cyclopentadithiopehenes[9]. In fact, the highest performing polymer-based BHJ OPV reported in the literature contains such a tetrahedral germanium atom yielding devices with PCEs in excess of 8%[41] (figure 4.2, **4B**).

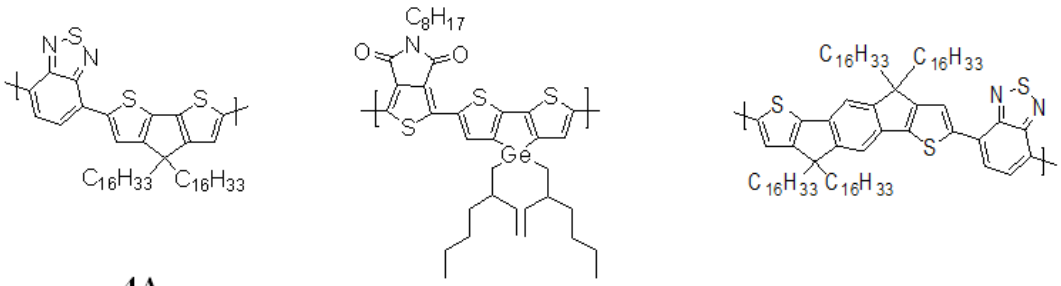

Figure 4.2: Examples of high performance polymers containing orthogonal side chains.[9,41,151]

Polymers based on indacenodithiophene donors (**4C**, figure 4.2) containing two sp^3 carbons and 4 orthogonal side chains in the backbone per repeat unit produced OTFT devices with mobilites as high as 1.0 cm^2/Vs.[151] Furthermore, it was found by GIXS that this polymer was, in fact, semi-crystalline with a π-stacking distance of 4.1 Å and displayed good solubility in a wide range of common organic solvents.

These observations from the literature suggest that the presence of sp^3 (hetero)atoms in the polymer backbone does not necessarily impede efficient self assembly and close π-stacking. Furthermore, as illustrated in Chapter One and figure 4.2, all of the top performing polymers to date contain branched and/or orthogonal side chains. Frechet et al. recently performed a study on the bulkiness of the side chains in PAT derivatives. They found polymers with increased side chain bulkiness in close vicinity to the polymer backbones displayed enhanced exciton dissociation and improved photocurrent.[152] However, one large difference between the proposed indanedione acceptor and the structures shown in figure 4.2 is that the branched chains are located on the acceptor unit, rather than the donor unit. Placing the sp^3 carbon on the acceptor

portion of the conjugated backbone, to my knowledge, has not been reported in the literature. Not only does the indanedione motif present an opportunity to tune FMO energies and solubility of our polymers (relative to phthalimide), it presents an opportunity to study the fundamental aspects of OPV operation. As shown in Chapter One, one of the mechanistic steps in OPV operation is charge transfer from the donor polymer to fullerene. It is generally accepted that in D-A type polymers the LUMO is localized on the acceptor units in the polymer backbone.[153-155] If this mechanism is operative with these polymers, placing orthogonal side chains on the acceptor unit, while likely detrimental to OPV device performance, could present an interesting opportunity to study the fundamental operations of OPVs.

4. 2 Synthesis

Synthesis of the indanedione acceptor monomers began with 3,6-dibromophthalic anhydride, first described in Chapter Three. Condensation with *tert*-butyl acetoacetate in the presence of triethylamine and acetic anhydride followed by *in situ* decarboxylation[156] smoothly afforded the 3,6-dibromoindanedione building block.

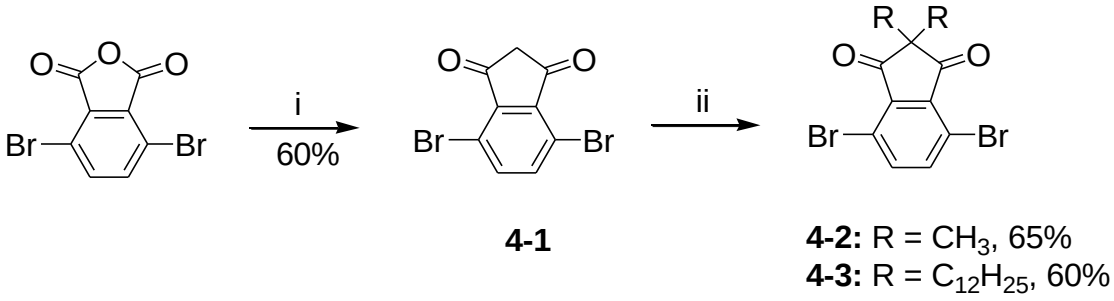

4-1

4-2: R = CH_3, 65%
4-3: R = $C_{12}H_{25}$, 60%

Scheme 4.1 Synthesis of indanedione acceptor monomers. *Conditions and Reagents: i)* 1) Ac_2O, NEt_3, *tert*-butyl acetoacetate, 2) HCl (aq) 70 °C. *ii)* KF/celite, R-I, MeCN, 50 or 70 °C (for R = CH_3 and $C_{12}H_{25}$ respectively), 2 d.

1,3-indanedione is known to be a sensitive material; prolonged heating or changes in pH cause self condensation to bindone.[157] This material was used crude for the next step of the synthesis. Alkylation of the indanedione acceptor **4-1** was easily carried out with a suspension of KF adsorbed on Celite using alkyl iodides in acetonitrile.[158]. The final monomers **4-2** and **4-3** were stable to elevated temperatures and low pH. They were chromatographed on silica gel and recrystallized before polymerization. Polymerizations were carried out as described in earlier chapters to produce the polymers in acceptable yields with reasonable molecular weights (scheme 4.2 and table 4.1).

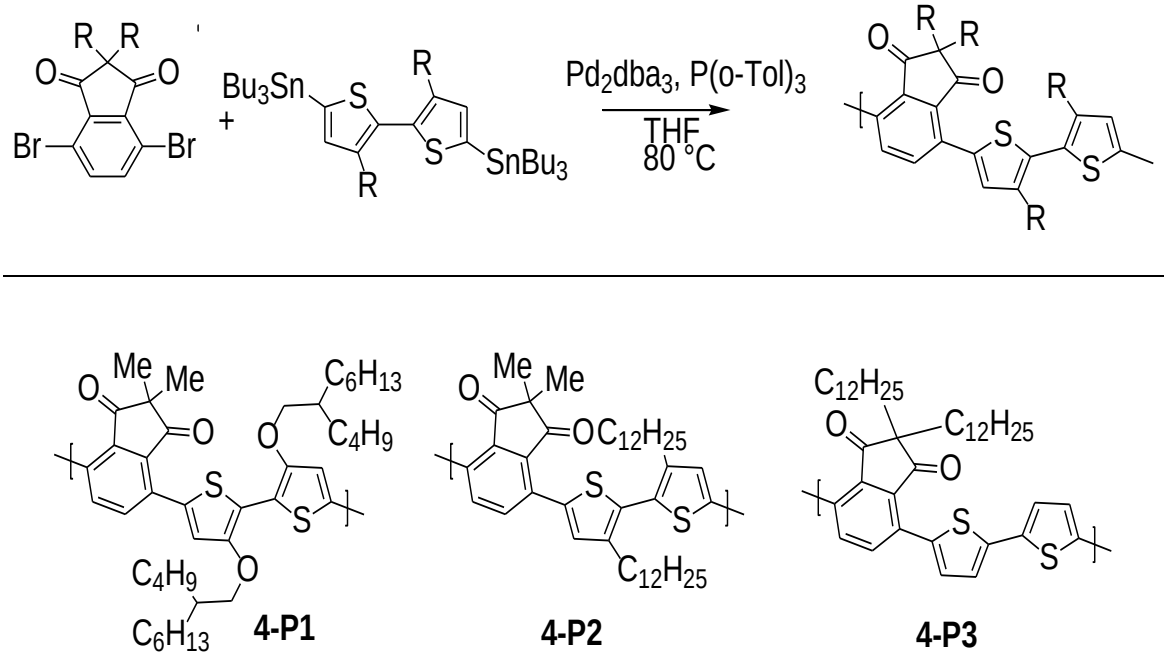

Scheme 4. 2. Polymer synthesis and structures.

Polymers **4-P1** and **4-P2** were very soluble in common organic solvents, including warm hexanes. The solubility of **4-P3** was decreased relative to **4-P1** and **4-P2** due to the unsubstituted-bithiophene donor unit in this polymer. However, it was soluble in chlorinated solvents and warm aromatic solvents such as toluene and anisole.

Table 4.1: Yields, molecular weights, melting points and optical properties of the polymers.

	Yield (%)	Mn (kDa) [PDI][a]	λ_{max} soln[b]/film[c]	T_m[d]
4-P1	88	24.0 [2.01]	594/663	241
4-P2	67	45.0 [1.40]	424/435	80
4-P3	92	N/A[e]	487/535(576)	243

[a]By GPC relative to polystyrene standards [b]10^{-5} $CHCl_3$ solutions. [c]Spin-coated from 1 mg/mL toluene solutions. [d]Measured by DSC at a scan rate of 10 °C/min. [e]Insoluble in THF

4. 3 Optical Properties

Figure 4.3 shows the absorption profiles for the polymers as chloroform solutions and as thermally annealed thin-films. It can be seen, as demonstrated in the previous chapters, that the polymers containing 3,3'-ROT2 donors are far red-shifted relative to the unsubstituted bithiophene donors. The solution spectra are featureless and fairly narrow, indicative of a molecularly-dissolved solution, owing to the high chloroform solubility for all of the polymers. Fairly large red-shifts are observed in λ_{max} upon going from solution to the solid state implying increased backbone coplanarity and conjugation for the polymers in films. Fine structure is observed for both **4-P1** and **4-P3** after thermal annealing, suggesting that these materials have the ability to "thermally relax" and form structures with increased order and crystallinity. In particular, **4-P1** displays a broad absorption profile with a low-energy shoulder at ~ 750 nm with an onset of absorption at ~ 815 nm, suggesting this material could be an efficient photon harvester in OPV applications. Two separate, well defined peaks are present in films of **4-P3** at 535 and 576 nm. Fine structure is also present on the high energy side of λ_{max} for **4-P3**. Polymer

4-P2, containing the HH-dialkylbithiophene donor motif is far blue-shifted relative **4-P1** and **4-P3** as observed for polymers in the previous chapters containing the same donor motif.

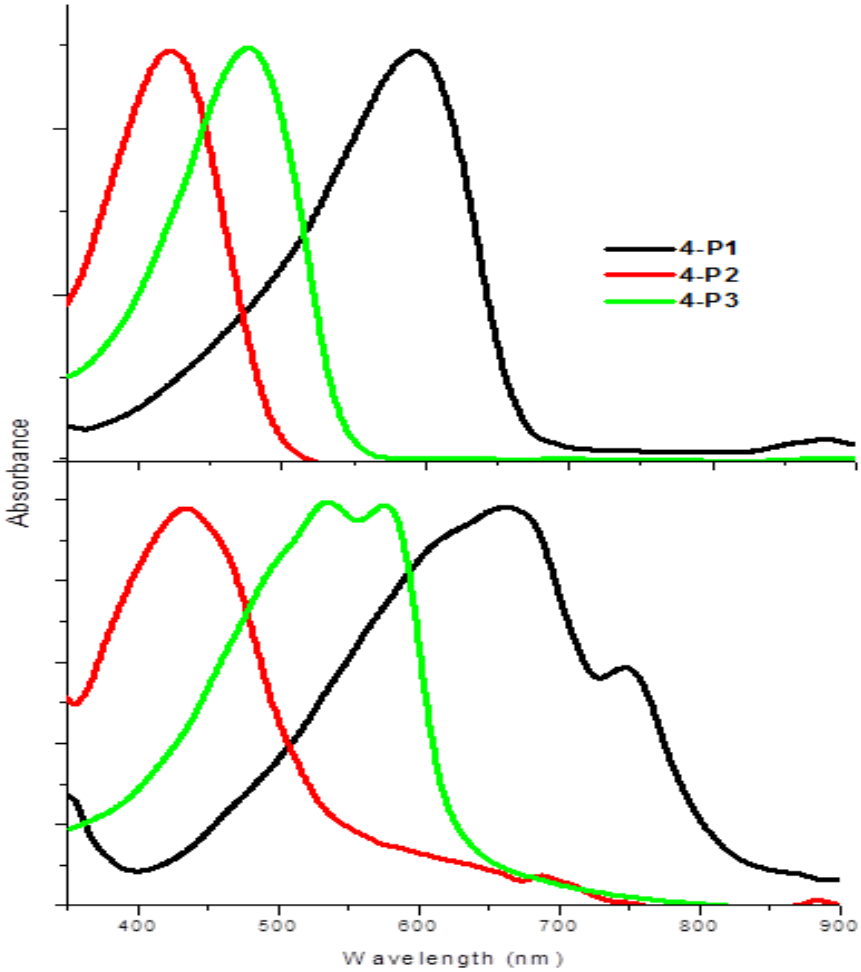

Figure 4.3: Solution (top) and annealed thin-film (bottom) UV-Vis spectra.

4. 4 Electrochemistry

Table 4.2 lists the DPV results for the polymers. **4-P1** had a similar E_{HOMO} as the other polymers with β-branched 3,3'-ROT2 donors in Chapters One and Three at -5.25 eV. Our hypothesis, that the stronger electron accepting indanedione group would slightly lower the HOMO energy for these polymers is not consistent with this observation. This

is likely a result of decreased FMO orbital mixing between the donor acceptor units in these polymers. A decrease in the energy gap, and therefore a decrease in E_{LUMO} by 0.5 eV relative to phthalimide was observed. This picture is consistent with the LUMO level of these D-A polymers being dependent on the acceptor unit while the HOMO is dependant on the donor unit.[103,104] Similar observations were made with the other two polymers relative to their phthalimide counterparts. A decrease in the energy gaps as well as decreases in LUMO levels was measured for both materials.

Table 4.2: Electrochemical results for the polymers.

	E_{HOMO}[a]	E_{LUMO}[b]	E_g[c]
4-P1	-5.25 ± 0.01	-3.74	1.51
4-P2	-5.86 ± 0.03	-3.61	2.25
4-P3	-5.69 ± 0.02	-3.79	1.90

[a]DPV measurements of thin-films drop cast from 1 mg/mL PhMe solutions versus Fc/Fc^+. [b]Estimated from $E_{LUMO} = E_{HOMO} + E_g$. [c]Optical energy gap estimated from the absorption edge of thin-films annealed at 200 °C.

4. 5 WAXD

The final question to address with the indanedione based polymers was the solid state ordering; whether or not the orthogonal side chains had a dramatic impact on the π-stacking and ordering of the polymers. As can be seen from figure 4.4, the WAXD profiles for both **4-P1** and **4-P3** display clear diffraction attributable to π-stacking. **4-P1** in particular clearly shows many diffractions suggesting that the presence of orthogonal side chains does not interfere with the ability of these polymers to form ordered structures. The π-stacking distances for **4-P1** and **4-P3** were measured to be 4.0 and 3.7

Å, respectively. These values are identical to those with phthalimide-based polymers containing bithiophene and 3,3'-ROT2 donors.

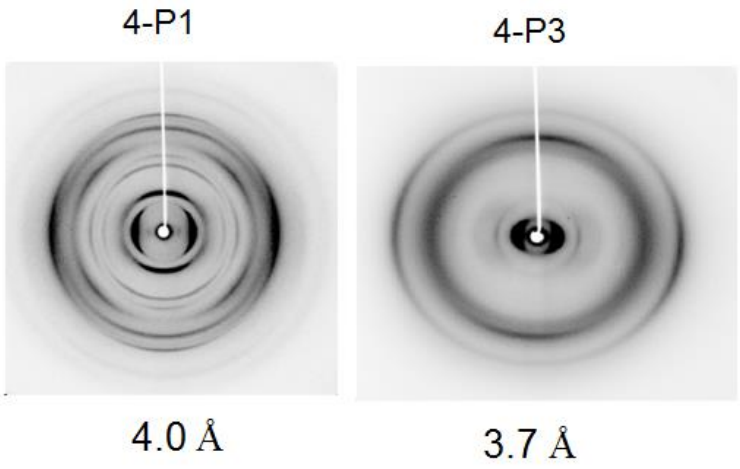

Figure 4.4: WAXD for the polymers.

4. 6 Comparison with Phthalimde-Based Polymers

The structures of indanedione- and phthalimide-based copolymers with identical donor units used for comparison in this section are shown in figure 4.5.

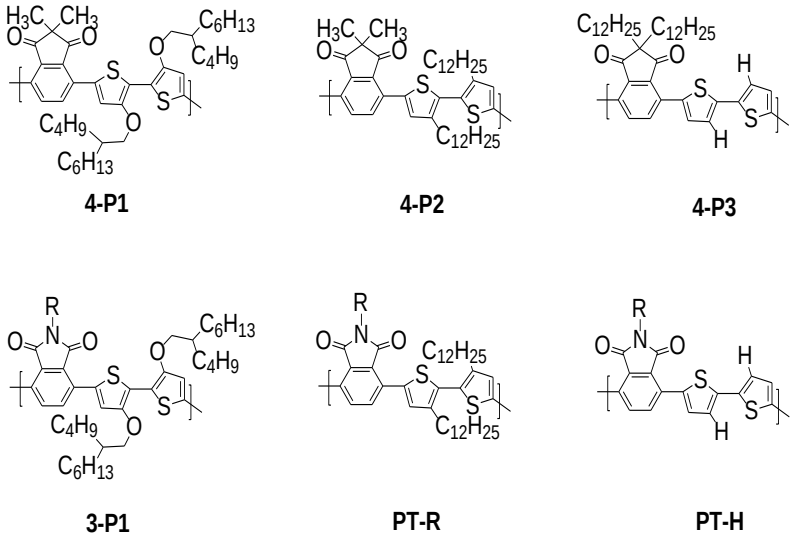

Figure 4.5: Structures of phthalimide and indanedione-based copolymers. Phthalimide polymers **PT-R** and **PT-H** are unpublished and were synthesized and studied in our lab by Xugang Guo.

4. 6. 1 Optical Properties

Figure 4.6 shows the absorption spectra of indanedione and phthalimide derivatives. If the indanedione moiety is a stronger electron acceptor relative to phthalimide, it would be expected that a smaller E_g, both in solution and the solid state would be observed due to

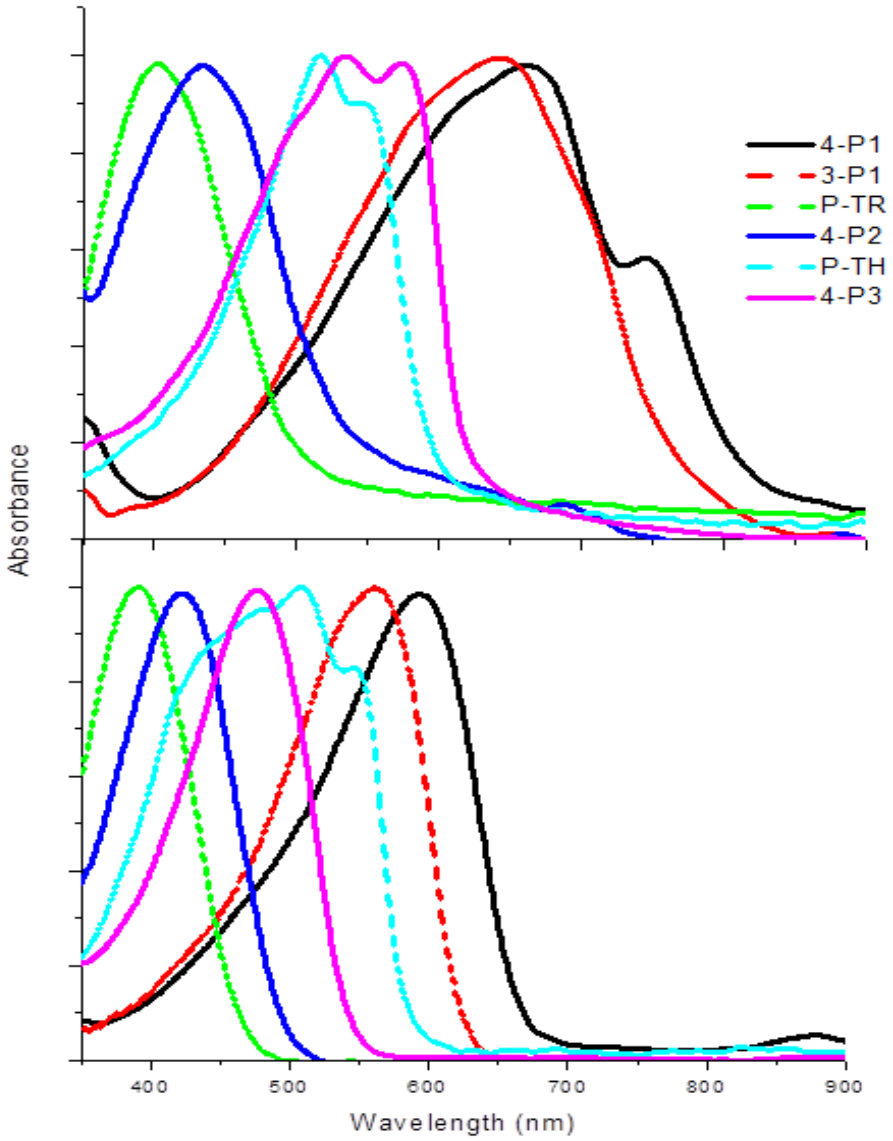

Figure 4.6: Thermally annealed thin-film (top) and solution (bottom) absorption spectra for indanedione and phthalimide polymers.

Increased D-A interactions between the units and lower LUMO molecular orbital energies. As can be seen, λ_{max} and the onset of absorption are red-shifted for the indanedione polymers relative to phthalimide. Additionally, fine structure is present with greater intensities for **4-P1** and **4-P3** relative to their phthalimide counterparts **3-P1** and **P-TH** suggesting that these indanedione-based polymers have a higher level of solid state

ordering. Polymers **4-P1** and **4-P2** show red-shifts in solution of ~ 30 nm, while polymer **4-P3** shows a blue-shift of the same magnitude relative to the phthalimide polymers. The unsubitiuted bithiophene donor, in the case of , severely hampers the solubility of these polymers and the insolubility of **P-TH**, in this case, is probably is reason for the relative blue-shift. The structured and broad absorption of **P-TH** suggests this. **4-P3** on the other hand, containing orthogonal dodecyl side chains on the acceptor, easily dissolved in $CHCl_3$ and likely represents a more molecularly dissolved solution.

4. 6. 2 Electrochemistry

An FMO energy diagram for the polymers is shown in figure 4.7. There is little difference in the HOMO energies for the indanedione-based polymers relative to phthalimide-based polymers. The LUMO energies for polymers containing indanedione-acceptors are ~ 0.1 eV more negative than the analogous phthalimide-based polymers, corresponding to the 0.1 eV decrease in E_g for those polymers. This suggests that FMO mixing between donor and acceptor fragments is likely not occurring to a great extent in these systems, rather the HOMO energies and LUMO energies are governed by the donor and acceptor units, respectively.

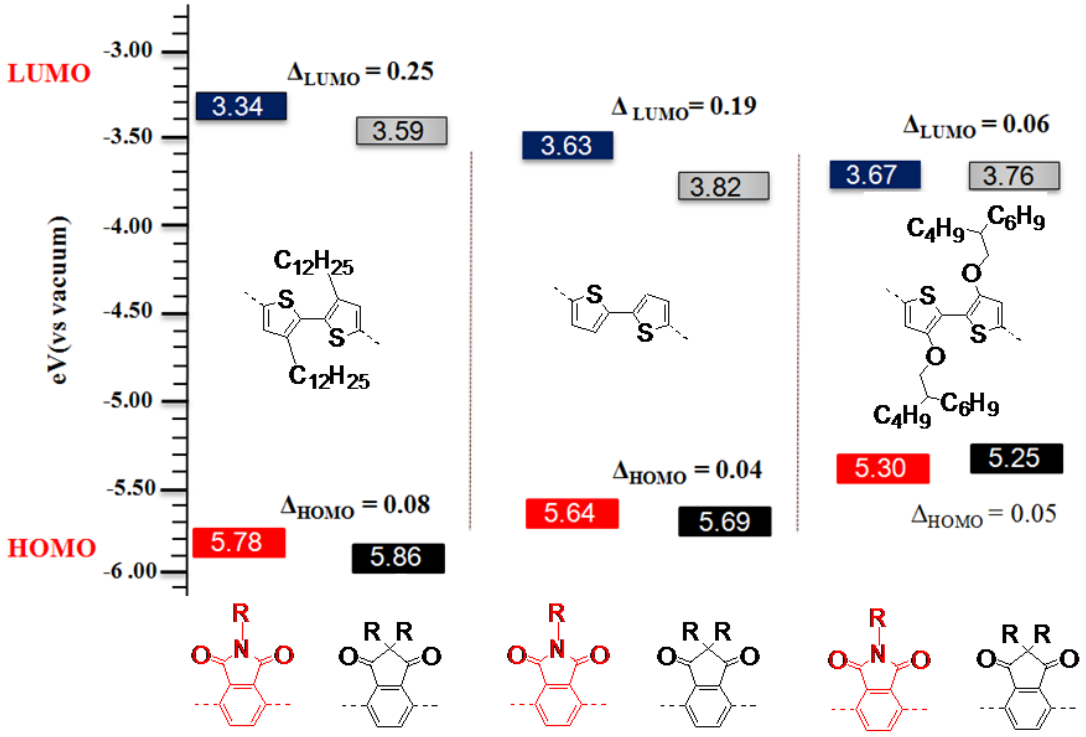

Figure 4.7: FMO energy graph of phthalimide and indanedione polymers (negative signs were omitted for clarity).

4. 7 Conclusions

Novel indanedione-based D-A polymers were synthesized and copolymerized with three different donor units. Despite the hypothesis of a diketo-moiety being a stronger electron accepting group than an imide moiety, the HOMO energies of the indanedione based polymers were nearly equal to that of phthalimide, likely due to localization of the HOMO and LUMO and the donor and acceptor polymer units, respectively. LUMO energies were found to be ~ 0.1 eV more negative than phthalimide donors, suggesting that the indanedione motif may play a role in n-type semiconductors after appropriate functionalization.

Chapter Five: 3,3'-Dialkynyl-2,2'-bithiophene Donor Units in Donor-Acceptor Copolymers

5. 1 Introduction

5. 1. 1 Fused-Ring Donor Units

The highest performing materials in OPVs and OTFTs (as shown in Chapter One) to date are D-A polymers incorporating strong electron accepting groups and weak, fused electron donating groups. Examples of these groups, shown in figure 5.1, include diketopyrrolopyrrole (DKPP)[159] and thiophene-dimide (TDI)[40] as acceptors and benzodithiophene (BDT)[119,160] and (hetero)cyclopentadithiophene (CPDT) derivatives as donors.[9,40,41] Specifically, the donors shown in figure 5.1 fulfill three important

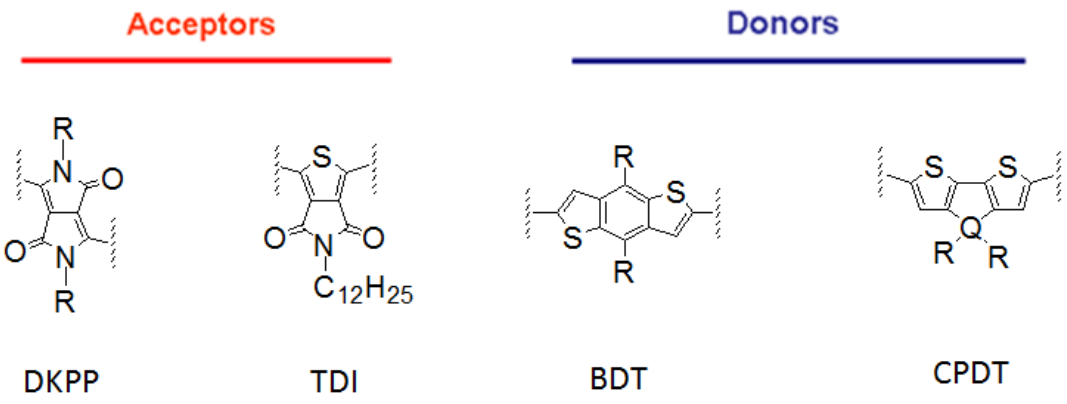

Figure 5.1: Structures of commonly used acceptors and donors for high performance OE materials (CPDT: Q = C, Si or Ge).

requirements when copolymerized with various acceptors. First, they enforce backbone rigidity and planarity through their covalently-fused structures. Free rotation is restricted between the fused thiophene units and the donor portion of the polymer is locked in a coplanar geometry. Second, the placement of the alkyl side chains on the donor motif

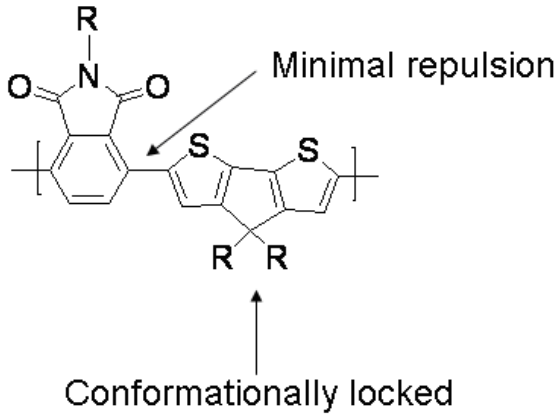

Figure 5.2: Example of a polymer containing the cyclopentadithiophene donor motif.

minimizes steric interactions between the donor and acceptor units of the polymer, allowing for full conjugation between the donor and acceptor units (figure 5.2). Finally, the weak electron-donating nature of side chains allows reasonably deep HOMO energy levels to be achieved. The desirable consequences of this design tends to be small HOMO-LUMO energy gaps, satisfactorily deep HOMO energy levels and highly soluble polymers, all of which are beneficial to overall device performance.[23]

5. 1. 2 Alkyl Chain Position in PATs and D-A Polymers

Early work on PATs with non-fused backbones showed that the most beneficial placement for the alkyl chains was in the head-to-tail (HT) position.[161] This placement of alkyl side chains minimizes the steric repulsion between the adjacent monomer units in thiophene homopolymers, resulting in minimal backbone twisting as illustrated by structure A in figure 5.3. This, approach, however, is not applicable to D-A copolymers; large steric interactions are introduced between the alkylated-thiophene rings and the acceptor units, causing twisting of the polymer backbone as illustrated by structure B in

figure 5.3. To overcome this drawback in D-A systems, insertion of unsubstituted spacer groups within the polymer backbones (C) has been applied to reduce twisting of the

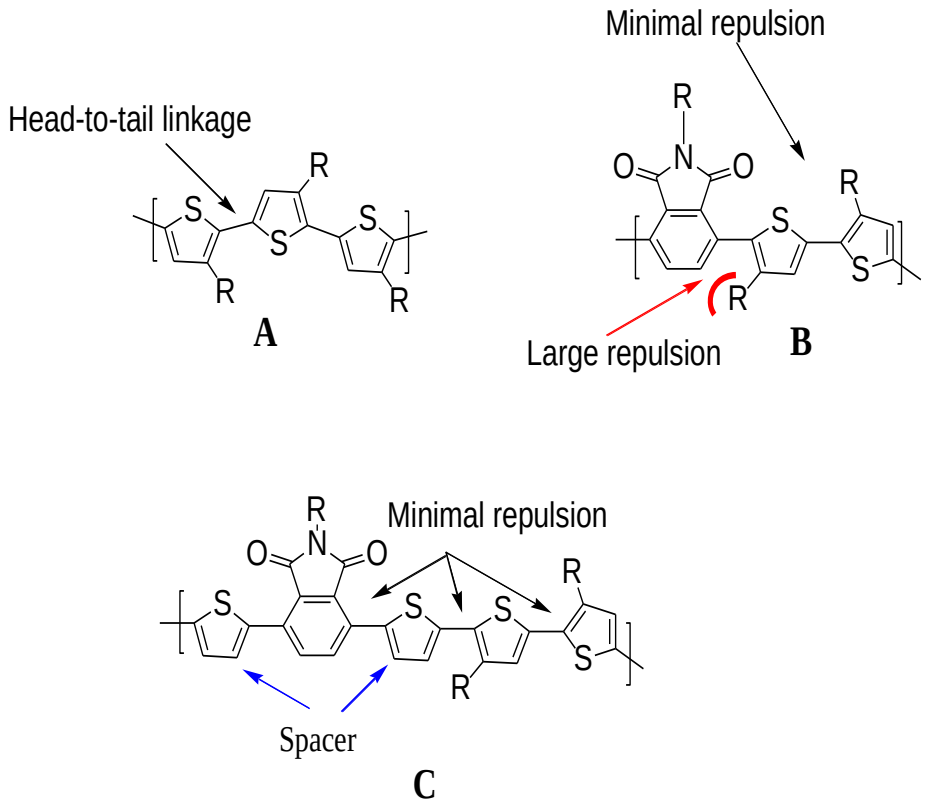

Figure 5.3: HT-P3HT (A), HT bithiophene motif in a D-A polymer (B) and D-A polymer with spacer groups (C)

adjacent units.[18] This approach, however, has two deleterious consequences. First, the solubility of these polymers will likely be reduced due to a smaller fraction of side chains per repeat unit. This can lead to precipitation of the polymers from the reaction medium during synthesis and low molecular weights. Additionally, reduced solubility makes processing these polymers into devices more difficult. Second, dilution of the acceptor units within the polymer backbone has consequences on the FMO energies of the resulting polymers. Koch and coworkers have shown that insertion of an increasing percentage of tetrafluorobenzene units in the backbone of polythiophenes increases the IP of the resulting polymers as a function of the percentage of TFB added.[19] As stated in

Chapter One, polymers possessing high IPs can possibly lead to materials with increased ambient stability and higher V_{OC} in devices.

5. 1. 3 Head-to-Head Coupled Bithiopehene Donor Units

Our group is one of the few interested in head-to-head (HH) coupled bithiophene donor units in our conjugated polymers (figure 5.4). This motif removes the need for the use of "spacer" groups within the polymer backbone between donor and acceptor groups to maintain conjugation. However, the presence of the adjacent alkyl groups on the adjacent thiophene rings generally causes large repulsion and twisting within the bithiophene donor unit, resulting in loss of conjugation throughout the polymer backbone.

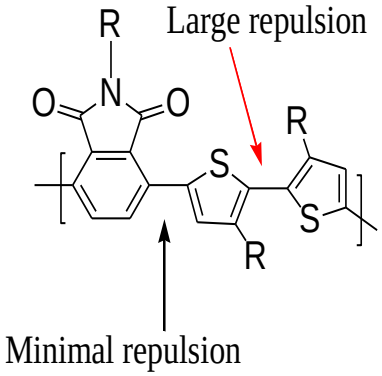

Figure 5.4: D-A polymer with HH bithiophene linkages.

It has been shown that in the special case of using tetrafluorobenzene acceptors, long range order was not disturbed by the presence of HH-dialkyl donor units and the HOMO energy levels of the polymers were very deep.[122] However, when this donor motif was used with nearly any other electron acceptors, as shown in Chapters One and Four, the polymers were usually amorphous and lacked long range order, presumably due to sterically driven backbone twisting from the 3,3'alkyl-subsitiuted linkages. Following

these observations the use of 3,3'-ROT2 was adopted; these donor monomers form attractive S··O interactions and enforce coplanarity of the adjacent thiophene units[36,162] rather than causing steric twisting of the polymer backbones as discussed in Chapter One. Polymers containing this donor unit have been reported to have some very attractive features such as low optical energy gaps, high degrees of intermolecular ordering, and in some cases high charge carrier mobility.[61,113] It has become apparent however, that this design has one major drawback. The strong electron donating nature of the alkoxy groups attached to thiophene backbone, and/or the enforcement of coplanarity by attractive S···O interactions leads to polymers with HOMO energies that are below the ambient stability threshold. Electrochemical measurements as well as long term device instability[113] have clearly demonstrated this point.

5. 1. 4 Proposal for Using Alkyne Spacer Units

The above observations led to the realization that a new donor motif was needed for incorporation into our D-A copolymers. Ideally, a suitable donor would retain the attractive properties of the 3,3'-ROT2 donor units when copolymerized such as low E_g and allow close π-stacking of polymer backbones and simultaneously increase air stability and V_{OC} in device performance. To this end a series of 3,3'-dialkynyl-2,2'-bithiophene donor monomers was developed to achieve this purpose (figure 5.5).

This motif will allow a coplanar backbone to be achieved by reducing steric interactions between the alkyl chains on the adjacent thiophene units. Additionally, the HH linkages will result in minimal steric interactions between bithiophene donor units and adjacent acceptor units, without the use of a spacer in the polymer backbone. Finally, the alkynyl linkages will not act as strong electron donors into the π-system.

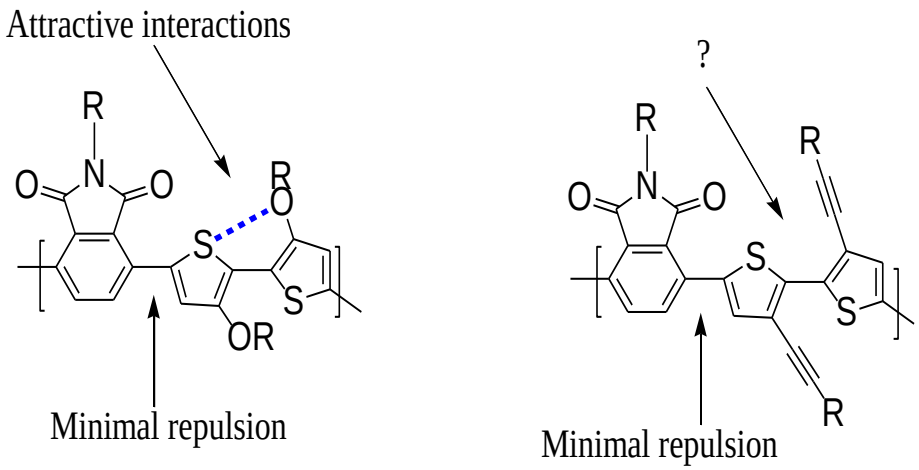

Figure 5.5: 3,3'-dialkoxy- and 3,3'-dialkynyl-2,2'-bithiophene motifs.

All of these factors together should produce polymers with relatively coplanar backbones and deep HOMO energy levels.

5. 1. 5 Literature Precedents

Indeed, some work based on this idea has already been performed by Yamaoto and co-workers. They were the first to prepare a copolymer of 3-(dodec-1-yn-1-yl)thiophene with 1,4-bis-dodecyloxy benzene via Suzuki coupling and compare the polymer with its alkylated counterpart (figure 5.6, **D** and **F**). [163] In-depth studies of the optical and electronic properties were not performed but both solution and solid state absorption maxima for polymer **D** were red-shifted relative to polymer **F** by greater than 80 nm. By comparison, the absorption maximum of the unsubstituted-thiophene based polymer **E** lies in middle of **D** and **F**, with λ_{max} at 486 nm.[164] The absorption profile of the alkynylated-polymer **D** also showed a bathochromic shift of λ_{max} of greater than 60 nm upon going from solution to thin-film with the appearance of fine structure. These observations suggest the polymers were not greatly aggregating in solution and

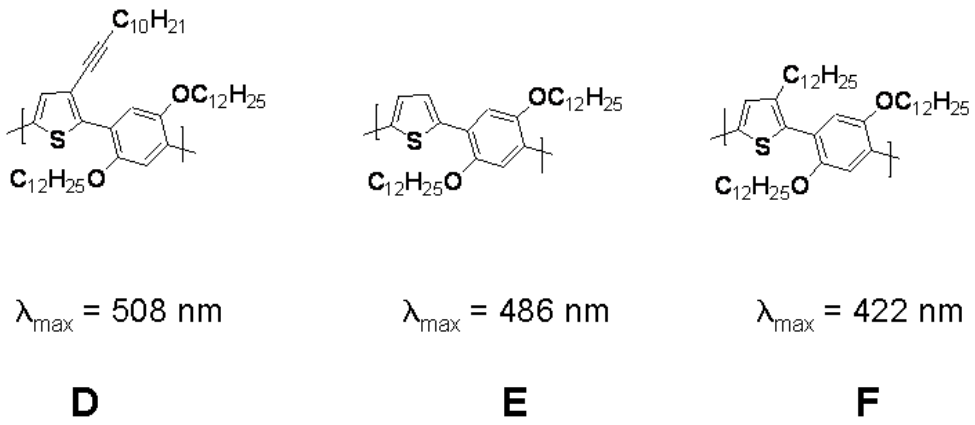

Figure 5.6: Structures and listed thin-film absorption maxima of alkylated (**F**),[163] alkynylated (**D**),[163] and unsubstituted (**E**)[164] polymers.

planarization of the polymer backbone was occurring in the solid state.[165]

They also synthesized the 3,3'-didodecynyl-2,2'-bithiophene homopolymer (**G**, figure 5.7) by palladium-catalyzed polycondensation with $(SnBu_3)_2$.[166] The soluble fraction of the isolated polymer had fairly low number-average molecular weight of 4.4 kDa, but nonetheless had a red-shifted film absorption maximum of 157 nm relative to HH-P3HT[166] (M_n = 37 kDa) and was even slightly red-shifted relative to unsubstituted P3DDT[96](structures **I** and **H**, respectively). Furthermore, single crystal X-ray analysis of 3,3'-didodecynyl-2,2'-bithiophene monomers showed the sp carbons of the alkynyl unit were coplanar with the thiophene ring, and a dihedral angle of only 1° was measured between the adjacent thiophene rings.[166] The monomer crystal structure alone, however, does not necessarily mean that the thiophene units will remain coplanar once incorporated into a polymer. The evidence as a whole from the literature, including both

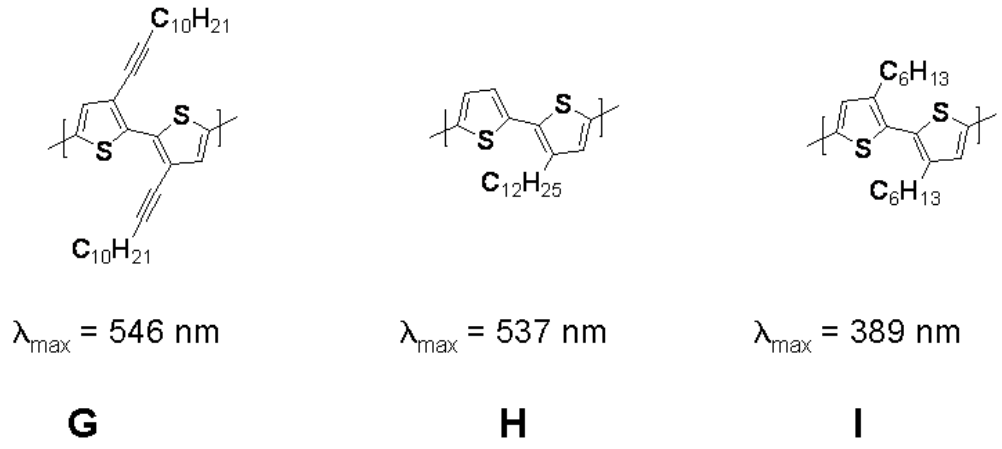

Figure 5.7: Structures and thin-film absorbance maxima for HH-dialkynylated- (**G**), [166] HH-alkylated- (**I**)[166], and unsubstituted-(**H**)[96] polythiophene polymers.

the monomer crystal structure and the polymer UV-Vis data, however, suggested that these units likely to do remain coplanar once incorporated into polymers and warranted the synthesis of these materials.

5. 1. 6 Purpose of This Project

The purpose of this project was to synthesize 3,3'-dialkynyl-2,2'-bithiophene units as donors for D-A polymers, using phthalimide as the acceptor unit. The side chain length and branching pattern on the donor monomers were varied and the structure-property relationships were studied using UV-Vis, electrochemical and WAXD analysis. Finally, comparisons are made of the new polymers with known similar phthalimide based polymers containing 3,3'-dialkyl-, 3,3'-dialkoxy- and unsubsitiuted 2,2'-bithiophene donor units .

5. 2 Synthesis

Initially, I proposed that a large number of terminal alkynes could be synthesized from trimethylsilylacetylene (TMSA) using S_N2 reactions with the appropriate alkyl halides. Despite reports[167] of 50% yields using BuLi as base and stoichiometric HMPT with stirring overnight, the reactions were very sluggish under these conditions. Increasing the temperature and changing from alkyl bromides to iodides did little to increase the reaction rate. After 7 days only 20% conversion could be detected by GC-MS and only 10% yield could be isolated after 1 week, even at elevated temperature. An alternate route, shown in scheme 5.1 was then adopted to isolate the desired alkynes. Commercial alcohols were used to generate the corresponding aldehydes via Swern oxidation.[168] The aldehydes were converted to the final alkynes, **5-3,** by standard Corey-Fuchs methodology.[169] With the alkynes in hand, Sonogashira coupling was attempted using common intermediate **1-15** following Yamamoto's published procedure.[163] The authors reported 80% yield after 24 h reaction time using identical substrates. A complex mixture of products was obtained after work-up that could not be separated. Application of microwave heating and shorter reaction times did not circumvent the problems either. Negishi methodology produced similar results. Finally, a Kumada-type coupling was attempted using palladium as catalyst yielding the alkynylated bithiophenes **5-4** in reasonable overall yields. Lithiation and stannylation were to be carried out

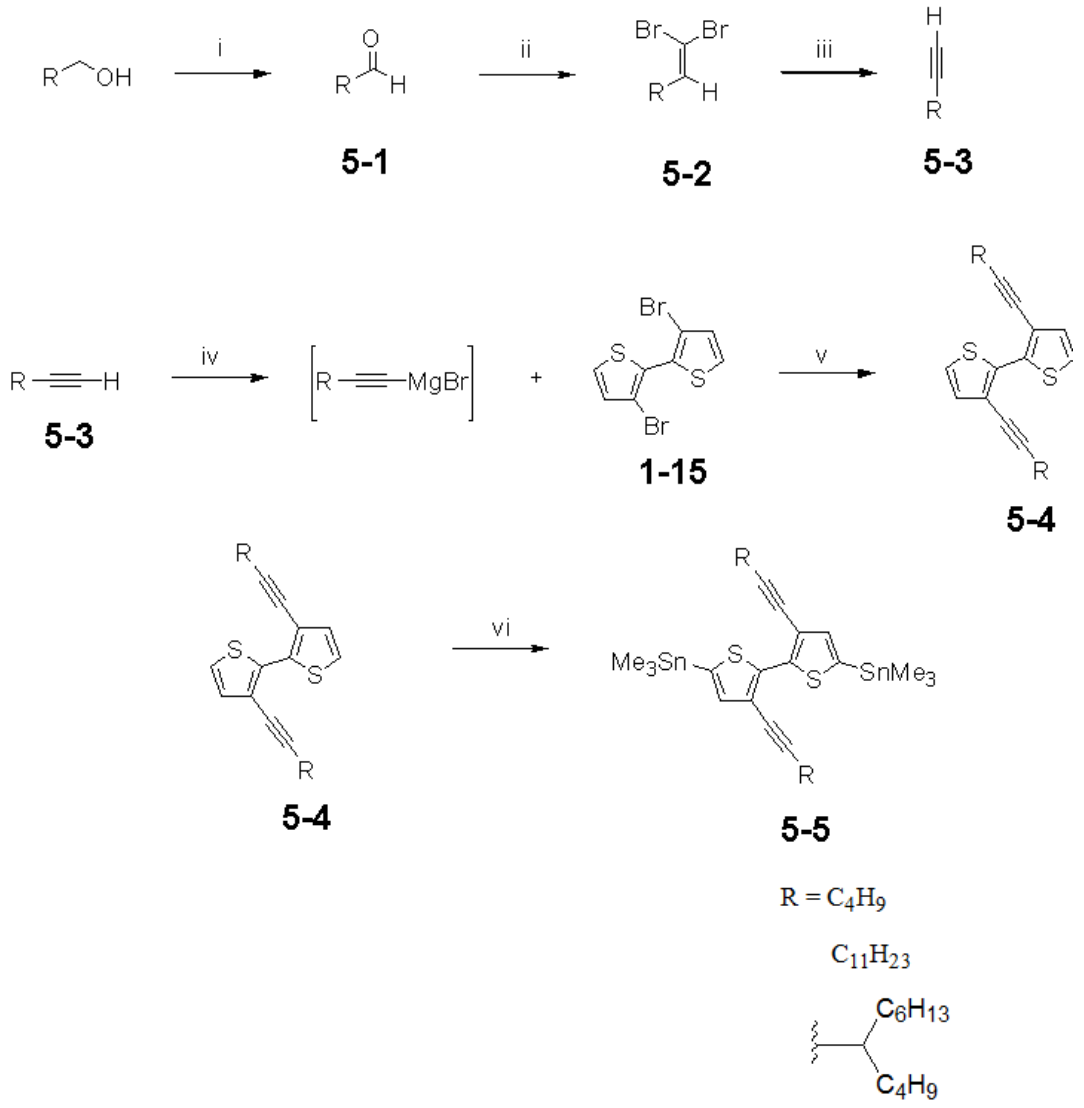

Scheme 5.1: Synthesis of monomers. Reagents and Conditions: i. a) oxalyl chloride, DMSO, DCM, -78 °C. b) ROH. c) NEt_3 -78 °C → rt. ii. a) PPh_3, CBr_4, Zn dust, DCM, 24h. b) RCHO (0.5 eq) 5 h, rt. iii. a) BuLi, THF. b) NH_4Cl (aq). iv) EtMgBr, THF, rt → 50 °C, 2 h. v) $Pd(PPh_3)_4$, THF, 110 °C bath, sealed tube. vi) a) BuLi, Et_2O, -78 °C, 2 h. b) Me_3SnCl/hexanes, -78 °C → rt 4 h.

under the conditions used for the donor monomers described in the previous chapters (3 equivalents of BuLi followd by 3 equivalents Bu_3SnCl). Surprisingly, a complex mixture of products was obtained after work-up via ^1H NMR. Experience with the other bithiophene donor monomers has shown that reacting excess BuLi with the substrates and

quenching with excess Bu_3SnCl gives complete conversion to product. The only contaminate from these reactions is Bu_4Sn produced from reaction of excess BuLi and Bu_3SnCl as evidenced by NMR. Precipitation of the salts from the crude reaction products of **5-5** with pentane followed by solvent evaporation and ^1H NMR analysis provided a spectrum identical to that obtained after aqueous work-up. Returning to the published procedure[163] the solvent was changed to diethyl ether (Et_2O) and 4 eq. of BuLi was used, still producing a mixture of products.

To gain further insights to the reaction pathways small scale reactions were performed using both THF and Et_2O as solvents, with both excess and stoichiometric amounts of BuLi from a freshly titrated bottle and trimethylsilyl chloride as anion trapping agent. Figure 5.8 shows the GC traces of the extreme cases (4 eq. BuLi in THF and 2 eq. BuLi in Et_2O). Excess BuLi in either solvent produced isomeric products as well as tri-silylated products, the proportion being much lower in Et_2O. Even stoichiometric quantities of BuLi in THF led to isomeric mixtures of products. Two equivalents of BuLi using Et_2O as solvent produced the desired product after trapping with TMSCl as evidenced by GC-MS and NMR analysis.

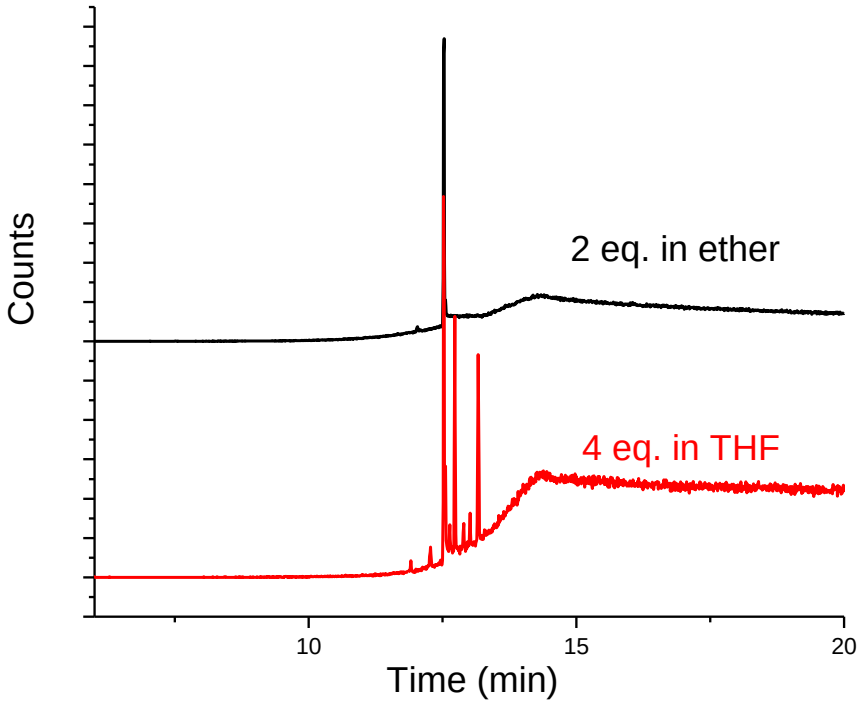

Figure 5.8: GC traces of the product mixture from **5-4** and 2 eq. of BuLi in Et_2O (black) and 4 eq. of BuLi in THF (red)

Finally, Bu_3SnCl was replaced with Me_3SnCl on this project to produce crystalline solids so recrystallization of these monomers could be used as purification. Stille polymerizations were carried out under standard conditions to produce polymers with reasonably high molecular weights (table 5.1).

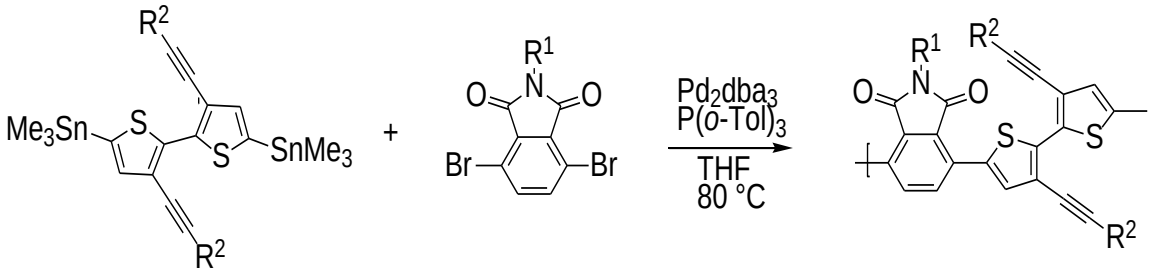

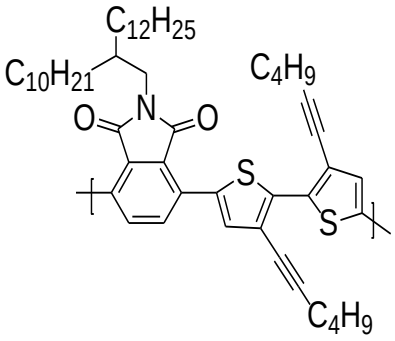

5-P1

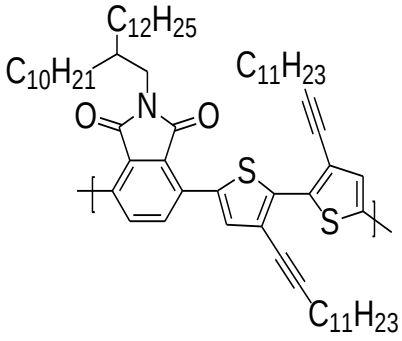

5-P2

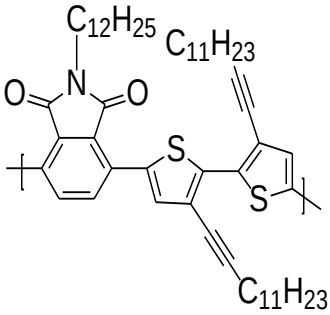

5-P3

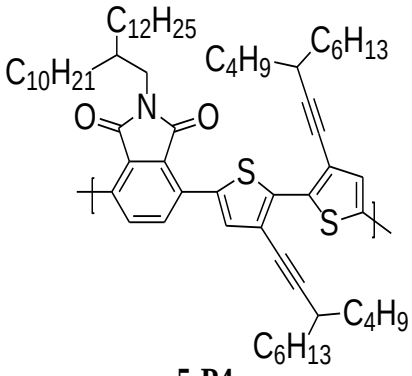

5-P4

Scheme 5.2: Polymerization reaction and structures of the polymers.

Table 5.1: Yields, molecular weights and optical properties of the polymers.

	Yield (%)	Mn (kDa) [PDI]	λ_{max} soln[a]/film[b] (nm)	E_g (eV)[c]	$\Delta\lambda_{max}$ film/soln (nm)
5-P1	66	75 [3.58]	494/520	2.07	26
5-P2	67	101 [3.61]	492/524	2.06	32
5-P3	8[d]	30.1 [5.51]	491/527	2.01	36
5-P4	75	95 [3.45]	478/514	2.16	36

[a] 10^{-5} M in chloroform [b] Spin-coated from 1 mg/mL chlorobenzene solutions and thermally annealed. [c]Estimated from the low-energy absorption edge of annealed thin films using E = 1240 eV· nm/λ. [d] Chloroform soluble fraction.

5. 3 Optical Properties

Figure 5.9 shows the thin-film and solution absorption profiles the polymers. The solution spectra are featureless with λ_{max} values around 490 nm for all of the polymers. Small blue-shifts in λ_{max} occur (table 5.1) as the steric bulk of the side chains increases. **5-P1**, carrying the smallest butyl alkyl-side chain attached to the alkyne spacer, has λ_{max} located at 494 nm. Increasing the alkyl chain length on the alkynyl units to undecyl, **5-P2**, only causes a small blue-shift of 2 nm relative to **5-P1.** Changing the side chains on the phthalimide acceptor from branched N-2-decyltetradecyl to linear N-dodecyl (**5-P2** to **5-P3**) induces a slightly larger blue-shift of 3 nm relative to **5-P1**. This subtle difference is likely due to the large differences in molecular weights of the polymers and solution aggregation effects. Branching the alkyl chains on the donor units in the propargyl position in **5-P4** leads to the largest blue-shift of 16 nm relative to **5-P1**. This is likely due to the steric bulk of the side chains in close proximity to the polymer backbone, as well as increased solubility and reduced aggregation of the polymers in solution. The

onset of absorption is nearly the same for all of the polymers in solution with the exception of **5-P4**, suggesting that they all have similar same main chain conformations regardless of the side chain length used in this study. The UV-Vis measurements suggest these polymers are relatively conjugated in solution, being red-shifted greater than 30 nm relative to rr-P3HT.[170]

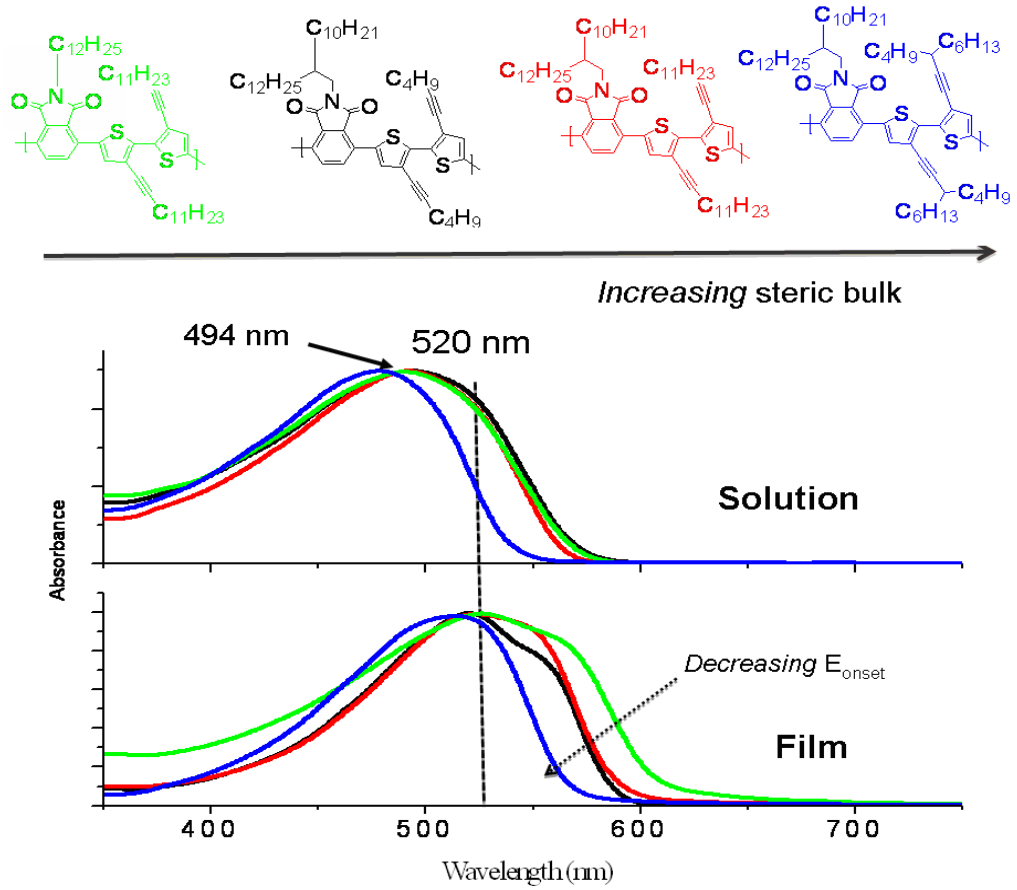

Figure 5.9: Solution (top, 10^{-5} M $CHCl_3$) and annealed thin-film (bottom) absorption spectra.

The thin-film absorption profiles show red-shifts in both λ_{max} and the onset of absorption for all of the polymers, suggesting an increase in conjugation and ordering for the polymers upon going from solution to the solid state. The magnitude of the absorption shifts is dependent on the size of the alkyl chains attached to the alkynyl

spacer. Interestingly, the bulkier side chains produced greater red-shifts upon going from solution to the solid state ($\Delta\lambda_{max}$ film/soln, table 5.1). These effects, however small, are likely a product of aggregation in solution; smaller shifts are observed for the less soluble polymers with shorter side chains due a larger fraction of strongly aggregated species in solution. The absorption maxima in the solid state are similar for all of the polymers. A slight decrease in the E_g for the polymers occurs as the steric bulk on both the donor and acceptors units decrease as shown in figure 5.9. **5-P1** and **5-P2** have a difference in the energy gap of only 0.01 eV, suggesting little impact of the length of the alkyl side chains attached to the alkynyl spacer on conjugation in the solid state. There is however, a small shoulder present in **5-P1** that is absent in **5-P2** suggesting a higher degree of solid state ordering for **5-P1.**[171] A larger difference is noticeable between **5-P1** and **5-P3**. The E_g for **5-P3** is the smallest of the series, 2.01 eV, with a small shoulder present at ~ 560 nm. The difference in the spectra for all of the polymers with regard to fine structure suggests that only the polymers with short, straight side chains are adopting ordered structures in the films (this will be examined further with WAXD below). Similar observations on the degree of polymer ordering have been made for PATs of varying side chain lengths.[172] The relatively high energy λ_{max} and large E_g values suggests that the polymers may be relatively coplanar such as rr-P3HT, however there are likely no strong D-A interactions between the monomer units such as for polymers in Chapter Three based on phthalimide with 3,3'-ROT2 donors.

5. 4 WAXD

To gain a deeper understanding of the nature of the solid state ordering of these polymers, WAXD was measured. The data showed a lack of long-range order for all of the polymers; indeed they are mostly amorphous. Only the polymers with the short butyl chains on the bithiophene donor, **5-P1**, and straight chains on the imide nitrogen and bithiophene unit, **5-P3**, show weak diffractions. Indeed, these are the only two polymers showing small shoulders in the absorption spectra of thin-films. The π-stacking distances measured for **5-P1** and **5-P3** are 3.78 and 3.70 Å, respectively. The weak diffractions from these materials suggest they are forming relatively disordered structures in the solid

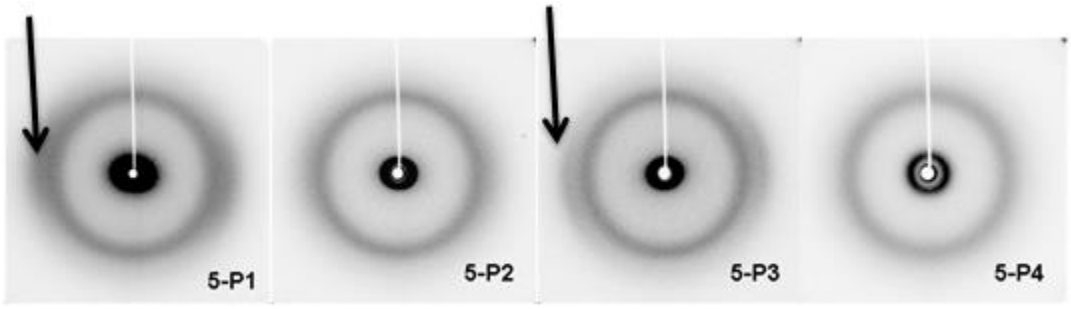

Figure 5.10: WAXD of the dialkynyl polymers. Arrows indicate the diffractions attributed to π-stacking.

state. The absorption spectra suggests that these materials are still relatively conjugated so it is likely that the absence of strong D-A interactions in these polymers does not provide a strong driving force for self-assembly in the solid state. Therefore, the solid state behavior observed in the WAXD is solely is function of space filling and packing of the polymer side chains. Only the materials with smallest and non-branched alkyl side chains can pack in a somewhat ordered fashion. More details on the solid state behavior of these materials will be discussed below.

5. 5 Electrochemistry

DPV results for the polymers are listed in table 5.2 and an FMO energy graph is provided in figure 5.11. Interestingly, a correlation between the side chain length and FMO energies is observed. Increasing the alkyl chain length from 4 carbons in **5-P1** to 11 carbons in **5-P2** results in a ~ 0.1 eV decrease in E_{HOMO} and ~ 0.15 eV decrease in E_{LUMO} with a constant E_g. **5-P3**, the only polymer containing straight chains on both the donor and acceptor units was found to have an E_{HOMO} 0.1 eV shallower than **5-P1** and a lower optical energy gap by 0.6 eV. Branching of the side chains in **5-P4** produces the deepest E_{HOMO} of -5.89 eV of the group with an E_{LUMO} similar to **5-P2**.

Table 5.2: Electrochemical results for the polymers

	E_{HOMO} (eV) [a]	E_{LUMO} (eV) [b]	E_g [c]
5-P1	-5.64 ± 0.03	-3.57	2.07
5-P2	-5.76 ± 0.02	-3.70	2.06
5-P3	-5.54 ± 0.02	-3.53	2.01
5-P4	-5.89 ± 0.06	-3.73	2.16

[a]DPV measurements of drop-cast thin-films versus Fc/Fc^+. [b]Estimated from $E_{LUMO} = E_{HOMO} + E_g$. [c]Optical energy gap estimated from the absorption edge of thin-films annealed at 200 °C.

The electrochemical results in combination with the UV-Vis and WAXD studies suggests that self-assemble these materials is quite sensitive to side chain length and branching, both on the imide nitrogen and alkynyl positions. According to Roncali[25] and as discussed in Chapter One, the energy gap of conjugated polymers, hence the HOMO and LUMO energy levels depend on five factors: bond length alteration, deviation of the

polymer backbone from planarity, electronic effects of the substituents, aromatic resonance energy, and intermolecular (chain) coupling the solid state. The first four "terms" should be the same within this series of polymers, identical aromatic cores were used and the environment in the immediate vicinity of the conjugated backbones is similar due to the alkynyl spacers. The similar solution absorption profiles further support this for polymers **5-P1** through **5-P3**. Branching the alkyl chains in **5-P4** likely results in backbone twisting and a relative blue-shift in the solution absorption profile. Therefore, the origin of the electrochemical differences is likely intermolecular;

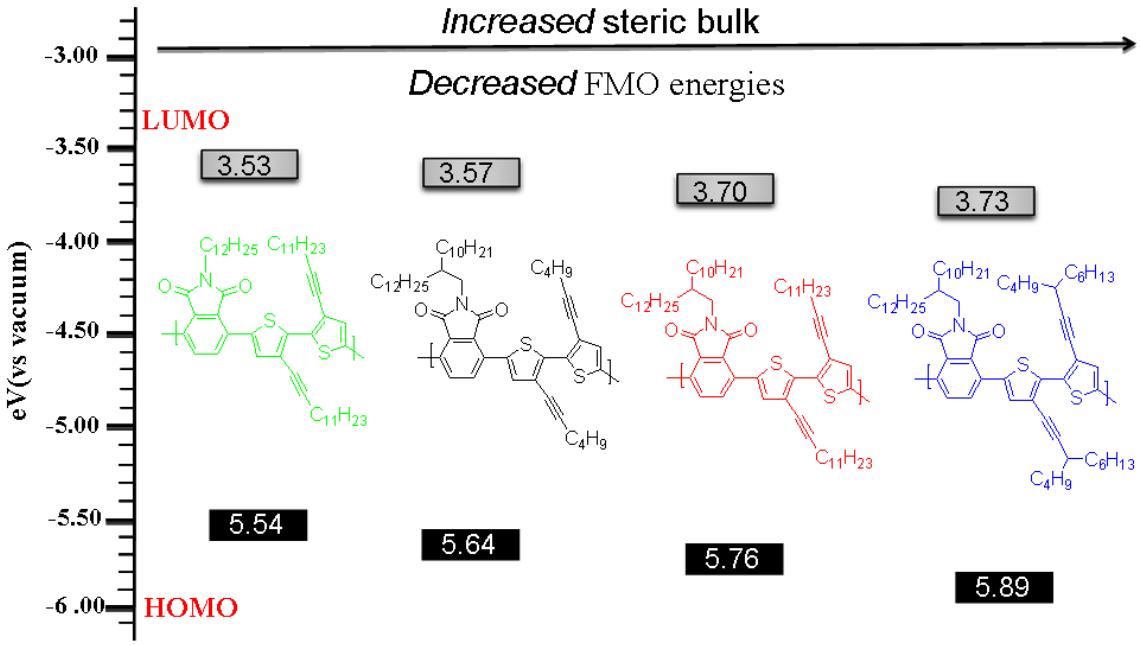

Figure 5.11: FMO energy graph of the polymers as a function of increasing steric bulk.

stronger interchain coupling in the solid state occurs only with those polymers carrying smaller side chains due to space filling demands, as evidenced by lower FMO energies and by the absorption spectra. WAXD further supports this conclusion. The only polymers with discernable diffractions are **5-P1** and **5-P3**, the materials with least

sterically demanding side chains. As the bulkiness of the side chains increases in **5-P2** and **5-P4** WAXD diffractions are not observed, fine structure in the absorption profiles disappear and the FMO energies decrease.

5. 6 Comparison of the "Spacer" Groups Used in Bithiophene Donor Units

5. 6. 1 Polymer Structures Compared in This Study

The goal of synthesizing these monomers was to find a suitable replacement for dialkoxy- and dialkyl-bithiophene donors. The following section discusses the influence of the side chains of the donor monomers using phthalimide acceptor monomers. It is noted here that the structures (figure 5.12) are very similar, but slightly vary in the chain lengths on the N-imide nitrogen atoms. However, we have found that the length of the branched chains on the N-imide positions does not greatly affect the absorption profiles and oxidation potentials of these polymers. These factors are mainly dependant on backbone torsion and electronic properties of the donors. Polymer **5-P2** will be used for comparison throughout this section due to the similarity of its alkynyl side chain length with the other polymers shown in figure 5.12.

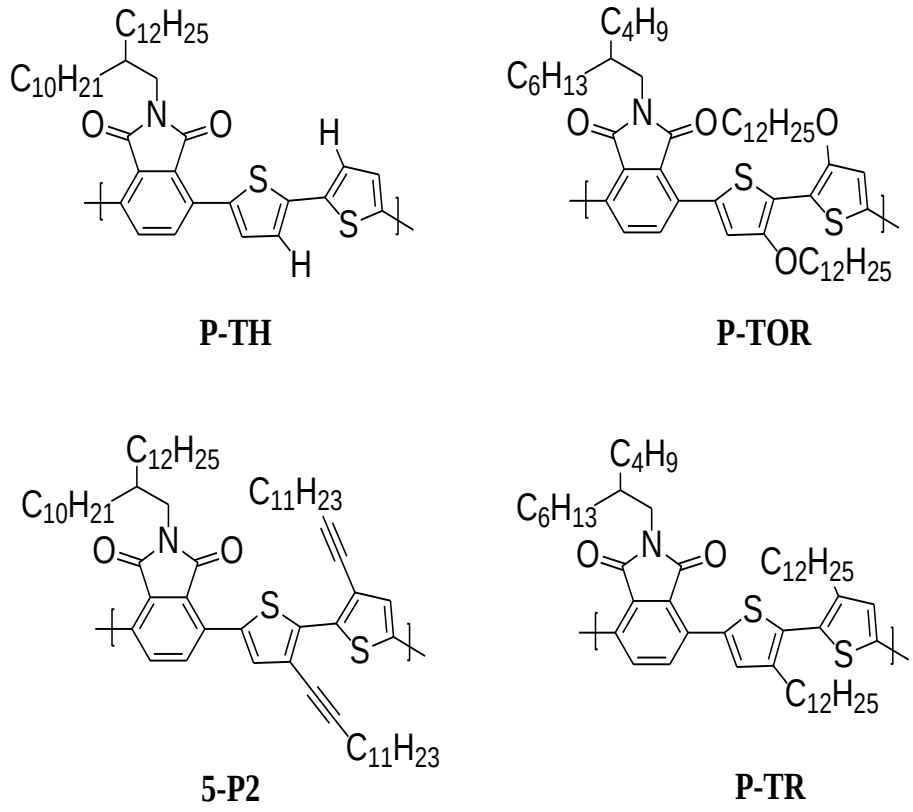

Figure 5.12: Structures of the polymers in discussion. **P-TH** and **P-TR** are unpublished materials that were synthesized and studied in our lab by Xugang Guo.

5. 6. 2 Optical Properties

The thin-film absorption maximum for **5-P2** is red-shifted relative to **P-TR** by > 110 nm and even slightly red-shifted by 6 nm relative to **P-TH**. Figure 5.13 shows the thin-film absorption profiles for the polymers. The large blue-shift for **P-TR** of > 110 nm relative to **5-P2** and **P-TH** clearly shows the effects of the HH-dialkyl units and the loss of conjugation in this polymer. A well defined shoulder, present for **P-TH** is absent for both **P-TR** and **5-P2**. It is noted, however, that the absorption profiles for the films of **5-P2** and **P-TH** are nearly the same regarding the λ_{max} values, peak widths and energy

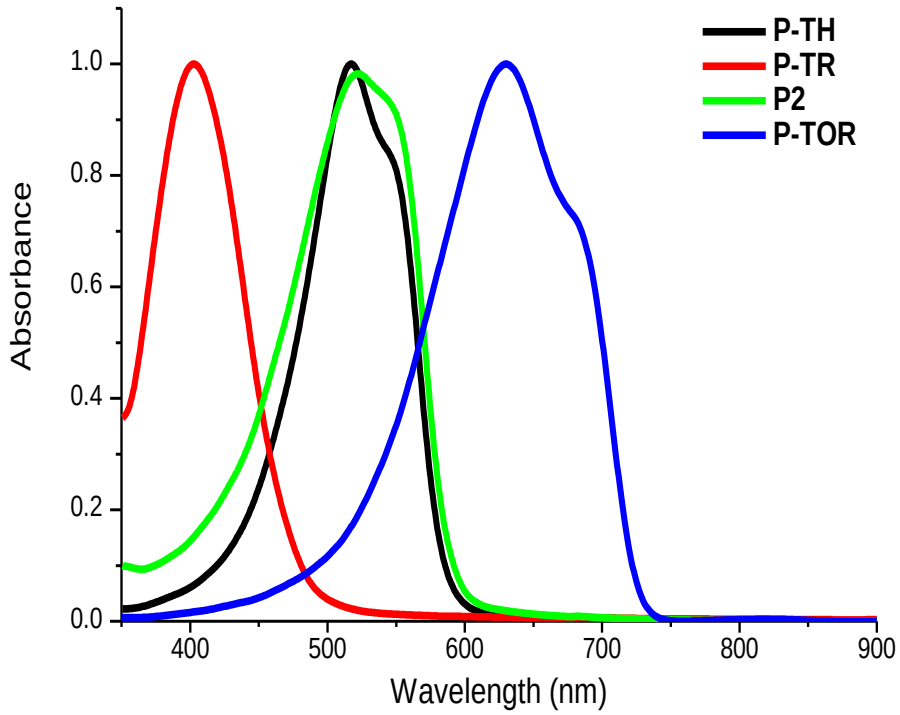

Figure 5.13: Comparison of annealed thin-film absorption profiles for phthalimide based polymers with donors of varying strength.

gaps. This implies that the effective conjugation for **5-P2** is not disrupted by the presence of the alkynyl spacers between the alkyl side chains. Comparing **5-P2** relative to **P-TOR**, a large blue-shift in both λ_{max} and E_g is observed. This is due to the absence of strongly electron donating side chains and/or attractive S···O interactions.

5. 6. 3 Electrochemistry

The estimated FMO energies for the polymers are listed in table 5.3. **5-P2** and **P-TR** have similar HOMO energies of -5.76 and -5.78 eV, respectively, compared to unsubstituted **P-TH** with an E_{HOMO} of -5.64 eV. The UV-Vis data shows that **5-P2** and **P-TH** each have an E_g of ~ 2.01 eV and that **P-TR** is a twisted species with a 0.4 eV

larger energy gap than **5-P2** and **P-TH**. The similar optical energy gaps and thin-film absorption profiles of **5-P2** and **P-TH** suggests that these materials have the same

Table 5.3: Electrochemical results for polymers with various donor side chains.

	E_{HOMO} (eV)[a]	E_{LUMO} (eV)[b]	E_g (eV)[c]
5-P2	-5.76	-3.74	2.02
P-TH	-5.64	-3.63	2.01
P-TR	-5.78[d]	-3.37	2.41
P-TOR	-5.12	-3.43	1.69

[a]DPV measurements of drop cast thin-films versus Fc/Fc^+. [b]Estimated from $E_{LUMO} = E_{HOMO} + E_g$. [c]Optical energy gap estimated from the absorption edge of thin-films annealed at 200 °C. [c]Measured by CV.

relative conjugation. The electrochemical data shows that **5-P2** has both a deeper E_{HOMO} and E_{LUMO} than **P-TH** by ~ 0.1 eV, suggesting that the alkynyl donors are in fact not acting as donors at all relative to hydrogen, rather then, acceptors. However, recalling the side chain length dependence on the FMO energies for the alkynyl polymers (figure 5.11), comparison of **P-TH** and shorter chain **5-P1**, shows that their FMO energies are nearly the same. If the alkynyl linkages were indeed acting purely as acceptors (relative to hydrogen) with all other factors being equal, a relative decrease for the FMO energies should be observed with **5-P1** as well. This again suggests that the variation in FMO energies is purely a manifestation of solid state effects. Comparing with **P-TOR**, a large difference in FMO values are observed, again highlighting the effects of the electron donating oxygen atom attached to the polymer backbone.

5. 6. 4 WAXD

The WAXD for the four polymers discussed above is shown in figure 5.14. As can be seen for **5-P2** and as was discussed above, intense diffractions are absent. This gives rise to a similar WAXD profile as that for the alkylated polymer, **P-TR**. The UV-Vis data suggests the length of conjugation for **5-P2** and **P-TH** are similar. If the complete lack of any D-A interactions alone is to blame for the lack of order in **5-P2** then

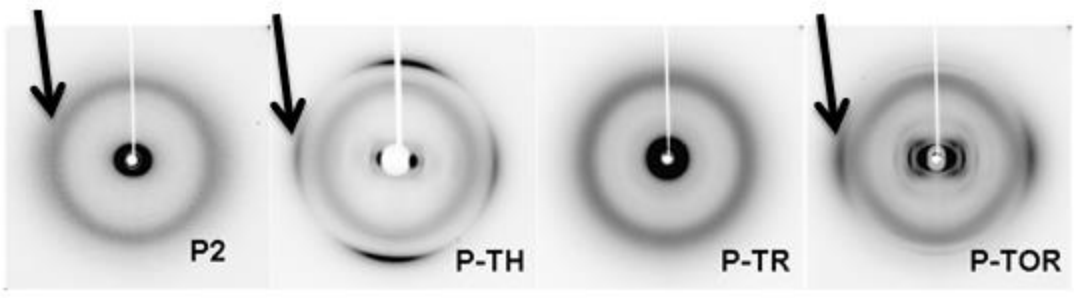

Figure 5.14: WAXD of polymers with varying donor side chain motifs. **P-TH** and **P-TR** were measured by Xugang Guo (unpublished). Arrows indicate the diffractions attributed to π-stacking.

it is reasonable to expect a WAXD pattern similar to that of **P-TH**. As can be seen in figure 5.14 however, this is not the case. This suggests that the lack of solid state ordering is due to presence of the alkyl chains attached to the alkynyl spacer. Indeed the diffractions attributable to π-stacking are more intense for the short chain alkynyl polymers **5-P1** and **5-P3**. Finally, **P-TOR** produces the most structured patterns of the series with π-stacking distance of 3.8 Å. This is likely a combination of enforced backbone coplanarity due to S···O interactions and strong D-A interactions within the polymer backbone, producing a strong driving force for self organization.

5. 7 Conclusions

3,3'-Dialkynyl-2-2'-bithiophene donor units were successfully synthesized and copolymerized with phthalimide acceptor units. The initial goals of retaining a coplanar polymer backbone while decreasing HOMO energies relative to vacuum were achieved with the new donor. Conjugation within the polymer backbone does not appear to be disrupted by the HH-linkages in these polymers; a stark contrast to what is generally observed with HH-dialkyl bithiophene containing polymers as seen in Chapters 1 and 4. The optical properties for this particular class of phthalimide-based material are similar to those of unsubstituted bithiophene donor units. Both HOMO and LUMO energies are decreased by ~0.1 eV relative to the bithiophene based polymer, implying an electron withdrawing effect of the alkyl linkages relative to hydrogen. Finally, these materials lacked long range order as evidenced by WAXD measurements. Apparently, the side chains, while not destroying conjugation of adjacent monomer units, do not allow long range registry of the polymers in the solid state and would likely be detrimental in OE applications.

Chapter Six: Summary and Future Outlook

6. 1 Summary

The field of OE has witnessed impressive growth over the past five years due to advances in materials chemistry, materials science, and device engineering. The major goal of this research was to further this technology by contributing novel polymers to this field. Cyanoarene acceptor units were synthesized and shown to produce D-A polymers with FMO energy levels sufficient for p-type operation. FMO energy levels were found to be dependant on the type of aromatic core that the cyano-groups were attached to. Cyanobenzene-based polymers had deeper HOMO energy levels and larger energy gaps than cyanothiophene-based polymers in agreement with Roncali's E_g model presented in Chapter One.

Branched side chains on 3,3'-ROT2 donor units were shown to effectively increase the solubility for phthalimide-based polymers relative to 3,3'-ROT2 donors carrying non-branched side chains. The HOMO energy levels for the branched chain polymers were also deeper relative to polymers with non-branched side chains on the donor units, suggesting that they may produce devices with greater performance in OPV applications. Spin-coating polymer films from a wide range of solvents and SVA experiments showed that the solid state behavior of two of these polymers can be controlled simply by spin-coating from "marginal" solvents or annealing the films for prolonged periods with the casting solvents. Additionally, a novel, fluorinated phthalimide acceptor unit was synthesized and used for polymerization with a 3,3'-ROT2 unit. The resulting copolymer was found to have identical HOMO energies then the non-fluorinated polymers and a larger E_g.

Novel indanedione functionalized D-A polymers were reported for the first time in Chapter Four. An alternative route to produce the key precursor to phthalimide and indanedione acceptors, 3,6-dibromophthalic anhydride, was also devised. The polymers in Chapter Four were shown to achieve long ranger order despite the presence of orthogonal side chains within the polymer backbone. HOMO energies relative to phthalimide-based D-A polymers were not greatly affected by incorporation of this unit into the polymer backbones. The E_g and LUMO energies for these polymers were found to decrease slightly relative to polymers containing identical donors with phthalimide-based acceptors.

In Chapter Five 3,3'-dialkynyl-2,2'-bithiophene units were reported and copolymerized with phthalimide acceptors. Copolymerization with this unit produced materials that had similar properties to polymers containing unsubstituted bithiophene donors. Additionally, it was found that properties of these polymers were very sensitive to the side chain length of the alkyl units attached to the alkyne spacer.

6. 2 Outlook

The obvious next-step for these materials is device testing and device optimization. Many of the cyanoarene polymers presented in Chapter One possessed the appropriate FMO energy levels and favorable solid state ordering (by WAXD) for device operation. The decreased HOMO energies and increased solubility for the polymers in Chapter Three based on branched chain 3,3'-ROT2 units suggests that they may display increased OPV performance in relative to **PhBT-12**. There is much room for further expansion of the indanedione-based polymers. WAXD and UV-Vis spectroscopy

suggests that these materials display good long-range order. A derivative of fluorene-based polymers based on a 9-alkylidene-9H-fluorene unit has been reported in the literature and is shown (**6-P1**) in figure 6.1.[180] The authors found that the alkylidene-based polymer produced OPVs with PCE twice as high as the analogous fluorene-based polymer. Furthermore, they found that **6-P1** possessed higher crystallinity than **6-P2**, resulting in higher charge carrier mobility, and lower E_g. Therefore, it would be reasonable to expect that moving the branching position farther away from the polymer backbones would impart similar

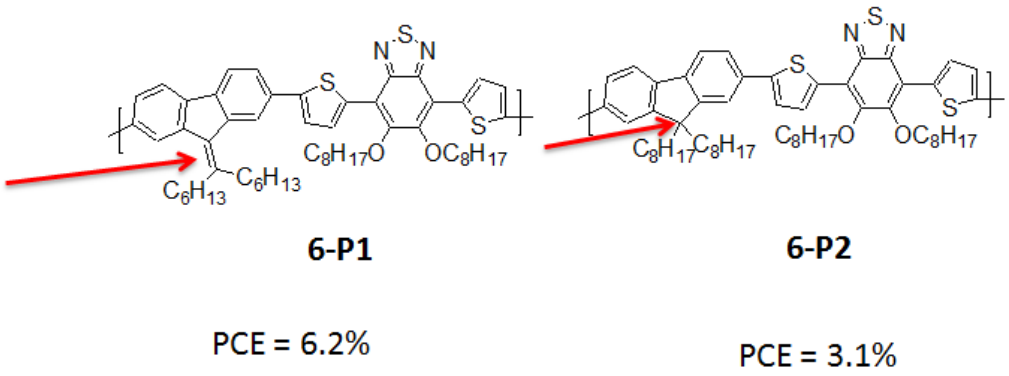

Figure 6.1: Structures and PCEs of alkylidene- and alkyl-fluorene-containing polymers.[180]

improvements in the indanedione-based polymers. I have synthesized two alkylidene-dione based acceptor monomers, shown in scheme 6.1. Copolymerization of the

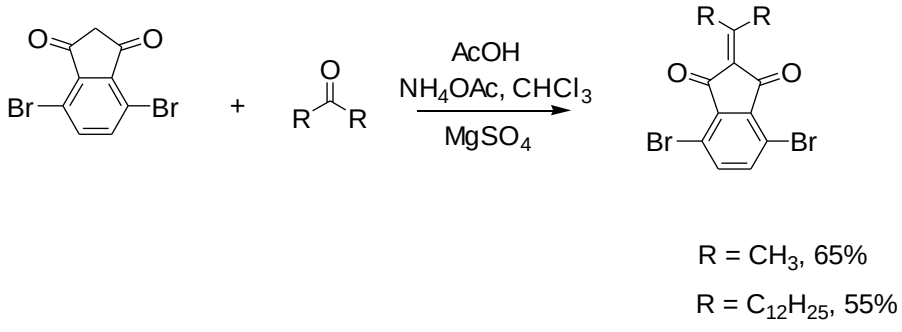

Scheme 6.1: Synthesis of alkylidene-dione acceptor monomers.

monomers with the branched chain 3,3'-ROT2 donors used in Chapters Three and Four will produce polymers **6-P3** and **6-P4.** The properties of these polymers, including device performance, can then be compared with the materials in Chapter Four and the function of the orthogonal side chains on the indanedione motif can be further studied.

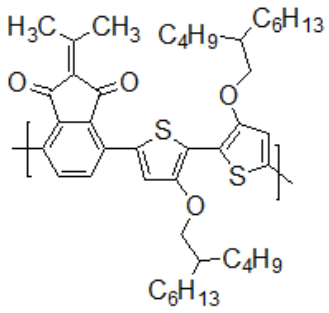

6-P3

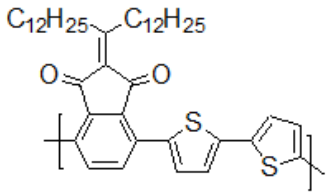

6-P4

Figure 6.2: Proposed alkylidene-indanedione-based polymers.

The indanedione acceptors can also be functionalized with electron withdrawing groups to produce polymers with deeper FMO energy levels and possibly n-type OTFT properties. 2-Dicyanomethyleneindane-1,3-dione is a known compound and its synthesis has been reported in the literature.[175-177] The proposed synthesis of di-brominated 2-dicyanomethyleneindane-1,3-dione is shown in scheme 6.2. Direct bromination of the phenyl ring of ninhydrin to produce **6-4** would likely not occur without decomposition of indanedione moiety. Therefore, this synthesis begins with the di-brominated indanedione derivative as described in Chapter Four. A similar synthesis reported in the literature to produce 5-bromo-ninhydrin will then produce **6-4**.[178] Finally Knoevengal reaction with malonitrile will produce the final monomer **6-5.**[179] Polymers based on this acceptor will likely suffer from poor solubility as did the cyanoarene polymers in Chapter One.

Therefore, it will be necessary to copolymerize this unit with donors that have large branched side chains.

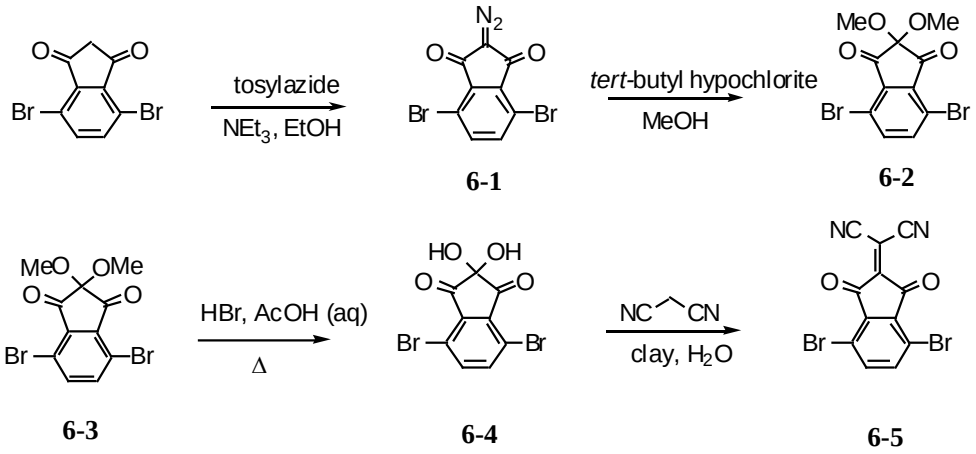

Scheme 6.2: Proposed synthesis of the brominated 2-Dicyanomethyleneindane-1,3-dione monomer.

It is possible that the dicyanomethylene moiety in **6-5** will not be chemically inert during polymerization reactions. Small molecule studies on the Stille reaction of monomer **6-5** with aromatic bromides, complete with careful product characterization will be necessary before polymerization. Nevertheless, the potential reactivity of **6-5** could provide a synthetic handle for further functionalization of the monomer before polymerization (see references 183 and 184 for examples of this reactivity).

Finally, fluorination of the indanedione moiety may also be achieved to lower FMO energy levels and serve to increase self ordering. A brominated difluorodioxocyclopenta-[*c*]thiophene has been reported in the literature, the reaction is shown in scheme 6.3. Fluorination of the indanedione can be achieved in a similar manner, using an electrophilic source of fluorine, either N-fluoro-6-(trifluoromethyl)pyridinium-2-sulfonate (MEC-O4B)[181] or Selectfluor®[182].

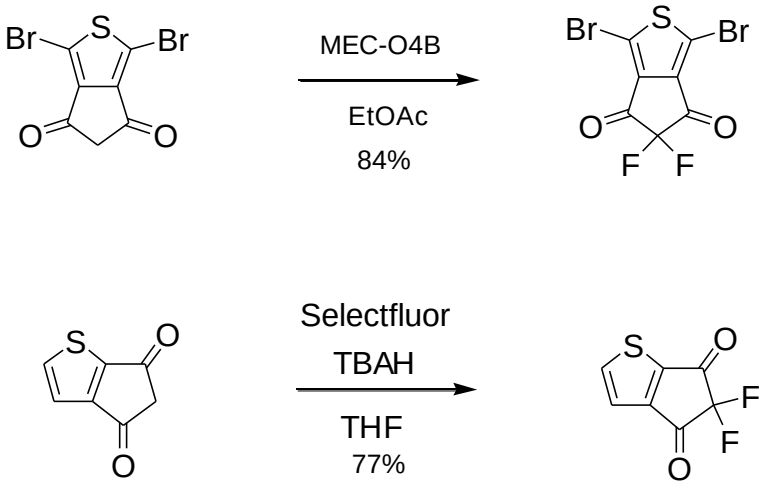

Scheme 6.3: Synthesis of fluorinated thiophene-dione derivatives reported in the literature.[181,182]

The resulting acceptor unit may then be copolymerized with a variety of donor units for the fabrication of n-type OFET materials.

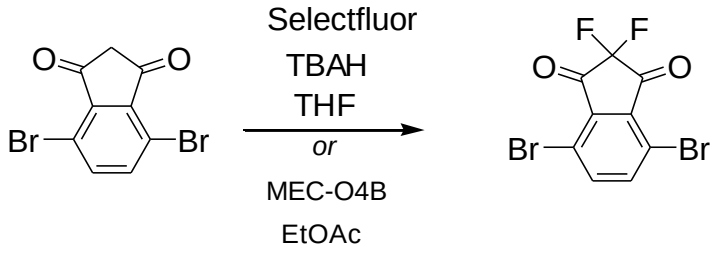

Scheme 6.4: Proposed synthesis of fluorinated indanedione acceptor.

Chapter Seven: Experimental Details

7. 1 General Experimental Details

All solvents used for synthesis were distilled from appropriate drying agents and stored under N_2 over molecular sieves. THF was freshly distilled from Na/K alloy before use. n-butyllithium was purchased from Acros as a 2.5 M solution in hexanes. Anhydrous DMF was purchased from Acros and used for all reactions without further purification. All other materials were used as purchased unless otherwise stated. All reactions were carried out in oven dried glassware under N_2 atmosphere using standard Schlenk techniques unless otherwise stated. ^{1}H and ^{13}C NMR spectra were recorded on a Varian INOVA 400 MHz spectrometer (purchased under the CRIF program of the National Science Foundation, grant CHE-9974810) and referenced to residual protio-solvent signals. Relative molecular weight determinations of polymers were made at room temperature with THF as eluent at a flow rate of 1 mL/min using a Waters 600E HPLC system, driven by Waters Empower Software and equipped with two linear mixed-bed GPC columns (American Polymer Standards Corporation, AM Gel Linear/15) in series. Eluting polymers were detected with both refractive index and photodiode array detectors. The system was calibrated with 11 narrow PDI polystyrene samples in the range of 580 - 2 $x10^6$ Da. GC-MS data were collected from an Agilent Technologies 6890N GC with 5973 MSD.

Polymer melting points are reported as the endothermic maxima of 1^{st} order transitions measured by differential scanning calorimetry using a Mettler 822^e DSC, with a heating rate of 10 ºC/min, under nitrogen. Differential pulsed voltammograms were collected on a BAS 100 B/W electrochemical analyzer. A three electrode setup using a platinum

button working electrode, platinum wire counter electrode and silver wire reference electrode was used and referened to Fc/Fc^{+}. Thin-films were drop cast from 1 mg/mL toluene solutions and measured using 0.1 M tetra-*n*-butylammonium hexafluorophosphate as electrolyte in acetonitrile at a scan rate of 20 mV/s. The electrolyte solution was thoroughly purged with N_2 before all measurements. UV-Vis spectra were collected on Varian Cary 1 UV-Visible spectrometer. All of the final 3,3'-dialkyl-, and 3,3'-dialkoxy-2,2'-bithiophene donor monomers were synthesized following published procedures.[61]

7. 2 Synthetic Details for Chapter Two

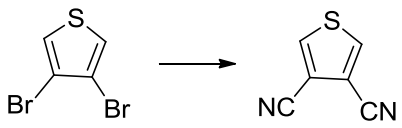

3,4-Dicyanothiophene A solution of 3,4-dibromothiophene (15.00 g, 62.00 mmol) and CuCN (16.66 g, 186.0 mmol) in DMF (65 mL) was refluxed for 7 h. The oil bath was cooled to 60 °C and a solution of $FeCl_3$ (16.0 g) in 80 mL of 1.7 M HCl was added. The reaction was cooled to room temperature after 1 h and filtered. The filtrate was extracted with dichloromethane (5 x 100 mL) and the combined organic layers were washed with 10% HCl (2 x 150 mL) and brine. After drying over $MgSO_4$ and evaporating the solvent under reduced pressure a yellow solid was obtained. The crude product was filtered through a silica gel plug using dichloromethane as eluent followed by precipitation from

a minimum amount of dichloromethane into hexanes to yield 5.00 g (60%) of colorless solid. ^{1}H NMR ($CDCl_3$) δ 8.14 (s, 2H). ^{13}C NMR δ 141, 111, 120.

3-Thiophenecarbonitrile A solution of 3-bromothiophene (10.00 g, 63.30 mmol) and CuCN (8.24 g, 92.0 mmol) in DMF (15 mL) was heated to 170 °C for 7 h. The flask was cooled to 60 °C and a solution of $FeCl_3$ (16.0 g) in 80 mL of 1.7 M HCl was added. The reaction was cooled to room temperature after 1 h and filtered. The filtrate was extracted with dichloromethane (5 x 100 mL) and the combined organic layers were washed with 10% HCl (2 x 150 mL) and brine. After drying over $MgSO_4$ and evaporating the solvent under reduced pressure a dark green liquid was obtained. The crude product was chromatographed on silica gel using dichloromethane as eluent yielding 4.667 g (70%) colorless liquid. ^{1}H NMR ($CDCl_3$) δ 7.93 (dd, 1 H), 7.42 (m, 1 H), 7.29 (dd, 1 H). ^{13}C NMR δ 142, 135, 130, 111, 116.

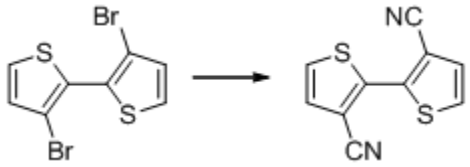

3,3'-Dicyano-2,2'-bithiophene 3,3'-Dibromo-2,2'-bithiophene (1.501 g, 4.629 mmol), CuCN (1.658 g, 18.51 mmol) and DMF (10 mL) were stirred at reflux under N_2 overnight. After cooling to 60 °C a solution of 1.26 g $FeCl_3$ in 24 mL of 1.7 M HCl was

added and the mixture was stirred for 1 h. The solution was filtered and the filtrate was extracted with DCM (4 x 100 mL). The combined organic layers were washed with 10% HCl, brine and concentrated to give 2.01 g yellow solid. The crude product was chromatographed using DCM as eluent to give 1.07 g light yellow solid (87%). ^{1}H NMR (CDC l_3) δ 7.51 (d, 2 H), 7.34 (d, 2 H). ^{13}C NMR ($CDCl_3$ 100 MHz) δ 141, 130, 128, 114, 110.

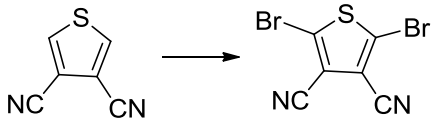

2,5-Dibromo-3,4-dicyanothiophene. 3,4-Dicyanothiophene (0.4293 g, 3.669 mmol), N-bromosuccimide (1.6327 g 9.173 mmol) and trifluoroacetic acid (10 mL) were combined in a vacuum flask. The mixture was stirred until homogeneous (~ 5 minutes) and sulfuric acid (2.5 mL, 18 M) was added drop wise. After 5 h the reaction was quenched by slow addition of a saturated sodium bicarbonate solution. DCM was added and the layers were separated. The aqueous layer was extracted (3 x 25 mL) with DCM, dried over $MgSO_4$ and concentrated. The resulting yellow solid was purified by vacuum sublimation (0.1 torr, 120 °C) followed by recrystallization from ethanol yielding colorless needles, 0.516 g (48 %). ^{1}H NMR ($CDCl_3$) No proton observed. ^{13}C NMR ($CDCl_3$ 100 MHz) δ 125, 116, 110.

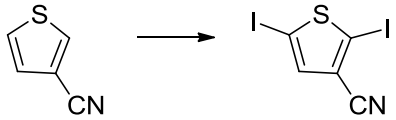

2,5-Diiodo-3-thiophenecarbonitrile This compound was prepared in the same manner as 3,6-diiodophthalonitrile (below). The product was purified by silica gel chromatography using dichloromethane as eluent followed by recrystallization from ethanol (35%). ^{1}H NMR (CDC l_3) 7.20 (s). ^{13}C NMR ($CDCl_3$ 100 MHz) δ 139, 122, 113, 90, 78.

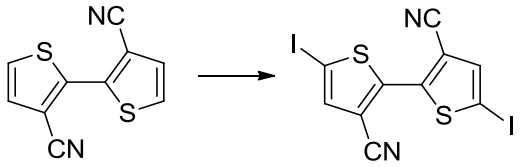

3,3'-Dicyano-5,5'-diiodo-2,2'-bithiophene This compound was prepared in the same manner as 3,6-diiodophthalonitrile. The product was recrystallized from DMSO four times. The recrystallized solid was sonicated in THF for 15 minutes and collected by filtration to give yellow powder, 60%. ^{1}H NMR (DMSO, 80 °C) δ 7.90. Due the very poor solubility of this monomer in organic solvents ^{13}C was not recorded.

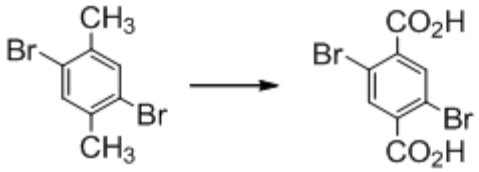

2,5-Dibromoterephthalic acid To a refluxing solution of 2,5-dibromo-*p*-xylene (10.00 g, 38.01 mmol) in pyridine (166 mL) was added a solution of potassium permanganate (40.46 g, 63.34 mmol) in water (110 mL). The solution was stirred at reflux overnight

and cooled. The resulting brown solid was collected on a Buchner funnel and washed with hot water. The filtrate was filtered through a pad of celite and acidified with 6 M HCl. A colorless solid was collected by filtration and added to a solution of 5.06 g KOH in 85 mL water. The mixture was heated to reflux and 12.0 g $KMnO_4$ in 175 mL of water was added. After stirring overnight methanol was slowly added to the solution until the purple color disappeared. The heterogeneous solution was filtered through a pad of Celite and concentrated to approximately 75 mL. 6 M HCl was added until the solution was acidic to pH paper and the colorless precipitate was collected by filtration. The crude product was used without further purification (10.05 g, 82%).

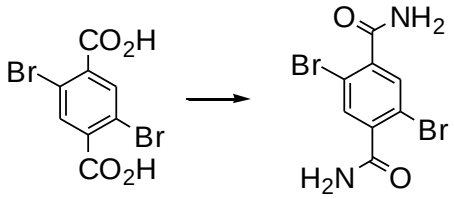

2,5-Dibromoterephthalamide To a stirring solution of 2,5-dibromoterephthalic acid (5.00 g, 15.4 mmol), benzene (70 mL) and two drops of DMF was added oxalyl chloride (2.69 g, 21.2 mmol) in one portion. The mixture was refluxed for 2 h. After cooling, 250 mL of 3 M ammonium hydroxide was added to the solution in one portion and the resulting tan solid was collected by filtration, thoroughly washed with water, methanol and ether to yield 4.35 g, (88%.) of tan solid. ^{1}H NMR (DMSO) δ 8.01 (s, 1 H), δ 7.72 (s, 1H), δ 7.63 (s, 2H). ^{13}C (DMSO) δ 167, 141, 133, 117.

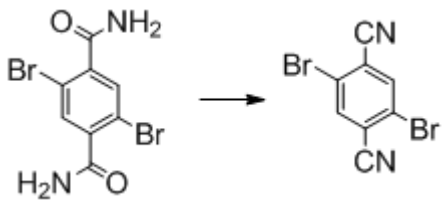

2,5-Dibromoterephthalonitrile 2,5-Dibromoterephthalamide (0.2792 g, 0.8674 mmol) and P_2O_5 (0.4925 g, 3.470 mmol) were combined and thoroughly ground together under N_2. The solid mixture was heated to 140 °C for 2 h. Ice water was carefully added and the aqueous layer was extracted with ethyl acetate (5 x 50 mL). The combined organic layers were washed with brine, dried and evaporated to give a light yellow solid which was chromatographed on silica gel using a gradient elution (4:5 hexane/DCM → DCM). The light yellow solid was recrystallized from ethyl acetate to give colorless powder (0.1041 g, 42%). ^{1}H NMR (dioxane) δ 8.23, (s, 1H). ^{13}C NMR (dioxane 100 MHz) δ 142, 128, 125, 119.

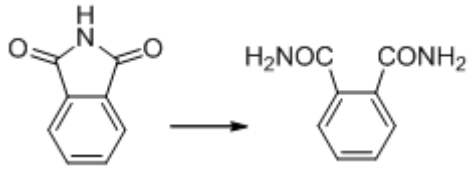

Benzene-1,2-dicarboxamide Phthalimide (10.5 g, 71.2 mmol), concentrated ammonium hydroxide (40 mL) and absolute ethanol (25 mL) were combined and the heterogeneous solution was stirred overnight at room temperature. The solid was collected by filtration and washed with equal volumes of ammonium hydroxide, water and ethanol. The

colorless solid was dried and used without further purification, 9.80 g. Due to poor solubility in all tested solvents analytical data were not collected.

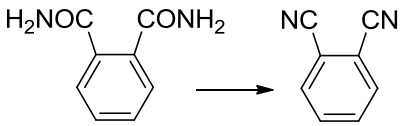

Phthalonitrile Benzene-1,2-dicarboxamide (9.80 g, 59.7 mmol) was suspended in 90 mL DMF and thionyl chloride (8.71 mL) was added slowly at 0 °C . The yellow homogenous solution was stirred for 30 minutes, allowed to warm to room temperature and then heated to 60 °C overnight. The mixture was poured into 5% HCl (300 mL) to produce white precipitate that was collected on a Buchner funnel, washed with 5% HCl, water and methanol to give 7.20 g pure product (94%). ^{1}H NMR (DMSO, 500 MHz) δ 8.14, 7.90. ^{13}C NMR (DMSO, 100 MHz) δ 140, 120, 115, 100.

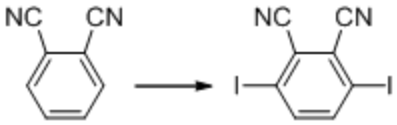

3,6-Diiodophthalonitrile 2,2',6,6'-Tetramethylpiperidine (2.000 g, 14.16 mmol) was dissolved in 60 mL of THF and cooled to -78 °C. BuLi (5.66 mL, 2.5 M) was added dropwise and the mixture was allowed to warm to room temperature and stirred for 1 h. After cooling to -78 °C, a 0.71 M solution of phthalonitrile in THF (10 mL total volume) was added slowly via cannula. The green solution was stirred at this temperature for 1.5 h. A solution of I_2 (3.95 g 15.72 mmol) in 12 mL THF was added in one portion and the mixture was stirred overnight reaching ambient temperature. Water was added and the

aqueous layer was extracted with ether. The organic extracts were combined and washed with 10 % HCl, water, aqueous sodium thiosulfate, water and finally brine. After drying and removing the solvent under reduced pressure the crude tan solid was chromatographed using dichloromethane as eluent to give 1.90 g off yellow solid. The product was further purified recrystallization from ethyl acetate to yield 0.650 g colorless solid (24%). ^{1}H NMR (DMSO) δ 7.98. ^{13}C NMR (DMSO 100 MHz) δ 144, 124, 117, 102.

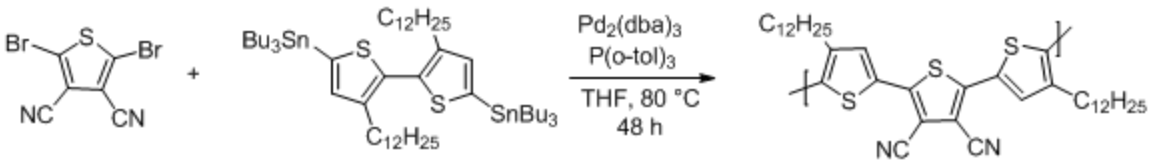

General Procedure for Polymerizations, Chapter Two

The diaryl halide and tributyltin monomers were sequentially added to a vacuum flask (1:1 molar ratio). The flask was evacuated and backfilled with N_2 three times. A mixture of $Pd_2(dba)_3$ and P(*o*-tol)$_3$ was added (1:8 molar ratio, 0.03 eq Pd based on the monomers) and the mixture was pump-purged two additional times. Freshly distilled THF was added via syringe to bring the monomers to a final concentration of 0.05 M. The flask was sealed and placed in an 80 °C oil bath. After stirring for two days the mixture was cooled to room temperature and dripped into 100 mL of acetone containing 5 mL of 12 M HCl. The precipitated solids were stirred vigorously in the acidic acetone solution for 4 hours and poured into a Soxhlet thimble. The solids were thoroughly washed with methanol in the thimble and dried under a stream of N_2. Sequential Soxhlet

extractions (24 h each) followed using acetone, hexanes and chloroform (the final solvent used for **T_2CN_2DBT** was chlorobenzene). The soluble chloroform fraction was concentrated with a N_2 stream to ~ 20 mL and precipitated into MeOH. The polymers were collected by centrifugation and dried under reduced pressure. ^{13}C spectra could not be recorded to the limited solubility and strong solution aggregation of the polymers.

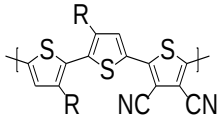

R = $C_{12}H_{25}$ **TCN_2DBT**

R = $OC_4H_9CHC_6H_{13}$ **TCN_2BOBT**

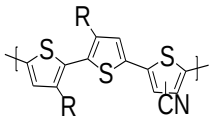

R = $C_{12}H_{25}$ **TCNDBT**

R = $OC_{14}H_{29}$ **$TCNOC_{14}$**

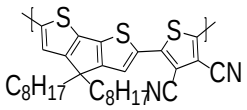

TCN_2CPDT

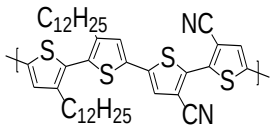

T_2CN_2DBT

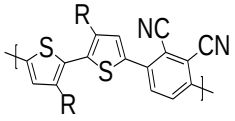

R = $C_{12}H_{25}$ **$1,2\text{-}PhCN_2DBT$**

R = $OC_4H_9CHC_6H_{13}$ **$1,2\text{-}PhCN_2BOBT$**

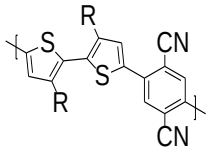

R = $C_{12}H_{25}$ **$1,4\text{-}PhCN_2DBT$**

R = $OC_4H_9CHC_6H_{13}$ **$1,4\text{-}PhCN_2BOBT$**

TCN_2DBT: Purple solid. 89%. ^1H NMR ($C_2D_2Cl_4$ 120 °C): δ 7.61 (s, 2H) (end groups observed in aromatic region) 2.69 (t, 4H) 1.71 (m, 4H) 1.33 (m, 36 H) 0.94 (t, 6 H).

TCN_2BOBT: Blue solid. 15% from the $CHCl_3$ fraction, solid remained in the Soxhlet thimble. ^1H NMR ($C_2D_2Cl_4$ 120 °C): 7.56-7.49 (br m, 2 H) 4.20-4.18 (br m, 4 H) 3.15

(br s, 2 H) 2.01 (br m, 4 H) 1.65-1.32 (br m, 32 H) 0.99-0.91 (br m, 12 H). Note: Poorly resolved spectra were obtained due to the insolubility of this polymer.

TCNDBT: Orange solid. 89%. ^{1}H NMR ($C_2D_2Cl_4$ 80 °C): δ 7.58 (s, 1H) 7.57 (s, 1H) 7.30 (s, 1H) 2.66 (br m, 4H) 1.70 (br m, 4H) 1.40 (br m, 36 H) 0.95 (t, 6H).

$TCNOC_{14}$: Blue solid. 89% ^{1}H NMR ($C_2D_2Cl_4$ 120 °C): δ 7.47 (br s, 1H) 7.26 (br s, 1H) 7.02 (br s, 1H) 4.27 (br m, 4H) 2.02 ((br m, 4H) 1.45 (br m, 44H) 0.95 (t, 6H).

TCN_2CPDT: Purple solid. 90%. ^{1}H NMR ($C_2D_2Cl_4$ 120 °C): δ 7.57 (s, 2H) 1.94 (br m, 4 H) 1.20 (br m, 18H) 0.85 (t, 6 H).

T_2CN_2DBT: Red solid. 49%. ^{1}H NMR ($C_2D_2Cl_4$ 120 °C): 7.40 (s, 2 H) 7.27 (s, 2H) 2.66 (br m, 4 H) 1.70 (br m, 4 H) 1.36 (br m, 36 H) 0.96 (t, 6H).

1,2-$PhCN_2DBT$: Orange solid. 92%. ^{1}H NMR ($C_2D_2Cl_4$ rt): δ 7.90 (s, 2 H) 7.73 (s, 2 H) 2.75 (t, 4 H) 1.76 (m, 4 H) 1.35 (br m, 36 H) 0.95 (t, 6 H).

1,2-$PhCN_2BOBT$: Purple solid. 91%. ^{1}H NMR ($C_2D_2Cl_4$ 120 °C): δ 7.87 (s, 2 H) 7.74 (s, 2 H) 4.27 (d, 4 H) 2.05 (m, 2 H) 1.71-1.40 (br m, 32 H) 1.02-0.95 (br m, 12 H).

1,4-$PhCN_2DBT$: Orange solid 92%. ^{1}H NMR ($CDCl_3$ rt): 7.99 (s, 2H) 7.66 (s, 2H) 2.62 (t, 4H) 1.53 (m, 4H) 1.22 (br m, 4H) 1.22 (br m, 36H) 0.86 (t, 6H).

1,4-PhCN$_2$BOBT: Blue solid. 61%. 8.05 (s, 2H) 7.60 (s, 2H) 2.62 (t, 4H) 1.53 (m, 4H) 1.22 (br m, 4H) 1.22 (br m, 32H) 0.86 (br m, 12 H).

7. 3 Synthetic Details for Chapter Three

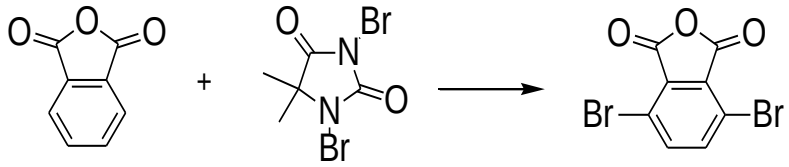

3,6-Dibromophthalimide - alternate procedure Phthalic anhydride (25.0 g, 169 mmol) was dissolved in concentrated sulfuric acid (100 mL) in a 500 mL flask open to air. 1,3-dibromo-5,5-dimethylhydantoin was added portion wise over 30 min (1 eq.). The reaction mixture was stirred at 60 °C overnight. A colorless precipitate formed. After cooling to room temperature 300 mL of DCM was added and the solids dissolved. The layers were separated and the H_2SO_4 phase was extracted with DCM (5 x 175 mL). Solid $NaHCO_3$ (5 g) was added portion-wise to the DCM layer with vigorous stirring. After bubbling ceased the solution was transferred to a separatory funnel and water was slowly added. After bubbling ceased the phases were separated and the organic layer was washed with water (3 x 100 mL), dried and evaporated. A colorless solid was obtained that was recrystallized from AcOH twice to give 13.33 g of colorless product, 26%. ^{1}H NMR ($CDCl_3$) δ 7.80 (s), ^{13}C NMR ($CDCl_3$) δ 160, 140, 130, 120.

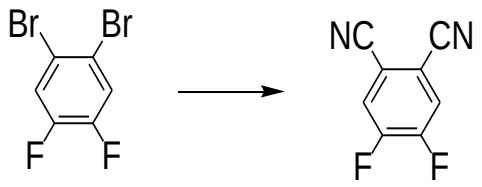

1,2-Difluoro-*o*-phthalonitrile 1,2-Dibromo-4,5-difluorobenzene (5.44 g, 20.0 mmol) was dissolved in anhydrous DMAc (15 mL) and N_2 was bubbled into the solution for 15 minutes. The solution was placed in a 100 °C preheated oil bath and Pd_2dba_3 (366 mg, 0.4 mmol) and DPPF (300 mg, 0.5 mmol) were added in one portion. $Zn(CN)_2$ was added in ~ 550 mg portions every 30 minutes (2.82 g, 24 mmol total). The solution was stirred overnight. The solvent was removed under vacuum and the residue was diluted in EtOAc (50 mL). The solids were removed by filtration and the mother liquor was washed with water (2 x 50 mL), brine and dried. After evaporation of the solvent the solid was dissolved in DCM in filtered through a pad of silica gel. Recrystallization from EtOH followed by vacuum sublimation (0.9 torr, 100 °C) yielded 500 mg yellow solid, 15%. ^{1}H NMR ($CDCl_3$) δ 8.30 (m)

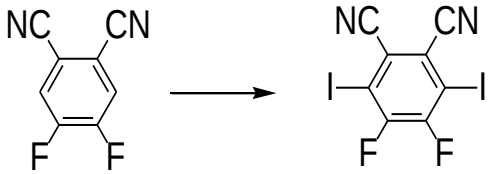

4,5-Difluoro-3,6-diiodo-phthalonitrile 1,2-Difluoro-phthalonitrile (200 mg, 1.22 mmol) and iodine (928 mg, 3.66 mmol) were stirred in DMF (1 mL) and a solution of freshly prepared lithium *tert*-butoxide in DMF (1.14 mL, 3.2 M) was added in one portion. After the exothermic reaction cooled, the solution was placed in a 60 °C oil

bath. The reaction was monitored by GC-MS and was complete after 1 h. The solution was cooled to room temperature and poured into a saturated solution of sodium thiosulfate (20 mL). The precipitated solid was collected by filtration and washed with water, followed by diethyl ether and dried under vacuum to yield 0.458 g tan solid, 91%. ^{1}H NMR (DMSO) no proton observed. ^{13}C NMR (DMSO) δ 155 (d), 151 (d), 122, 116. ^{19}F (DMSO, $CFCl_3$) δ -102.

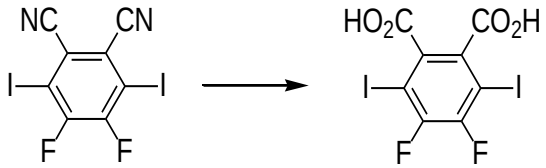

4,5-Difluoro-3,6-diiodo-phthalic acid 4,5-Difluoro-3,6-diiodo-phthalonitrile (458 mg, 1.10 mmol) and aqueous H_2SO_4 (70%, 5 mL) were heated to 150 °C in a sealed screw-cap tube overnight. The cooled solution was poured into ice water and extracted with dichloromethane (3 x 10 mL). The combined organics were washed with water (until the aqueous layer was neutral to litmus), brine and then dried. Evaporation of the solvent yielded 273 mg yellow solid that was used without further purification, 55%.

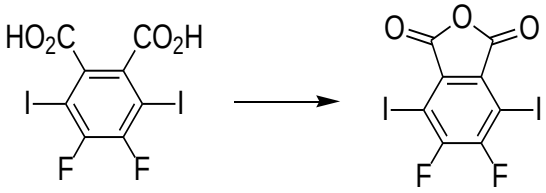

4,5-Difluoro-3,6-diiodophthalic anhydride 4,5-Difluoro-3,6-diiodo-phthalic acid 500 mg, 1.10 mmol) and acetic anhydride (15 mL) were placed in a screw cap tube and sparged with N_2 for 15 minutes. The tube was sealed and placed in a 150 °C oil bath and

the mixture was stirred overnight. The solution was cooled to room temperature and concentrated to ~ 50% of the original volume and cooled in an ice bath. The precipitated solid was collected on a Buchner funnel, washed with ice cold acetic anhydride followed by a minimum amount of ice cold methanol and dried under vacuum. The colorless solid was used without further purification, 450 mg, 93%.

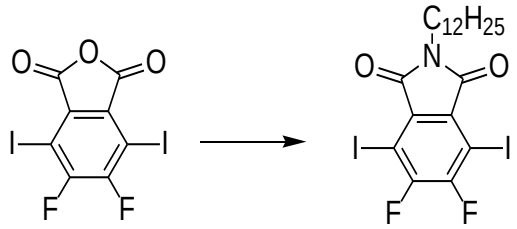

N-dodecyl-4,5-difluoro-3,6-diiodo-phthalimide 4,5-Difluoro-3,6-diiodo-phthalic anhydride (270 mg, 0.062 mmol), N-dodecylamine (150 mg, 0.0809 mmol) and glacial acetic acid (10 mL) were combined in a round bottom flask and sparged with N_2. The mixture was refluxed for 6 h, cooled to room temperature and the solid precipitate was collected by filtration and washed with acetic acid, then water. The brown precipitate that formed in the mother liquor after the water wash was then also collected by filtration. The mother liquor was evaporated and TLC of the three crops showed nearly the same level of purity. The three crops were combined and purified by column chromatography using 1:1 DCM/hexane as eluent. 170 mg of colorless solid was isolated, 45%. ^{1}H NMR ($CDCl_3$) δ 3.66, (t) 3 H, δ 1.64, (m) 2 H, δ1.29-1.22, (m) 18 H, δ 0.84, (t) 3 H. ^{13}C NMR ($CDCl_3$) δ 164, 154 (d), 152 (d), 130, 39, 32, 29.5-29.1, 28, 26, 23, 14. ^{19}F ($CDCl_3$, $CFCl_3$) δ -107.

General Procedure for Polymerizations, Chapter Three

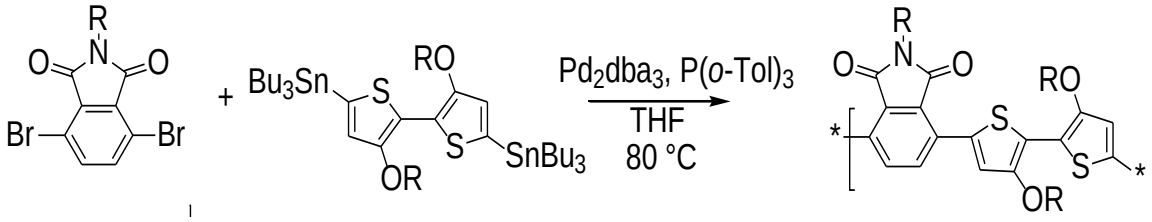

The same synthetic procedure described for Chapter One was followed. The polymers were precipitated from the reaction mixture into an acidic methanol solution instead of acetone. The Soxhlet solvents for **3-P3a** and **3-P2** were methanol, acetone, hexanes and chloroform. Polymers **3-P1**, **3-P3b** and **3-3c** were isolated from the hexane fraction with no solid left in the Soxhlet thimble.

3-P1: Blue solid. 92%. ($CDCl_3$, 50 °C): δ 8.00 (br s, 2 H), δ 7.82 (br s, 2 H), δ 4.22 (br s, 4 H), δ 3.70 (br s, 2 H), δ1.95 (br s, 2 H), δ 1.68 (br m, 4 H), δ 1.67-1.28 (br m, 44 H), δ 0.94-0.85 (br m, 18 H).

3-P2: Blue solid. 85%. ^{1}H NMR ($C_2D_2Cl_4$ 120 °C): δ 7.52 (s, 2 H), δ 4.30 (br s, 4 H), δ 3.71 (br s, 2 H), δ 2.00 (br s, 2 H), δ 1.65 (br s, 4 H), δ 1.32 (br m, 46 H) δ 0.92 (br m, 15 H). ^{19}F NMR ($C_2D_2Cl_4$, $CFCl_3$, 120 °C): δ -126.

3-P3a: Blue solid. 81%. ^{1}H NMR ($C_2D_2Cl_4$ 120 °C): δ 7.95-7.89 (br m, 4 H), δ 4.61 (br s, 2 H), δ 3.75 (br s, 2 H), δ 2.05 (br s, 2 H), δ 1.63 (br s, 4 H), δ 1.55-1.32 (br m, 30 H), δ 0.99-0.93 (br m, 9 H).

3-P3b: Blue solid. 83%. ^{1}H NMR ($CDCl_3$ 50 °C): δ 8.00 (br s, 2 H), δ 7.86 (br s, 2 H), δ 4.43 (br s, 2 H), δ 3.71 (br s, 2 H), δ 1.92 (br s, 2 H), δ 1.80-1.56 (br m, 8 H), δ 1.40-1.27 (br m, 32 H), δ 1.11 (br m, 8 H), 0.89 (br m, 12 H).

3-P3c: Blue solid. 89%. ^{1}H NMR ($CDCl_3$ 50 °C): δ 8.00 (br s, 2 H), δ 7.86 (br s, 2 H), δ 4.48 (br s, 2 H), δ 3.71 (br s, 2 H), δ 1.94 (br s, 2 H), δ 1.80 (br s, 6 H), δ 1.59 (bs s, 12H) δ 1.40-1.28 (br m, 8 H), δ 1.02 (br m, 16 H), δ 0.91 (t, 6 H) 0.89 (m, 9 H).

7. 4 Synthetic Details for Chapter Four

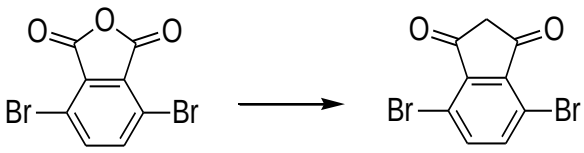

4,7-Dibromo-*2H*-indene-1,3-dione 2,5-Dibromophthalic anhydride (2.00 g, 6.54 mmol) was suspended in acetic anhydride (4 mL). Triethylamine (2 mL) was added and the mixture became homogenous. *tert*-butyl acetoacetate (0.141 g ,0.893 mmol) was added and the solution was stirred overnight. Ice (1 g) and concentrated HCl (0.5 mL) was

added to the heterogeneous yellow suspension followed by 5 M HCl (5 mL). After the exotherm subsided, the solution was heated to 70 °C until gas evolution ceased (~ 1 h). The aqueous phase was extracted with dichloromethane (4 x 10 mL). The combined organic layers were washed with water until neutral to litmus, then brine. After drying and concentrating, the product can be used without further purification. If purification is required, the brown solid may be filtered through a silica gel plug using DCM as eluent (note: a color change occurs on the column, the product is not stable to SiO_2 chromatography). The purple solid may be further purified by recrystallization from anhydrous, degassed acetonitrile to give green needles, 60 %. ^{1}H NMR (DMSO) δ 7.94 (s), 2 H, δ 3.41 (s), 2 H. ^{13}C NMR (DMSO) δ 194, 159, 141, 116, 46.

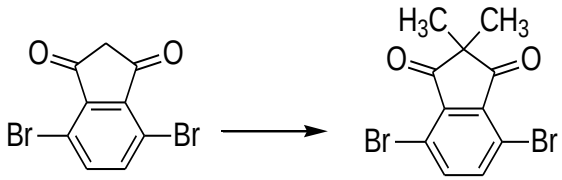

4,7-Dibromo-2,2-dimethyl-*2H*-indene-1,3-dione *The potassium fluoride/celite reagent was prepared as follows:* Celite 545 was suspended in water (0.0581 g/mL) and poured into a solution of aqueous KF (0.116 g/mL, 1:1 final mass ratio, KF / Celite). The mixture was gently stirred for 1 h and the solvent was removed on a rotory evaporator (note: the solids were not completely dried to allow for easier manipulation of the reagent). Acetonitrile was added (1.16 g KF-Celite mix/mL) and the suspension was briefly shaken. The solid was collected on a Buchner funnel, washed with acetonitrile,

then finely ground with a mortar and pestle. The reagent was dried under vacuum overnight.

4,7-Dibromo-*2H*-indene-1,3-dione (0.200 g, 0.658 mmol), iodomethane (0.280 g ,1.97 mmol) and acetonitrile (3 mL) were combined in a vacuum flask. Under vigorous stirring the potassium fluoride/Celite reagent (0.41 g) was added; the flask was sealed and stirred at 50 °C for two days. After cooling to room temperature the mixture was filtered through a pad of Celite and the mother liquor was concentrated under vacuum. The golden solid was purified by column chromatography using 1:1 pentane/dichloromethane as eluent to yield light yellow solid, 63%. ^{1}H NMR ($CDCl_3$): δ 7.77 (s, 2H), δ 1.29 (s, 6 H). ^{13}C ($CDCl_3$) δ 201, 141, 139, 119, 50, 21.

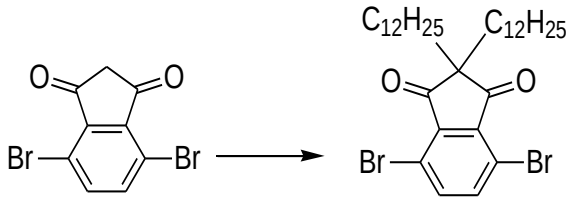

4,7-Dibromo-2,2-didodecyl-*2H*-indene-1,3-dione This was prepared in an analogous fashion to 4,7-dibromo-2,2-dimethyl-*2H*-indene-1,3-dione, (SiO_2, 1:3 DCM/hexane eluent), 56% yield. ^{1}H NMR ($CDCl_3$): δ 7.76 (s, 2H), δ 1.77 (m, 4H), δ 1.27 (m, 36 H), δ 0.99 (m, 4 H) δ 0.85 (m, 6 H). ^{13}C ($CDCl_3$) δ 201, 143, 138, 120, 55, 33-30 (multiple), 26, 25, 23, 14

General Procedure for Polymerizations, Chapter Four

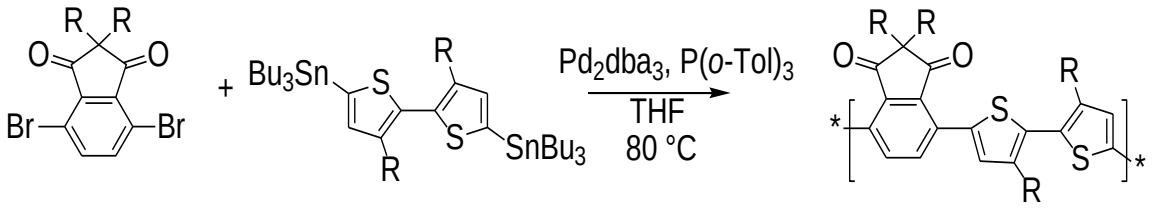

The same synthetic procedure described for Chapter One was followed. The polymers were precipitated from the reaction mixture into an acidic methanol solution instead of acetone. The Soxhlet solvents for **4-P1** and **4-P2** were methanol, acetone, hexanes. The same sequence of solvents was used for **4-P3,** the final solvent was chloroform.

4-P1: Blue solid. 88%. ^{1}H NMR ($CDCl_3$, 55 °C): δ 7.92 (br s, 2 H), δ 7.82 (br s, 2 H), δ 4.21 (br s, 4 H), δ 1.94 (br s, 2 H), δ 1.66 (m, 4 H) δ 1.53-1.29 (br m 40 H), δ 0.92 (m, 6 H), δ 0.84 (m 6 H).

4-P2: Orange solid. 67%. ^{1}H NMR ($CDCl_3$, rt) δ 7.90 (d, 2H), δ 7.65 (d, 2 H), δ 2.68 (t, 4 H), δ 1.69 (m, 4 H) δ 1.45-1.23 (br m, 36 H), δ 0.85 (t, 6 H).

4-P3: Red solid. 90%. ^{1}H NMR ($C_2D_2Cl_4$, 110 °C); δ 7.96 (br s, 2 H), δ 7.73 (br s, 2 H) δ 7.40 (br s, 2 H), δ 1.87 (br m, 4 H) δ1.29-1.26 (br m, 40 H), δ 0.91 (br m, 6 H).

7.5 Synthetic Details for Chapter Five

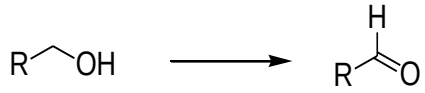

General procedure for the oxidation of alcohols to aldehydes[6] **(**all listed equivalents based on the alcohol) Freshly distilled dimethyl sulfoxide (2 eq.) was dissolved in DCM (0.4 M final concentration of DMSO) and placed in a – 78 °C bath. Oxalyl chloride (1.05 eq.) was added slowly via syringe (~0.1 mL/min). The mixture was stirred for 30 minutes and the alcohol was added slowly via addition funnel (~0.1 mL/min). Triethylamine (3 eq.) was added dropwise after stirring the mixture for 40 minutes. The whole was stirred for 15 minutes and then removed from the cooling bath. The mixture was stirred overnight. 1 M HCl was added and the aqueous layer was extracted with DCM. The combined organics were washed with water, brine, dried and evaporated. The aldehydes were filtered through a plug of silica gel using hexanes as eluent and used without further purification.

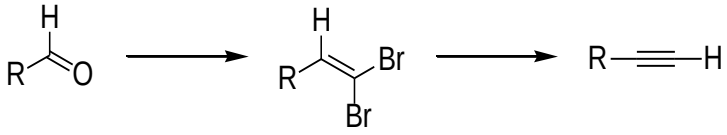

General procedure for the conversion of aldehydes to terminal alkynes *Zinc and CBr_4 were purified before use as follows:* CBr_4 was dissolved in DCM (0.1 g/mL) and $MgSO_4$ was added with stirring. After 20 minutes the dessicant was filtered off and the solvent removed by rotary evaporation. The solid was further dried under vacuum and quickly weighed in air before being transferring to the reaction flask.

Zinc dust was activated by stirring in 10% HCl for ~ 3 minutes. The liquid was decanted and the zinc was washed with water 3 times. This process was repeated three times; after the final water wash the activated zinc was washed with THF three times and dried under vacuum.

Dibromoolefin synthesis Purified zinc dust (2 eq.) and CBr_4 (2 eq.) were dissolved in DCM (to a concentration of 0.36 M) and chilled to 0 °C. Triphenylphosphine (2 eq.) dissolved in DCM (1.6 M solution) was added slowly through a dropping funnel. The solution was stirred overnight and produced a pink solution with white precipitate. The aldehyde was then added neat via syringe. After 3 h pentane was added (4 x DCM by volume) and the white precipitate was filtered off. The solvents were evaporated and the residue was dissolved in a minimum amount of DCM and precipitation was carried out again. After filtration and evaporation of the solvent, the residue was dissolved in pentane and filtered through a silica gel plug yielding the dibromoolefin as clear oil which was used without further purification.

R = $C_{11}H_{23}$: 82 %

R = 1-butyl-1-hexyl: 60 %

Terminal alkyne synthesis The dibromoolefin was dissolved in THF (1.8 M solution) and the solution was cooled to – 78 °C. BuLi (2.1 eq.) was added dropwise and the reaction was stirred for 1 h at – 78 °C. The mixture was allowed to reach room temperature and stirred for 1 h. Water was added to the solution and the aqueous phase

was extracted with diethyl ether three times. The combined organics were washed with water once, brine, dried and evaporated to yield the terminal alkyne as clear oil that was used without further purification.

R = $C_{11}H_{23}$: 98 %

R = 1-butyl-1-hexyl: 93%

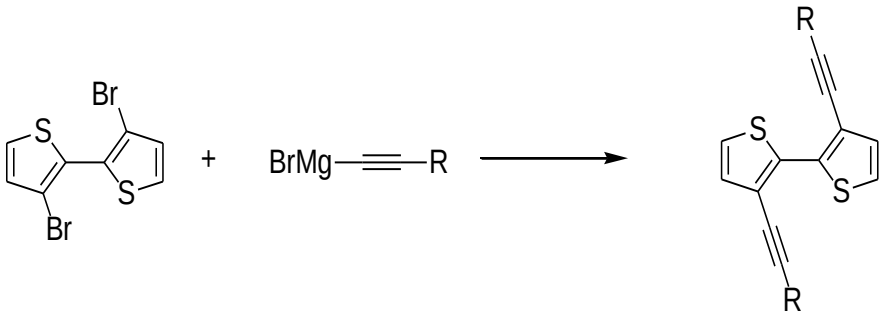

General procedure for coupling of alkynes to bithienyl dibromide. *Prepartion of alkynyl magnesium bromide reagents:* Neat bromoethane (distilled from CaH_2, 0.3 mL) was added to Mg turnings (1.2 eq.) in THF (containing a small crystal of I_2) to initiate the reaction. If the I_2 color remained the flask was heated with a heat gun. The remaining bromoethane was then added dropwise as a solution in THF (1.8 M). The reaction was heated to 60 °C for 1 h. After cooling, the alkyne was added dropwise to the solution of the Grignard reagent. Once gas evolution ceased the mixture was heated to reflux for 1 h. In a separate screw cap flask, 3,3'-dibromo-2,2'-bithiophene was dissolved in THF (0.08 M) and the cooled Grignard reagent was transferred over via cannula. N_2 was bubbled into the mixture for 15 minutes and $Pd(PPh_3)_4$ was added. The solution was sealed and placed in a 110 °C oil bath for 3 days. After cooling, the reaction was quenched by the

addition of 5 % HCl and extracted with Et_2O three times. The combined organics were washed with water, brine, dried over $MgSO_4$ and evaporated. The products were purified by column chromatography followed by recrystallization as listed below.

R = C_4H_9: SiO_2, 7:1 hexanes/DCM EtOH recrystallization. 20 % ^{1}H NMR ($CDCl_3$) δ 7.12 (d) 2 H, δ 7.01 (d) 2 H, δ 2.48 (t) 4 H, δ 1.60, (m) 4 H, δ 1.46, (m) 4 H, δ 0.89, (t) 6H. ^{13}C NMR ($CDCl_3$) δ 137, 131, 123, 120, 97, 77 (resolved inside of the $CDCl_3$ resonances), 30, 22, 17, 18.

R = $C_{11}H_{23}$: SiO_2, hexanes, EtOH recrystallization 26 %. ^{1}H NMR ($CDCl_3$) δ 7.15 (d) 2 H, δ 7.02 (d) 2 H, δ 2.48 (t) 4 H, δ 1.65, (m) 4 H, δ 1.46, (m) 4 H, δ 1.26, (m) 28 H, δ 0.88, (t) 6 H. ^{13}C NMR ($CDCl_3$) δ 137, 130, 123, 120, 97, 77 (resolved inside of the $CDCl_3$ resonances), 32, 29-28 (multiple) 23.

R = 1-butyl-1-hexyl: SiO_2, hexanes, EtOH recrystallization, 30 % ^{1}H NMR ($CDCl_3$) δ 7.11 (d) 2 H, δ 7.01(d) 2 H, δ 2.58 (m) 2 H, δ 1.55, (m) 16 H, δ 1.28, (m) 16 H, δ 0.88 (m) 12 H. ^{13}C NMR ($CDCl_3$) δ 137, 131, 123, 120, 100, 77 (resolved inside of the $CDCl_3$ resonances), 35, 34, 33, 32, 30, 29, 28, 22, 14.

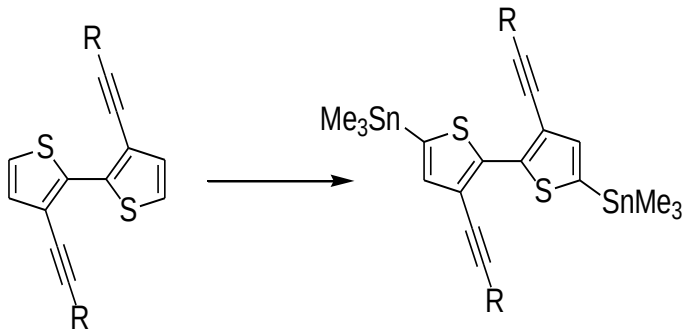

General procedure for stannylation of the di-alkynyl monomers Freshly titrated BuLi (from N-benzylbenzamide,[185] 2.0 eq.) was added to a Schlenk flask and chilled to -40 °C. Diethyl ether was added to bring the final concentration of BuLi to 0.16 M. In a separate flask, 3,3-dialkynyl-2,2'-bithiophene was dissolved in Et_2O (0.13 M). The monomer solution was slowly added to the BuLi solution dropwise at – 40 °C. The mixture was stirred at this temperature for 15 minutes, then at room temperature for 1.5 h. After cooling the reaction to – 40 °C, trimethyltin chloride (1.0 M in hexanes, 2.0 eq.) was added dropwise and the solution was stirred overnight. Ice cold water was added and the organic layer was washed with water twice then brine. After drying, the solvent was removed under reduced pressure at room temperature to yield colorless crystals. The products were pure enough by ^{1}H NMR to be used directly for polymerization but could be recrystallized from EtOH or a mixture of acetone and EtOH if necessary.

R = C_4H_9: Recrystallized from EtOH, colorless crystals, 87 %. ^{1}H NMR ($CDCl_3$) δ 7.07 (s), 2 H, δ 2.50 (t), 4 H, δ 1.66 (m) 4 H, δ 1.52 (m) 4 H, δ 0.95 (m) 6 H, δ 0.37 (m) 18 H. ^{13}C NMR ($CDCl_3$) δ 143, 139, 136, 121, 97, 31, 22, 20, 14, - 8.

R = $C_{11}H_{23}$: Evaporation of solvent after workup yielded 90 % light yellow crystals ^{1}H NMR ($CDCl_3$) δ 7.07 (s), 2 H, δ 2.49 (t), 4 H, δ 1.66 (m) 4 H, δ 147 (m) 4 H, δ 0.1.25 (m) 29 H, δ 0.87 (m) 6 H δ0.37 (m) 18 H. ^{13}C NMR ($CDCl_3$) δ 143, 138, 136, 121, 97, 32, 29.7-29.0 (multiple), 28, 23, 20, 14, -8.

R = 1-butyl-1-hexyl: Recrystallized from acetone/EtOH , 88%. ^{1}H NMR ($CDCl_3$) δ 7.07 (s), 2 H, δ 2.60 (t), 2 H, δ 1.58 (m) 4 H, δ 1.45 (m) 13 H, δ 1.28 (m), 13 H, δ 0.98 (m) 6 H, δ 0.87, (m) 4 H, δ 0.37 (m) 18 H. ^{13}C NMR ($CDCl_3$) δ 143, 139, 135, 121, 100, 78, 35-33 (multiple), 32, 30, 29, 28, 23, 14, -8.

General Procedure for Polymerizations, Chapter Five

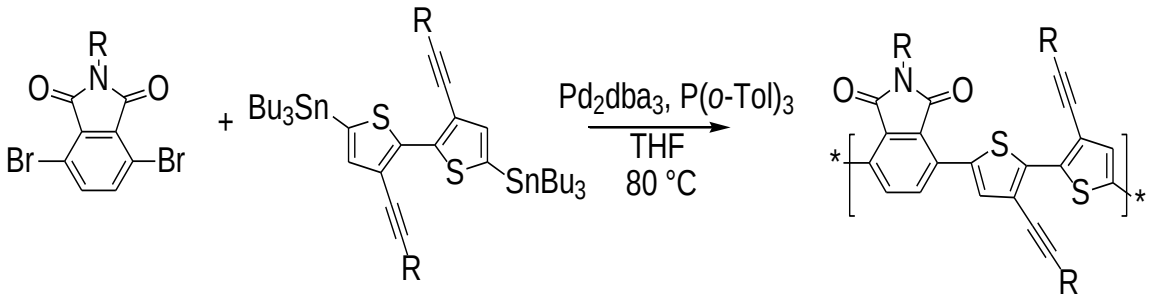

The same synthetic procedure described for Chapter One was followed. The polymers were precipitated from the reaction mixture into an acidic methanol solution instead of acetone. The Soxhlet solvents for **5-P1**, **5-P2** and **5-P3** were methanol, acetone, hexanes, chloroform and chlorobenzene. **5-P4** was collected from the chloroform fraction. Data reported below and in the text for **5-P3** are from the chloroform fraction.

5-P1: Red solid. 66%. ^{1}H NMR data, even at 130 °C, could not be collected due to the poor solubility/strong aggregration of this polymer.

5-P2: Red solid. 67%. ^{1}H NMR ($C_2D_2Cl_4$, 120 °C): δ 7.87-7.84 (br m, 4 H), δ 3.74 (m, 2 H), δ 1.87 (m, 4 H), δ 1.77-1.57 (br m, 69 H), δ 0.90 (br m, 12 H).

5-P3: Red solid. 8%. ^{1}H NMR ($CDCl_3$, 50 °C): δ 7.87 (br s, 2 H), δ 7.54 (br s, 2 H), δ 3.72 (bs s, 2 H), δ 2.66-2.58 (m, 4 H), δ 1.77 (br, s 8 H), δ 1.28 (br m, 48 H), δ 0.87 (br m, 9 H).

5-P4: Red solid. 75%. ^{1}H NMR ($CDCl_3$ 50 °C): δ 7.86-7.82 (br m, 4 H), δ 3.63 (br m, 2 H), δ 2.71 (br m, 2 H), δ 1.98 (br m, 2 H), δ 1.63 (br m, 8 H), δ 1.28 (br m, 61 H), δ 0.89 (br m, 18 H).

7. 6 Polymer NMR for Chapter Two

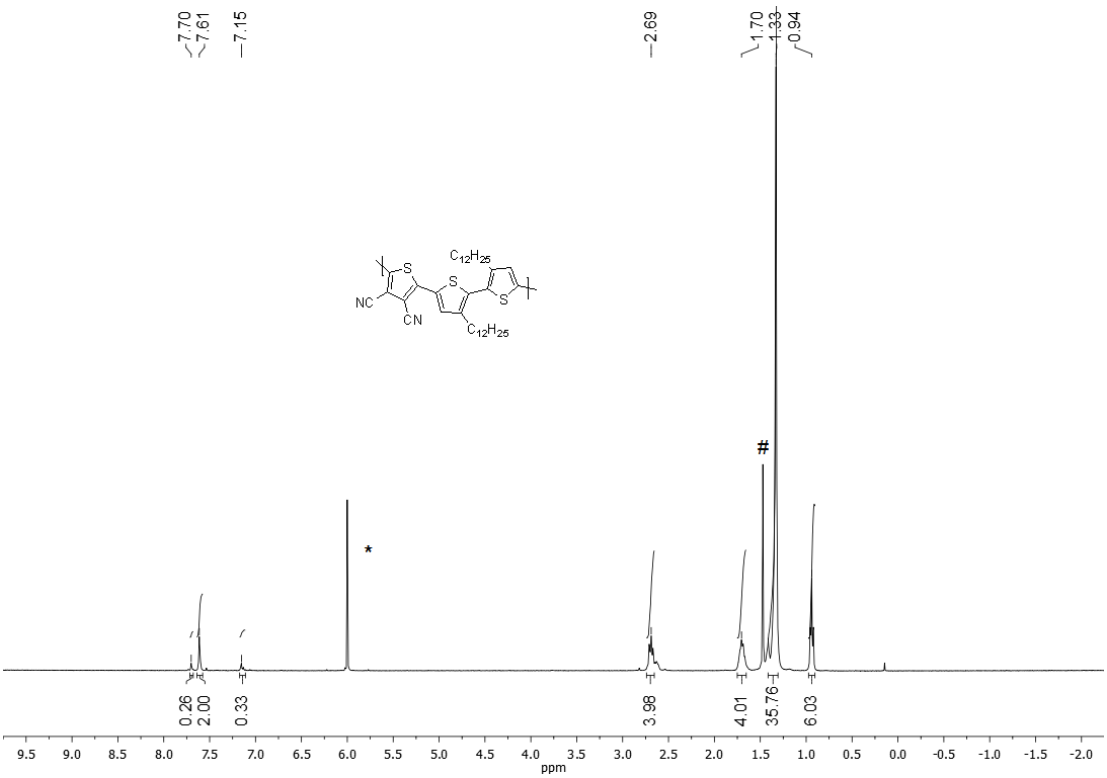

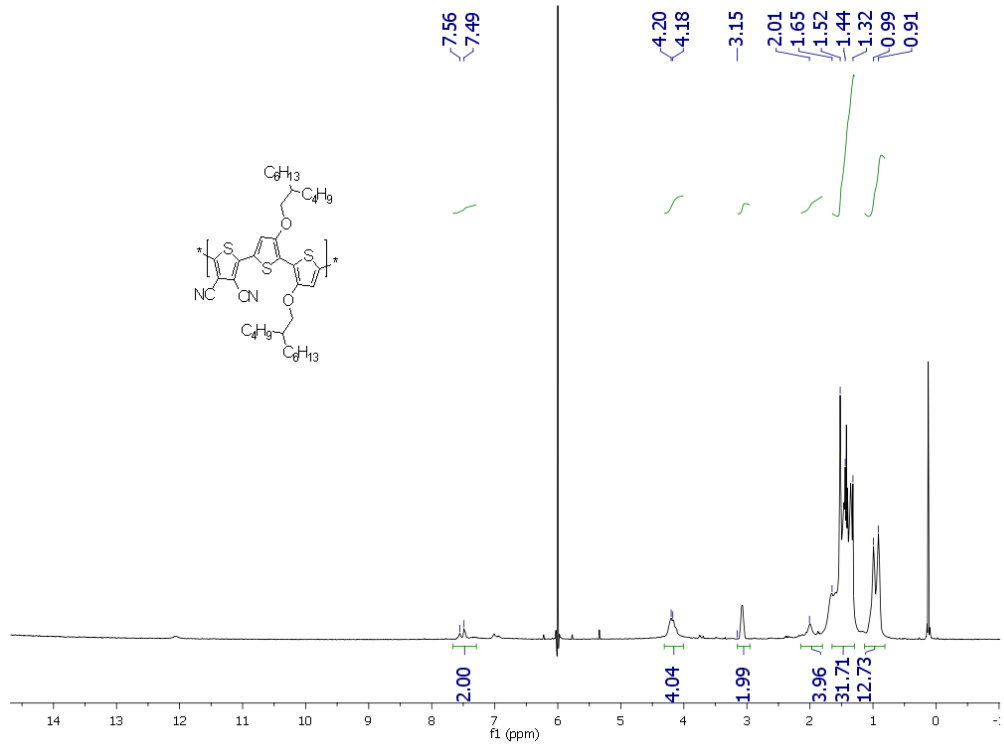

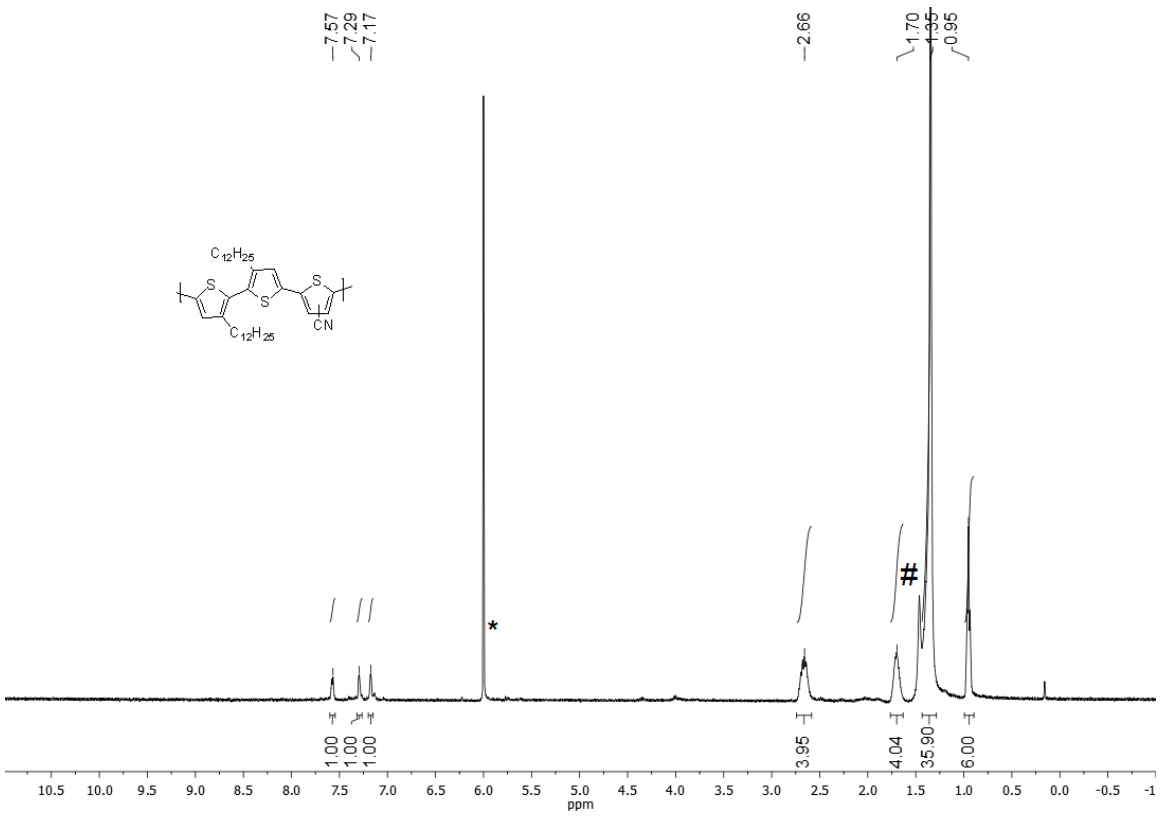
7.57
7.29
7.17
2.66
1.70
1.35
0.95
C12H25
S
S
S
CN
C12H25
*
#
1.00
1.00
1.00
3.95
4.04
35.90
6.00
10.5 10.0 9.5 9.0 8.5 8.0 7.5 7.0 6.5 6.0 5.5 5.0 4.5 4.0 3.5 3.0 2.5 2.0 1.5 1.0 0.5 0.0 -0.5 -1
ppm

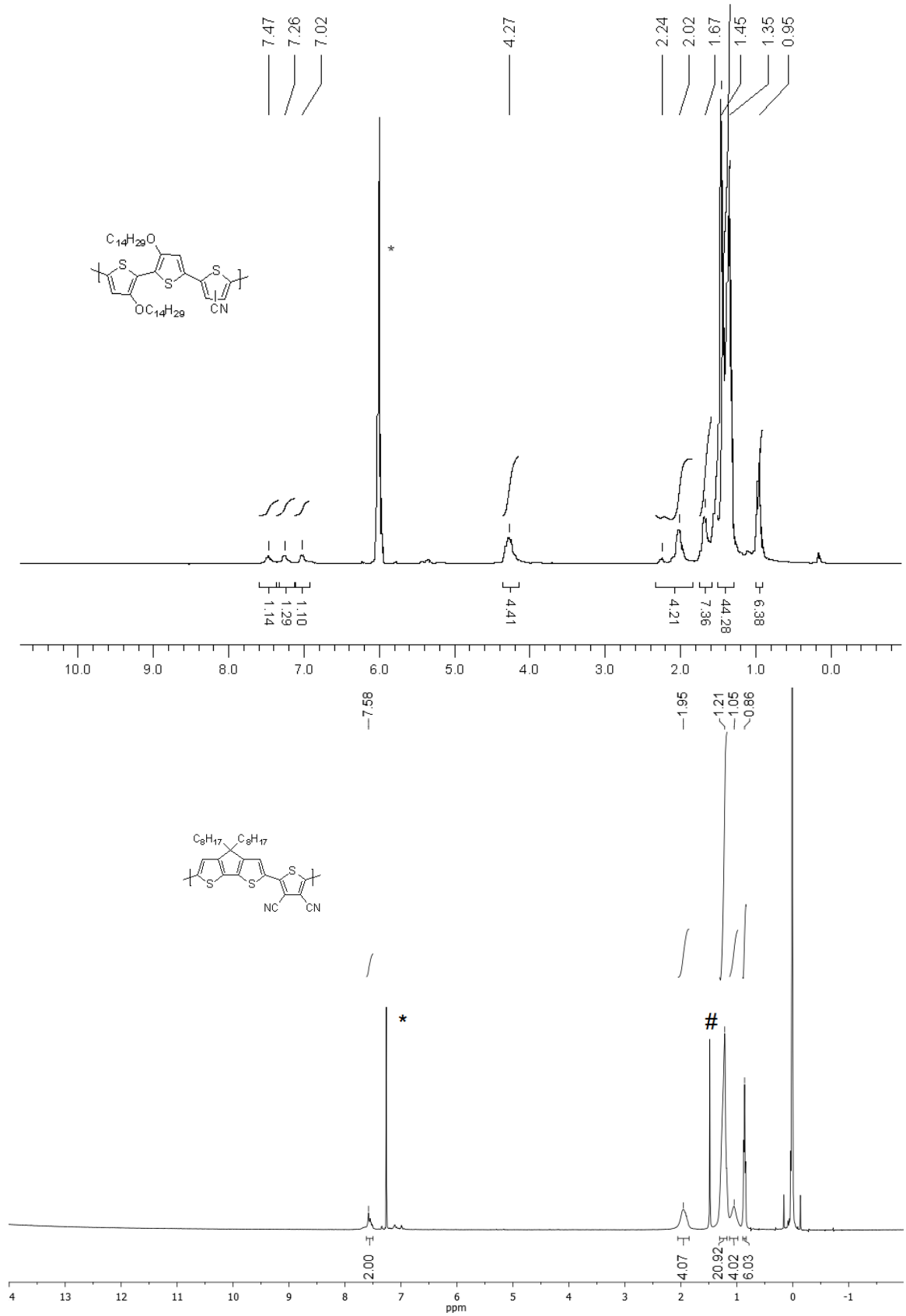
7.47
7.26
7.02
4.27
2.24
2.02
1.67
1.45
1.35
0.95
C14H29O
OC14H29
S
CN
*
1.14
1.29
1.10
4.41
4.21
7.36
44.28
6.38
10.0
9.0
8.0
7.0
6.0
5.0
4.0
3.0
2.0
1.0
0.0
7.58
1.95
1.21
1.05
0.86
C8H17
C8H17
NC
CN
*
#
2.00
4.07
20.93
4.02
6.03
ppm

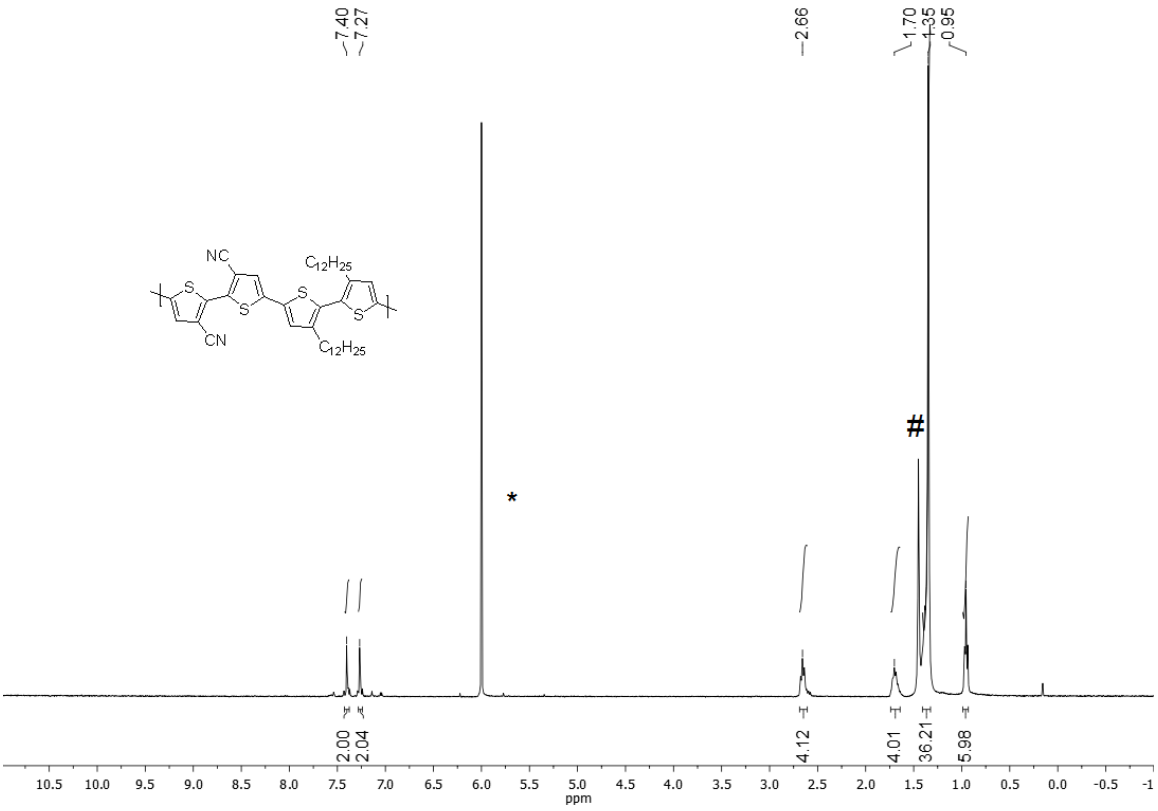
7.40
7.27
2.66
1.70
1.35
0.95
NC
CN
$C_{12}H_{25}$
$C_{12}H_{25}$
*
#
2.00
2.04
4.12
4.01
36.21
5.98
ppm

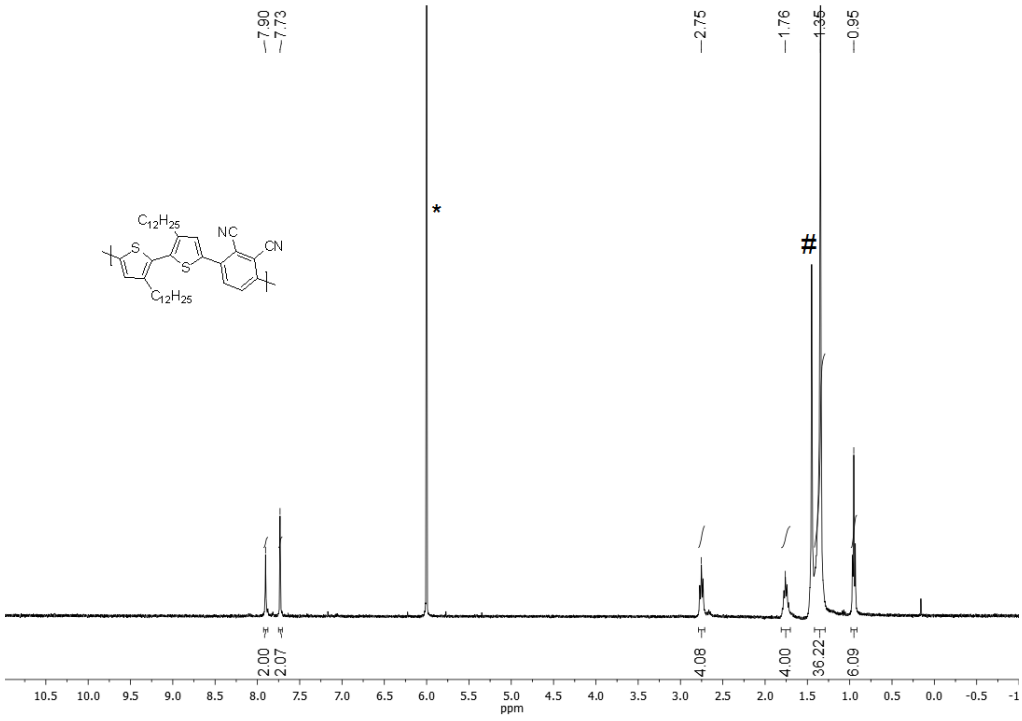
7.90
7.73
2.75
1.76
1.35
0.95
*
#
NC
CN
S
S
$C_{12}H_{25}$
$C_{12}H_{25}$
2.00
2.07
4.08
4.00
36.22
6.09
10.5 10.0 9.5 9.0 8.5 8.0 7.5 7.0 6.5 6.0 5.5 5.0 4.5 4.0 3.5 3.0 2.5 2.0 1.5 1.0 0.5 0.0 -0.5 -1
ppm

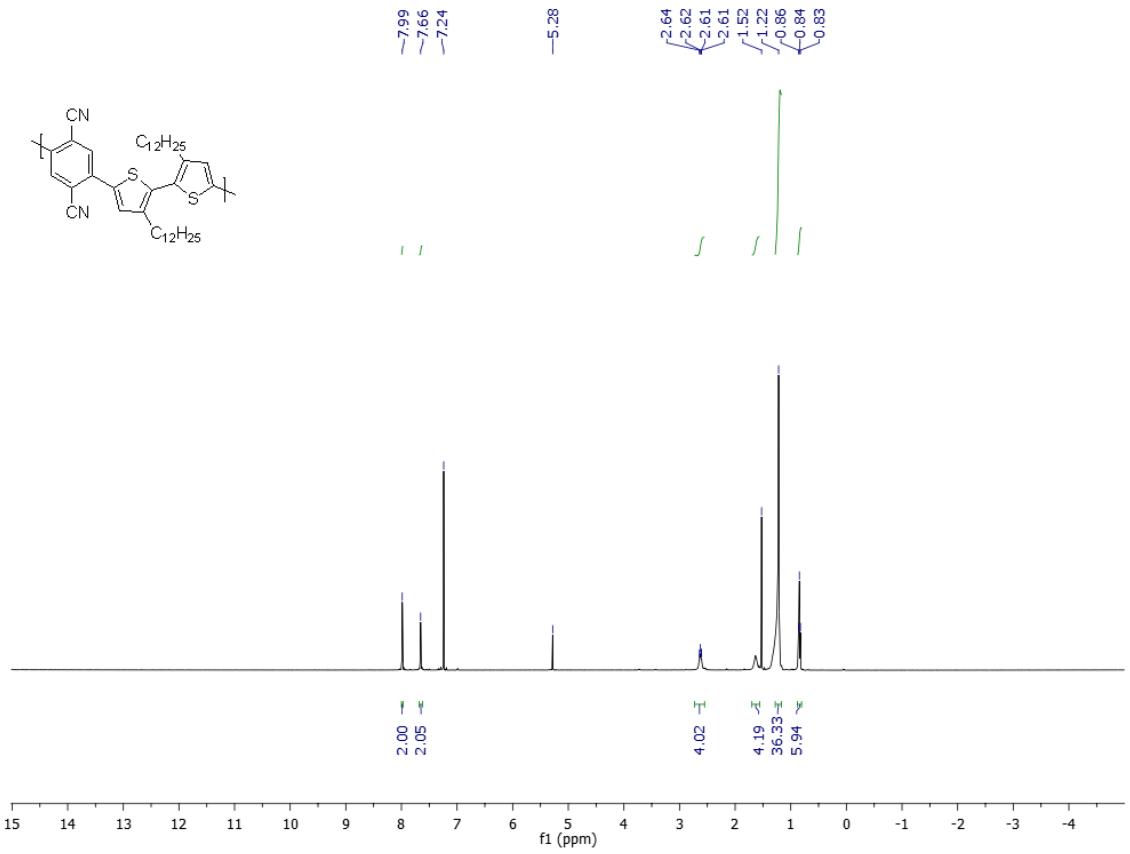
CN
CN
$C_{12}H_{25}$
$C_{12}H_{25}$
S
S
7.99
7.66
7.24
5.28
2.64
2.62
2.61
2.61
1.52
1.22
0.86
0.84
0.83
2.00
2.05
4.02
4.19
36.33
5.94
15 14 13 12 11 10 9 8 7 6 5 4 3 2 1 0 -1 -2 -3 -4
f1 (ppm)

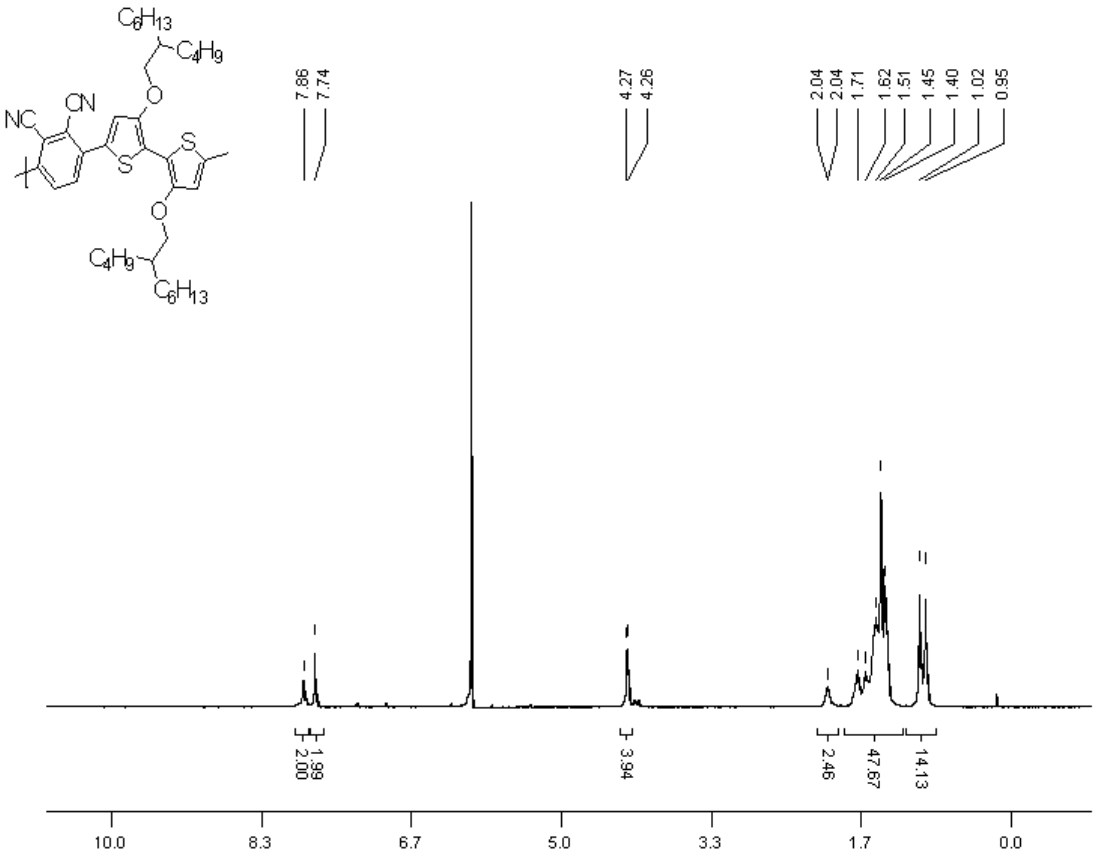
C6H13
C4H9
NC
CN
O
S
S
O
C4H9
C6H13
7.86
7.74
4.27
4.26
2.04
2.04
1.71
1.62
1.51
1.45
1.40
1.02
0.95
1.99
2.00
3.94
2.46
47.67
14.13
10.0
8.3
6.7
5.0
3.3
1.7
0.0

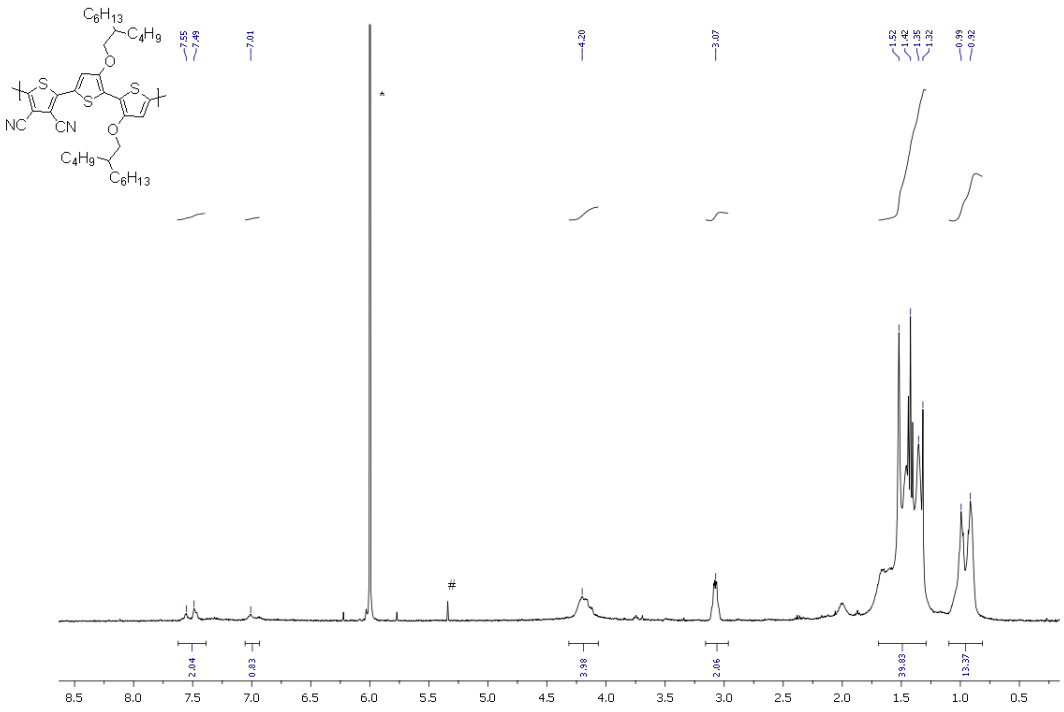
C6H13
C4H9
O
S
S
S
NC
CN
O
C4H9
C6H13
7.55
7.49
7.01
4.20
3.07
1.52
1.42
1.35
1.32
0.99
0.92
*
#
2.04
0.83
3.38
2.06
39.83
13.37
8.5
8.0
7.5
7.0
6.5
6.0
5.5
5.0
4.5
4.0
3.5
3.0
2.5
2.0
1.5
1.0
0.5

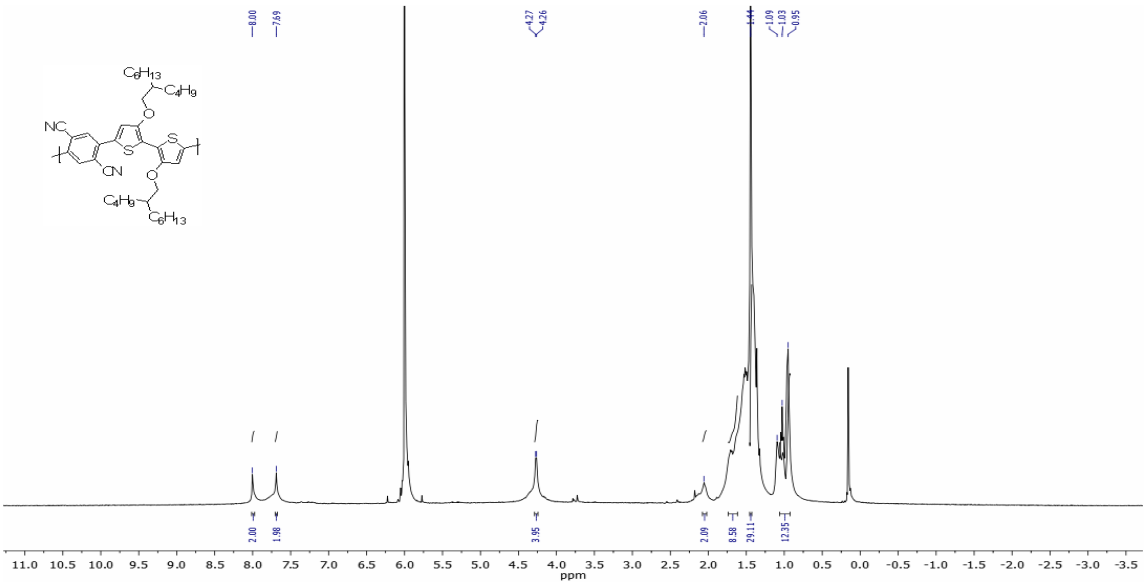
8.00
7.69
4.27
4.26
2.06
1.09
1.03
0.95
2.00
1.98
3.95
2.09
8.58
29.11
12.35
11.0 10.5 10.0 9.5 9.0 8.5 8.0 7.5 7.0 6.5 6.0 5.5 5.0 4.5 4.0 3.5 3.0 2.5 2.0 1.5 1.0 0.5 0.0 -0.5 -1.0 -1.5 -2.0 -2.5 -3.0 -3.5
ppm

7. 7 Polymer NMR for Chapter Three

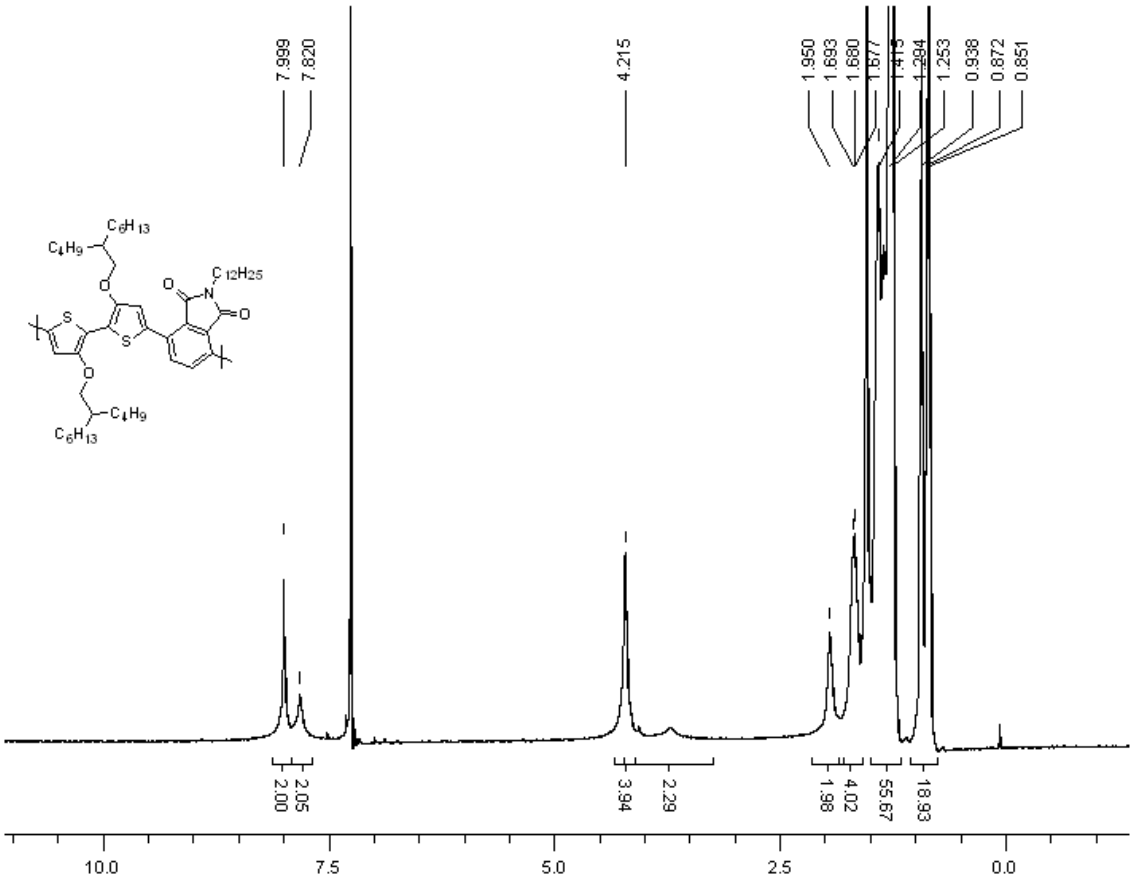

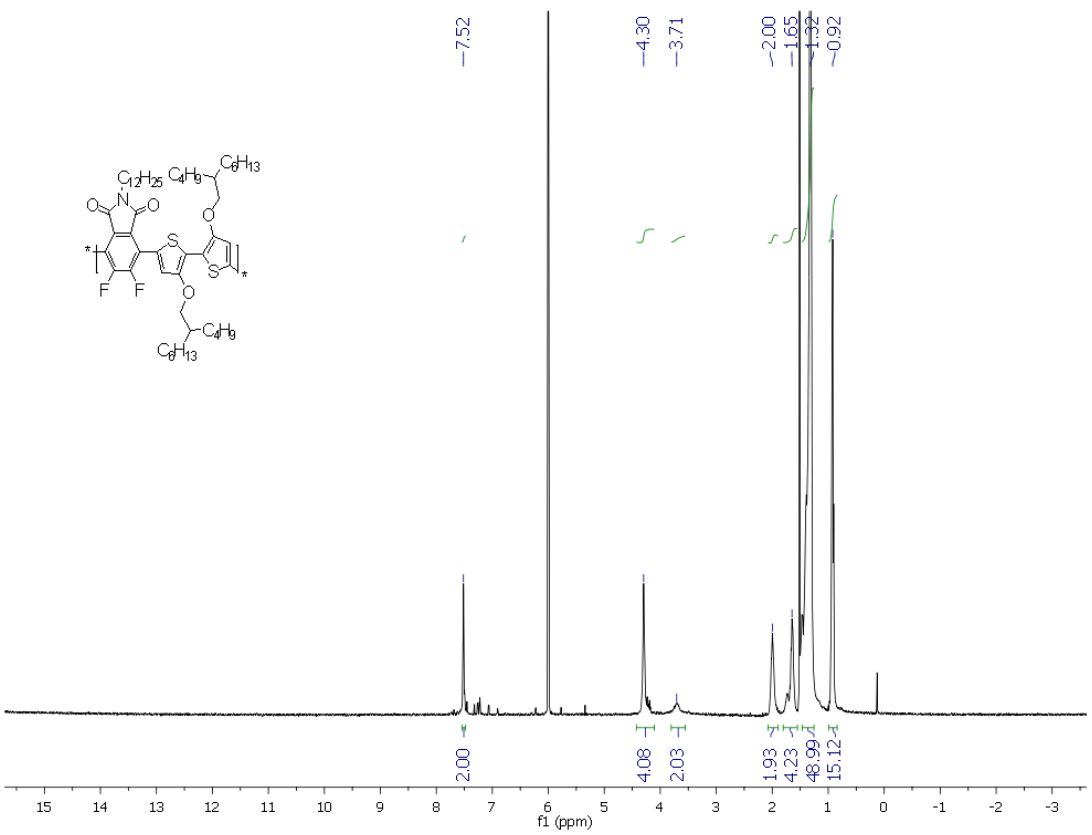
7.52
4.30
3.71
2.00
1.65
1.32
0.92
2.00
4.08
2.03
1.93
4.23
48.99
15.12
f1 (ppm)

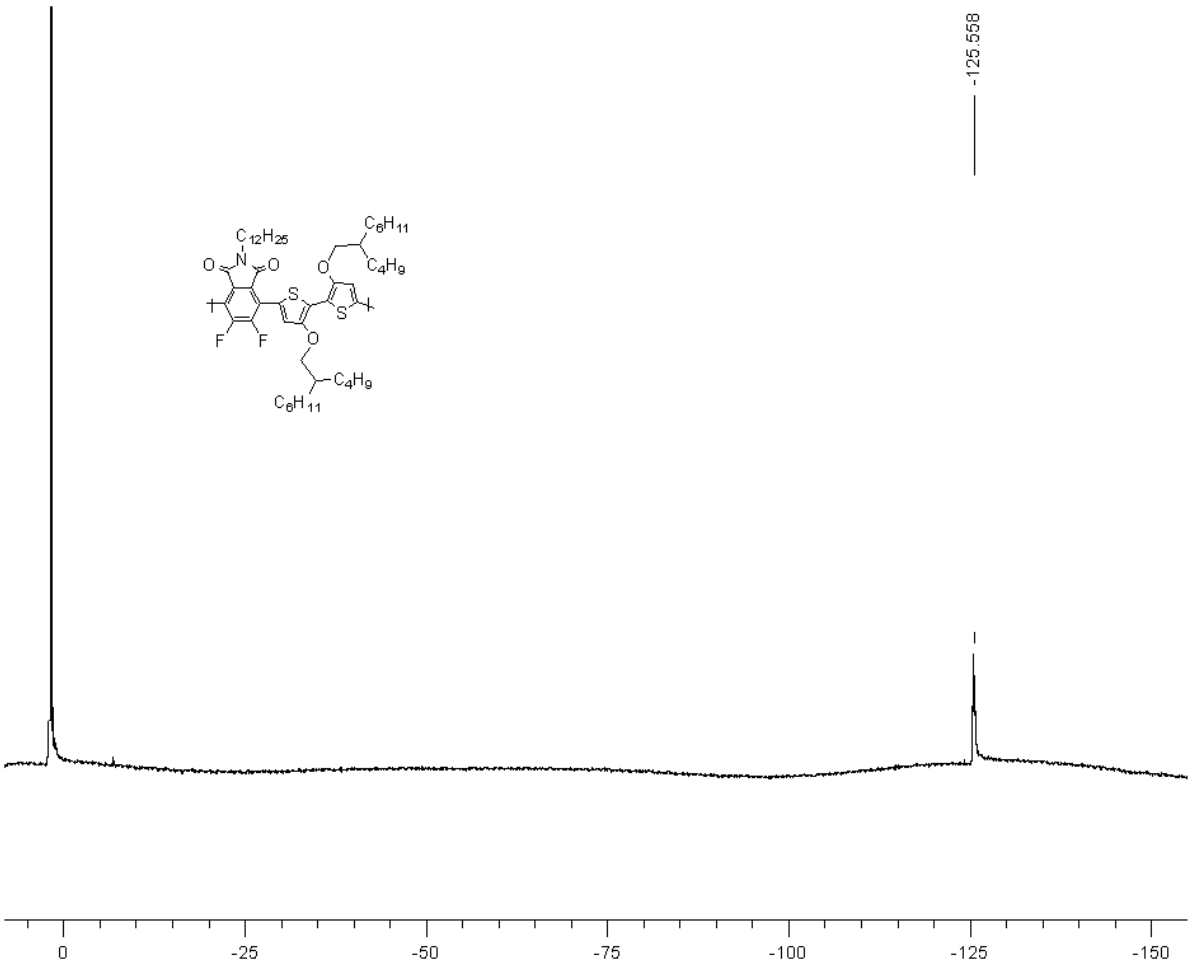
-125.558
C12H25
N
O
O
C6H11
C4H9
O
S
S
F
F
O
C4H9
C6H11
0
-25
-50
-75
-100
-125
-150

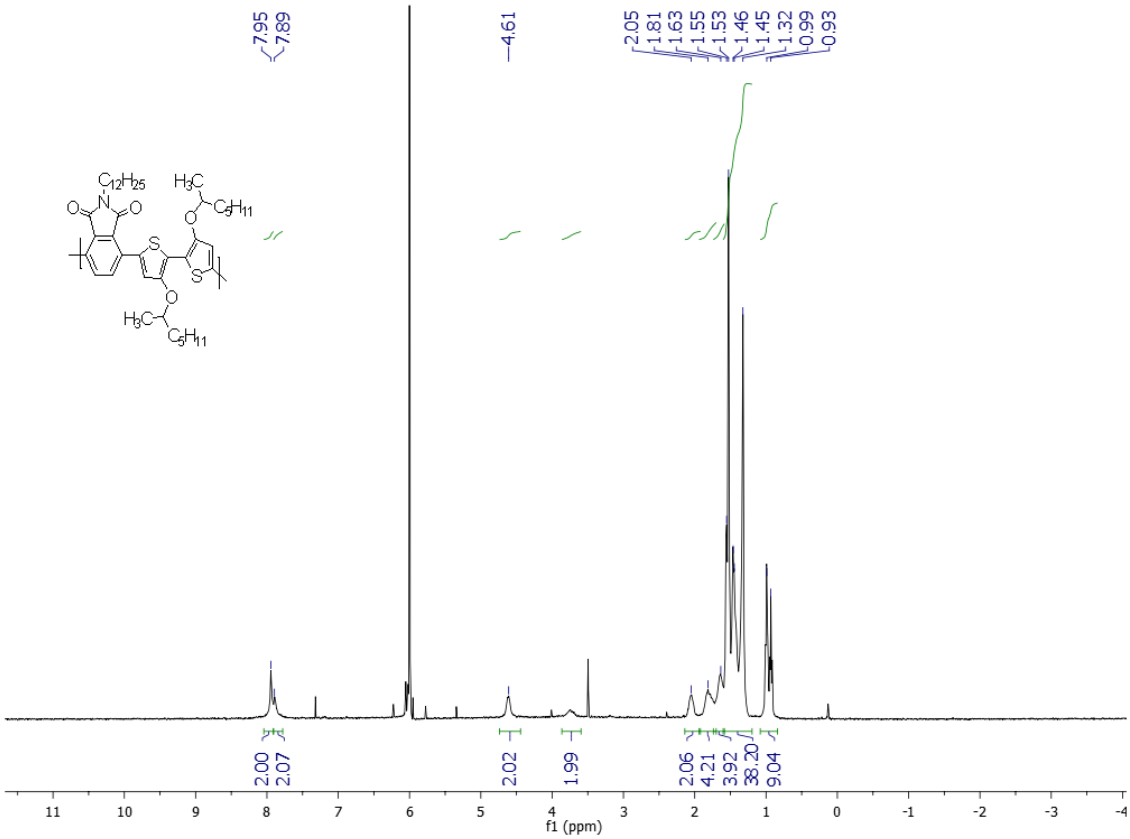
7.95
7.89
4.61
2.05
1.81
1.63
1.55
1.53
1.46
1.45
1.32
0.99
0.93
2.00
2.07
2.02
1.99
2.06
4.21
3.92
38.20
9.04
f1 (ppm)

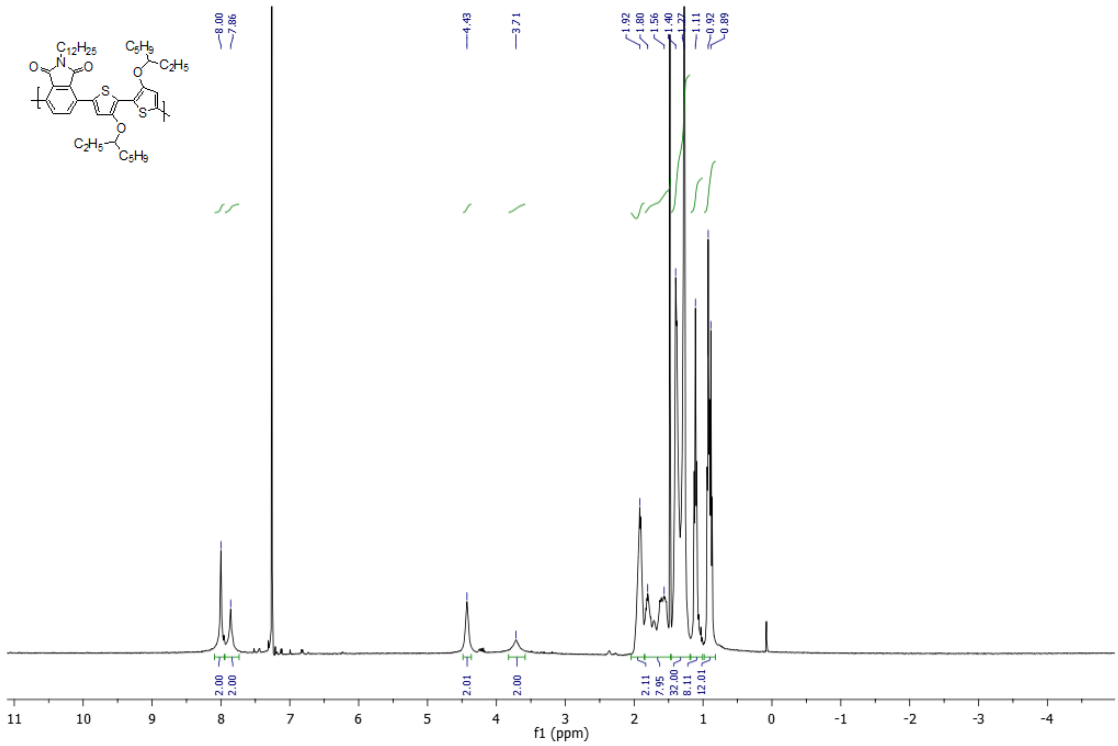
8.00
7.86
4.43
3.71
1.92
1.80
1.56
1.40
1.22
1.11
0.92
0.89
f1 (ppm)

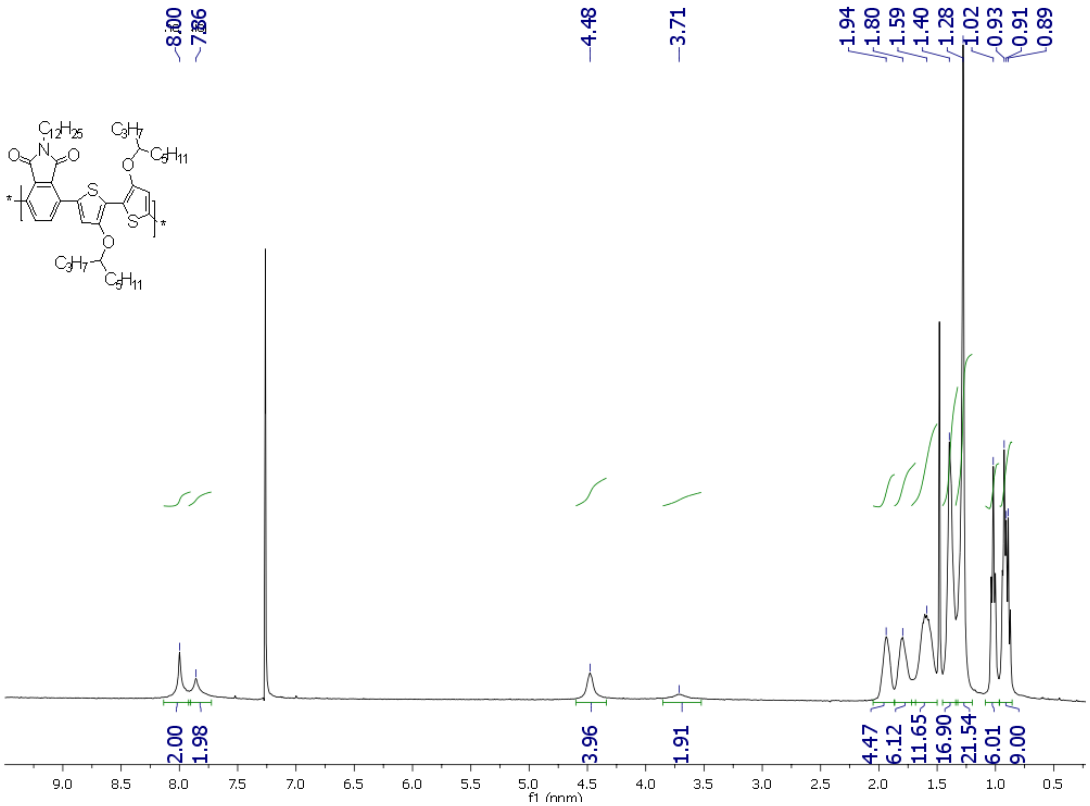
8.00
7.96
4.48
3.71
1.94
1.80
1.59
1.40
1.28
1.02
0.93
0.91
0.89
2.00
1.98
3.96
1.91
4.47
6.12
11.65
16.90
21.54
6.01
9.00
f1 (ppm)

7. 8 Polymer NMR for Chapter Four

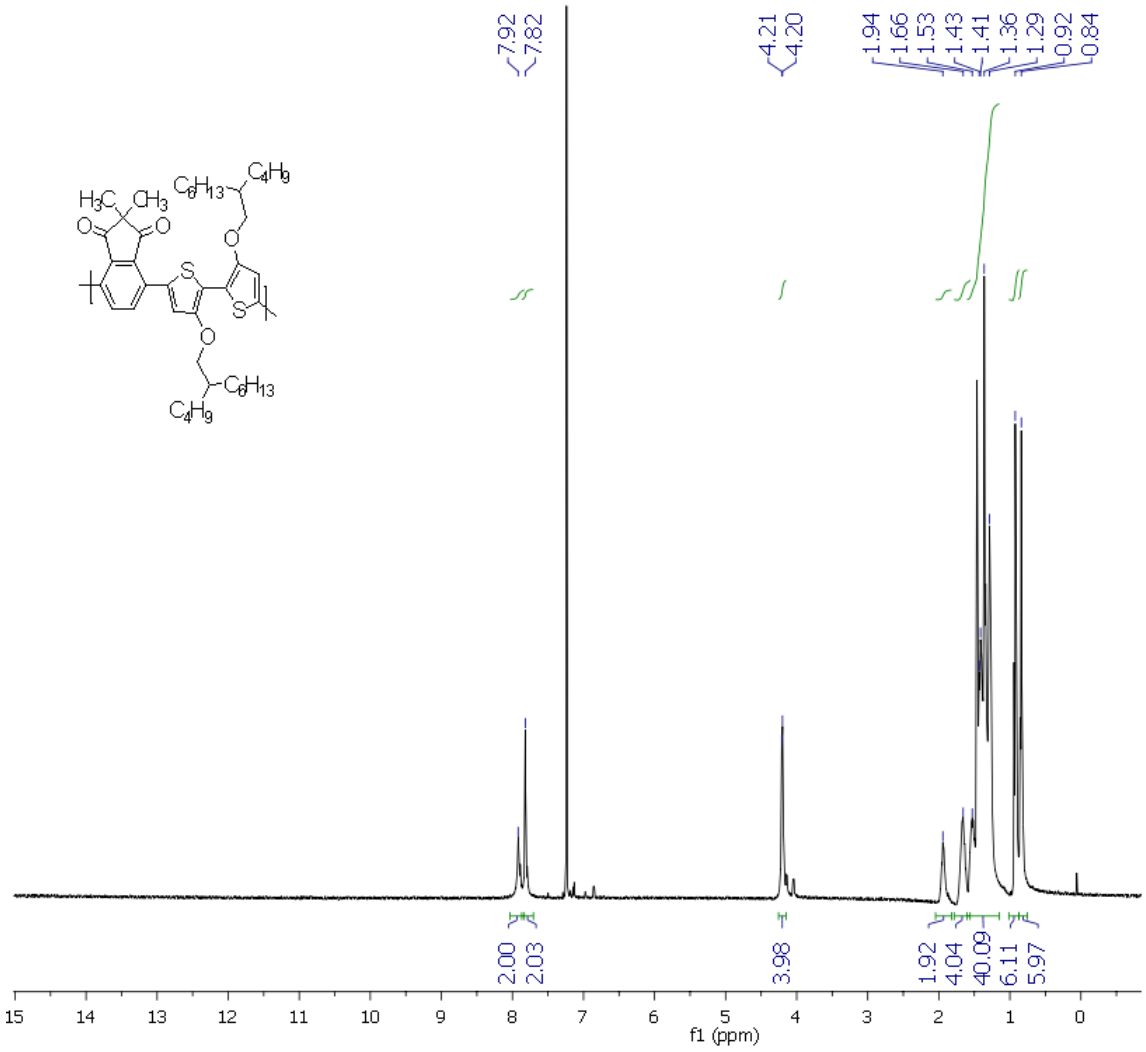

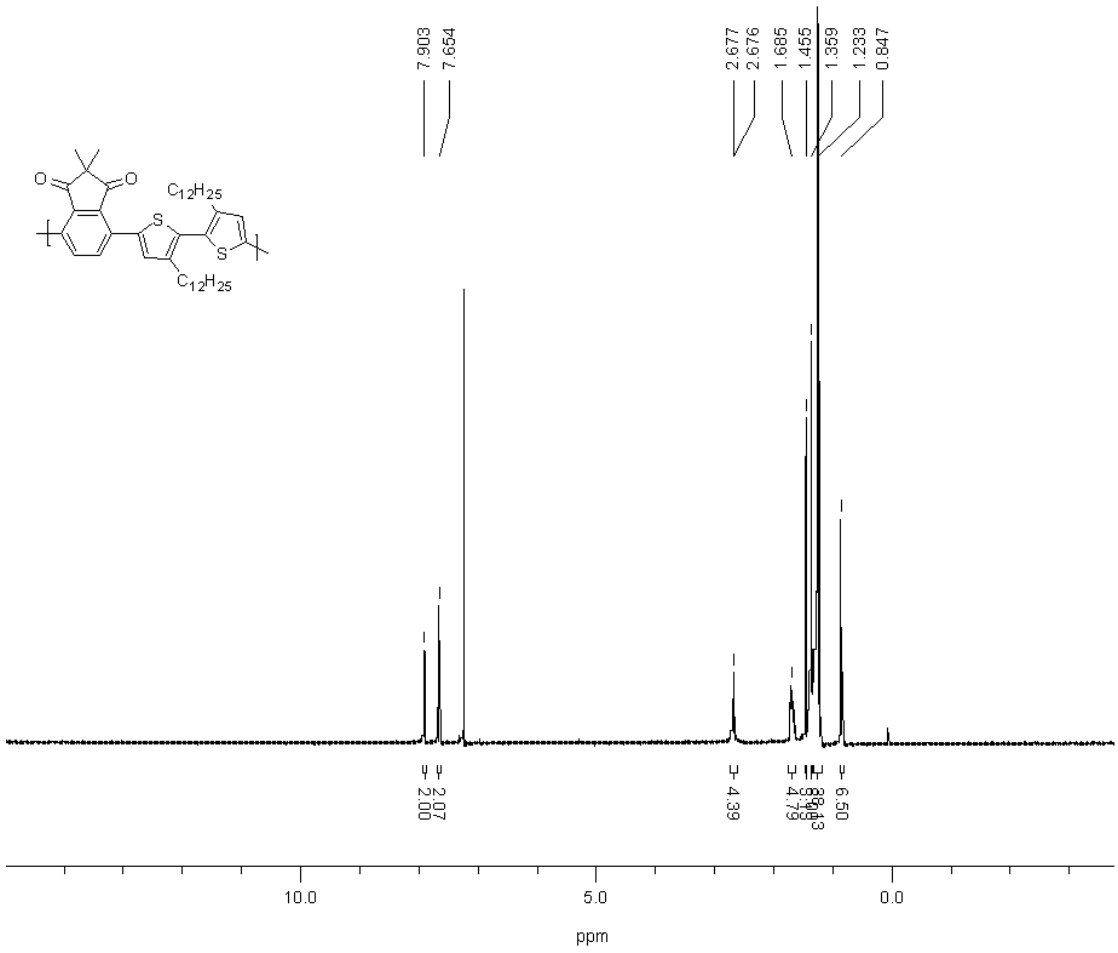
7.903
7.654
2.677
2.676
1.685
1.455
1.359
1.233
0.847
O
O
$C_{12}H_{25}$
S
S
$C_{12}H_{25}$
= 2.00
= 2.07
= 4.39
= 4.79
= 6.50
10.0
5.0
0.0
ppm

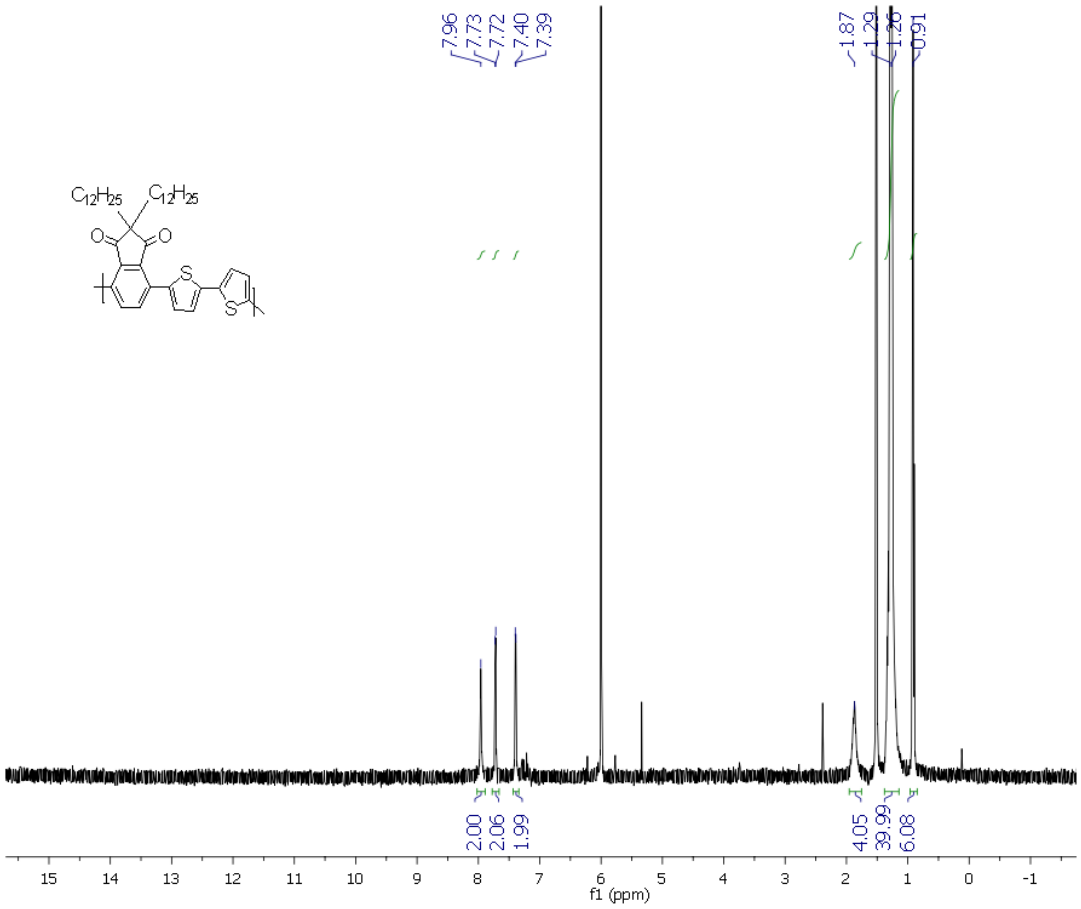
C12H25
C12H25
O
O
S
S
7.96
7.73
7.72
7.40
7.39
1.87
1.29
1.26
0.91
2.00
2.06
1.99
4.05
39.99
6.08
15
14
13
12
11
10
9
8
7
6
5
4
3
2
1
0
-1
f1 (ppm)

7. 9 Polymer NMR for Chapter Five

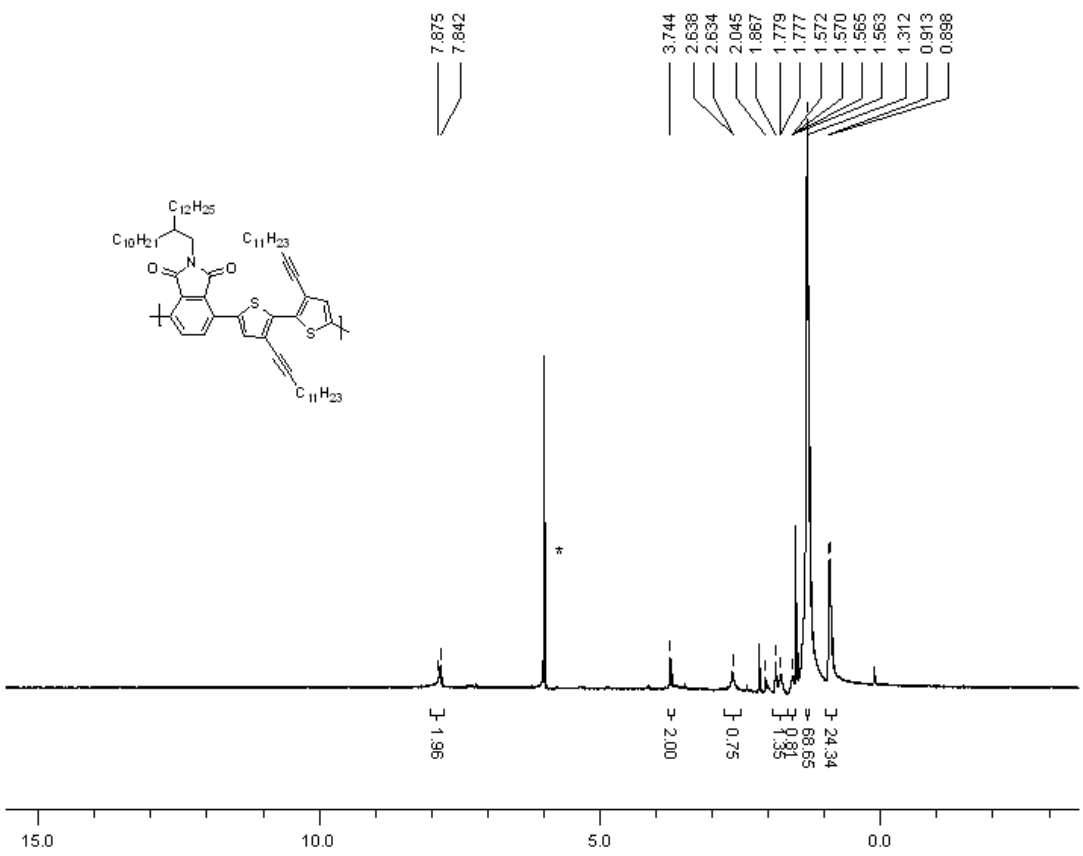

[%]Contamination in $C_2D_2Cl_4$ at ~ 2 ppm

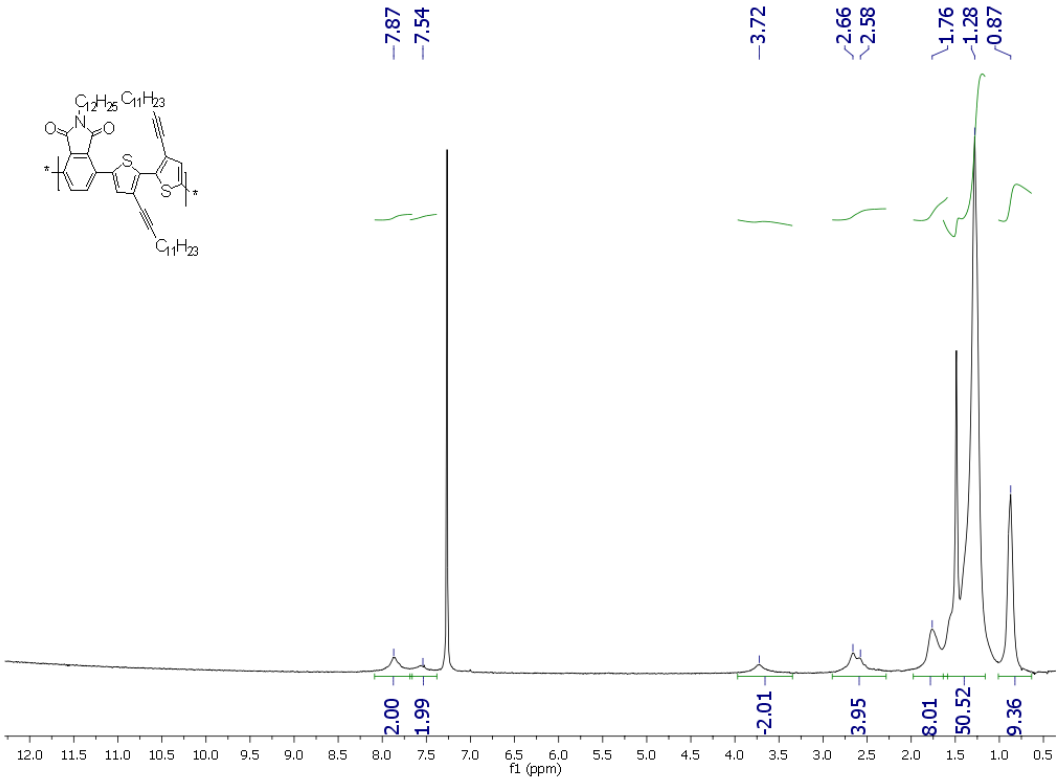
7.87
7.54
3.72
2.66
2.58
1.76
1.28
0.87
2.00
1.99
2.01
3.95
8.01
50.52
9.36
f1 (ppm)

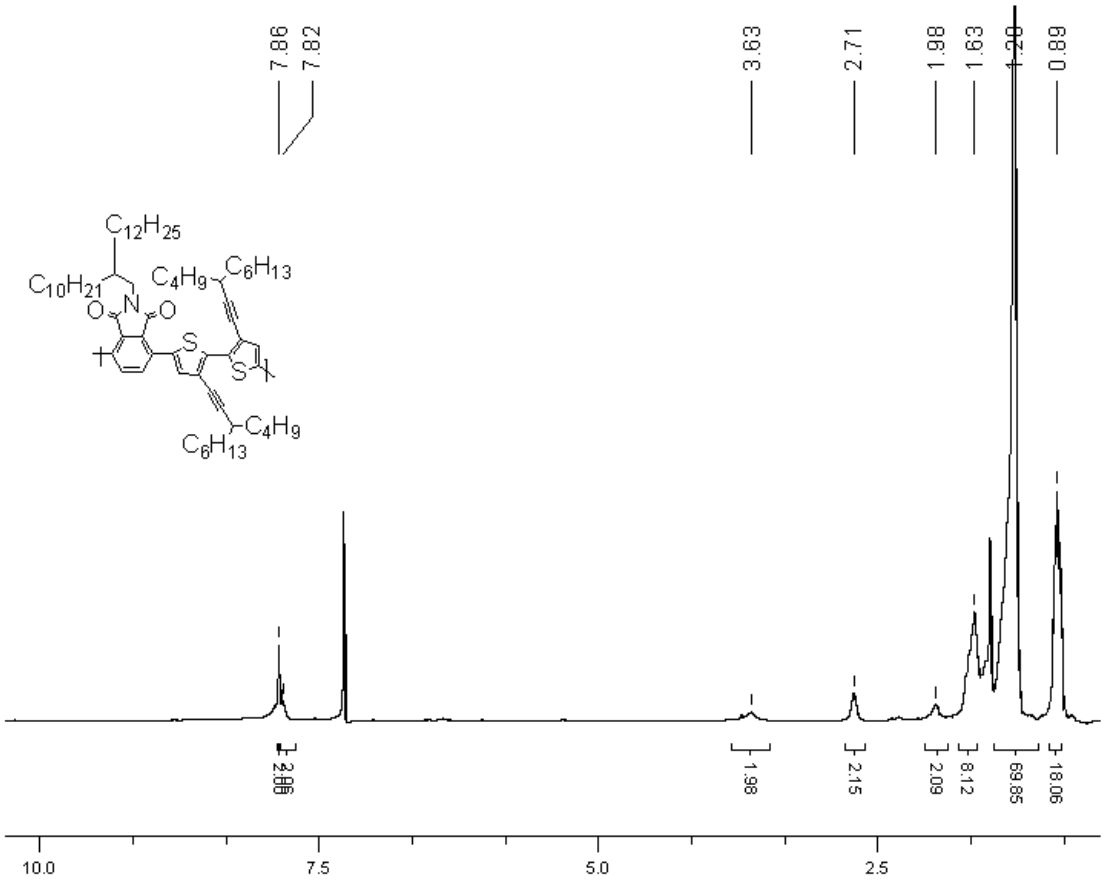

References

1. Shirakawa, H.; Louis, E. J.; Macdiarmid, A. G.; Chiang, C. K.; Heeger, A. J. *J. Chem. Soc. Chem. Comm.* **1977,** 578.
2. Newman, C. R.; Frisbie, C. D.; da Silva Filho, D. A.; Bredas, J-L.; Ewbank, P. C.; Mann, K. R. *Chem. Mater.* **2004,** *16,* 4436.
3. Po, R.; Maggini. M.; Camaioni, N. *J. Phys. Chem. C* **2010,** *114,* 695.
4. Thomas, S. W.; Joly, G. D.; Swager, T. M. *Chem. Rev.* **2007,** *107,* 1339.
5. Rotzoll, R.; Mohapatra, S.; Olariu, V.; Wenz, R.; Grigas, M.; Dimmler, K.; Shchekin, O.; Dodabalapur, A. *App. Phys. Lett.* **2006,** *88,* 123502/1.
6. Wen, Y.; Liu, Y.; Guo, Y.; Yu, G.; Hu, W. *Chem. Rev.* **2011,** *111,* 3358.
7. Bao, Z.; Rogers, J. A.; Katz, H. E. *J. Mater. Chem.* **1999**, *9,* 1895.
8. Chen, H.; Guo, Y.; Yu, G.; Zhao, Y.; Zhang, J.; Gao, D.; Liu, H.; Liu, Y. *Adv. Mater.* **2012,** DOI: 10.1002/adma.201201318.
9. Tsao, H. N. Cho, D. M.; Park, I.; Hansen, M. R.; Mavrinskiy, A.; Yoon, D. Y.; Graf, R.; Pisula, W.; Spiess, H. W.; Müllen, K. *J. Am. Chem. Soc.* **2011,** *133,* 2605.
10. Chen, H.; Guo, Y.; Yu, G.; Zhao, Y.; Zhang, J.; Gao, D.; Liu, H.; Liu, Y. *Adv. Mater. **2012,*** DOI: 10.1002/adma.201201318
11. Meijer, E. J.; Detcheverry, C.; Baesjou, P. J.; Van Veenendaal, E.; De Leeuw, D. M.; Klapwijk, T. M. *J. Appl. Phys.* **2003**, *93,* 4831
12. Vieira, S. M. C. Hsieh, G-W.; Unalan, H. E.; Dag, S.; Amaratunga, G. A. J.; Milne, W. I. *Appl. Phys. Lett.* **2011,** *98,* 102106.
13. Chabinyc, M. L.; Street, R. A.; Northrup, J. E. *Appl. Phys. Lett.* **2007,** *90,* 123508.
14. Po, R.; Maggini, M.; Camaioni, N. *J. Phys. Chem. C* **2010,** *114,* 695.
15. Coakley, K. M.; McGehee, M. D. *Chem. Mater.* **2004,** *16,* 4533.
16. Dennler, G.; Scharber, M. C.; Brabec, C. J. *Adv. Mater.* **2009,** *21,* 1323.
17. http://www.polyera.com/newsflash/polyera-achieves-world-record-organic-solar-cell-performance accessed 8/1/2012
18. Thompson, B. C.; Fréchet, J. M. J. *Angew. Chem. Int. Ed.* **2008,** *47,* 58.
19. Allemand, P. M.; Koch, A.; Wudl, F. *J. Am. Chem. Soc.* **1991,** *113,* 1050.
20. Gunes, S.; Neugebauer, H.; Sariciftci, N. S. *Chem. Rev.* **2007,** *107,* 1324.
21. Bredas, J. L.; Beljonne, D.; Coropceanu, V.; Cornil, J. *Chem. Rev.* **2004**, *104,* 4971.
22. Brabec, C. J.; Cravino, A.; Meissner, D.; Sariciftci, N. S.; Fromherz, T.; Rispens, M. T.; Sanchez, L.; Hummelen, J. C. *Adv. Funct. Mater.* **2001,** *11,* 374.
23. Scharber, M. C.; Wuhlbacher, D.; Koppe, M.; Denk, P.; Waldauf, C.; Heeger, A. J.; Brabec, C. J. *Adv. Mater.* **2006,** *18,* 789
24. Moliton, A.; Nunzi, J.-M. *Polym. Int.* **2006,** *55,* 583.
25. Roncali, J. *Chem. Rev.* **1997,** *97,* 173.
26. Lee, Y. S.; Kertesz, M. *J. Chem. Phys.* **1988**, *88,* 2609.
27. Brédas, J. L. *J. Chem. Phys.* **1985**, *82,* 3808.
28. de Leeuw, D. M.; Simenon, M. M. J.; Brown, A. R.; Einerhand, R. E. F. *Synth. Met.* **1997,** *87,* 53.
29. Maior, R.M. S.; Hinkelman, K.; Eckert, H.; Wudl, F. *Macromolecules* **1990**, *23,* 1268.

30. Wang, Y.; Watson, M. D. *Macromolecules* **2008,** *41,* 8643.
31. Irvin, J. A.; Schwendeman, I.; Lee, Y.; Abboud, K. A.; Reynolds, J. R. *J. Poly. Sci. A.* **2001,** *39,* 2164.
32. Sotzing, G. A.; Reynolds, J. R.; Steel, P. J. *Chem. Mater.* **1996,** *8,* 882.
33. Turbiez, M.; Frére, P.; Allain, M.; Videlot, C.; Ackermann, J.; Roncali, J. *Chem. Eur. J.* **2005,** *11,* 3742.
34. Hergué, N.; Mallet, C.; Savitha, G.; Allain, M.; Frére, P.; Roncali, P. *Org. Lett.* **2011,** *13,* 762.
35. Spencer, H. J.; Skabara, P. J.; Giles, M.; McCulloch, I.; Coles, S. J.; Hursthouse, M. B. *J. Mater. Chem.* **2005,** *15,* 4783.
36. Vangheluwe, M.; Verbiest, T.; Koeckelberghs, G. *Macromolecules,* **2008,** *41,* 1041.
37. Cloutier, R.; Leclerc, M. *J. Chem. Soc. Chem. Comm.* **1991,** 1194.
38. Bleiholder, C.; Gleiter, R.; Werz, D. B.; Koppel, H. *Inorg. Chem.* **2007,** *46,* 2249.
39. Lei, T.; Dou, J.-H.; Pei, J. *Adv. Mater.* **2012,** *24,* 6457
40. Chu, T. Y.; Lu, J. Beaupré, S.; Zhang, Y.; Pouliot, J. R.; Wakim, S.; Zhou, J.; Leclerc, M.; Li, Z.; Ding, J.; Tao, Y. *J. Am. Chem. Soc.* **2011,** *133,* 4250.
41. Small, C. E.; Chen, S.; Subbiah, J.; Amb, C. M.; Tsang, S.-W.; Lai, T.-H.; Reynolds, J. R.; So, F. *Nature Photonics,* **2012**, *6,* 115.
42. Liang, Y.; Xu, Z.; Xia, J.; Tsai, S. Z.; Wu, Y.; Li, G.; Ray, C.; Yu, L. *Adv. Mater.* **2010,** *22,* E135.
43. Zhou, H.; Yang, L.; Stuart, A. C.; Price, S. C.; Liu, S.; You, W. *Angew. Chem.* **2011,** *123,* 3051.
44. Murphy, A. R.; Fréchet, J. M. J. *Chem. Rev.* **2007,** *107,* 1066.
45. Lu, G.; Usta, H.; Risko, C.; Wang, L.; Facchetti, A.; Ratner, M. A.; Marks, T. J. *J. Am. Chem. Soc.* **2008,** *130,* 7670
46. D'Andrade, B. W.; Datta, S.; Forrest, S. R.; Djurovich, P.; Polikarpov, E.; Thompson, M. E. *Organic Electronics*, **2005,** *6,*11.
47. Cardona, C. M.; Li, W.; Kaifer, A. E.; Stockdale, D.; Bazan, G. C.; *Adv. Mater.* **2011,** *23,* 2367.
48. Pavlishchuk, V. V.; Addison, A. W. *Inorganica Chimica Acta* **2000,** *298,* 97.
49. Johansson, T.; Mammo, W.; Svensson, M.; Andersson, M.R.; Inganas, O. *J. Mater. Chem.* **2003** , *13* , 1316
50. Flato, J. B. *Anal. Chem.* **1972,** *44,* 75 A.
51. Steckler, T. T.; Abboud, K. A.; Craps, M.; Rinzler, A. G.; Reynolds, J. R. *Chem. Commun.* **2007,** 4904.
52. Mei, J.; Heston, N. C.; Vasilyeva, S. V.; Reynolds, J. R. R.; *Macromolecules,* **2009,** *42,* 1482.
53. Nietfeld, J. P.; Heth, C. L.; Rasmussen, S. C. *Chem. Commun.*, **2008,** *0,* 981-983.
54. Meyer, D. J.; Osteryoung, J. *Anal. Chem.*, 1974, **46**, 357
55. Choulis, S.A.; Nelson, K. J.; Bradley, D. D. C.; Giles, M.; Shkunov, M.; McCulloch, I. *App. Phys. Lett.***2004,** *85,* 3890.
56. Chao, Y-C.; Xie, M-H.; Dai, M-Z.; Meng, H-F.; Horng, S-F.; Hsu, C-S. *App. Phys. Lett.***2008,** *92,* 093310.
57. Stille, J. K. *Angew. Chem*. **1986,** *98,* 504 – 519.
58. Facchetti, A. *Materials Today,* **2007,** *10,* 28.

59. Farina, V.; Krishnan, B. *J. Am. Chem. Soc.* **1991,** *113*, 9585.
60. Bao, Z.; Chan, W. K.; Yu, L. *J. Am. Chem. Soc.* **1995,** *117*, 12426-12435.
61. Guo, X.; Watson, M. D. *Org. Lett.* **2008,** *10*, 5333.
62. Osaka, I,; McCullough, R. D. *Acc. Chem. Res.* **2008,** *41*, 1202.
63. Kohn, P.; Huettner, S; Komber, H.; Senkovskyy, V.; Tkachov, R.; Kiriy, A.; Friend, R. H.; Steiner, U.; Huck, W. T. S.; Sommer, J.; Sommer, M. *J. Am. Chem. Soc.* **ASAP,** DOI: 10.1021/ja210871j.
64. Espinet, P.; Echavarren, A. M. *Angew. Chem. Int. Ed.* **2004,** *43*, 4704.
65. Goodson, F. E.; Wallow, T. I.; Novak, B. M. *Macromolecules,* **1998,** *31*, 2047.
66. Goodson, F. E.; Wallow, T. I.; Novak, B. M. *J. Am. Chem. Soc.* **1997,** *119*, 12441.
67. Ziegler, C. B.; Heck, R. F. *J. Org. Chem.* **1978,** *43*, 2941.
68. Bendikov, M.; Wudl, F. *Chem. Rev.* **2004,** *104*, 4891.
69. Jones, B. A.; Facchetti, A.; Wasielewski, M. R.; Marks, T. J. *J. Am. Chem. Soc.* **2007,** *129*, 15259.
70. Mikhnenko, O. V.; Azimi, H.; Scharber, M.; Morana, M.; Blom, P. W. M.; Loi, M. A. *Energy Enviorn. Sci.* **2012,** *5*, 6960.
71. Tsao, H. N.; Müllen, K. *Chem. Soc. Rev.* **2010,** *39*, 2372.
72. Reichenbächer, K.; Süss, H. I.; Hullinger, J. *Chem. Soc. Rev.* **2005,** *34*, 22.
73. Zhang, Z. –G.; Wang, J. *J. Mater. Chem.* **2012,** *22*, 4178.
74. Ahmed, E.; Kim, F. S.; Xin, H.; Jenekhe, S. A. *Macromolecules,* **2009,** *42*, 8615.
75. Mcculloch, I.; Heeney, M.; Bailey, C.; Genevicius, K.; Macdonald, I.; Shkunov, M.; Sparrowe, D.; Tierney, S.; Wagner, R.; Zhang, W. M.; Chabinyc, M. L.; Kline, R. J.; Mcgehee, M. D.; Toney, M. F. *Nature Materials* **2006,** *5*, 328.
76. Anthony, J. E. *Chem. Rev.* **2006,** *106*, 5028.
77. Allemond, P. M.; Koch, A.; Wudl, F.; Rubin, Y.; Diederich, F.; Alvarez, M. M.; Anz, S. J.; Whetten, R. L. *J. Am. Chem. Soc.* **1991**, *113*, 1050.
78. Singh, T. B.; Marjanovic, N.; Matt, G. J.; Gunes, S.; Sariciftci, N. S.; Montaigne Ramil, A.; Andreev, A.; Sitter, H.; Schwodiauer, R.; Bauer, S. *Org. Electron.* **2005**, *6*, 105.
79. Salleo, A.; Kline, R. J.; DeLongchamp, D. M.; Chabinc, M. L. *Adv. Mater.* **2010,** *22*, 3812.
80. http://www.heliatek.com/newscenter/latest_news/neuer-weltrekord-fur-organische-solarzellen-heliatek-behauptet-sich-mit-12-zelleffizienz-als-technologiefuhrer/?lang=en Last accessed 03/09/2012.
81. Morgado, J.; Cacialli, F.; Friend, R. H.; Chuah, B. S.; Rost, H.; Holmes, A. B. *Macromolecules*, **2001,** *34*, 3094.
82. Greve, D. R.; Apperloo, J. J.; Janssen, R. A. J. *Eur. J. Org. Chem.* **2001,** *18*, 3437.
83. Jonforsen, M.; Johansson, T.; Spjuth, L.; Inganas, O.; Andersson, M. R. *Synth. Met.* **2002,** *131*, 53.
84. Kokubo, H.; Sato, T.; Yamamoto, T. *Macromolecules* **2006,** *39*, 3959.
85. Demanze, F.; Cornil, J.; Garnier, F.; Horowitz, G.; Valat, P.; Yassar, A.; Lazzaroni, R.; Brédas, J. *J. Phys. Chem. B.* **1997,** *101*, 4553.
86. Kuo, M. -Y.; Chen, H. Y.; Chao, I. *Chem. Eur. J.* **2007,** *13*, 4750.
87. Barclay, T. M.; Cordes, A. W.; MacKinnon, C. D.; Oakley, R. T. Reed, R. W. *Chem. Mater.* **1997,** *9*, 981.

88. Swartz, C. R.; Parkin, S. R.; Bullock, J. E.; Anthony, J. E.; Mayer, A. C.; Malliaras, G. G. *Org. Lett.* **2005,** *7,* 3163.
89. Lim, Y. F.; Shu, Y.; Parkin, S. R.; Anthony, J. E.; Malliaras, G. G. *J. Mater. Chem.* **2009,** *19,* 3049.
90. Anthony, J. *Chem. Mater*. **2011,** *23,* 583.
91. Chen, Y. J.; Hsiung, S.; Hsu, C. S. *Chem. Rev.* **2009,** *109,* 5868.
92. Holcombe, T. W.; Woo, C. H.; Kavulak, D. F. J.; Thompson, B. C.; Fréchet, J. M. J. *J. Am. Chem. Soc.* **2009,** *131,* 14160.
93. Sang, G.; Zou, Y.; Huang, Y.; Zhao, G.; Yang, Y.; Li, Y. *Appl. Phys.Lett.* **2009,** *94,* 193302.
94. Greenwald, Y.; Xu, X.; Fourmigué, M.; Srdanov, G.; Koss, C.; Wudl, F.; Heeger, A. J. *J. Poly. Sci. A.* **1998,** *36.* 3315.
95. Greve, D. R., Aperloo, J. J.; Janssen, R. A. J. *Eur. J. Org. Chem.* **2001,** 3437.
96. Friedman, L; Shechter, H. *J. Org. Chem.* **1961,** *26,* 2522. b) Yassar, A.; Demanze, F.; Jaafari, A.; El Idrissi, M.; Coupry, C. *Adv. Funct. Mater.* **2002,** *12,* 699.
97. Liu, M. S.; Jiang, X.; Herguth, P.; Jen, A. K. Y. *Chem. Mater.* **2001,** *13,* 3820.
98. Pletnev, A. A.; Tian, Q.; Larock, R. C. *J. Org. Chem.* **2002,** *67,* 9276.
99. Guo, X.; Watson, M. D.; *Org. Lett.* **2008,** *10,* 5333.
100. Turbiez, M.; Frere, P.; Allain, M.; Videlot, C.; Ackermann, J.; Roncali, J. *Chem. Eur. J.* **2005,** *11,* 3742.
101. McCullough, R. D.; Lowe, R. S. *Chem. Comm.* **1992,** 70.
102. Amrutha, S. R.; Jayakannan, M. *J. Phys. Chem. B.* **2008,** *112,* 1119.
103. Blouin, N.; Michaud, A.;Gendron, D.; Wakim, S.; Blair, E.; Neagu-Plesu, R.; Belletete, M.; Durocher,G.; Tao, Y.; Leclerc, M. *J. Am. Chem. Soc.* **2008**, *130*, 732.
104. Thompson, B. C.; Kim, Y. G.; McCarley, T. D.; Reynolds, J. R. *J. Am. Chem. Soc.* **2006**, *128*, 12714.
105. Maior, R. M. S.; Hinkelmann, K.; Eckert, H.; Wudl, F. *Macromolecules,* **1990,** *23,* 1268.
106. Holland, E. R.; Bloor, D.; Monkman, A. P.; Brown, A.; De Leeuw, D.; Bouman, M. M.; Meijer, E. W. *J. Appl. Phys.* **1994,** *75,* 7954.
107. Liu, M. S.; Jiang, X.; Herguth, P.; Jen, A. K.Y. *Chem. Mater.* **2001**, *13*, 3820.
108. Chang, J. F.; Sun, B.; Breiby, D. W.; Nielsen, M. M.; Solling, T. I.; Giles, M.; McCulloch, I.; Sirringhaus, H. *Chem. Mater*. **2004,** *16,* 4772.
109. Yang, H.; Shin, T. J.; Yang, L.; Cho, K.; Ryu, Y.; Bao, Z. *Adv. Funct. Mater.*, **2005,** *15,* 671.
110. C. Hansch and A. Leo, "Substituent Constants for Correlation Analysis in Chemistry and Biology," Wiley-Interscience, NY, 1979.
111. Osaka, I.; McCullough, R. D., *Accounts of Chemical Research* **2008,** *41,* 1202.
112. Halkyard, C. E.; Rampey, M. E.; Kloppenburg, L.; Studer-Martinez, S. L.; Bunz, U. H. F. *Macromolecules* **1998,** *31,* 8655.
113. Guo, X.; Kim, F. S.; Jenekhe, S. A.; Watson, M. D. *J. Am. Chem. Soc.* **2009,** *131,* 7206.
114. Xin, H.; Guo, X.; Ren, G.; Watson, M. D.; Jenekhe, S. A. *Adv. Energy Mater.* **2012,** *2,* 575.

115. Guo, X.; Ortiz, R. P.; Kim, M. G.; Zhang, S.; Hu, Y.; Lu, G.; Facchetti, A.; Marks, T. J. *J. Am. Chem. Soc.* **2011,** *133,* 13685.
116. Yan, H.; Chen, Z.; Newman, C.; Quinn, J. R.; Dotz, F.; Kastler, M.; Facchetti, A. *Nature* **2009,** *457,* 679.
117. Chen, Z.; Zheng, Y.; Yan, H.; Facchetti, A. *J. Am. Chem. Soc.* **2009,** *131,* 8.
118. Letizia, J. A.; Salata, M. R.; Tribout, C. M.; Facchetti, A.; Ratner, M. A.; Marks, T. J. *J. Am. Chem. Soc.* **2008,** *130,* 9679.
119. Piliego, C.; Holcombe, T. W.; Douglas, J. D.; Woo, C. H.; Beaujuge, P. M.; Frechet, J. M. J. *J. Am. Chem. Soc.* **2010,** *132,* 7595.
120. Xin, H.; Guo, X.; Kim, F. S.; Ren, G.; Watson, M. D.; Jenekhe, S. A. *J. Mater. Chem.* **2009,** *19,* 5303.
121. Burkhart, B.; Khlyabich, P. P.; Thompson, B. C. *Macromolecules,* **2012,** *45,* 3740.
122. Wang, Y.; Watson, M.D. *Macromolecules,* **2008,** *41,* 8643.
123. Babudri, F.; Farinola, G. M.; Naso, F.; Ragni, R. *Chem. Comm.* **2007,** 1003
124. Wang, Y.; Parking, S. R.; Gierschner, J.; Watson, M. D. *Org. Lett.* **2008,** *10,* 3307.
125. Liang, Y.; Xu, Z.;' Xia, J.; Tsai, S. T.; Wu, Y.; Li, G.; Ray, C.; Yu, L. *Adv. Mater.* **2010,** *22,* 135.
126. Zhou, H.; Yang, L.; Stuart, A. C.; Price, S. C.; Liu, S.; You, W. *Angew. Chem.* **2011,** *123,* 3051.
127. Allen, C. F. H.; Frame, G. F.; Wilson, C. V. *J. Org. Chem.* **1941**, *6*, 732.
128. Rajesh, K.; Somasundaram, M.; Saiganesh, R.; Balasubramanian, K. K. *J. Org. Chem.* **2007,** *72,* 5867.
129. Eguchi, H.; Kawaguchi, H.; Yoshinaga, S.; Nishida, A.; Nishiguchi, T.; Fujisaki, S. *Bull. Chem. Soc. Jpn.* **1994,** *67,* 1918.
130. Iqbal, Z.; Lyubimtsev, L.; Hanack, M. *Synlett,* **2008,** *15,* 2287.
131. Anbarasan, P.; Schareina, T.; Beller, M. *Chem. Soc. Rev.* **2011,** *40,* 5049.
132. Do, H. Q.; Daugulis, O. *Org. Lett.*, **2009,** *11,* 421.
133. Schroeder, B. C.; Huang, Z.; Ashraf, R. S.; Smith, J.; D'Angelo, P.; Watkins, S. E.; Anthopoulos, T. D.; Durrant, J. R.; McCulloch, I. *Adv. Funct. Mater.* **2012,** *22,* 1663.
134. Clarke, T. M.; Ballantyne, A. M.; Nelson, J.; Bradley, D. D. C.; Durrant, J. *Adv. Funct. Mater.* **2008,** *18,* 4029.
135. Nguyen, L. H.; Hoppe, H.; Erb, T.; Gunes, S.; Gobsch, G.; Sariciftci, N. S.; *Adv. Funct. Mater.* **2007,** *17,* 1071.
136. Chabinyc, M. L.; Salleo, A. *Chem. Mater.* **2004,** *16,* 4509.
137. Dang, M. T.; Wantz, G.; Bejbouji, H.; Urien, M.; Dautel, O. J.; Vignau, L.; Hirsch, L. *Sol. Energy Mater. Sol. Cells* **2011,** *95,* 3408.
138. Holland, E. R.; Bloor, D.; Monlman, A. P.; Brown, A.; De Leeuw, D.; Bouman, M. M.; Meijer, E. W. *J. Appl. Phys.* **75,** *12,* 7954.
139. Sun, S.; Salim, T.; Wong, L. H.; Foo, Y. L.; Boey, F.; Lam, M. Y. *J. Mater. Chem.* **2011,** *21,* 377.
140. Motaung, D. E.; Malgas, G. F.; Arendse, C. J. *Syn. Met.* **2010,** *160,* 876.
141. Dang, M. T.; Hirsch, L.; Wantz, G.; Wuest, J. D. *Chem. Rev.* **ASAP,** dx.doi.org/10.1021/cr300005u

142. Gierschner, J.; Huang, Y.-S.; Van Averbeke, B.; Cornil, J.; Friend R. H.; Beljonne, D. *The J. Chem. Phys.* **2009**, *130*, 044105.
143. Dickey, K. C.; Anthony, J. E.; Loo, Y.-L. *Adv. Mater.* **2006,** *18,* 1721.
144. Watson, M. D. U.S. Pat. Appl. Publ. **2010**, US 20100252112 A1 20101007.
145. Xin, H.; Guo, X.; Ren, G.; Watson, M. D.; Jenekhe, S. A. *Adv. Energy Mater.* **2012,** *2,* 575.
146. Hansen, C. M.; *J. Paint. Technol.* **1967,** *39,* 104.
147. Taken from the solvents respective MSDS.
148. Guo, X.; Ortiz, R. P.; Zheng, Y.; Hu, Y.; Noh, Y.-Y.; Baeg, K.-J.; Facchetti, A.; Marks, T. J. *J. Am. Chem. Soc.* **2011,** *133,* 1405.
149. Scherf, U.; List, E. J. W. *Adv. Mater.* **2002,** *14,* 477.
150. Sloof, L. H.; Veenstra, S. C.; Kroon, J. M.; Moet, D. J.; Sweelssen, J. *Appl. Phys. Lett.* **2007,** *90,* 143506.
151. Zhang, W.; Smith, J.; Watkins, S. E.; Gysel, R.; McGehee, M.; Salleo, A.; Kirkpatrick, J.; Ashraf, S.; Anthopoulos, T.; Heeney, M.; McCulloch, I. *J. Am. Chem. Soc.* **2010,** *132,* 11437.
152. Holcombe, T. W.; Norton, J. E.; Rivnay, J.; Woo, C. H.; Goris, L.; Piliego, C.; Griffini, G.; Sellinger, A.; Bredas, J.-L.; Salleo, A.; Frechet, J. M. J. *Journal of the American Chemical Society* **2011**, *133*, 12106.
153. Cornil, J.; Gueli, I.; Dkhissi, A.; Sancho-Garcia, J. C.; Hennebicq, E.; Calbert, J. P.; Lemaur, V.; Beljonne, D.; Bredas, J-L. *J. Chem. Phys.* **2003,** *118,* 6615.
154. Karsten, B. P.; Bijleveld, J. C.; Viani, L.; Cornil, J.; Gierschner, J.; Janssen, R. A. J. *J. Mater. Chem.* **2009,** *19,* 5343.
155. Cornil, J.; Beljonne, D.; Calbert, J-P.; Bredas, J-L. *Adv. Mater.* **2001,** *13,* 1053.
156. Buckle, D. R.; Morgan, N. J.; Ross, J. W.; Smith, H.; Spicer, B. A. *J. Med. Chem.* **1973,** *16,* 1334.
157. Gruen, H.; Norcross, B. E. *J. Chem. Educ.* **1965,** *42,* 268.
158. Kuck, D. *Chem. Ber.* **1994,** *127,* 409.
159. Chen, H.; Guo, Y.; Zhao, Y.; Zhang, J.; Gao, D.; Liu, H.; Liu, Y. *Adv. Mater.* **2012,** *24,* 4618.
160. Chen, H-Y.; Hou, J.; Zhang, S.; Liang, Y.; Yang, Y.; Yang, G.; Yang, Y.; Yu, L.; Wu, Y.; Li, G. *Nature Photonics,* **2009,** *3,* 649.
161. Maior, R. M.; Hinkelmann, K.; Eckert, H.; Wudl, F. *Macromolecules,* **1990,** *23,* 1268.
162. Irvin, J. A.; Schwendeman, I.; Lee, Y.; Abboud, K. A.; Reynolds, J. R. *J. Polym. Sci. Part A: Polym Chem.* **2001,** *39,* 2164.
163. Sato, T.; Kokubo, H.; Fukumoto, H.; Yamamoto, T. *Bull. Chem. Soc. Jpn.* **2005,** *78,* 1368.
164. Tanese, M. C.; Farinola, G. M.; Pignataro, B.; Valli, L.; Giotta, L.; Conoci, S.; Lang, P.; Colangiuli, D.; Babudri, F.; Naso, F.; Sabbatine, L.; Zambonin, P. G.; Torsi, L. *Chem. Mater.* **2006,** *18,* 778.
165. Gierschner, J.; Mack, H. G.; Egelhaaf, H. J.; Schweizer, S.; Doser, B.; Oelkrug, D. *Syn. Met.* **2003**, *138*, 311.
166. Sato, T.; Cai, Z.; Shiono, T.; Yamamoto, T. *Polymer,* **2006,** *47,* 37.
167. Yuan, M.; Rice, A. H.; Luscombe, C. K. *J. Poly. Sci. A.* **2011,** *49,* 701.
168. Price, S. C.; Stuart, A. C.; You, W. *Macromolecules,* **2010,** *43,* 797.

169. Corey, E. J.; Fuchs, P, L. *Tetrahedron. Lett.* **1972,** *36,* 3769.
170. Chen, T-A.; Wu, X.; Rieke, R. D.; *J. Am. Chem. Soc.* **1995,** *117,* 233.
171. Friedel, B.; McNeill, C. R.; Greenham, N. C. *Chem. Mater.* **2010,** *22,* 3389.
172. Oosterbaan, W. D.; Bolsee, J.-C.; Gadisa, A.; Vrindts, V.; Bertho, S.; D'Haen, J.; Cleij, T.
173. Wang, M.; Li, J.; Zhao, G.; Wu, Q.; Huang, Y.; Hu, W.; Gao, X.; Li, H.; Zhu, D. *Adv. Mater.* **2013,** DOI: 10.1002/adma.201204469.
174. C. Liu, T. Minari, X. Lu, A. Kumatani, K. Takimiya, K. Tsukagoshi, *Adv. Mater.* **2011**, *23*, 523.
175. Chatterjee, S. *J. Chem. Soc. (B)* **1969,** 725.
176. Schonberg, A.; Singer, E. *Chem. Ber.* **1970,** *103*, 3871.
177. Bryce, M. R.; Davies, S. R.; Hasan, M.; Ashwell, G. J.; Szablewski, M.; Drew, M. G. B.; Short, R.; Hursthouse, M. B. *J. Chem. Soc. Perkin Trans.* **1989,** *2,* 1285.
178. Hark, R. R.; Hauze, D. B.; Petrovskaia, O.; Joullie, M. M. *Tet. Lett.* **1994,** *35,*7719.
179. Chakrabarty, M.; Mukherji, A.; Arima, S.; Harigaya, Y.; Pilet, G. *Monatsh. Chem.* **2009,** *140,* 189.
180. Du, C.; Li, C.; Li, W.; Chen, X.; Bo, Z.; Veit, C.; Ma, Z.; Wuerfel, U.; Zhu, H.; Zhang, F. *Macromolecules,* **2011,** *44,* 7617.
181. Ie, Y.; Umemoto, Y.; Kaneda, T.; Aso, Y. *Org. Lett*. **2006**, *8*, 5381-5384.
182. Ie, Y.; Umemoto, Y.; Okabe, M.; Kusunoki, T.; Nakayama, K.-I; Pu, Y.-J.; Kido, J.; Tada, H.; Aso, Y. *Org. Lett.* **2008,** *10,* 833.
183. Nesterov, V. N.; Aitov, I. A.; Sharanin, Y. A.; Struchkov, Y. T. *Russ. Chem. Bull.* **1996,** *45,* 164.
184. Freeman, F. *Chem. Rev.* **1980,** *80,* 329.
185. Burchat, A. F.; Chong, J. M.; Nielsen, N. *J. Organomet. Chem.* **1997,** *542,* 281.
186. www.sigmaaldrich.com

VITA

Mark Seger was born in Ft. Thomas, Kentucky. He attended Northern Kentucky University and participated in undergraduate research focused on the synthesis of annulenes. He earned a Bachelor of Science degree in Chemistry in 2007. After graduation, he was admitted into the graduate program at the University of Kentucky and starting his research on conjugated polymers with Professor Mark Watson. His research focused on the synthesis of donor-acceptor copolymers for (opto)electronic applications.

Publications:

1. "Naphthalene Diimide-Based Polymer Semiconductors: Synthesis, Structure-Property Correlations and n-Channel and Ambipolar Field-Effect Transistors." Xugang Guo, Felix Sunjoo Kim, **Mark J. Seger**, Samson A. Jenekhe, Mark D. Watson, *Chemistry of Materials*, **2012,** *24* (8) 1434-1442.
2. "Cyanoarene Semiconducting Polymers" **Mark J. Seger**, Mark D. Watson, *in preparation.*

Presentations:

3. "Synthesis and Properties of Soluble Flavobenzocyclynes." **Mark Seger** and KC Russell, 233rd ACS National Meeting. Chicago, IL, March 2007. (Poster)
4. " Synthesis and Characterization of Soluble Flavobenzocyclynes." **Mark Seger** and KC Russell, Northern Kentucky University Celebration of Student Research and Creativity, Highland Heights, KY; April 2007. (Poster)
5. " Caffeine Analysis of Decaffeinated Coffee Samples within the Tri-State Area." T. Fabre, P. Hogan, B. Holcomb, J. Leslie, S. Proctor, S. Schumacher, **M. Seger**, R. Wilson, and H. A. Bullen. NKU Celebration of Student Research and Creativity April 2006.– part of a class project for Channel 5 News (Poster)
6. "Synthesis of Soluble Falvobenzocyclynes." **Mark Seger** and KC Russell 92nd annual KAS meeting, Moorehead, KY; November 2006. (Poster)